Investigating the roles of the ADMA-DDAH1 pathway in cerebral artery function and ischaemic stroke pathogenesis

Arun Flynn BSc (Hons) MRes

PhD Thesis

Submitted in fulfilment of the requirements for the Degree of

Doctor of Philosophy

School of Cardiovascular & Metabolic Health
College of Medical, Veterinary, and Life Sciences
University of Glasgow

December 2023

Abstract

Nitric oxide (NO), which is produced by endothelial NO synthase (eNOS) in the cerebral endothelium, is crucial for maintaining cerebrovascular homeostasis in health and disease. Asymmetric dimethylarginine (ADMA) is an endogenous inhibitor of eNOS and the dimethylarginine dimethylaminohydrolase (DDAH) 1 and 2 enzymes regulate ADMA levels. Several studies have shown that ADMA levels are elevated following ischaemic stroke and that loss-of-function DDAH1 polymorphisms are associated with increased stroke risk. However, causal evidence linking elevated ADMA levels and stroke pathogenesis are lacking. Furthermore, in contrast to the systemic circulation, direct evidence showing the functional importance of DDAH1 in the cerebral circulation is also lacking. The overall hypotheses of this thesis are that elevated ADMA plays a causal role in ischaemic stroke pathogenesis by perturbing the eNOS-NO signalling pathway, and that the ADMA-metabolising enzyme DDAH1 plays an important physiological role in regulating endothelial NO signalling in cerebral arteries by controlling ADMA levels.

For the main aims of this thesis, we used a selective DDAH1 inhibitor or endothelial-specific DDAH1 knockout mice to investigate the effect of elevated ADMA levels on stroke outcomes in mice following experimental stroke; and to evaluate the functional importance of DDAH1 for the maintenance of NO-dependent physiological processes (e.g., vasoreactivity and angiogenesis) in mouse cerebral vessels. Firstly, we found that DDAH1 inhibition using the selective DDAH1 inhibitor L-257 disrupts eNOS-derived NO signalling in cerebral arteries *in vitro* and increases brain ADMA levels *in vivo* without altering cardiovascular haemodynamics. Importantly, however, the major new finding of this work was that DDAH1 inhibition using L-257 had no effect on ischaemic brain injury or neurological outcomes in mice following focal cerebral ischaemia. These findings indicate that elevated ADMA levels following DDAH1 inhibition does not influence stroke outcomes in this mouse model of stroke. Secondly, using endothelial-specific DDAH1 knockout mice, we found that endothelial DDAH1 is a crucial regulator of cerebral eNOS-NO signalling and resultant endothelial and smooth muscle function, likely through the metabolism of endothelial ADMA, however, we found that it does not appear to play a critical role in ischaemic stroke outcomes. Lastly, using L-257 and endothelial-specific DDAH1 knockout mice, we provide the first evidence that DDAH1 is also critically important for the angiogenic activity of the cerebral endothelium.

In summary, cerebral vascular DDAH1 is a functionally important regulator of cerebral endothelial NO signalling by controlling ADMA levels, however, so far, our work suggests that elevated ADMA levels or DDAH1 dysfunction does not play a causal role in ischaemic stroke pathogenesis. As discussed in this thesis, further studies are required to establish the roles of the ADMA-DDAH1 pathway in ischaemic stroke outcomes.

Contents

List of tables

List of figures

Acknowledgements

First of all, I would like to express my gratitude to the British Heart Foundation, without whom this PhD project and thesis would not have been possible.

To my primary supervisor, Alyson, I cannot adequately put into words how thankful I am to have had you as a supervisor, mentor, and friend throughout my PhD. I am also truly grateful that you saw in me what others did not, which was the ability and determination to undertake a PhD (albeit in a field I was unfamiliar with), and subsequently offered me the chance to prove it. Your help, guidance, and understanding has been paramount in my journey, and I have learned so much and grown both as a scientist and person under your mentorship! There is little I can do to mitigate the number of grey hairs that I will have caused you, but I hope that my recognition of it helps a little, as you have been incredibly patient with me during the last 4 years. Lastly, it is difficult to know whether to be thankful for not for all the nicknames that you developed for me over the years, such as Fireman Flynn and Pablo.

I would also like to thank Professor James Leiper, as well as members of the Leiper group. Your knowledge, expertise, and guidance on all things ADMA and DDAH have been instrumental in my pursuit of understanding the roles of the ADMA-DDAH1 pathway in the cerebrovasculature. Also, your generous provision of the unique selective DDAH1 inhibitor, L-257, as well as the endothelial-specific DDAH1 knockout mouse line made my PhD scholarship and project possible. A special thanks also goes to Laura Dowsett, who was unofficially my third supervisor. You were incredibly helpful and reliable, and your frequent pockets of wisdom throughout my project was hugely appreciated.

A huge thanks and shout out also goes to current and former members of the Miller Lab. Alex and Gabbie, thank you both so much for your help and support in the lab with experiments, surgery inductions, and much more. It has been great working alongside you both. Ashton, my brother from another mother, I believe that our friendship in the lab when I was a research technician was pivotal in my introduction to the Miller Lab, and I may not have sufficiently demonstrated my abilities to Alyson without our undertaking of the PVMs project. You have been hugely missed in the lab but thank you for your friendship and inclusivity. Jawza, Erika, and Emily, it was a pleasure to work with you all too.

To my three musketeers: Dan ‘The Man’, our frequent coffee trips, dark room hangouts and tennis matches. You were a huge support system for me in my final year in Glasgow, I am eternally grateful of our friendship. Simon AKA ‘The Guvna’, you are the most considerate and generous guy I’ve ever met, I thank you for taking time developing automated analysis tools using Python for all my imaging analysis, even though I didn’t

get to use them in the end. Never change! Talha, rumour has it you are still optimising your hydrogels… I joke, it has been a pleasure to work alongside you and all the times we hung out in the lab. To all three of you, our Munro expeditions were the perfect escape from a busy PhD life, and I hope we will continue going on hikes in the future.

Special mentions for other staff and students in SCMH: Josie and Nic, you both were great support systems for me across both my technical post and PhD. Erin, Antoniya, Eleni, Sonya, Julian, Tuuli, Aisling, Lisa, Sheon, Zaniah, Ryszard – you all set high standards through your work and presence in the lab, which set a threshold for me to aim for throughout my PhD, thank you all for your dedication and your camaraderie in the lab. John, thank you for all of your help and patience with me in myography, I enjoyed working with you and having all our chats. Christian, Stuart, Martin, John Mercer, John McClure, Wai, Delyth, Lorraine, and Scott, thank you all for the opportunity to work with you as a research technician, I learned so much from you all. Wendy, Andy, Elaine, Michael, Linda, and Steven, each of you were incredibly welcoming in my first moments in the GCRC which helped it feel like home to me for the following 5-6 years. Stuart, Seonagh, Marianne, Joanne, thank you for all of your help and support in the CVRU and with all surgical/animal related matters.

My friends and members of the 'Friday Club': Kieran, Cameron, Scott, Fraser, Kieran (Kiwi), Callum. Thanks for all the laughs, the memories, the fun, the 'drops' in lockdown, and 'the derts'. I am grateful for all of you.

Last but not least, I would like to thank my family. Mum, thank you for your unwavering support and encouragement, as well as your interest in my research and all of your inquisitive questions. You are wonderful! Kiran, thank you for all of your words of encouragement and support. You have always been my role model and I am lucky to have such an inspiring sister. Dad, I could not have completed writing my thesis without you. Thank you so much for your support, understanding, and generosity which provided me with the shelter and stability I needed to get this over the line. It feels inadequate to say that I am truly grateful for you.

Author's declaration

I hereby declare that the work presented in this thesis is my own, and that no material has been used or accepted for any other degree at the University of Glasgow or any other institution. To the best of my knowledge, this thesis contains no material which has previously been published or written by another person, except where the relevant sources have been referenced.

The central subject of this thesis is "Defining the roles of the ADMA-DDAH1 pathway in cerebral artery function and ischaemic stroke pathogenesis". The concepts, ideas, development, and writing of all chapters in this thesis were the principal responsibility of myself under the supervision of Dr Alyson A. Miller and Professor James Leiper.

Signature: Date: 08/04/2024

Arun Flynn

Abbreviations and definitions

Abbreviation	Description
4124W	Weak competitive DDAH inhibitor
ACh	Acetylcholine
Acta2	Alpha-smooth muscle actin
ADMA	Asymmetric dimethylarginine
ADP	Adenosine diphosphate
AGXT2	Alanine-glycoxylate aminotransferase
Akt	Protein kinase B
ANOVA	Analysis of variance
ApoE$^{-/-}$	Apolipoprotein E knockout
ARRIVE	Animals in research: reporting *in vivo* experiments
AWERB	Animal welfare and ethics review board
BBB	Blood-brain barrier
BDNF	Brain-derived neurotrophic factor
bFGF	Basic fibroblast growth factor
BH_4	Tetrahydrobiopterin
BP	Blood pressure
BSA	Bovine serum albumin
CAD	Carotid artery disease
CARM1	Coactivator-associated arginine methyltransferase 1 (PRMT4)
CBF	Cerebral blood flow
CCA	Common carotid artery
cDNA	Complementary DNA
cGKI	cGMP-dependent kinase I
cGMP	Cyclic guanosine monophosphate
CIV	Corrected infarct volume
C_{max}	Maximal contraction
Contra	Contralateral hemisphere
COX	Cyclooxygenase
CSF	Cerebrospinal fluid
Ct	Cycle threshold
DAPI	4’,6-diamidino-2-phenylindole
DDAH	Dimethylarginine dimethylaminohydrolase
DDAH1$^{fl/fl}$	DDAH1 floxed control
DDAH1$^{En-/-}$	DDAH1 endothelial-specific knockout
DEGs	Differentially expressed genes
Dll-4	Delta-like ligand 4
DMA	Dimethylamine
DNA	Deoxyribonucleic acid
EDHF	Endothelium-derived hyperpolarising factor

eNOS	Endothelial nitric oxide synthase
ET-1	Endothelin-1
FAD	Flavin adenine dinucleotide
FBS	Foetal bovine serum
Flox	$DDAH1^{fl/fl}$
FMN	Flavin mononucleotide
GAPDH	Glyceraldehyde 3-phosphate dehydrogenase
GERF	Glasgow experimental request form
GTP	Guanosine triphosphate
HBSS	Hank's buffered salt solution
hCMEC/D3	Human cerebral microvascular endothelial cells
HDL	High-density lipoprotein
HIF	Hypoxia-inducible factor
HPLC-MS	High performance liquid chromatography-mass spectroscopy
ICA	Internal carotid artery
ICD	International classification of disease
iNOS	Inducible nitric oxide synthase
Ipsi	Ipsilateral hemisphere
JAG1	Jagged-1
KO	$DDAH1^{En-/-}$ (knockout)
KPSS	High potassium physiological salt solution
L-257	Selective DDAH1 inhibitor
L-Arg	L-arginine
LDL	Low-density lipoprotein
LHA	Left hemisphere area
L-NMMA	Monomethyl-L-arginine
$logEC_{50}$	Half-maximal effect concentration
MA plot	Microarray plot
MCA	Middle cerebral artery
mGlu	Metabotropic glutamate [receptor]
MMA	Monomethylamine
mNSS	Modified neurological severity score
MRA	Magnetic resonance angiography
MYH11	Smooth muscle myosin heavy chain
NADPH	Nicotinamide adenine dinucleotide phosphate
NIHSS	National Institutes of Health Stroke Scores
NGS	Next-generation sequencing
NMDA	N-methyl-aspartate [glutamate receptor]
NO	Nitric oxide
NOX	NADPH oxidase
nNOS	Neuronal nitric oxide synthase
NVU	Neurovascular unit

OCT	Optimal cutting temperature compound
OGD	Oxygen-glucose deprivation
ONOO	Peroxynitrite
OV	Oedema volume
PBS	Phosphate-buffered saline
PC1/2	Principle component 1 or 2
PCR	Polymerase chain reaction
PDGF	Platelet-derived growth factor
PE	Phenylephrine
PI3K	Phosphoinositide 3-kinase
PKG	cGMP-dependent protein kinases
POI	Protein of interest
PRMT	Protein arginine methyltransferase
PSS	Physiological salt solution
PVDF	Polyvinylidene fluoride
rCBF	Regional cerebral blood flow
RHA	Right hemisphere area
RIA	Right hemisphere infarct area
ROS	Reactive oxygen species
RNS	Reactive nitrogen species
R_{max}	Maximal relaxation
RNA	Ribonucleic acid
RNA-seq	RNA sequencing
RT-qPCR	Reverse transcription quantitative polymerase chain reaction
SAH	Subarachnoid haemorrhage
SD	Standard deviation
SDMA	Symmetric dimethylarginine
SEM	Standard error
sGC	Soluble guanylate cyclase
SNAP	*S*-nitroso-*N*-acetyl-D,L-penicillamine
SNP	Sodium Nitroprusside
SOD	Superoxide dismutase
STAIR	Stroke therapy academic industry roundtable
TBS	Tris-buffered saline
TOAST	Trial of org 10172 in acute stroke trial
tMCAo	Transient middle cerebral artery occlusion
TUNEL	Transferase mediated dUTP nick end labelling
U4	Thromboxane A2 agonist (U46619)
VEGF	Vascular endothelial growth factor
VEGFR	Vascular endothelial growth factor receptor

Chapter 1 General introduction

1.1 Ischaemic stroke

1.1.1 The burden of ischaemic stroke and statistics

Stroke is the second leading cause of death and the third-largest cause of disability worldwide (Feigin *et al.*, 2022). There are two main types of stroke: ischaemic, and haemorrhagic (intracerebral and subarachnoid), which differ in disease pathology as well as treatment options. Notably, however, ischaemic stroke accounts for approximately 87% of all strokes (Virani *et al.*, 2020), and occurs when blood flow to a region of the brain is transiently or permanently disrupted by a blockage (thrombus or embolus) (Dirnagl, Iadecola and Moskowitz, 1999). Between 1990 and 2019, the estimated global cost of all stroke types was ~$721 billion, and approximately 62% of incident (first-time) strokes are ischaemic strokes, of which 60% occur in people over 70 years of age, and more than half of ischaemic stroke cases are in women compared to men (Feigin *et al.*, 2022). Due to the improved patient survival of stroke patients in recent years, the prevalence of ischaemic stroke has increased (Feigin *et al.*, 2022). However, the effects of post-stroke complications such as neurological impairments and disability also significantly impact the social and economic burdens of stroke. For example, the number of patients who survive ischaemic stroke and require rehabilitation is increasing, and the cost of early rehabilitation after stroke was recently shown to positively correlate with the degree of motor but not neurological disability (Angerova *et al.*, 2020). A recent systematic review also estimated that the global average healthcare cost per stroke patient, including rehabilitation costs, ranges from £5,000-120,000 (Lucas-Noll *et al.*, 2023). Thus, ischaemic stroke is becoming an increasing problem for healthcare systems worldwide, and it can have catastrophic consequences on the quality of life of patients and their families. Identifying new treatments for stroke which will improve patient outcomes, minimise disability and the resulting economic pressures is of great importance.

1.1.2 Risk factors and co-morbidities associated with stroke

There are numerous risk factors and co-morbidities linked with ischaemic stroke. Common risk factors for stroke are classified into potentially modifiable and non-modifiable risk factors. Modifiable risk factors for ischaemic stroke include hypertension, obesity, diabetes, and smoking (Allen and Bayraktutan, 2008; Boehme, Esenwa and Elkind, 2017). For example, hypertension is widely known as the single most modifiable risk factor for stroke, and each increase of 20 mmHg of systolic blood pressure in adults aged 40-69 was shown to cause a two-fold increase of mortality after stroke (Lewington *et al.*, 2002). In contrast, each 10 mmHg reduction in systolic blood pressure is associated with a reduced risk of stroke by one-third (Ettehad *et al.*, 2016). Non-modifiable risk factors include age, sex, and genetics. For example, there are well established sex differences in stroke risk and incidence. A recent study demonstrated a higher incidence of stroke in men than women, however, there are several risk factors for stroke that are more strongly

associated with women than men (Peters *et al.*, 2020). Furthermore, it is now widely accepted that post-menopausal women are at double the risk of ischaemic stroke compared to pre-menopausal women (Lisabeth and Bushnell, 2012). An individual's risk of stroke is further increased with the presence of existing cardiovascular conditions, referred to as co-morbidities. For example, atherosclerosis in the carotid arteries (carotid artery disease) is a major risk factor for ischaemic stroke by promoting the formation of thromboses (Bir and Kelley, 2022). Other co-morbidities associated with increased ischaemic stroke risk include atrial fibrillation, hypertension, coronary artery disease, and hyperlipidaemia (Kuriakose and Xiao, 2020). Therefore, the disease manifestation of ischaemic stroke is multifaceted, which explains the heterogenicity between stroke patients.

1.1.3 Ischaemic stroke pathogenesis

As mentioned, ischaemic stroke is caused by the occlusion of blood flow to a region of the brain either by an embolus or thrombus, and its association with risk factors and co-morbidities demonstrates the heterogenous aetiology of the disease. However, both clinical and pre-clinical research have revealed even greater complexity of stroke pathophysiology, comprising of both primary and secondary brain injury (Chen *et al.*, 2017). Firstly, cerebral blood flow (CBF), which is tightly controlled for maintaining constant cerebral perfusion pressure, is markedly reduced which leads to energy failure, excitotoxicity, and necrotic cell death in the downstream vascular territory (primary brain injury). Energy failure refers to the loss of energy (ATP) production which causes anoxic depolarisation of neurons and the release of excitatory amino acids such as glutamate. Also, cells in the affected area swell due to the passive flow of water in response to aberrant ion gradients (ionic oedema). Excitotoxicity resulting from excessive membrane depolarisations in response to increased extracellular glutamate subsequently occurs in the ischaemic core, thereby triggering necrosis and apoptosis (Dirnagl, Iadecola and Moskowitz, 1999). Secondly, a diverse range of pathophysiological events subsequently occur which exacerbate ischaemic injury (secondary brain injury) over the course of several days (Figure 1-1). The major processes involved in secondary brain injury are neuroinflammation, oxidative stress, blood-brain barrier (BBB) disruption, and apoptosis (Dirnagl, Iadecola and Moskowitz, 1999; Chen *et al.*, 2017). Cells in the ischaemic core also begin producing reactive oxygen species (ROS) and reactive nitrogen species (RNS) such as superoxide anion and peroxynitrite (ONOO), respectively, which can cause cell damage and inflammation (Dirnagl, Iadecola and Moskowitz, 1999). Furthermore, the loss of BBB integrity promotes the recruitment of circulating activated immune cells. Thus, a combination of circulatory and brain-resident immune cells become activated and contribute to neuroinflammation and oxidative stress in the brain which extends into the ischaemic penumbra. Interestingly, del Zoppo and colleagues previously

reported that the influx of circulating leukocytes after stroke contributes to ischaemic brain injury by occluding capillaries in the microvascular bed, clearly demonstrating the diversity and complexity of secondary injury events (del Zoppo *et al.*, 1991). Increased BBB permeability, which is considered to be biphasic, occurring in both the acute and chronic phases following stroke (Yang and Rosenberg, 2011), also contributes to oedema through the extravasation of water from the blood (vasogenic oedema) (Keaney and Campbell, 2015), which can ultimately lead to increased intracranial pressure and brain herniation which is a major predictor of patient survival (McKeown *et al.*, 2022). Furthermore, stroke exerts several other effects on the cerebral vasculature which in turn can exacerbate brain injury. The principal outcome of these secondary pathological events is increased cell death (apoptosis or necrosis), enlarged ischaemic brain injury, and worse patient outcomes (Dirnagl, Iadecola and Moskowitz, 1999). Many neuroprotective strategies have been investigated with the aim of mitigating the impact of these pathophysiological events following stroke (Connolly *et al.*, 1996; Turski *et al.*, 1998; Weisbrot-Lefkowitz *et al.*, 1998; Zeynalov, Jones and Elliott, 2017); however, clinical trials have failed to reproduce the findings of pre-clinical studies (Kuriakose and Xiao, 2020). Thus, the disparity of outcomes between pre-clinical and clinical neuroprotective studies highlights the difficulty of developing new therapies for ischaemic stroke.

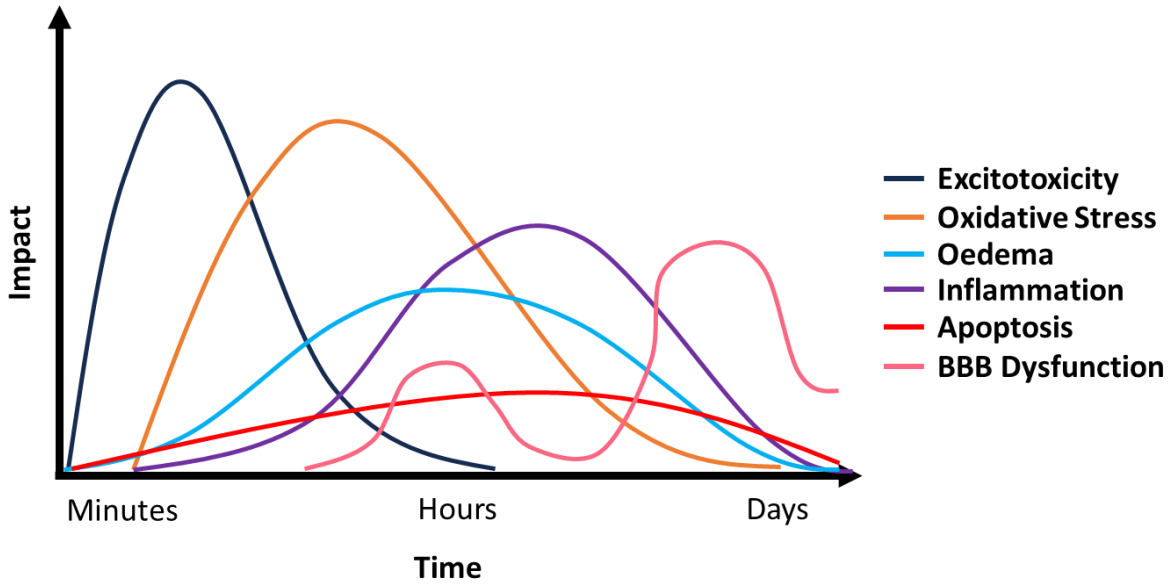

Figure 1-1. Pathophysiological events following ischaemic stroke onset.

1.1.4 Treatment options for ischaemic stroke

It is estimated that only approximately 10% of ischaemic stroke patients are eligible for therapeutic intervention due to a narrow therapeutic window of 4.5-6 hours (Zahuranec and Majersik, 2012; McMeekin *et al.*, 2017). Treatment for ischaemic stroke is limited to only two currently approved intervention methods – intravenous thrombolysis and

intraarterial mechanical thrombectomy (The NINDS and Stroke rt-PA Stroke Study Group, 1995; Berkhemer *et al.*, 2015). Thrombolysis using recombinant tissue plasminogen activator (rtPA) is normally given within 4.5 hours of stroke onset, however, thrombolytic treatment administered after this period correlates with increased risk of a haemorrhagic transformation and mortality (Lindley *et al.*, 2004; Whiteley *et al.*, 2012). In contrast, mechanical thrombectomy can be given within 6 hours of stroke onset, however, recent studies indicate that patients may benefit from a thrombectomy up to 24 hours after stroke onset depending on certain criteria (Albers *et al.*, 2018; Nogueira *et al.*, 2018; Rehani *et al.*, 2020). As mentioned previously, the identification and development of neuroprotective therapies for stroke have yielded promising results in pre-clinical studies, however, these findings have failed to translate into clinical trials of ischaemic stroke (Dirnagl, Iadecola and Moskowitz, 1999). Therefore, sufficient, and widely applicable treatment options for ischaemic stroke are lacking, thereby highlighting a need for new preventative and therapeutic treatment options.

1.2 Ischaemic stroke in research

1.2.1 Complexity of stroke research

A considerable amount of research is being devoted to the understanding of pathophysiological mechanisms underpinning ischaemic stroke as well as identification of new therapeutic strategies. However, appropriately modelling stroke is challenging given the heterogenous nature of stroke in humans. Most of the widely used experimental stroke models include limited pathophysiological features of the disease, and often lack the commonly associated risk factors and co-morbidities of stroke. Thus, there is a large translational gap in stroke research, and clinical studies have failed to reproduce the findings from pre-clinical studies (Kuriakose and Xiao, 2020), which led to the conceptualisation of the Stroke Therapy Academic Industry Roundtable (STAIR) (Stroke Therapy Academic Industry Roundtable (STAIR), 1999). The STAIR, which provides recommendations for improving the robustness and translatability of the findings from pre-clinical stroke research, has reconvened numerous times with the aim of reinforcing and improving the efforts of ischaemic stroke research (Fisher *et al.*, 2009; Albers *et al.*, 2011; Saver *et al.*, 2013; Jovin, Albers and Liebeskind, 2016; Savitz *et al.*, 2019), however, despite the efforts made following its conceptualisation, little success has arisen. Nevertheless, other guidelines have also been formed to aid the progression of pre-clinical and clinical stroke research. For example, the Trial of Org 10172 in Acute Stroke Trial (TOAST) developed a classification system for ischaemic stroke aetiological subtypes that is now widely used in clinical stroke trials (Adams *et al.*, 1993). Furthermore, inconsistencies in the reporting of translational research led to the development of the Animals in Research: Reporting *In Vivo* Experiments (ARRIVE) guidelines (Kilkenny *et al.*, 2010), and adherence to the ARRIVE guidelines has become increasingly standardised

across the stroke research community. Another limitation in stroke research was the misclassification of ischaemic stroke as merely a vascular disease under the International Classification of Disease (ICD) coding system by the World Health Organisation, which misled the efforts of researchers and healthcare systems (Shakir, 2018). However, in the recent ICD-11 update, ischaemic stroke was re-classified as a neurological disease which has created uniformity in the documentation, analysis, and funding acquisition of stroke research (Kuriakose and Xiao, 2020; Harrison *et al.*, 2021). Therefore, efforts are being made to address the roadblocks in ischaemic stroke research, so that the challenges may be overcome and ultimately lead to the development of novel treatments for stroke.

1.2.2 Experimental models of ischaemic stroke

There are numerous experimental models of ischaemic stroke, and each model offers a range of advantages and disadvantages for investigating the mechanisms of stroke pathophysiology. For example, the photothrombotic model involves the injection of a light-sensitive dye (e.g., Rose Bengal) followed by localised light exposure on the surface of the skull. This in turn, results in the formation of oxygen free radicals which damages the cerebrovascular endothelium, subsequently forming thrombi which occludes all vessels in the target brain region (Labat-gest and Tomasi, 2013). This approach is considered relatively non-invasive and is known for yielding consistent cortical lesions in rodents. However, although ischaemia is achieved by formation of thrombi to occlude blood flow, it fails to appropriately model stroke which typically occurs by the blockage of a singular cerebral artery or arteriole and its downstream vascular territory. Additionally, achieving sub-cortical lesions in this model requires stereotactic introduction of an optic fibre, thereby losing the advantage of being a minimally invasive technique (Labat-gest and Tomasi, 2013). Additionally, it often lacks the formation of a penumbra which is an important consideration of neuroprotective stroke research that aims to salvage the ischaemic penumbra (Sommer, 2017; Uzdensky, 2018). Alternatively, the embolic model simulates ischaemic stroke via the formation of thromboemboli which subsequently occludes a major cerebral artery (Durukan and Tatlisumak, 2007). In this model, artificial or biological clotting agents (micro-/macrospheres or thrombin, respectively) are injected into the common carotid artery (CCA) resulting in the generation of emboli which in turn travel along the internal carotid artery (ICA) and occlude blood flow to the middle cerebral artery (MCA) territory (DiNapoli *et al.*, 2006). A key advantage of this model is that it allowed researchers to examine the effects of thrombolytic agents combined with neuroprotective drugs in ischaemic stroke; however, it remains difficult to control for the site of vessel occlusion and the occurrence of spontaneous reperfusion which explains the large variability of infarct size and location (Liu *et al.*, 2009). Moreover, a major limitation of the thromboembolic models is the poor reproducibility of stroke outcomes due to the risk of multifocal ischaemia and variability

in size and location (Macrae, 2011). The endothelin-1 (ET-1) model is another such technique which utilises the vasoconstrictor peptide ET-1 either by topical application to a large cerebral artery or by intracerebral injection to a desired sub-cortical region of the brain, ultimately causing transient vasoconstriction and subsequent ischaemic lesions. This model is relatively simple and reliable; however, it is most effective when performed on rats (Windle *et al.*, 2006; Abeysinghe *et al.*, 2014). It was shown that mouse cerebral vessels are relatively unresponsive to ET-1 and in mice this model requires ligation of the CCA and inhibition of the nitric oxide synthases by L-NAME (Horie *et al.*, 2008). Another consideration stated by the STAIR guidelines is that a preclinical stroke study should be reproducible in multiple animal species which suggests the ET-1 model may not be ideal for translational stroke research (Stroke Therapy Academic Industry Roundtable (STAIR), 1999; Fisher *et al.*, 2009). Nevertheless, as discussed below, a fourth and commonly used model of ischaemic stroke is the MCA occlusion model (MCAo), which can reliably produce ischaemic lesions and simulate spontaneous reperfusion in a controlled manner.

1.2.3 The middle cerebral artery occlusion model of stroke

A significant feature of the MCAo model is that occlusion of the MCA is among the most common forms of ischaemic stroke in humans, accounting for over 50% of cases (Ng *et al.*, 2007), meaning it is a clinically relevant model. It typically involves the introduction of a silicon-coated monofilament to the origin of the MCA at the circle of Willis, thereby occluding blood flow to the territory of the brain supplied by the MCA. An advantage of this model is that MCAo periods can be easily modified by retracting the filament (transient MCAo; tMCAo) to induce reperfusion which simulates those patients who receive intervention or undergo spontaneous reperfusion; or keeping the filament in place to simulate those patients who do not. Importantly, however, the permanent MCAo (pMCAo) more closely resembles malignant stroke which produces maximal infarction in the territory of the MCA (Macrae, 2011). Considering that not all ischaemic stroke patients undergo spontaneous reperfusion or receive intervention, it could be argued that models simulating strokes in humans who don't receive treatment are more appropriate for investigating novel neuroprotective strategies, however, as mentioned in practice the pMCAo model more closely mimics malignant strokes. tMCAo on the other hand can mimic spontaneous reperfusion and/or the effects of successful thrombolysis by tPA in a highly controlled manner, and by adjusting the duration of MCAo, different severities of stroke can easily be achieved. For example, a study showed that relatively short tMCAo periods (e.g., 30-minutes) produced small infarcts that were predominantly located in the striata/sub-cortical brain regions, whereas longer tMCAo periods (e.g., 60-minutes) produced larger lesions that also extended into the cortex (Engel *et al.*, 2011). In addition to the chosen occlusion period, stroke severity in rodents after MCAo can be influenced by other factors. For instance, it is well documented that infarct size following tMCAo is

influenced by genetic background (Barone *et al.*, 1993; Hara *et al.*, 1996; Fujii *et al.*, 1997; Keum and Marchuk, 2009; Cheng *et al.*, 2012). Correspondingly, it was shown that C57BL6/J mice produced consistently larger infarcts compared to SV-129 mice (Fujii *et al.*, 1997). Nevertheless, although the MCAo model lacks the presence of a thrombus as observed in human thrombotic strokes, the MCAo model offers greater reproducibility of ischaemic lesions in the territory of the MCA and is more easily modified to achieve different stroke severities. As such, the MCAo model has become one of the most widely used experimental models of ischaemic stroke.

1.2.4 Assessment of neurological and functional outcomes

The neurological and functional disabilities caused by ischaemic stroke in humans can also be measured in rodents. The assessment of neurological and functional impairments in pre-clinical models of stroke is therefore an important endpoint measure and the use of functional tests can improve the translatability of such studies. As such, the goal of any therapeutic agent is to prevent or minimise the neurological and functional impairments following stroke (DeVries *et al.*, 2001). Consequently, behavioural tests and composite scores are commonly used in rodent models of stroke. Healthy mice typically present behaviours in a manner of functional symmetry, where unilateral ischaemia presents asymmetrically from contralateral impairment (Phipps, 1991; Li *et al.*, 2004; Schallert, 2006; Schaar, Brenneman and Savitz, 2010). There are numerous commonly used tests to assess neurological and functional impairments following tMCAo, which include the foot fault, cylinder, adhesive removal, balance beam, forelimb flexion, and body swing (tail suspension) tests. Such tests aim to detect changes in functional symmetry in mice following stroke, where asymmetrical forelimb use is symptomatic of the unilateral brain injury caused by stroke. However, while there are no perfect tests, it is important to select those which adequately measure deficits in the region of the brain where the ischaemic lesion forms. In addition to the aforementioned tests, composite neurological scores can be used to assess neurological deficits in rodents after stroke, which include the 3-, 4-, and 5-point Bederson scores, and the modified neurological severity score (mNSS) (Schaar, Brenneman and Savitz, 2010). Accordingly, the validity of these composite scores were evaluated to establish whether scores correlated with infarct size. Indeed, it was shown that neurological deficits measured by the 5-point Bederson and mNSS scores strongly correlated with infarct size (Bieber *et al.*, 2019). An emerging behavioural test in stroke research is the nest building activity test. Nest building is performed to provide shelter, heat conservation, and protection from predators, and research suggests that this activity can be used as a measure of motivation, pain (Rock *et al.*, 2014), general welfare (Gaskill *et al.*, 2013), and depressive-like behaviour in mice (Haley *et al.*, 2020). Interestingly, Rock and colleagues reported that mice begin interacting with nesting material within 10-minutes, indicating that nest building

behaviours are a useful qualitative and quantitative outcome measure in pre-clinical research (Rock *et al.*, 2014). However, it was previously reported that the quality, shape, and size of nests are dependent on the genetic background of mice, highlighting the complex nature of nest building assessments and the variety of nest building materials available further increase the complexity of the test (Lee, 1972). Importantly, recent work has highlighted that assessing nest building activity can be used to assess neurological deficits in mice following tMCAo. For example, Yuan and colleagues reported significantly impaired nest building activity in mice after 40- and 60-minutes of tMCAo compared to mice following 20-minute tMCAo and sham controls (Yuan *et al.*, 2018). Additionally, impaired nest building activity was detected as long as 3 weeks following the induction of ischaemia. Ultimately, neurological tests and composite scores should be carefully considered for measuring the extent of ischaemic brain injury in pre-clinical stroke studies.

1.3 The cerebral circulation

1.3.1 The cerebral circulation

The brain consumes approximately 20% of the body's oxygen and glucose supply, however, it also lacks sufficient energy reserves. Thus, the brain requires a constant supply of blood to ensure its metabolic demands are met. Consequentially, the cerebral circulation is equipped with numerous specialised and tightly regulated physiological mechanisms which ensures the brain always receives an adequate blood supply over a wide range of external and internal conditions. The cerebral circulation is supplied by four extracranial cerebral arteries (carotid and vertebral) which meet at the circle of Willis which distributes the cerebral blood supply via the anterior, middle, and posterior cerebral arteries (Hossmann, 2006). Unlike large arteries in the systemic circulation, the carotid arteries and large cerebral arteries originating from the circle of Willis are major contributors to cerebral vascular resistance, blood flow, and microvascular perfusion pressure. Indeed, it was previously established that the arterial pressure in large cerebral and pial arteries is approximately 50% of aortic pressure in the systemic circulation (Faraci and Heistad, 1990). One mechanism responsible for maintaining CBF is cerebral autoregulation, which is an active vascular mechanism which acts to maintain adequate brain perfusion during changes in mean arterial blood pressure of the systemic circulation (van Beek *et al.*, 2008). For example, in the range of 60-150 mmHg mean arterial blood pressure, pial arterial and parenchymal arteriolar tone changes in response to blood pressure variations and is demonstrated by vessels dilating during a drop in blood pressure or constricting to withstand an increase in blood pressure (Jackman and Iadecola, 2015). Functional hyperaemia, or neurovascular coupling, is defined as the coupling of neuronal activity and vascular perfusion (Iadecola and Nedergaard, 2007). For instance, upon increased metabolic demand in a specific brain region, blood supply subsequently

increases in a time- and location-dependent manner. Neurovascular coupling relies on the close association of several cell types referred to as the neurovascular unit (NVU) which includes neurons, endothelial cells, astrocytes, microglia, pericytes, smooth muscle cells, and perivascular macrophages (Iadecola, 2017). Following neuronal activation, it has been proposed that the subsequent release of glutamate triggers increased intracellular calcium of neighbouring astrocytes via the activation of glutamate (NMDA) or metabotropic glutamate (mGlu) receptors. This in turn, triggers the release of vasoactive factors such as nitric oxide (NO) from the neuronal NO synthase (nNOS) or the cyclooxygenase (COX) 2 product prostacyclin, which diffuse to nearby arterioles and results in relaxation of the vascular smooth muscle, thereby increasing regional CBF (Zonta *et al.*, 2003). Importantly, cardiovascular risk factors (e.g., age and hypertension) can cause cerebrovascular and neurovascular dysfunction which in turn disrupts crucial cerebral autoregulation and neurovascular coupling, and a loss of these processes ultimately increases the risk of brain injury (Jackman and Iadecola, 2015). For example, vascular hypertrophy and/or remodelling of cerebral vessels following hypertension requires greater pressures to achieve autoregulation (Tryambake *et al.*, 2013), whereas the vasodilation of these vessels can become impaired which is likely to increase the susceptibility of the brain to inadequate perfusion during a drop in blood pressure (Delles *et al.*, 2004).

In addition to the aforementioned pathophysiological events following stroke, ischaemic brain injury is also exacerbated by dysregulation of the cerebral circulation. For example, the regulation of vascular tone, cerebral blood flow and perfusion pressure are disrupted following stroke, which may, in part, be characterised by the loss of crucial endothelium-derived NO. Accordingly, a pre-clinical stroke study demonstrated that the impaired maintenance of vascular tone in large cerebral arteries occurs via the scavenging of endothelium-derived NO by superoxide anions (De Silva *et al.*, 2011), whereas another study reported a similar loss in tone of parenchymal arterioles after stroke (Cipolla and Bullinger, 2008; Cipolla et al., 2009). Furthermore, cerebral autoregulation is impaired in humans and in animal models of stroke, whereas functional hyperaemia (and associated neurovascular coupling) is impaired in animal models of stroke, but clinical studies have yielded variable results (Jackman and Iadecola, 2015). Ultimately, loss of these crucial regulatory processes can lead to exacerbated injury and cell death. As previously mentioned, another major consequence of ischaemic damage of the cerebral circulation is loss of BBB integrity. Indeed, the cerebral endothelium which differs from that of the systemic circulation, constitutes the major structural component of the BBB by possessing unique cell-cell junctions (tight junctions) (Faraci, 2011) and lacking fenestrations which limits paracellular permeability of molecules and cells between the CNS and the blood (Hu *et al.*, 2017). Cells of the NVU (pericytes, microglia, and macrophages) also become

activated during stroke which can further disrupt BBB integrity (Hu *et al.*, 2017). Thus, structural, and functional changes to the cerebral endothelium can have a profound influence on ischaemic brain injury. Therefore, identifying the mechanisms that underpin the vascular dysfunction following stroke may yield novel therapeutic targets, and there is an unmet need for studies which evaluate the importance of the cerebral vasculature in ischaemic stroke.

1.3.2 The central role of the cerebral endothelium

The cerebral endothelium is an important regulator of cerebral artery function and thus the maintenance of CBF. The major mechanism through which the endothelium influences cerebral vascular function is through the generation and release of diffusible vasoactive factors which regulate vasodilatation (e.g., NO, prostacyclin, and endothelium-derived hyperpolarising factor [EDHF]), or vasoconstriction (e.g., endothelins and thromboxane A2) (Faraci and Heistad, 1998). Central to the roles of the endothelium is the production and release of the gaseous signalling molecule NO. It is produced by the NO synthase (NOS) enzymes, of which there are three isoforms: nNOS, inducible NOS (iNOS), and endothelial NOS (eNOS). nNOS and eNOS are predominantly expressed in neurons and endothelial cells, respectively, they are constitutively expressed, and their activities are largely calcium-dependent. In contrast, iNOS is not normally expressed but its expression can be increased in numerous cell types (e.g., immune and endothelial cells) in response to cytokine signalling which becomes constantly active independent of calcium (Forstermann and Sessa, 2012). All three NOS enzymes utilise the substrate L-arginine, the co-substrates molecular oxygen and NADPH, and the cofactors flavin adenine dinucleotide (FAD), flavin mononucleotide (FMN), and tetrahydrobiopterin (BH_4). The products NO and L-citrulline are produced following a two-step process involving a series of electron transfer steps and redox reactions (Forstermann and Sessa, 2012). Specifically, the conversion of NADPH to NADP and a hydrogen ion releases an electron that transfers across FAD and FMN to the haem domain of NOS, which subsequently reduces molecular oxygen leading to the oxidisation of L-arginine (Stuehr, Pou and Rosen, 2001). In the endothelium, the constitutive expression of eNOS is required for producing basal levels of NO, however, its activity can be increased by numerous stimuli via calcium-dependent and -independent mechanisms. One mechanism is by receptor-mediated increases in intracellular calcium followed by binding to calmodulin in response to stimuli such as acetylcholine, bradykinin, and histamine (Faraci, 2011). In addition, eNOS expression can be increased in response to stimuli such as oestrogen (McNeill *et al.*, 2002) and insulin (Fisslthaler *et al.*, 2003). Alternatively, the activity of eNOS can be increased by Ser1177 phosphorylation via the phosphatidylinositol 3-kinase (PI3K)-protein kinase B (Akt) pathway in response to stimuli such as shear stress (Boo *et al.*, 2002) and vascular endothelial growth factor (VEGF) (Papapetropoulos *et al.*, 1997), whereas phosphorylation of Thr495 is regarded as a

negative regulator of eNOS activity (Forstermann and Sessa, 2012). NO production by eNOS in the cerebral endothelium rapidly diffuses into the vascular smooth muscle where it exerts chronic vasodilator signalling. Therefore, eNOS-derived NO (eNOS-NO) plays a critical role in regulating basal resting tone and thus cerebral perfusion, where eNOS-NO mediates vasodilator responses to receptor and non-receptor mediator stimuli as described above. Soluble guanylate cyclase (sGC) in the smooth muscle is a primary target of eNOS-NO, which becomes activated and, in turn, increases the conversion of GTP to cyclic guanosine monophosphate (cGMP). The primary downstream effector of cGMP are the cGMP-dependent protein kinases (cGKI), which when activated by cGMP results in a decrease in intracellular calcium and thus relaxation of the smooth muscle (Figure 1-2) (Faraci, 2011). In addition to influencing vascular tone in the brain, eNOS-NO has several other functions that are crucial for maintaining cerebrovasculature homeostasis. For example, it is well established that eNOS-NO inhibits vascular smooth muscle cell proliferation (Zuckerbraun *et al.*, 2007; Tsihlis *et al.*, 2011), platelet aggregation (Riddell and Owen, 1997) and leukocyte adhesion and migration (Kubes, Suzuki and Granger, 1991), as well as anti-inflammatory actions (De Caterina *et al.*, 1995), and mediates angiogenesis (Fiedler *et al.*, 2009). Thus, eNOS-NO signalling in cerebral vessels is vital, and the development of endothelial dysfunction via the loss of NO synthesis in the brain can have devastating consequences for brain health.

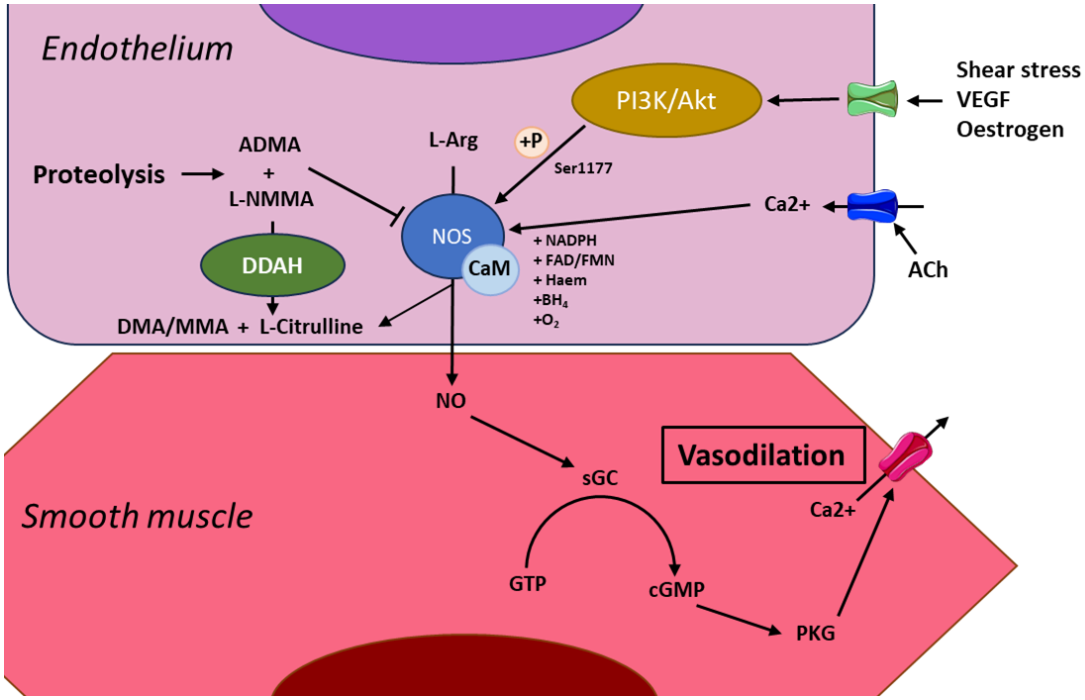

Figure 1-2. Endothelial nitric oxide synthesis pathway and influence of nitric oxide on cerebral artery tone. NOS, nitric oxide synthase; CaM, calmodulin; L-Arg, L-arginine; ADMA, asymmetric dimethylarginine; L-NMMA, N-monomethyl-L-arginine; DDAH, dimethylarginine dimethylaminohydrolase; DMA, dimethylamine; MMA, monomethylamine; NO, nitric oxide; PI3K, phosphatidylinositol 3 kinase; Akt, protein kinase B; VEGF, vascular endothelial growth factor; Ser1177, serine 1177 residue; ACh, acetylcholine, NADPH, reduced nicotinamide adenosine diphosphate; FAD, flavin adenosine diphosphate; FMN, flavin monophosphate; BH4, tetrahydrobiopterin; sGC, soluble guanylate cyclase; GTP, guanosine triphosphate; cGMP, cyclic guanosine monophosphate; PKG, cGMP-dependent protein kinases.

1.3.3 Endothelial dysfunction in the cerebral circulation

Endothelial dysfunction is a hallmark of all major cardiovascular risk factors (e.g., atherosclerosis (Dowsett *et al.*, 2020), diabetes (Hink *et al.*, 2003)). A key characteristic of endothelial dysfunction is the loss or reduction in endothelium-derived NO signalling; however, it encompasses several other pathological features such as pro-inflammatory and pro-fibrotic phenotypes (Theofilis *et al.*, 2021). The major consequences of endothelial dysfunction in the brain are vast, and include increased vascular tone and hypertrophy, loss of BBB integrity, and neuroinflammation which ultimately leads to impaired CBF and increased stroke risk (Faraci, 2011). There are several mechanisms which can cause endothelial dysfunction and exacerbate the risk of disease in cerebral vessels. An example of this is oxidative stress, which is defined as an imbalance between the generation of reactive oxygen species (ROS) and the antioxidants that scavenge them. The parent ROS molecule superoxide anion can react avidly with NO, resulting in its inactivation and therefore a reduced bioavailability of NO. Also, this reaction leads to the formation of the highly reactive RNS peroxynitrite, which can cause DNA damage and the S-nitrosylation of proteins (nitrosative stress) resulting in cell death (Forstermann and Sessa, 2012). Enzymatic sources of superoxide in cerebral vessels include the NADPH

oxidase (NOX) and COX enzymes (Didion, Hathaway and Faraci, 2001; Miller *et al.*, 2010; Montezano *et al.*, 2011). Interestingly, expression of the NOX enzymes was shown to be greater in cerebral arteries compared to arteries in the systemic circulation (Miller *et al.*, 2005), suggesting that cerebral arteries generate greater physiological amounts of ROS and thus may be more susceptible to developing endothelial dysfunction. Additionally, if eNOS uncoupling occurs (which is another mechanism of endothelial dysfunction), eNOS itself can generate superoxide rather than NO, thereby contributing to oxidative stress. For example, activation of the NOX enzymes was previously reported to increase superoxide and peroxynitrite levels in cultured primary endothelial cells via the uncoupling of eNOS (Zhang *et al.*, 2011), which involves an incomplete transfer of electrons leading to the production superoxide anions from molecular oxygen. Another mechanism of eNOS uncoupling is by the endogenous NOS inhibitors such as the methylarginines (e.g., asymmetric dimethylarginine [ADMA]) (Forstermann and Sessa, 2012). Indeed, it was previously reported that high serum ADMA levels were associated with decreased vascular function and higher superoxide production in human peripheral arteries (Antoniades *et al.*, 2009). The effects of the methylarginines in cardiovascular and cerebrovascular disease are discussed below in section 1.4. Nevertheless, the superoxide dismutase (SOD) enzymes are responsible for scavenging superoxide anions to form molecular oxygen or hydrogen peroxide (Wang *et al.*, 2018). The functional importance of SODs in maintaining cerebrovascular homeostasis is well documented, with studies showing that the activity of SODs in mice protect against carotid endothelial dysfunction (Ohashi *et al.*, 2006) and cerebral vascular dysfunction (Faraci *et al.*, 2006). Taken together, it is clear that a loss of homeostatic eNOS-NO signalling in cerebral vessels can have profound consequences on cerebral endothelial and vascular function and in turn, may contribute to cerebrovascular diseases such as ischaemic stroke. Thus, it is important to improve our understanding of the mechanisms that underpin endothelial dysfunction and how these impact the pathogenesis of cerebrovascular disease.

1.3.4 The roles of nitric oxide in ischaemic stroke

As mentioned above, there are three enzymes responsible for NO synthesis: nNOS, iNOS, and eNOS. It is now well established that each of the NOS enzymes is involved in ischaemic stroke pathogenesis, and that NO has protective or deleterious roles depending on the cellular or enzymatic source, the amount of NO produced, and the stage of evolution of the ischaemic cascade (Figure 1-3). Specifically, the activity of nNOS and iNOS play a role in neurotoxicity and exacerbate ischaemic injury, whereas eNOS plays a neuroprotective role (Chen *et al.*, 2017). In the hyperacute phase after stroke, excitotoxicity leads to excess NO production by nNOS in neurons which reacts with superoxide to form large quantities of peroxynitrite which subsequently leads to nitrosative stress and rapid cell death. Previous studies have demonstrated that mice deficient in nNOS, or mice treated

with nNOS inhibitors, develop smaller infarcts following experimental stroke (Huang *et al.*, 1994; Nagafuji *et al.*, 1995; Zhang *et al.*, 1996; Zhou *et al.*, 2010). With respect to iNOS, experimental stroke studies have shown that *de novo* expression increases 12-hours after stroke onset and is sustained for up to 1 week with expression levels peaking on day 4 (Iadecola *et al.*, 1997; Li *et al.*, 2022). The amount of NO generated by iNOS is substantially greater than nNOS which exacerbates nitrosative stress and promotes neuroinflammation and the production of ROS (Pannu and Singh, 2006; Chen et al., 2017). Mice deficient in iNOS or mice treated with iNOS inhibitors have small infarcts and improved functional outcomes following experimental stroke compared to controls (Iadecola *et al.*, 1997; Zhang and Iadecola, 1998; Li *et al.*, 2022). Unlike nNOS and iNOS, eNOS releases NO at much smaller quantities which is crucial for maintaining brain perfusion and for the recruitment and maintenance of collateral vessels in the early phases after ischaemic stroke (Huang *et al.*, 1994; Faraci, 2011; Maguida and Shuaib, 2023). eNOS-NO is also important for mediating angiogenesis and neurogenesis in the later phase after ischaemic stroke (Terpolilli, Moskowitz and Plesnila, 2012). Correspondingly, eNOS-deficient mice develop larger infarcts after experimental stroke (Huang *et al.*, 1996; Cui *et al.*, 2013), whereas treatment of rats with the flavonoid Nicotiflorin was shown to promote neuroprotection after experimental stroke by upregulating eNOS expression and activity (Li *et al.*, 2006). Thus, there is sufficient evidence indicating that NO is both deleterious and protective during stroke, and understanding the mechanisms which regulate each of the NOS enzymes during stroke pathogenesis is of great importance.

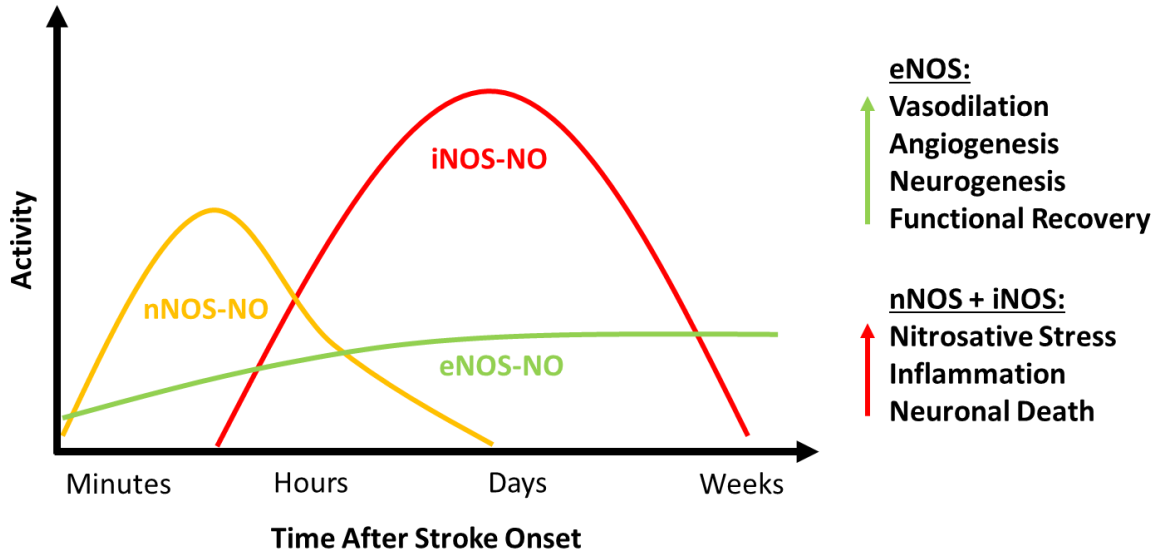

Figure 1-3. Dual roles of NO following ischaemic stroke.

1.4 The ADMA-DDAH1 pathway

1.4.1 Origins of the methylarginines

Methylarginines are methylated derivatives of the semi-essential amino acid L-arginine, and includes ADMA, N_G-monomethyl-L-arginine (L-NMMA), and symmetric

dimethylarginine (SDMA) (Fuhrmann, Clancy and Thompson, 2015). The methylation of arginine residues in proteins is controlled by the protein arginine methyltransferase enzymes (PRMTs), which catalyse the addition of one or more methyl groups on the guanidino nitrogen atoms of L-arginine side chains (Kakimoto and Akawaza, 1970). There are three subtypes of PRMTs: the type I PRMTs, yielding ADMA and L-NMMA and include PRMT1-4, 6, and 8; the type II PRMTs, yielding L-NMMA and SDMA and include PRMT5 and 9; whereas a single type III PRMT exists, PRMT7, which yields only L-NMMA (Fulton, Brown and Zheng, 2019). Protein methylation of arginine residues by the PRMTs is a common post-translational modification of histones for regulating epigenetic gene expression, however, the methylation of proteins by the PRMTs are also known to regulate mRNA splicing, DNA repair, protein localisation, and intracellular signalling (Fuhrmann, Clancy and Thompson, 2015). All type I PRMTs are expressed in the brain, however, unlike the other PRMT subtypes which are ubiquitously expressed in cells and tissues, PRMT8 is the only membrane-bound and cell-specific isoform, expressed exclusively in neurons. Although the roles of PRMT8 in neurons are unclear, it is believed to be important for neuronal development and function (Couto e Silva *et al.*, 2020). Importantly, PRMT1 is the most highly expressed isoform and accounts for approximately 85% of all PRMT activity in the body (Tang *et al.*, 2000). Interestingly, however, PRMT4 (also known as CARM1) expression was previously shown to be markedly increased following myocardial infarction in mice (Wang *et al.*, 2019). During proteolysis of methylated proteins, free methylarginines are released into the cytosol and circulation. Importantly, it is well documented that ADMA and L-NMMA are endogenous inhibitors of the NOS enzymes by competing with L-arginine for the NOS active site, thereby reducing NO synthesis (Figure 1-4) (Caplin and Leiper, 2012). In contrast, SDMA does not inhibit NOS, however, it was shown to indirectly inhibit NO synthesis by competing with L-arginine for the CAT-2B amino acid transporter (Closs *et al.*, 1997; Grosse *et al.*, 2020).

Plasma methylarginine levels in healthy humans are approximately 0.5 μM, 48 nM, and 0.53 μM for ADMA, L-NMMA, and SDMA, respectively (Martens-Lobenhoffer, Bode-Böger and Clement, 2016). Considering the biological importance of NO signalling and the higher quantities of ADMA over L-NMMA, ADMA is therefore the most extensively studied methylarginine. All mammals constitutively express the dimethylarginine dimethylaminohydrolase (DDAH) 1 and 2 enzymes which account for approximately 80% of ADMA and L-NMMA clearance, whereas the remaining 20% and also total SDMA are eliminated in urine by the kidneys (Teerlink, 2007). However, another minor pathway exists for the metabolism of ADMA and SDMA which is controlled by the alanine-glycoxylate aminotransferase (AGXT2) enzyme (Ogawa, Kimoto and Sasoaka, 1990). The DDAH enzymes have identical catalytic capabilities of methylarginine metabolism in the form of a ‘catalytic triad’ of Asp126, His172, and Cys273 residues in the enzyme active

sites, and the metabolism of ADMA and L-NMMA by the DDAH enzymes yields L-citrulline and dimethylamine or monomethylamine, respectively (Leiper *et al.*, 1999; Nandi *et al.*, 2012). Genetic knockout of either DDAH isoform has been shown to elevate methylarginine levels which subsequently disrupts systemic artery function by the inhibition of eNOS-NO signalling (Leiper *et al.*, 2007; Lambden *et al.*, 2015). However, there is conflicting evidence about the functions of DDAH2 as studies have argued that DDAH2 may not function as a metabolising enzyme of ADMA or L-NMMA (Altmann *et al.*, 2012; Ragavan *et al.*, 2023). The DDAH isoforms have distinct tissue distributions with DDAH1 predominantly expressed in the brain, liver, and kidneys whereas DDAH2 is predominantly expressed in the heart, placenta, and immune tissues. Notably, however, both isoforms were shown to be expressed in the systemic vasculature (Leiper and Nandi, 2011; Dowsett *et al.*, 2015; Lambden *et al.*, 2015). In the brain, it was recently shown that DDAH1 is expressed in numerous cell types, including endothelial cells, neurons, astrocytes and other glial cells, whereas DDAH2 expression was restricted to neurons in specific brain regions (Kozlova *et al.*, 2022). Notably, as will be discussed in section 1.4.3, in contrast to the systemic circulation the roles of the DDAH enzymes in the brain and cerebral circulation are largely unknown.

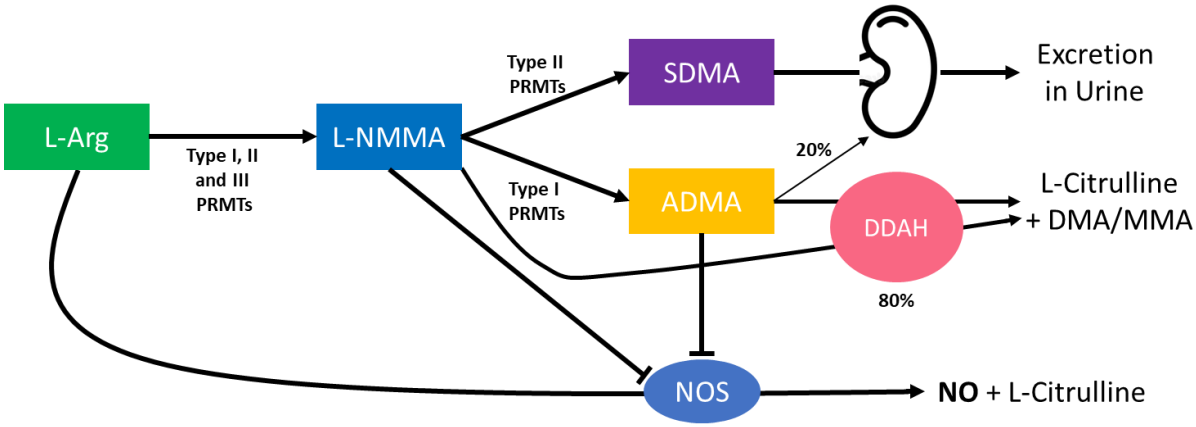

Figure 1-4. Methylation of protein arginine residues by the protein arginine methyltransferase enzymes and methylarginine clearance. L-Arg, L-arginine; PRMTs, protein arginine methyltransferases; L-NMMA, N-monomethyl-L-arginine; NOS, nitric oxide synthase; ADMA, asymmetric dimethylarginine; SDMA, symmetric dimethylarginine; DDAH, dimethylarginine dimethylaminohydrolase; NO, nitric oxide; DMA, dimethylamine; MMA, monomethylamine.

1.4.2 Significance of methylarginines in cardiovascular disease

As mentioned previously, endothelium-derived NO signalling is an important regulator of vascular function in the systemic and cerebral circulation (Furchgott and Zawadzki, 1980; Faraci, 2011). Furthermore, the methylarginines are known to disrupt eNOS-NO signalling either directly or indirectly. There is a large body of evidence linking elevated circulating ADMA levels and cardiovascular risk factors, and cardiovascular disease, which relate to the inhibitory actions of ADMA on eNOS-derived NO. For example, it is well documented that elevated ADMA levels are associated with endothelial dysfunction which is a

precursor to many cardiovascular diseases (Leone *et al.*, 1992). Indeed, studies have demonstrated that elevated ADMA levels are associated with hypertension (Surdacki *et al.*, 1999), atherosclerosis (Bӧger *et al.*, 1998), type 2 diabetes (Abbasi *et al.*, 2001), coronary artery disease (Krempl *et al.*, 2005), renal disease (Fleck *et al.*, 2003), and hypercholesterolaemia (Bӧger *et al.*, 1998). More importantly, however, studies have subsequently established that a causal relationship exists between elevated ADMA levels and cardiovascular disease, including hypertension and cardiac disease (Achan *et al.*, 2003), and atherosclerosis (Jacobi *et al.*, 2010). Similarly, L-NMMA (Liu *et al.*, 2018) and SDMA (Kiechl *et al.*, 2009; Staniszewska *et al.*, 2015; Schlesinger *et al.*, 2016; Zewinger *et al.*, 2017; Zobel *et al.*, 2017) are also associated with cardiovascular risk and disease, however, the exact pathobiological mechanisms of SDMA remain unclear. Notably, there are several mechanisms which might contribute to the increased circulating methylarginine levels during disease. One potential mechanism is through increased expression and/or activity of the type I PRMTs, thereby yielding increased free methylarginines after proteolysis. Another mechanism could be reduced methylarginine (ADMA and L-NMMA) metabolism by the DDAH enzymes, where DDAH inhibition or knockout have been used extensively in research for assessing the impact of elevated ADMA levels (Leiper and Nandi, 2011). As mentioned previously, oxidative stress is a common pathological process in endothelial dysfunction, which underpins numerous cardiovascular diseases such as atherosclerosis (Sena *et al.*, 2018; Higashi, 2022). Furthermore, it was previously shown that the expression and/or activity of type I PRMTs are increased while the activity of the DDAH enzymes are decreased by oxidative and nitrosative stress (Bӧger *et al.*, 2000; Leiper *et al.*, 2002; Sydow and Münzel, 2003). Therefore, it is conceivable that elevated levels of ADMA and L-NMMA during cardiovascular disease arises from an imbalance of methylarginine production and metabolism. Unlike ADMA, SDMA is almost entirely eliminated in the urine by the kidneys, and SDMA accumulates in the plasma of patients with renal disease (Schwedhelm and Böger, 2011), and thus the relevance of elevated SDMA in cardiovascular disease may be predominantly associated with renal insufficiency or disease (Marescau *et al.*, 1997). Therefore, this raises the question whether SDMA merely serves as a marker of renal dysfunction, or does it also exert pathobiological effects in the vasculature. Correspondingly, one study demonstrated that elevated SDMA accumulates in the high-density lipoprotein (HDL) of patients with chronic kidney disease, which was subsequently linked with endothelial dysfunction (Speer *et al.*, 2013). Additionally, elevated uremic HDL (SDMA-HDL) in patients was correlated with increased mortality (Zewinger *et al.*, 2017), suggesting that SDMA may indeed play a pathological role in disease whilst also serving as a marker of renal function. Taken together, elevated methylarginine levels are associated with a diverse range of cardiovascular diseases which highlights the

importance of understanding the mechanisms responsible for elevated methylarginine levels and their pathobiological roles in disease.

1.4.3 The ADMA-DDAH1 pathway, cerebrovascular function, and ischaemic stroke pathogenesis

Although there is a wealth of evidence implicating the pathobiological effects of elevated ADMA in the cardiovascular system, much less is known about its effects in the cerebral circulation. Additionally, it is well established that DDAH1 is an important regulator of eNOS-NO signalling in the systemic vasculature by controlling ADMA levels, indicating that DDAH1 activity is crucial for maintaining cardiovascular health. Indeed, numerous studies have shown that DDAH1 dysfunction arising from pharmacological inhibition or genetic knockout leads to an increase in circulating ADMA which contributes to endothelial dysfunction and the resultant cardiovascular disease. For example, loss of DDAH1 activity by inhibition or heterozygous DDAH1 knockout markedly impairs vascular NO signalling of peripheral blood vessels (Leiper *et al.*, 2007), and impairs pulmonary endothelial barrier function (Wojciak-Stothard *et al.*, 2009). Furthermore, selective DDAH1 knockout in mouse cardiomyocytes markedly exacerbates left ventricular hypertrophy and dysfunction following transverse aortic constriction (Xu *et al.*, 2017). Notably, the overexpression of DDAH1 in heterozygous DDAH1 knockout mice reverses vascular dysfunction (Torondel *et al.*, 2010) and impaired pulmonary endothelial barrier function (Wojciak-Stothard *et al.*, 2009). Genetic variants of DDAH1 (single nucleotide polymorphisms) have also been identified that are associated with cardiovascular diseases such as coronary heart disease (Ding *et al.*, 2010), chronic kidney disease (Caplin *et al.*, 2010), and type 2 diabetes (Abhary *et al.*, 2010). However, importantly, the functional importance of DDAH1 for maintaining eNOS-NO signalling in the cerebral circulation is largely unknown. It was previously shown, however, that the endothelium-dependent function of human MCA rings was markedly impaired following the application of exogenous ADMA or L-NMMA to the vessels (Segarra *et al.*, 1999), and that ADMA infusion decreases cerebral blood flow in healthy humans (Kielstein *et al.*, 2006). Furthermore, overexpression of DDAH1 was shown to ameliorate the harmful effects of ADMA on cerebral artery eNOS-NO function (Dayoub *et al.*, 2008). Nevertheless, direct evidence showing the functional importance of DDAH1 in the cerebral circulation is lacking.

With respect to ischaemic stroke pathogenesis, the importance of the ADMA-DDAH1 pathway is unknown, and causal evidence linking elevated ADMA and worse stroke outcomes is lacking. Indeed, several studies have established ADMA as a potential biomarker for ischaemic stroke in humans (Yoo and Lee, 2001; Wanby *et al.*, 2006; Nishiyama *et al.*, 2010). Furthermore, other studies have demonstrated that ADMA levels are significantly increased in the cerebrospinal fluid (CSF) and plasma of ischaemic stroke patients (Brouns *et al.*, 2009; Worthmann *et al.*, 2011), the latter of which also correlated

with adverse clinical outcomes following stroke (Worthmann *et al.*, 2011). In contrast, previous studies have reported that DDAH1 polymorphisms are associated with increased risk of thrombotic stroke (Ding *et al.*, 2010), and delayed cerebral ischaemia after subarachnoid haemorrhage (Hannemann *et al.*, 2020). Although it is now established that ADMA levels increase after ischaemic stroke, few studies have sought to address the functional importance of DDAH1 in ischaemic stroke pathogenesis. Also, the same studies did not test whether there are causal roles of the ADMA-DDAH1 pathway in ischaemic stroke pathogenesis. One study did however investigate the effect of global DDAH1 overexpression in mice on ischaemic brain injury but showed no differences in infarct size. However, they also showed that neither DDAH1 expression and activity were elevated in the brain, nor was there a change in ADMA levels (Leypoldt *et al.*, 2009). More recently, studies by Zhao and colleagues reported that global DDAH1 knockout in rats increases infarct size, however, the mean arterial blood pressures of these DDAH1 knockout rats was elevated at baseline and post-stroke which likely influenced stroke outcomes independently of DDAH1 activity (Zhao *et al.*, 2021, 2022). Therefore, there is an unmet need for establishing causal roles of the ADMA-DDAH1 pathway in ischaemic stroke pathogenesis.

1.5 Cerebral angiogenesis

1.5.1 Mechanisms of angiogenesis

Angiogenesis refers to the generation of new blood vessels from pre-existing ones. There are two main types of angiogenesis; sprouting and intussusceptive, which differ in the way new vessels are formed. Sprouting angiogenesis is the most widely described and understood type, whereas the mechanisms of intussusceptive angiogenesis are poorly understood. The normal function of cells and tissues requires an adequate supply of oxygen and glucose from the blood. Notably, however, when the supply to a region of tissue becomes inadequate, cells become hypoxic and upregulate hypoxia-inducible factors (HIF) such as HIF1-α. Activation of HIF-1α activity subsequently upregulates a range of pro-angiogenic factors, namely the vascular endothelial growth factors (VEGFs), the angiopoietins, and basic fibroblast growth factor (bFGF), which are key regulators of angiogenesis (Krock, Skuli and Simon, 2011). Notably, VEGF-A is widely accepted as the master regulator of angiogenesis, and it controls the migration, proliferation, and survival of endothelial cells (Gerhardt *et al.*, 2003). Hypoxic cells release factors such as VEGF-A which serve as a chemoattractant for target endothelial cells in nearby vessels, which subsequently initiate the sprouting angiogenic process (Figure 1-5). There are multiple steps associated with angiogenesis, ranging from the initiation of sprout formation to the maturation of newly perfused vessels. However, for sprouting angiogenesis to occur, the vessel wall and surrounding extracellular matrix must first be destabilised to allow for the liberation and migration of an advancing tip cell (Carmeliet, 2000). The second stage

of angiogenesis involves the differentiation of two types of endothelial cell: an endothelial 'tip' cell which polarises to direct sprout migration toward the hypoxic tissue, and endothelial 'stalk' cells which mainly proliferate to extend the emerging sprout (Ribatti and Crivellato, 2012). Ultimately, newly emerging sprouts continue to extend until reaching the source of pro-angiogenic factors or until the tip cell filopodia embrace the filopodia of a sprout forming from a vessel in the opposing direction. Interestingly, tip cells and stalk cells possess different and highly specialised phenotypes which depend on the balance of pro- and anti-angiogenic signals. For example, tip cells express increased VEGF receptor 2 (VEGFR2) during the formation of filopodia which aid migration, as well as delta-like ligand 4 (Dll-4) which binds the notch receptor which suppresses cellular proliferation. In contrast, stalk cells express more VEGF receptor 1 (VEGFR1) and have increased Jagged-1 (JAG1)-notch signalling in order to proliferate without the risk of more tip cells forming in response to VEGF (Eilken and Adams, 2010; Ribatti and Crivellato, 2012). Next, endothelial migration and proliferation stops and is followed by the formation of a lumen from the rearrangement of cell-cell junctions and morphological changes in the endothelial stalk cells (Lubarsky and Krasnow, 2003). At this stage there is a plexus of endothelial sprouts which require pruning and remodelling to establish a differentiated vascular network capable of being perfused and delivering oxygenated blood. For example, redundant sprouting channels experience low shear stress and blood pressure, which stimulates vascular pruning (Skalak and Price, 1996). Lastly, newly formed vessels in the late stage of angiogenesis undergo stabilisation and maturation by the recruitment of pericytes from the pre-existing vascular network (Nicosia *et al.*, 2005; Ribatti and Crivellato, 2012).

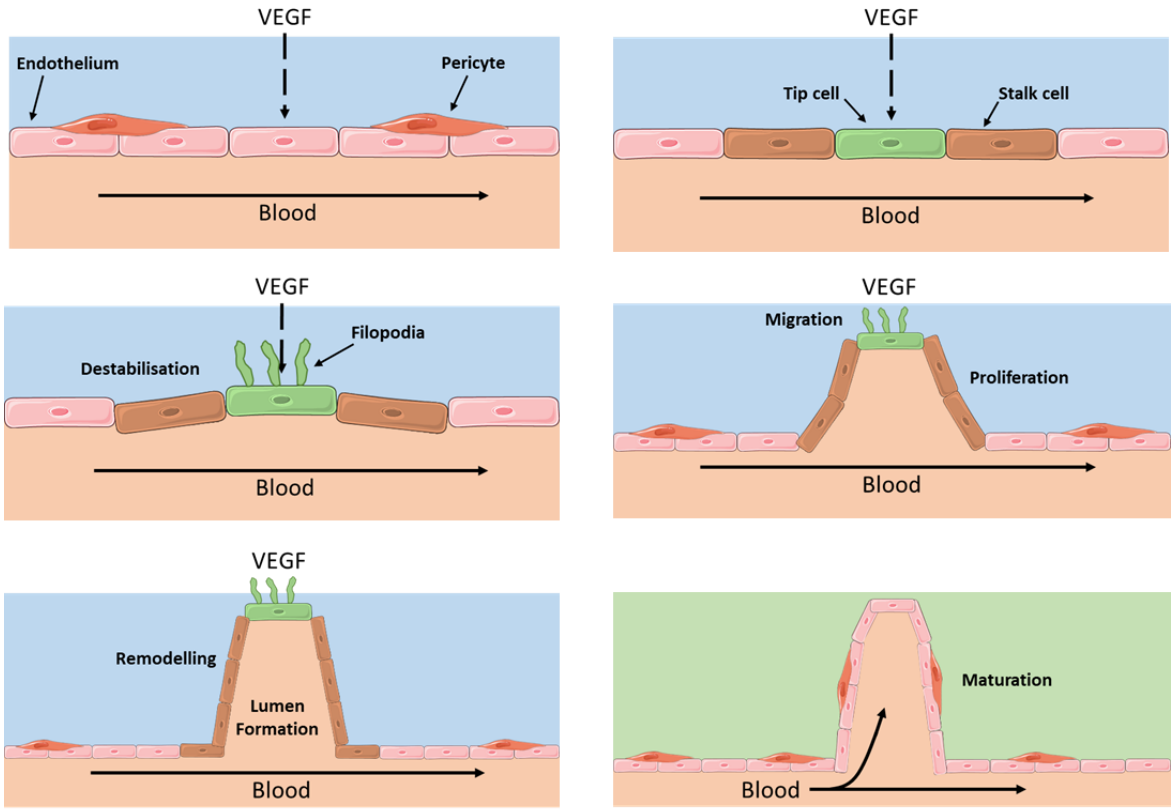

Figure 1-5. Sprouting angiogenesis of a blood vessel in response to vascular endothelial growth factor (VEGF).

1.5.2 Experimental models of angiogenesis

Angiogenesis, which begins during embryo development and continues throughout adult life, is important for tissue repair and remodelling prosses such as during wound healing. However, angiogenesis in adults also occurs during diseases such as cancer, diabetic retinopathy, and chronic inflammation (Carmeliet and Jain, 2011; Fallah *et al.*, 2019), and reports also suggest a role for neovascularisation in atherogenesis and atherosclerotic plaque destabilisation (Khurana *et al.*, 2005). Common characteristics of angiogenesis-associated diseases often involve conditions such as hypoxia, inflammation, and defective angiogenic growth factor production (Carmeliet and Jain, 2011). Alternatively, it is known that diseases such as myocardial infarction or ischaemic stroke may benefit from the therapeutic utilisation of angiogenesis to salvage the injured tissue. Thus, a significant amount of research has focused on understanding the mechanisms of sprouting angiogenesis in health and disease. Notably, however, angiogenesis involves a number of complex mechanisms which makes it challenging to model and thus study experimentally (Nowak-Sliwinska *et al.*, 2018). Commonly used approaches are the endothelial cell migration assays such as the *in vitro* scratch or wound closure assay, in which a monolayer of cells is disrupted, and the lateral migration of cells to close the gap is measured (Liang, Park and Guan, 2007). Although cell migration assays are simple to perform with or without chemotaxis, these assays have several limitations including the lack of a directed chemical gradient, and the requirement of large flasks of cells which limits their

applicability with specialised primary cell lines. Alternatively, the *in vivo* plug assay is often used, which provides greater physiological relevance of the mechanisms of angiogenesis in living hosts such as mice. This assay involves the subcutaneous placement of a Matrigel plug containing test compounds or angiogenic growth factors which is subsequently excised and evaluated for angiogenic growth (Malinda, 2009). Although this technique enables quantitative assessment of pro- and anti-angiogenic compounds in living mammals, angiogenic agents often leak out of the plug before being effective, generating considerable variability between animals (Nowak-Sliwinska *et al.*, 2018). Coupled with the cost and time-consuming nature, researchers have often turned to using the aortic ring assay, which is regarded as a relatively quick and easy technique used for measuring sprouting angiogenesis. In this assay, explanted rings of rat or mouse aorta are cultured *ex vivo* in an extracellular matrix (e.g., collagen) using culture media containing angiogenic growth factors such as VEGF-A or bFGF (Baker *et al.*, 2012). As with any technique, there are however several limitations. For example, the lack of blood flow through the vessel lumen means there will be a lack of angiogenic mechanochemical signalling and given that sprouting angiogenesis typically occurs in post-capillary venules rather than large arteries it raises questions about the relevance of the technique for modelling angiogenesis *ex vivo* (Baker *et al.*, 2012; Nowak-Sliwinska *et al.*, 2018). In contrast to existing *in vitro* models of angiogenesis, this technique utilises native vascular endothelial cells, devoid of modifications or the influence of passaging and are in the presence of other vascular cell types that are important for angiogenesis such as pericytes and fibroblasts (Nicosia, 2009). Importantly, studies using the aortic ring assay have reported positive correlations with *in vivo* models of angiogenesis (Nowak-Sliwinska *et al.*, 2018), and the technique can easily be applied to venous explants (Nicosia *et al.*, 2005). Thus, the *ex vivo* aortic ring assay offers a balance between *in vitro* and *in vivo* techniques and is therefore a suitable option for studying sprouting angiogenesis. It may be that the adaptability of the technique between venous and arterial explants allows for evaluation of other vessel types. To date, only one study reported the use of the aortic ring assay for other artery types. Stiffey-Wilusz and colleagues successfully modified the technique for explanted porcine carotid arteries for screening inhibitors of angiogenesis (Stiffey-Wilusz *et al.*, 2001). Notably, however, the application of the aortic ring assay for smaller, tissue-specific vessel types, such as cerebral arteries, remains unknown.

1.5.3 Cerebral angiogenesis and stroke

As mentioned previously, the central region where CBF reduction is most severe is referred to as the ischaemic core, whereas the surrounding tissue that experiences a less severe reduction in CBF as it receives blood supply from collateral vessels is referred to as the ischaemic penumbra. Due to the limited supply of blood, brain cells in the penumbra are considered to be mild or moderately ischaemic and thus are considered to

be alive but functionally impaired. Indeed, there are several post-ischaemic events as described in section 1.1.3 which dictate whether these cells die, whereas the restoration of blood flow dictates whether they survive and/or recover. Cerebral angiogenesis, the process of forming new cerebral vessels from existing ones, is important for improving blood flow to the ischaemic penumbra and promoting neurorepair following ischaemic stroke. Neurogenesis (the generation of new neurons) and neuronal plasticity (the anatomic regulation of brain circuitry) are other processes that occur after ischaemic stroke and are important determinants of neurological outcomes (Font, Arboix and Krupinski, 2010). Notably, it has been reported that cerebral angiogenesis is an important mediator of neurogenesis and neuronal plasticity by enabling the migration of neural progenitor cells to the border of the ischaemic penumbra (Kojima *et al.*, 2010). Thus, these three processes of neurorepair have become the subject of therapeutic neuroprotection research after ischaemic stroke with the aim of salvaging penumbral tissue. Pro-angiogenic factors such as VEGF, bFGF, and PDGF were previously shown to be upregulated in the brain after ischaemic stroke as early as 1-hour after reperfusion (Kovács *et al.*, 1996; Speliotes *et al.*, 1996; Hayashi *et al.*, 1997; Krupinski *et al.*, 1997), suggesting that augmentation of cerebral angiogenesis in the acute phase after stroke may help to mitigate the extent of ischaemic brain injury. Angiogenesis and neurogenesis have been observed in ischaemic stroke patients which positively correlated with microvessel density in the ischaemic hemisphere as well as patient survival (Krupinski *et al.*, 1994). It has also been reported that increased regional cerebral blood flow after focal cerebral ischaemia-reperfusion in rats corresponded with an increase of Tie-1-dependent pro-angiogenic factors in cerebral endothelial cells between day 1 and 7 (Lin *et al.*, 2001), indicating that increased angiogenesis can indeed improve cerebral perfusion in the ischaemic penumbra. Furthermore, another study reported that rats treated with recombinant human erythropoietin 24-hours after experimental stroke exhibited increased microvessel density in the ischaemic penumbra and improved functional recovery via enhanced VEGF and brain-derived neurotrophic factor (BDNF) expression (Wang *et al.*, 2004). Therefore, cerebral angiogenesis has great therapeutic potential for ischaemic stroke, however, there has been no success in the development of pro-angiogenic treatments for the disease. Thus, further exploration is required to understand the mechanisms which regulate cerebral angiogenesis and lead to improved outcomes following ischaemic stroke.

1.5.4 NO, angiogenesis, and the ADMA-DDAH1 pathway

It is well documented that endothelium-derived NO is a mediator of angiogenesis by contributing to endothelial proliferation (Ziche *et al.*, 1997), migration (Ziche *et al.*, 1994), and survival (Dimmeler, *et al.*, 1999; Rössig *et al.*, 1999). Pro-angiogenic factors such as VEGF and bFGF are known to activate eNOS and also increase its expression,

thereby increasing NO synthesis (Cooke, 2003). Indeed, VEGF has been shown to activate eNOS in a calcium-independent manner via the PI3K/Akt pathway which, in turn, leads to ser1177 phosphorylation of eNOS and subsequently increased NO synthesis (Dimmeler, *et al.*, 1999). Furthermore, there is evidence that eNOS-NO can increase VEGF synthesis in smooth muscle cells, thereby augmenting the angiogenic response in a positive feedback loop (Dulak *et al.*, 2000). Importantly, studies suggest that the ADMA-DDAH pathway may be an important regulator of angiogenesis. Indeed, numerous studies have demonstrated that ADMA inhibits angiogenesis. For example, a study found that exogenous ADMA inhibits endothelial cell motility of cultured porcine pulmonary endothelial cells in an effect which was reversed by the overexpression of DDAH1, or treatment with NO donors or an activator of cGMP-dependent protein kinases (PKG), the downstream target of cGMP (Wojciak-Stothard *et al.*, 2007). Another study showed that ADMA inhibited VEGF-induced angiogenesis *in vitro* using human umbilical vascular endothelial cells and *in vivo* using Matrigel plugs in mice (Fiedler *et al.*, 2009). The inhibitory effects were shown to be in a NO-dependent manner which were prevented by the overexpression of DDAH. Other studies have also demonstrated the functional importance of DDAH as a regulator of angiogenesis by showing that inhibitors of both DDAH enzymes or selective DDAH1 inhibitors impair NO-dependent tubule formation (a measurement of angiogenic activity) of human endothelial cells *in vitro* (Smith *et al.*, 2003; Ghebremariam, Erlanson and Cooke, 2014). Furthermore, using an endothelial-specific DDAH1 knockout mouse line, a more recent study demonstrated the importance of endothelial DDAH1 as a regulator of sprouting angiogenic activity in aortic rings (Dowsett *et al.*, 2015). Importantly, however, no studies have evaluated the impact of ADMA or explored the functional importance of DDAH1 on cerebral angiogenesis. This information is critical given evidence for elevated ADMA levels in stroke patients and also evidence that DDAH1 dysfunction may occur in response to ischaemia.

1.6 Hypothesis and aims of this thesis

The overall hypotheses of this thesis are that elevated ADMA plays a causal role in ischaemic stroke pathogenesis by perturbing the eNOS-NO signalling pathway, and that the ADMA metabolising enzyme DDAH1 plays an important physiological role in regulating endothelial NO signalling in cerebral arteries by controlling ADMA levels. Thus, the work presented in this thesis is expected to provide a new insight into the importance of the ADMA-DDAH1 pathway for cerebrovascular regulation and ischaemic stroke pathogenesis. To address my hypotheses, the main aims of this thesis are to:

1. Compare the impact of different durations of transient middle cerebral artery occlusion on the extent of ischaemic brain injury with the goal of establishing a

clinically relevant model of focal cerebral ischaemia without exceeding the ethical severity limits stipulated in our Home Office Project Licence (Chapter 3).

2. Explore the mechanisms responsible for elevated ADMA levels following ischaemic stroke in mice by examining the effect of focal cerebral ischaemia on expression levels of type I PRMT and DDAH enzymes; and using a selective DDAH1 inhibitor, examine the effect of elevated ADMA levels on ischaemic stroke outcomes after ischaemic stroke in mice (Chapter 4).

3. Evaluate the functional importance of endothelial DDAH1 for regulating eNOS-NO signalling by examining the impact of endothelial-specific DDAH1 knockout on endothelial and vascular smooth muscle function in mouse cerebral arteries; and examine the importance of endothelial DDAH1 for outcomes after ischaemic stroke in mice (Chapter 5).

4. Investigate the roles of the ADMA-DDAH1 pathway in cerebral angiogenesis by examining the impact of selective DDAH1 inhibition or endothelial-specific DDAH1 knockout on the sprouting angiogenic activity of mouse cerebral arteries (Chapter 6).

Chapter 2 General materials & methods

2.1 Experimental work using mice

2.1.1 Animals and ethics

All experiments were performed under a UK Home Office Project Licence (P486284C3) and Personal Licences (Arun Flynn: I56229F14; Alexandra Riddell: I8DA11C7A), in accordance with the Animals (Scientific Procedures) Act 1986 and approved by the University of Glasgow's Animal Welfare and Ethics Review Board (AWERB). These experiments were also covered by Glasgow Experimental Request Form (GERFs) numbers 003 and 105 and followed the ARRIVE guidelines for the reporting of animal research (Kilkenny *et al.*, 2010). Male C57BL6/J wild-type mice were purchased from Envigo (Blackthorn, UK) at 7 weeks of age and acclimatised for at least one week before experiments.

Male and female endothelial-specific DDAH1 knockout ($DDAH1^{En-/-}$) and floxed littermate control ($DDAH1^{fl/fl}$) mice were bred in-house under the Project Licence stated above (Figure 2-1). Heterozygous DDAH1 floxed mice with LoxP sites flanking exon 1 of the *DDAH1* gene and heterozygous mice expressing Cre recombinase under the Tie-2 promoter (both of a C57BL6/J genetic background) were obtained from Professor Leiper. Mating cages were set up using 8-week-old male $DDAH1^{En-/-}$ (Cre-positive) and female $DDAH1^{fl/fl}$ (Cre-negative) mice. All $DDAH1^{En-/-}$ and $DDAH1^{fl/fl}$ mice were aged to 8 weeks old before experiments. Successful homozygous endothelial DDAH1 knockout was validated by Dowsett and colleagues using the DDAH1 genotyping primers described below and a unique upstream primer, 5'- GCTGGGTTCTTGCAGTCTTC -3' which indicates successful knockout when PCR product is yielded (Dowsett *et al.*, 2015).

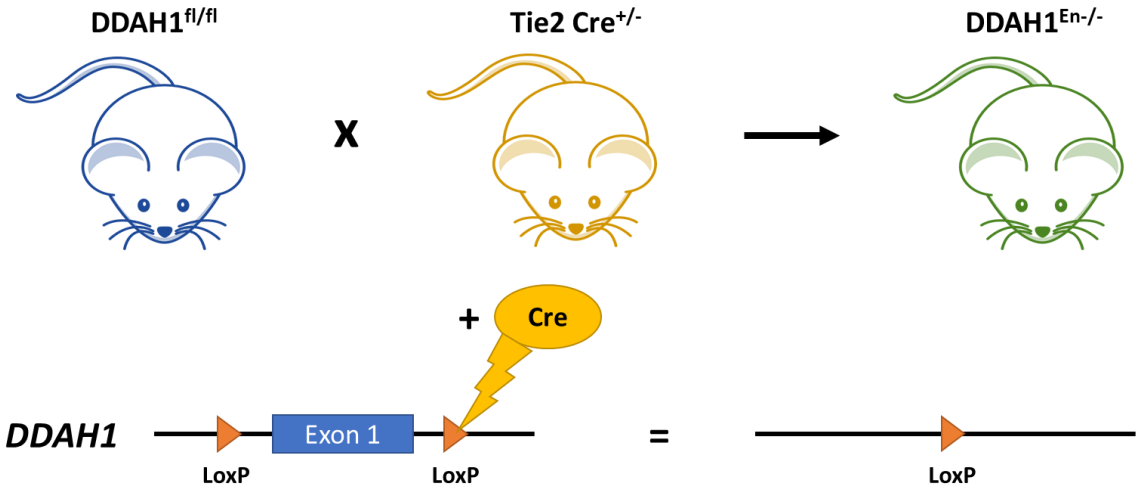

Figure 2-1. Generation of endothelial-specific DDAH1 knockout mice by crossing homozygous DDAH1 floxed mice with heterozygous Tie2 Cre mice. Floxed mice possessed LoxP sites flanking *DDAH1* exon 1, while heterozygous Tie2 Cre mice expressed Cre recombinase under the endothelial-specific Tie2 promoter.

Ear notches taken from three-week old DDAH1 Tie2 Cre mice were digested in 100 µL alkalising buffer (25 mM NaOH, 0.2 mM EDTA) for 1 hour at 98°C, followed by the addition

of 100 µL neutralising buffer (40 mM Tris HCl). DNA extracts were vortexed for 15 seconds and stored at -20°C until ready for PCR. PCR experimental parameters for genotyping are described in Table 2-1.

Presence of homozygous floxed DDAH1 alleles and Cre recombinase were confirmed using polymerase chain reaction (PCR) using the following primers, respectively. DDAH1 (Forward: (GX2738) 5'- TGAGTTGGAGTGTAGTGACGAGGACTTGG -3', Reverse: (GX2735) 5'- CTCCCATTGCTAATGAAACGGAGC -3'), Tie2 Cre (Forward: 5'- GCCTGCATTACCGGTCGATGCAACGA-3', Reverse: 5'- GTGGCAGATGGCGCGGCAACACCATT -3'). PCR reactions were made for DDAH1 and Tie2 Cre for each DNA sample using 3 µL DNA sample, DreamTaq Green PCR Master Mix (2X, ThermoFisher, UK), dNTPs, combined forward and reverse primers, and made up to 20 µL reaction volumes with dH_2O. PCR reaction conditions are described in Table 2-1. PCR reactions were run on a 1.5% agarose gel in 100 mL 1X TBE buffer and contained 3µL GelRed Nucleic Acid Gel Stain (SCT123, Merck, UK), at 60-90 V for 1-2 hours. Gels were visualised using a ChemiDoc XRS+ Imager (Bio-Rad Laboratories Ltd., UK).

Stage	DDAH1			Tie2 Cre		
	Temperature	**Duration**	**Cycles**	**Temperature**	**Duration**	**Cycles**
Initial Denaturation	95°C	5 Minutes	1 Cycle	95°C	5 Minutes	1 Cycle
Denaturation	95°C	30 Seconds	40 Cycles	94°C	30 Seconds	34 Cycles
Annealing	60°C	40 Seconds		70°C	30 Seconds	
Extension	72°C	1 Minute		72°C	1 Minute	
Final Extension	72°C	10 Minutes	1 Cycle	72°C	1 Minute	1 Cycle

Table 2-1. PCR running parameters for DDAH1 and Tie2 Cre genotyping of crude DNA lysates from endothelial-specific DDAH1 knockout (Cre-positive) and control (Cre-negative) mice.

In total, 306 mice (8-15 weeks of age) were used. Mice had access to water and standard chow *ad libitum* and were housed under a 12 h light/12 h dark cycle. All mice were euthanised by a rising concentration of CO_2 (Schedule 1 of the Act) using a Pre-Set Automated CO_2 System-1 Chamber-Trespa Housing Unit (Vet-Tech Solutions, UK) for tissue collection or at the study end-points.

2.1.2 Rodent model of focal cerebral ischaemia by transient middle cerebral artery occlusion (tMCAo)

Ischaemic stroke accounts for approximately 87% of cases in humans and is characterised by occlusion of cerebral arteries by a blood clot. Furthermore, blockage of the middle

cerebral artery (MCA) is the most common and accounts for >50% of ischaemic stroke cases (Satoh, Shirane and Yoshimoto, 1991; Ng *et al.*, 2007; Vital and Gavins, 2016). Therefore, in this thesis ischaemic stroke was induced in mice using the well-characterised and clinically relevant transient MCA occlusion (tMCAo) technique. Mice were anaesthetised before and during surgery using Isoflurane with 97-98% O_2 from an oxygenator (3% for induction, 2% for maintenance, Zoetis Ltd, UK). All sites of incision were treated with local anaesthetic (Naropin, 4 mg/kg, s.c.; AstraZeneca, UK) and 1 mL saline (i.p.) was given for hydration prior to surgery. Body temperature was monitored and maintained at 37±0.5°C throughout surgery using a heat lamp (ExoTerra, USA) and a rectal probe (Testronics, Victoria, Australia). Surgeries were performed using an aseptic technique which included the use of sterile drapes, autoclaved dissection instruments, Sterillium® hand disinfectant (Hartmann, UK) for the surgeon's hands and arms, and the wearing of sterile surgical gloves and a surgical gown.

To measure changes in regional CBF (rCBF) at the territory supplied by the right MCA, a 1 cm incision was made between the right ear and eye to expose the surface of the skull. Next, a laser-Döppler flowmetry probe was attached to the skull (5 mm lateral and 2 mm posterior to Bregma; Perimed, Sweden) using super glue and accelerator. rCBF was recorded at 5-minute increments prior to and during ischaemia, and during the first 10-minutes of reperfusion (Figure 2-2B). Under a surgical dissection microscope, a 1 cm incision was made along the midline of the neck. The revealed salivary glands, surrounding membranes and subcutaneous fat were separated to expose the common carotid artery (CCA) and external carotid artery (ECA). The ECA was ligated using two sutures followed by an incision between the sutures to create an ECA stump. The CCA was separated from the adjacent vagus nerve and the internal carotid artery (ICA) was separated from surrounding membranes. A suture was looped around the ICA and secured to a haemostat. Blood flow to the ECA stump was then restricted by applying tension to the haemostat and by placing an arterial clamp on the CCA. A small incision was then made on the ECA to allow the insertion of a silicone-coated nylon monofilament. A 0.21 mm (6-0 fine MCAO suture L12 PK10; 602112PK10) or 0.23 mm (6-0 medium MCAo suture L12 PK10; 602312PK10) diameter monofilament was used for mice weighing 21-25 g or 25-30 g, respectively (Doccol Corporation, US). After insertion of the filament into the ECA stump, the tension applied to the haemostat was released and the arterial clamp was removed to restore rCBF. Next, the filament was turned into the ICA and advanced approximately 11 mm to occlude the origin of the MCA at the circle of Willis (Figure 2-2A). Successful tMCAo required a ≥70% reduction of rCBF. Details on the durations of ischaemia are described in the methods sections of the relevant results chapters. After ischaemia, the filament was withdrawn from the ICA and turned back into the ECA stump, to allow for reperfusion of the cerebral tissue supplied by the MCA. Successful reperfusion required

a restoration of ≥80% of baseline rCBF within 10-minutes of filament withdrawal. Analgesia (Buprenorphine, 0.05 mg/kg; Ceva Animal Health Ltd., UK) and 0.5 mL saline were administered 10-minutes before reperfusion. After the surgery, the midline neck incision was closed using simple interrupted vicryl-coated 5-0 nylon sutures (Nu-Care Products Ltd., UK) followed by removal of the laser-doppler probe and closing of the incision on the head with fresh sutures. Sham-operated mice underwent the same procedures as tMCAo mice apart from the restriction of blood flow at the ECA stump and insertion of the monofilament. Sham and tMCAo mice were terminated at either 24- or 72-hour end-points, depending on the study.

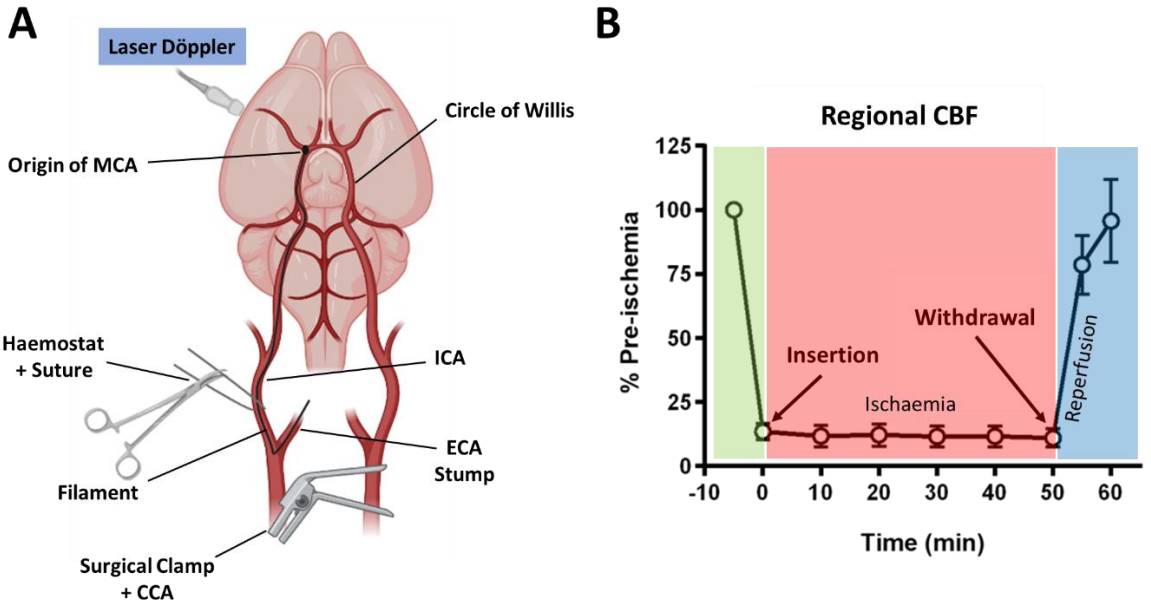

Figure 2-2. Schematic of surgery and example of changes of rCBF after tMCAo in mice. A surgical clamp and bridge suture are used to occlude blood flow to the ECA stump before a monofilament is inserted into the ICA and advanced to the origin of the MCA at the circle of Willis (**A**). Regional CBF at the cerebral territory of the MCA (**B**) is reduced by ≥70% after insertion of a monofilament followed by restoration of rCBF by ≥80% after withdrawal. Schematic made with BioRender.com.

Post-surgery, mice were recovered on a heat pad for at least the first 24-hours and provision of a softened diet (chow and Heinz baby food (Heinz, UK)) and HydroGel® (ClearH_2O®, US) *ad libitum*. Mice were monitored for at least 4 hours post-surgery and at least once daily thereafter until the study end-point using a clinical severity scoring system. This included assessment of the following criteria: hunching, body weight, breathing behaviour, grimace scale, eye paleness, and provoked behaviour. Additionally, appetite, faeces and urine output, and the sutured incision sites were checked for infection daily. Each criterion was assigned a score of 0-4 and a total score was calculated. Mice which scored 4 for a single criterion, a total of ≥10, or had ≥20% weight loss (relative to baseline weight) at any stage of recovery exceeded the severity limits of the study and were terminated immediately. Mice with a total score of 6-9 were monitored several times each day whereas mice scoring 0-5 were monitored once each day.

2.1.3 Slow-freezing with liquid nitrogen and cryosectioning of ischaemic mouse brains

Mice were culled on day 3 following stroke induction by a rising concentration of CO_2 (Schedule 1 of the Act) followed by decapitation. Brains were then removed, slow-frozen over liquid nitrogen, and then stored at -80°C until use. Using a cryostat, brains were embedded in OCT and coronally sectioned. A total of 15 sections (10 µm thickness, spaced 420 µm apart) covering three regions of the brain (region 1: +2.8 to +0.76 mm; region 2: +0.25 to -1.79 mm; region 3: -2.3 to -4.34 mm, relative to Bregma) were collected in replicates of 9. Sections were then thaw mounted onto poly-L-lysine coated glass slides and stored at -80°C. Sections 1-15 (covering regions 1-3) were used for infarct and oedema volume analyses, and section 7 (from region 2) was used for TUNEL analysis.

2.1.4 Determining cerebral infarct and oedema volume in mice after tMCAo

Thionin stains the Nissl bodies of living cells blue, which in turn, leaves the infarct region of tissue colourless allowing for identification and quantification of infarct size. Thus, a total of 15 frozen mouse brain sections (10 µm) covering approximately the whole brain and excluding the cerebellum were stained with thionin to delineate the infarct. Briefly, brain sections were immersed in 0.125% acidified thionin solution followed by two washes in distilled water (dH_2O). Sections were then dehydrated for 2-minutes in 70% ethanol (EtOH) followed by 2-minutes in 100% EtOH. Tissues were air dried before being dipped in xylene and mounted onto cover slips using DPX mounting media. Thionin-stained sections were imaged using a CCD Digital Camera (Canon, Japan). Total, cortical, and subcortical infarct and oedema volumes were quantified using ImageJ Image Processing and Analysis software (NIH, US).

Total infarct volume corrected for oedema was calculated using the following formula:

$$CIV = [RIA - (RHA - LHA)]\ x\ [section\ thickness + \ distance\ between\ sections\ (mm)]$$

CIV is the corrected infarct volume, RIA is right hemisphere infarct area, LHA is left hemisphere area, RHA is right hemisphere area.

Total oedema volume was measured using the following formula:

$$OV = \ [RHA - LHA]\ x\ [section\ thickness + \ distance\ between\ sections\ (mm)]$$

Infarct and oedema volumes were each totalled and expressed as mm^3.

To allow comparisons to be made with the typical infarct sizes found in human stroke, total infarct volume was also calculated as a percentage relative to left hemisphere volume (LHV; non-ischaemic) using the following formula:

$$\%\ Infarct\ Volume = \left(\frac{CIV}{LHV}\right)\ x\ 100$$

LHV was calculated by expressing LHA relative to total distance between sections (mm) for all 15 sections per brain.

Finally, total, cortical, and subcortical infarct area (mm^2) were also expressed relative to Bregma to examine the distribution of the infarct.

2.1.5 Assessing neurological function in mice after tMCAo

In addition to the histological analysis of infarct size, it is also important to evaluate behavioural and neurological outcomes and selecting appropriate behavioural tests are pivotal for investigating the consequences of ischaemic stroke. Therefore, stroke and sham-operated mice were tested for neurological and functional deficits 24- and 72-hours post-surgery compared to baseline. For this, the frequently used modified Neurological Severity Score (mNSS) composite scoring system as well as cylinder, foot fault, and forelimb grip strength tests were used. Unilateral ischaemia in both humans and rodents typically presents as deficits of symmetrical function, termed hemiparesis (Rogers *et al.*, 1997; Lang, MacDonald and Gnip, 2007; Schaar, Brenneman and Savitz, 2010). Therefore, tests such as these can measure a loss of forelimb function, and the mNSS also includes tests which are sensitive to the effects of unilateral ischaemia. Furthermore, nest building is an innate behaviour in rodents which is considered crucial for shelter, heat conservation, reproduction, and even depressive-like behaviour (Yuan *et al.*, 2018; Haley *et al.*, 2020). Nest building activity has been shown to be impaired after focal cerebral ischaemia in mice in a manner that reflects deficits after stroke in humans and is therefore an important test for rodent models of ischaemic stroke (Deacon, 2006; Yuan *et al.*, 2018).

2.1.5.1 Modified neurological severity score

The mNSS is composed of motor, sensory, reflex and balance tests, resulting in a deficit score from 0 (normal function) to 14 (maximum deficit) according to the scoring scheme summarised in Table 2-2 (Schaar, Brenneman and Savitz, 2010). Firstly, this approach used the walking and body swing tests to assess locomotion and sensorimotor function. MCAo and sham-operated mice were allowed to explore an open area of 30 cm x 15 cm for 2 minutes and their ability to walk was evaluated, followed by being suspended at the distal third of the tail for approximately 20 seconds (body swing test). Healthy mice walk freely in both directions and hang straight with their forelimbs extended towards the ground or swing 50% to either side with no preference. However, mice with unilateral ischaemic lesions often circle to one direction when walking and present with a dominant/biased swing direction favouring the side contralateral to the lesion. Severely affected mice often display uncontrollable circling or spasms when suspended from the tail. Secondly, pinna and corneal reflexes were also measured as part of the mNSS. Using a sterile cotton bud, the pinna of each ear and periphery of each eye were gently touched. Normal pinna reflex involves the flattening of the ear along the surface of the head, and

normal corneal reflex is demonstrated by blinking. The mNSS typically includes the balance beam test for measuring locomotion in mice, however, this study modified the mNSS by replacing the balance beam test with the foot fault test. This behavioural test assesses deficits of locomotion and sensorimotor coordination by quantifying asymmetrical foot faults and is described below. Scores measured the severity of the animal and the degree of asymmetry (foot fault index). The maximum scores for each test and their score allocations are described in Table 2-2.

Test & Purpose	**Score Range**	**Score Allocation**
Walking Test Locomotion	0-3	0 = Normal, no deficit 1 = Slight circling, mild deficit 2 = Clear circling and contralateral leaning, moderate deficit 3 = Minimal movement and contralateral leaning, severe deficit
Elevated Body Swing Test Locomotion	0-3	0 = Straight, normal 1 = Slight swing, mild deficit 2 = Clear swing, moderate deficit 3 = Circling/spasm, severe deficit
Pinna Reflex Test Reflex	0-1	0 = Reflexes present, normal 1 = ≥1 reflexes absent, clear deficit
Corneal Reflex Test Reflex	0-1	0 = Reflexes present, normal 1 = ≥1 reflexes absent, clear deficit
Foot Fault Test* Sensorimotor Locomotion	0-6	0 = Symmetrical, normal 1 = Positive asymmetry, mild deficit 2 = Negative asymmetry, mild deficit 3 = Positive asymmetry, moderate deficit 4 = Negative asymmetry, moderate deficit 5 = Positive asymmetry, severe deficit 6 = Negative asymmetry, severe deficit

Table 2-2. 14-point composite score criteria of the mNSS. The walking test score ranges from 0-3: 0, normal; 1, mild deficit with some circling or unilateral bias; 2, moderate deficit with clear circling; 3, severe deficit with little to no movement). The body swing test score also ranges from 0-3: 0, normal and straight; 1, mild deficit and swing <30°; 2, moderate deficit and swing >30°; 3, severe deficit and uncontrollable spasm. *Modified from commonly used balance beam test.

2.1.5.2 Cylinder test

The cylinder test was used to assess the asymmetry of spontaneous forepaw placements. A previous study showed that mice use ipsilateral forepaws at a greater frequency than their contralateral forepaws after focal cerebral ischaemia (Li *et al.*, 2004). This test requires a clear Perspex tube (10 cm diameter, 15 cm height, 0.5 cm thickness) with mirrors angled behind to gain a 360° view of the cylinder (Simply Plastics, UK; Figure 2-3). All forepaw placements were recorded for 60 seconds from the first paw placement made. Independent right (ipsilateral) and left (contralateral) paw placements, and simultaneous (both) paw placements were recorded. An asymmetry index value was calculated using

the following formula: (R - L) / Total paw placements (R, ipsilateral forepaw placements; L, contralateral forepaw placements; Total paw placements, L + R + (both paws x 2).

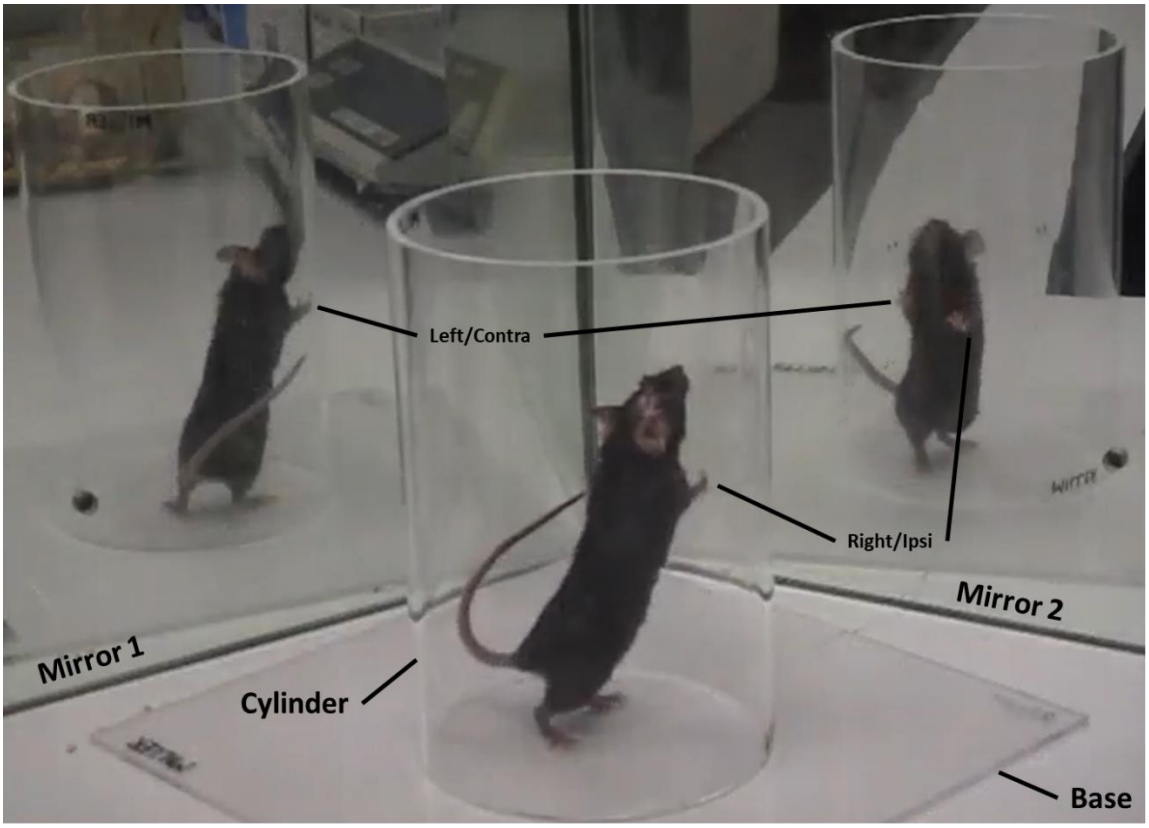

Figure 2-3. Diagram of the cylinder test with two mirrors for 360° visibility of mouse forepaw placements.

2.1.5.3 Foot fault test

The foot fault test was also presented independently of the mNSS. Normal mice typically make foot faults that are symmetrical. However, animals subjected to focal cerebral ischaemia often display deficits of locomotion and sensorimotor coordination asymmetrically. tMCAo and sham-operated mice were allowed to explore or cross an elevated wire grid (1.5 x 1.5 cm grid) for a maximum of 60 seconds, and the total forelimb steps and number of foot faults were recorded. Foot fault asymmetry was calculated using the following formula: (R - L) / Total steps taken (R, right (ipsilateral) forelimb faults; L, left (contralateral) forelimb faults).

2.1.5.4 Nest building activity test

As mentioned previously, nest building activity is an innate behaviour and indicates an animal's general well-being and cognition without the need for investigator interaction, and previous studies have demonstrated that this test can be used to assess sensorimotor and cognitive function as well as depressive-like behaviour (Deacon, 2006; Yuan *et al.*, 2018; Haley *et al.*, 2020). Therefore, tMCAo and sham-operated mice underwent a 24-hour nest building activity test before surgery and on day 2 post-surgery. Mice were singly housed in fresh, wood-chipped cages with minimal enrichment (wooden block and

cardboard tube) as per guidance by the Named Veterinary Surgeon at the University of Glasgow (Dr Michael Wilkinson), and food and water were provided *ad libitum*. Three grams of pressed cotton nestlets were then placed in the cage to assess nest building activity (Datesand group, UK; Deacon, 2006). After 24-hours, mice were returned to their original cages, nests were imaged and assessed. Nests were assigned a score on the following criteria based on a 5-point scale as shown in Figure 2-4, and % torn nestlet material was also calculated for each test using any untorn pieces weighing ≥0.1 g. Nest scores were assigned based on the criteria shown in Table 2-3 and any untorn pieces ≥0.7 g resulted in a deduction of 0.5 points. Also, nest scoring included the following amendments: nests with % torn and nest characteristics that were between two scores assignments were given as decimals of 0.5 between the available score assignments, e.g., 50% torn material and a visual nest with no shape or walls is between 3 and 4, thus assigned a score of 3.5. An example of nests before and after tests were performed is shown in section 8.1 in Appendix.

Score Assignment	**% Torn Material**	**Nest Characteristics**
0	0% torn	No visual interaction with material
0.5-1	10% torn	Minimal interaction with material or signs of a nest
1.5-2	10-50% torn	Some torn material but no visual nest or shape
2.5-3	50-90% torn	Nearly half torn but no visual shape of nest
3.5-4	90% torn	Mostly torn, visual nest but no shape or walls
4.5-5	100% torn	All material torn; clear nest with complete walls

Table 2-3. Scoring criteria for the nest building activity test as described by Deacon (Deacon, 2006)**.**

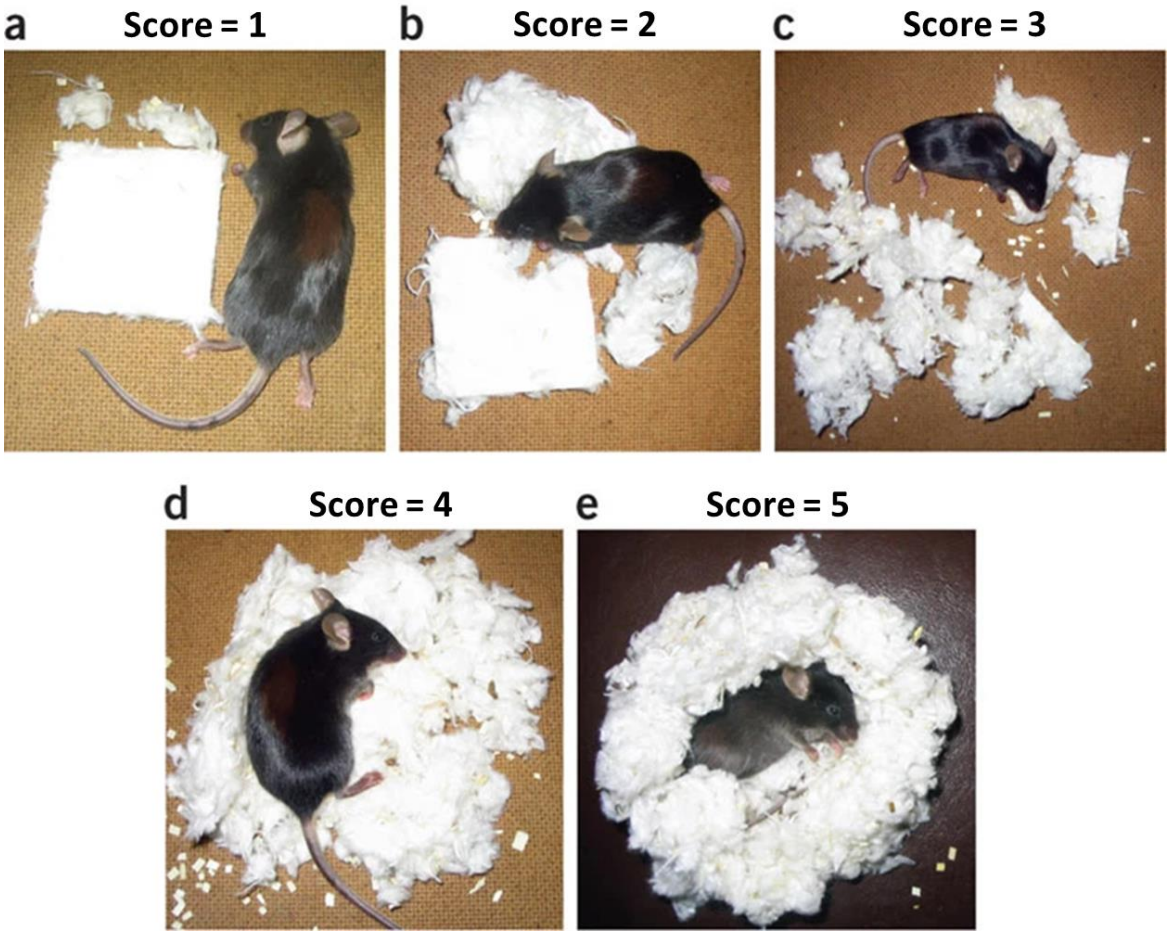

Figure 2-4. Visual representation of the 5-point scale for nest building activity of mice as described by Deacon (Deacon, 2006)**.**

2.1.5.5 Forelimb grip strength test

Grip strengths of both forelimbs were assessed prior to surgery and on day 2 post-surgery using a BIO-GS3 grip strength meter (BioSeb, UK). Mice were held by the base of the tail and lowered towards the T-bar of the strength meter. Once mice firmly grasped the T-bar with both forelimbs, the investigator gently pulled the mouse backwards in the horizontal plane until maximum grip strength of each mouse was measured (Figure 2-5). The force applied to the bar immediately before each mouse lost its grip was recorded as peak strength. Forelimb grip strength measurements were recorded in triplicate and an average was calculated.

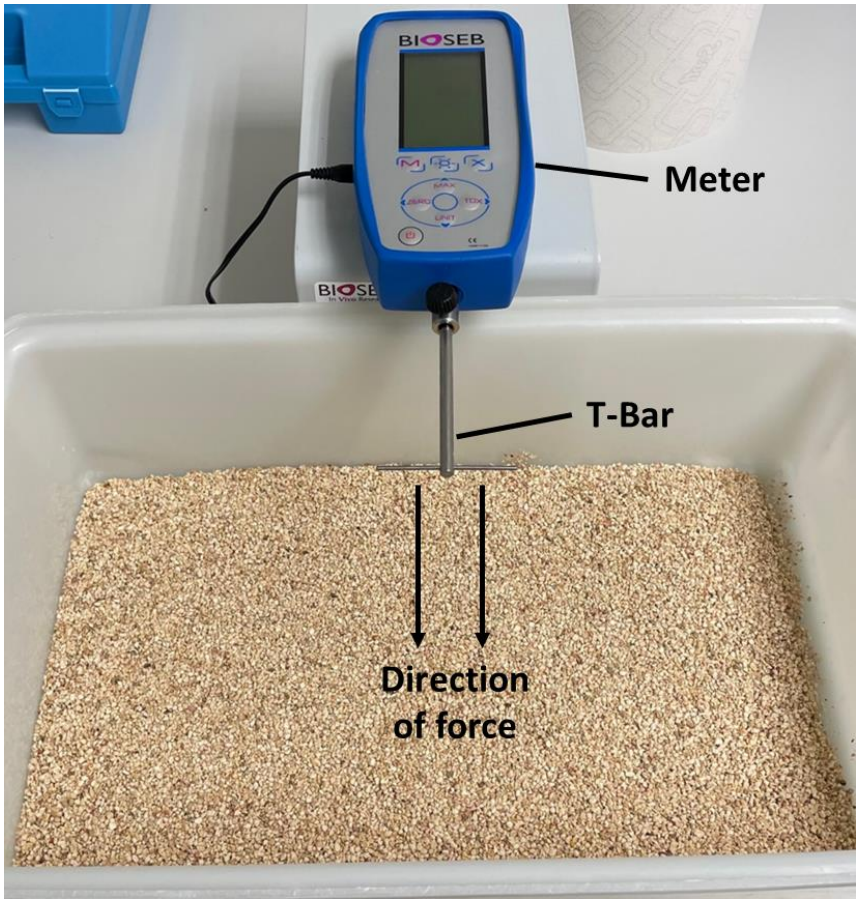

Figure 2-5. Diagram of the BioSeb forelimb grip strength meter with T-Bar attachment for assessing forelimb grip strength in mice.

2.1.6 Implantation of radiotelemetry probes and blood pressure measurement

Male C57BL6/J mice (8-15 weeks) were anaesthetised with isoflurane and 97-98% O_2 from an oxygenator (3% for induction and 2.5% for maintenance during the surgery; Zoetis Ltd, UK) and full aseptic technique was used throughout the procedure as described in section 2.1.2 in General Methods. A 2 cm midline neck incision was made, and the salivary glands were separated to reveal the left CCA. The CCA was cleared of connective tissue and a suture was looped around the artery distal to the bifurcation. A second suture was looped around the opposite end of the CCA relative to the bifurcation, and a third was placed along the midpoint of the CCA. Tension was applied to the suture near the bifurcation as well as the opposite end of the CCA to occlude blood flow. The tip of a 26G needle was used to pierce the CCA lumen and the end of the catheter of a radiotelemetry probe (PC-C10, DSI PhysioTel, US) was guided into the CCA lumen via the needle hole. The catheter was lined up parallel to the CCA and the middle suture was used to fasten the catheter and CCA together at the midpoint. A fourth suture was used to secure the catheter in place along the CCA. Blood flow was restored at the CCA by loosening and removal of the sutures at either end of the CCA. Blunt dissection of the subcutaneous tissue was used to create a cavity in the thoracic region of the abdomen where 1 mL warm, sterile saline was used to fill the ‘pocket’. Addition of saline creates the space required for placement

of the body of the probe. The surrounding tissues of the surgical site were returned into position and the incision site was closed using simple interrupted vicryl-coated 5-0 nylon sutures (Nu-Care Products Ltd., UK). Post-operatively, mice were given a softened diet of chow and Heinz baby food and HydroGel® *ad libitum* as previously described in section 2.1.2 in General Methods. Mice were allowed to recover for a minimum of 72 hours post-surgery before measurement of blood pressure. During this period, mice received a non-steroidal anti-inflammatory drug (0.5 mg/kg Meloxicam mixed with Nutella). Surgical implantation of the radiotelemetry probes in mice was performed by Dr Alexandra Riddell and Dr Delyth Graham, whereas post-surgical care, pharmacological treatments, and analyses described in Chapter 4 were performed by me.

Systolic and diastolic blood pressures, heart rates, and activity levels were measured for 10 seconds every 5 minutes throughout the duration of the study. Details of the experimental protocol are described in the methods section of Chapter 4.

2.1.7 Measurements of blood pressures using tail cuff plethysmography

Blood pressures were measured in mice using the minimally invasive tail cuff plethysmography technique (BP-2000 Blood Pressure Analysis System™; Visitech Systems Inc., US). Mice were acclimatised to the apparatus at least 3 times prior to blood pressure measurements. The temperature of the apparatus was set to 37°C, and systolic and diastolic blood pressures, and heart rates were measured every 30 seconds for a maximum of 15 recordings per mouse on each day of the study. Details of the experimental protocols are described in the methods sections of Chapters 4 and 5. Tail cuff measurements of C57BL6/J mice (Chapter 4) were performed by Miss Erika Trabold, whereas measurements of the male and female DDAH1$^{En-/-}$ and DDAH1$^{fl/fl}$ mice (Chapter 5) was performed by Dr Alexandra Riddell. All analyses were performed by me.

2.1.8 Measurement of brain and plasma ADMA/SDMA levels in naïve mice after L-257 treatment

L-257 was shown to be selective for DDAH1 over DDAH2 and has no effect on the NOS enzymes and arginase (Leiper and Nandi, 2011; Nandi *et al.*, 2012). Following intravenous administration, L-257 inhibits DDAH1 in rodents and thereby elevates circulating and peripheral tissue ADMA levels (Nandi *et al.*, 2012). Importantly, however, it is unknown whether systemic administration of L-257 to mice similarly increases ADMA levels in the brain. Therefore, 16 male C57BL6/J mice (8 weeks old) were randomised for intraperitoneal (i.p.) treatment with vehicle (saline) or L-257 (30 mg/kg). Randomisation of mice was performed using the random list generator using www.random.org/lists. Animals were returned to their cage for 1.5 hours before being euthanised. Brain tissues were collected and stored at -80°C. L-257 has a half-life in plasma of approximately 2 hours (personal communication by Prof James Leiper) and so a 1.5-hour duration was

chosen to allow for maximum DDAH1 inhibition before the half-life was reached. Thawed brains were weighed prior to homogenisation in ice-cold extraction solvent (chloroform/methanol/dH_2O; 1:3:1 ratio) using a 10 mm^3 dowse homogeniser at 4°C for the extraction of methylarginines. Sample homogenates were centrifuged at 13,000 x g at 4°C before collection and storage of the supernatants at -80°C.

Concentrations of ADMA, SDMA and L-NMMA (100 µmol/L) were used as standards for the detection of dimethylarginines. Brain and plasma methylarginine extracts were spiked with 10 µL of a 2 µM/L or a 500 nM/L stock of a labelled amino acid isotope ADMA-d7 internal standard, respectively, before being evaporated in nitrogen gas and reconstituted in mobile phase A (10 mM ammonium formate, 0.1% (v/v) formic acid in LC-MS-grade water). Reconstituted samples were separated using a silica column (150 x 3 mm I.D., 3 µm particle size; ACE) maintained at 37°C. Initial analysis conditions were 100%:0% mobile phase A:B with the percentage of mobile phase B (10 mM ammonium formate, 0.1% (v/v) formic acid in methanol/acetonitrile 1:1 (v/v)) increased from 0% to 2% over a 5-minute period. Flow rate was set to 300 µL/min, and samples were analysed in positive ion mode in the mass-to-charge (m/z) range of 100-1000. The capillary voltage was set to 4.3 kV with a temperature of 150°C and heater temperature of 350°C.

Separation and quantification of relative abundance by high performance liquid chromatography-mass spectrometry (HPLC-MS) was performed using a Thermo Scientific Ultimate 3000 RSLC system coupled to a Thermo Scientific Exactive Orbitrap mass spectrometer equipped with a heated electrospray ionisation (HESI II) probe (ThermoFisher Scientific, UK). Spectral processing was performed using the Thermo Xcalibur Quan Browser, matching ADMA and SDMA levels to pure standards by retention time and accurate mass and relative to the known internal standard concentration. All HPLC-MS experiments were performed by Professor Phil Whitfield and Dr Jennifer Haggarty at Glasgow Polyomics, whereas drug administration, tissue preparation and data analysis were performed by me.

2.1.9 Dissection of cerebral and systemic mouse arteries

Unlike in other vascular beds, large cerebral arteries account for >50% of total cardiovascular resistance (Faraci, 2011) and pial arteries such as the MCA are major contributors to cerebral blood flow and microvascular perfusion pressure (Faraci and Heistad, 1990). Moreover, occlusion of the MCA is a major cause of stroke in humans. Although extracranial cerebral arteries are not major contributors of cerebral vascular resistance, the carotid arteries are important conduit arteries of the cerebral circulation, they are a primary site for the development of atherosclerosis, and carotid artery disease is a major risk factor for ischaemic stroke and future cardiovascular events (Lorenz *et al.*, 2007; Faraci, 2011). Therefore, in addition to intracranial cerebral arteries, studies of

extracranial cerebral arteries (carotid arteries) are important with respect to understanding the underlying mechanisms of cerebral vascular disease and ischaemic stroke.

Extracranial (common carotid; CCA) and intracranial (middle cerebral; MCA) cerebral arteries and systemic (thoracic aorta and first order mesenteric) arteries were isolated from mice using a dissection light microscope. Vessels were placed in ice-cold phosphate-buffered saline (PBS), carbogen (95% O_2, 5% CO_2) bubbled physiological salt solution (PSS; 120 mM NaCl, 4.7 mM KCl, 1.2 mM $MgSO_4$, 25 mM $NaHCO_3$, 24 mM KH_2PO_4, 11 mM D-Glucose, 1 mM $CaCl_2$), serum-free OptiMEM media, or 4% paraformaldehyde (PFA) depending on the experiment being performed.

2.1.10 Wire myography of mouse CCA, thoracic aorta, and first-order mesenteric arteries

Wire myography is a widely used *in vitro* approach for studying the functional and mechanical properties of blood vessels. CCA, thoracic aorta, and first order mesenteric arteries were isolated and stored in ice-cold PBS and then transferred to a dissection dish containing ice-cold, carbogen (95% O_2, 5% CO_2) bubbled PSS. Under a dissection microscope, vessels were then cleared of connective tissue and cut into approximately 1.5-2 mm rings. A 0.4 mm diameter wire was carefully placed through the CCA or thoracic aorta, whereas a 0.25 mm diameter wire was used for mesenteric artery rings, and then vessels were mounted into a Mulvany-style small vessel wire myograph (Figure 2-6; Danish Myo Technology [DMT], Denmark) filled with ice-cold, carbogen bubbled PSS. Vessels were secured to the transducer and micrometer sides of the myograph using the metal wires and then left to equilibrate at 37°C for 30-minutes. After equilibration, vessels were stretched to a resting tension of 8 (thoracic aorta), 5 (CCA), or 2 (mesenteric) mN.

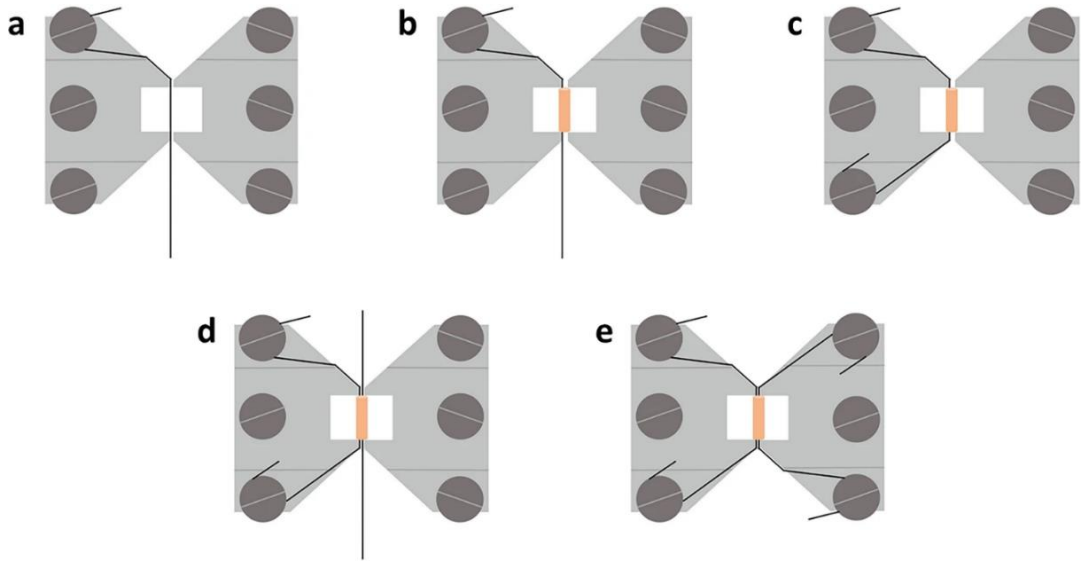

Figure 2-6. Diagram demonstrating the mounting of vessel rings to a wire myograph. Mouse CCA and thoracic aorta rings were mounted onto a transducer (left) and micrometer (right) sides of a wire myograph using metal wires and metal screws. Image from Griffiths and Madhani (Griffiths and Madhani, 2022).

Before conducting cumulative dose response curves (DRC), the following protocol was performed on all vessels. Firstly, the maximal physiological contractile response to modified high potassium PSS (61.5 mM KCl, KPSS) was recorded. Vessels with a maximal contractile response of ≥0.7 mN were deemed viable and were used in subsequent DRC experiments. After washing out KPSS, vessels were pre-contracted with the thromboxane A2 mimetic U46619 (40-60% of maximal KPSS response), and then the integrity of the endothelial layer was assessed by measuring the relaxation response to the endothelial NO-dependent agonist acetylcholine (ACh; 10^{-6} M). Vessels with ACh relaxation responses ≥50% of U46619-induced constriction were deemed to have an intact endothelium and were used for subsequent DRC experiments. Details of the DRC experimental protocols are described in the methods section of Chapters 4 and 5.

2.1.11 Perfusion myography of MCA

MCAs were dissected in ice-cold PSS from mouse brains and then mounted between microcannulas (~50 µm in diameter) in a pressure myograph (Living systems, US). Arteries were continuously superfused with warm (35°C to increase vessel longevity), carbogen-bubbled PSS. Intraluminal pressure was gradually raised to 60 mmHg with warm (35°C), carbogen bubbled PSS and maintained at this level using a pressure servo unit without further increases to intraluminal pressure (Living systems, US). Vessels were visualised on a Zeiss Axio Observer microscope (Carl Zeiss Ltd., UK) and a USB 3.0 Microscope Camera connected to IC Measure software (The Imaging Source Europe GmbH, Germany).

Following a 20-minute equilibration at 35°C, maximal contractile responses to KPSS were measured. Except for the very ends of each arterial segment, no part of the vessel touches the cannulae and the endothelium remains undisturbed (De Silva *et al.*, 2009; Miller *et*

al., 2010). Therefore, endothelium integrity was not assessed. Details of the experimental DRC protocols are described in the methods section of Chapters 4 and 5. Perfusion myography experiments were performed by Dr Alyson A. Miller and the analyses were performed by me.

2.1.12 Isolation of mouse brain microvessels for RNA extractions

For brain microvessel enriched preparations, I adapted the method used by Abbott and colleagues for use with mouse brains (Abbott *et al.*, 1992). In brief, mouse brains were isolated and washed with ice-cold PBS solution. In sterile conditions, the meninges were removed and the brains were subsequently homogenised using a 10 mm^3 Dowse homogeniser (Fisher Scientific, UK) in sterile Hank's Balanced Salt Solution (HBSS working buffer: 140 mM NaCl, 50 mM KCl, 3 mM Na_2HPO_4, 4 mM KH_2PO_4, 60 mM glucose, 1% penicillin-streptomycin (Merck, UK), 2% bovine serum albumin [43-50-850, 22% BSA, First Link Ltd, UK]), and then centrifuged at 800 x g for 5 minutes at 4°C. Pellets of brain homogenate were resuspended in 22% BSA solution (First Link Ltd, UK) and subsequently centrifuged at 300 x g for 20 minutes to separate cerebral microvessels from the brain parenchyma. Microvessel pellets were resuspended in ice-cold HBSS working buffer. This step was repeated 2-3 times for each sample until sufficient microvessels are separated from brain tissue samples. Mouse brain microvessel suspensions were centrifuged at 1800 x g for 5 minutes and supernatant discarded prior to either primary endothelial culture or RNA extractions.

2.1.13 TUNEL staining

The terminal deoxynucleotidyl transferase-mediated dUTP nick end labelling (TUNEL) assay is a commonly used approach for measuring late-stage apoptosis (Kyrylkova *et al.*, 2012). This assay detects free 3'-single or double-stranded DNA breaks by labelling 3'-hydroxyl terminal groups with deoxyuridine triphosphate nucleotides conjugated with fluorescein (FITC-dUTP), which is catalysed by the enzyme, terminal deoxynucleotidyl transferase (TdT).

One frozen 10 µm coronal section from region 2 of each mouse brain was thawed at room temperature for 10-minutes prior to fixation for 1 hour in 4% paraformaldehyde (PFA). Sections were washed three times for 10 minutes each in PBS, blocked in 3% H_2O_2 blocking buffer for 10-minutes, and washed a further three times before being permeabilised on-ice for 2-minutes. After permeabilisation, sections were washed twice with PBS before being blotted dry. Sections were then incubated with the TUNEL reaction mixture (Roche *In Situ* Cell Death Detection [TUNEL] kit, fluorescein [11684795910; Roche, Merck, UK]) for 1 hour at 37°C. After TUNEL staining, slides were washed three times with PBS before dry blotting and mounted in Vectashield® Antifade Mounting Medium containing DAPI (to counterstain nuclei), cover slipped, and left overnight before being sealed using

transparent colourless nail varnish. TUNEL-stained slides were stored at 4°C and protected from light. Stained sections were visualised and imaged using a Zeiss LSM 880 confocal microscope at 10X, 20X or 40X magnification (Zeiss, US). For each mouse, images were taken at 5 locations of the infarct core and peri-infarct of the ischaemic hemisphere (Figure 2-7).

TUNEL-stained images were analysed using the Cell Counter function on ImageJ Image Processing and Analysis software (NIH, US). In brief, the total number and area containing TUNEL-positive cells of each image were measured. An average of the 5 infarct and peri-infarct images was then taken and expressed as TUNEL-positive cells/mm^2.

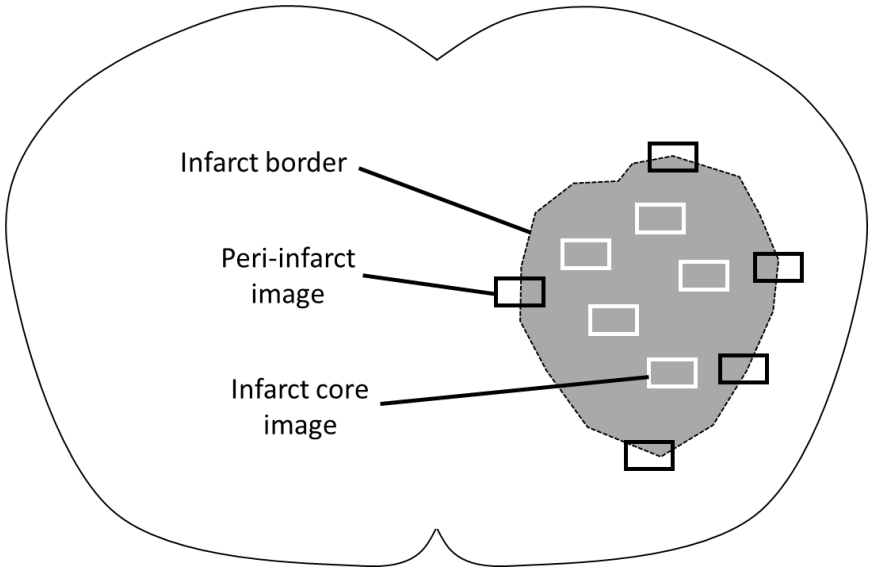

Figure 2-7. Imaging protocol for infarct core and peri-infarct brain regions after TUNEL staining.

2.2 Cell and Tissue Culture

2.2.1 Coating T75 cell culture flasks using rat collagen

Rat collagen I, lower viscosity (3443-100-01, R&D Systems Inc., US) was diluted 1:10 in sterile 1X PBS prior to incubation in fresh T75 cm flasks for 1 hour at 37°C in a humidified 5% CO_2 atmosphere. Flasks were then washed twice with 1X PBS and air-dried overnight in sterile conditions.

2.2.2 Culture of human cerebral microvascular endothelial cells (hCMEC/D3)

All cell culture experiments were performed under sterile conditions. Human cerebral microvascular endothelial cells (hCMEC/D3) were cultured in complete EndoGro™-MV media (Merck, UK) supplemented with 200 ng/mL human recombinant basic fibroblast growth factor (bFGF; F0291, Sigma-Aldrich, Merck, UK). Cells were maintained at 37°C in a humidified 5% CO_2 atmosphere and cultured in collagen-coated flasks. Cells were passaged every 4-5 days after approximately 80% confluency was achieved. Trypsin-EDTA was used to cleave the peptides that cells use to adhere to the base of the flask. Cells

were maintained between passages 26 and 36 for experiments and culture media was changed 24 hours after passaging. Exact experimental details are described in the methods section in Chapter 4.

2.2.3 *In Vitro* vessel sprouting assay of angiogenesis in thoracic aorta, common carotid, and middle cerebral artery rings

The aorta, and both CCAs and MCAs were dissected from mice, and placed in ice-cold PBS before being cut into ~1 mm rings. Rings of each vessel type were incubated in 12-well plates containing serum-free OptiMEM media (+ 1% Penicillin/Streptomycin) at 37°C in a humidified 5% CO_2 atmosphere for 24 hours to halt cell cycle progression. The next day, rat collagen (Sigma-Aldrich, UK) was diluted 1:2 in basal OptiMEM media, using 1 M NaOH drop-wise to restore pH, and 50 µL was loaded into wells of a 96-well plate. Sterile PBS was added to surrounding wells. Under a dissection microscope, vessel rings were transferred into individual wells and incubated at 37°C in a humidified 5% CO_2 atmosphere for 15 minutes for the collagen matrix to set. Vessel rings were then treated with 150 µL OptiMEM (2% FBS, 1% Penicillin/Streptomycin, 30 ng/mL VEGF [GF315, Merck, UK]) and incubated at 37°C in a humidified 5% CO_2 atmosphere (aorta and carotid, 7 days; MCA, 10 days). Media was replaced every 2-3 days. Details of the experimental protocols are described in the methods section of Chapter 6.

At the sprouting assay endpoints, vessel rings were imaged at 10X magnification using a bright field EVOS XL Core Imaging System microscope (ThermoFisher, UK). Sprouts were imaged in all planes surrounding the vessel rings. The number of sprouts, average sprout length, number of branch points, and vessel area (mm^2) were measured using ImageJ Image Processing and Analysis software (NIH, US), and each analysis criterion was normalised to vessel area.

2.3 Molecular Biological Techniques

2.3.1 RNA extraction of hCMEC/D3 cells and transgenic DDAH1 mouse microvessel pellets

RNA was extracted from cells and tissues in 1mL Qiazol™ lysis reagent (Qiagen, UK) followed by phase separation using 200 µL chloroform and vigorous mixing by fifteen inversions. Samples were centrifuged at 13,000 x g at 4°C for 15-minutes, followed by collection of the aqueous (clear) phase and precipitation of RNA using 70% EtOH. Subsequently, precipitated samples were transferred to Qiagen RNeasy® Mini Kit columns, and RNA was purified following the manufacturer's instructions until RNA elution (Qiagen, UK). Genomic DNA was digested using the RNase-free DNAse I kit (Qiagen, UK) and RNA was eluted from columns in 40 µL RNase-free dH_2O and re-eluted a second time for a maximum yield prior to quantification. RNA concentration was determined for all samples using a NanoDrop™ (ThermoFisher, UK) spectrophotometer before being stored at -20°C.

2.3.2 cDNA synthesis

RNA samples were converted to cDNA templates for RT-qPCR using the Qiagen QuantiTect Reverse Transcription kit (Qiagen, US), following the manufacturer's instructions. cDNA was converted from RNA stocks using multiples of ≥1 µg of RNA per reaction.

2.3.3 Quantitative SYBR green RT-qPCR

Quantitative SYBR Green reverse transcription PCR (RT-qPCR) was performed on cDNA samples using the Qiagen QuantiFast® SYBR Green RT-PCR Kit or QuantiNova® SYBR Green RT-PCR Kit, following the manufacturer's instructions (Qiagen, UK). Either QuantiTect® or QuantiNova® LNA® primer assays were used for measuring genes of interest. Primer details are described in Table 2-4 and running parameters are described in Table 2-5. Quantified expression of the target genes was determined and normalised to the housekeeping gene GAPDH and was achieved using the following formula: $2^{-\Delta\Delta Ct}$, where Ct is the cycle threshold, ΔCt = Ct (gene of interest) – Ct (control gene; GAPDH), ΔΔCt = ΔCt (OGD sample) – ΔCt (normoxic control sample). All $2^{-\Delta\Delta Ct}$ values were expressed relative to their relevant control sample value (Schmittgen and Livak, 2008).

Gene	Primer ID	Catalogue no.	Manufacturer
Ddah1	HS_DDAH1	SBH0345295-200	Qiagen
Ddah2	HS-DDAH2	QT00039592	Qiagen
Prmt1	HS_PRMT1	QT00005817	Qiagen
Prmt4 (Carm1)	HS_CARM1	SBH0380609-200	Qiagen
Gapdh	HS_GAPDH	SBH1220545-750	Qiagen

Table 2-4. Gene and primer details for assessing gene expression by SYBR Green RT-qPCR.

Stage		Temperature	Duration	Cycles
Hold Stage	Denaturation	95 °C	10 Minutes	1 Cycle
Amplification	Denaturation	95 °C	15 Seconds	40 Cycles
	Anneal and Extension	60 °C	60 Seconds	
Melt Curve	Denaturation	95 °C	15 Seconds	1 Cycle
	Anneal and Extension	60 °C	60 Seconds	(Continuous)
Final Stage	Dissociation	95 °C	15 Seconds	1 Cycle

Table 2-5. Running parameters for quantitative SYBR green RT-PCR.

2.3.4 Protein extraction from mouse brain tissue

Brain or kidney (positive control for DDAH enzymes) tissues were lysed with metal lysis beads in 1.5X Laemmli buffer (7.5% Glycerol, 3.75% 2-Mercaptoethanol, 0.225% SDS, 75 mM Tris HCl, 0.003% Bromophenol Blue) using a Qiagen MM300 Retsch TissueLyser at the frequency 30 shakes/second for 90 seconds (Qiagen, UK). Next, protein lysates were centrifuged at 13,000 x g for 30-minutes to separate protein and cellular debris fractions.

The protein-containing upper phase of the supernatant was collected and divided into aliquots. Protein concentration of all samples was determined using the RC DC™ protein quantification kit (Bio-Rad Laboratories Ltd, UK), as per the manufacturer's instructions. Afterwards, sample stocks were diluted in 1.5X Laemmli buffer to make 20, 40, or 60 µg running protein samples for Western blotting. All lysate stocks and running protein samples were stored at -80°C.

2.3.5 Western blotting

Protein samples of equal concentration were loaded on gels consisting of a lower phase 12.5% resolving gel (1.5M Tris-HCl, 40% Bis/Acrylamide, 10% SDS, 10% (w/v) Ammonium Persulfate, TEMED) with an upper phase 4% stacking gel (0.5M Tris-HCl, 40% Bis/Acrylamide, 10% SDS, 10% Ammonium Persulfate, TEMED). Protein samples were separated by SDS-PAGE for an initial 20-minutes at 60 V to stack proteins, followed by 1.5 hours at 120 V to resolve proteins. Gels were run in 1X running buffer (50 mM Tris-Base, 190 mM Glycine, 0.1% SDS, pH 8.8) and a Precision Plus Protein Dual Color Standards MW ladder was used (Bio-Rad Laboratories Ltd., UK). Proteins were transferred to an activated Immobilon-P Polyvinylidene Fluoride (PVDF; Merck, US) membranes by semi-dry electroblotting at 15 V for 1 hour, using a combination of three transfer buffers. Layout of the transfer layers is illustrated in Figure 2-8 (transfer buffer 1 [0.3 M Tris-Base, 20% v/v Methanol (MeOH), pH 10.4], transfer buffer 2 [0.025 M Tris-Base, 20% v/v MeOH, pH 10.4], transfer buffer 3 [0.038 M Tris-Base, 0.01 M ß-Alanine, 20% v/v MeOH, pH 9.4]). Next, protein-containing membranes were blocked in milk for 1 hour at room temperature before incubation with primary antibody overnight at 4°C. The following day, blots were washed with Tris-buffered saline (TBS) prior to incubation with a secondary antibody for 1 hour at room temperature. All secondary antibodies were designed for LiCor Odyssey fluorescence multiplex detection. After secondary antibody incubation, membranes were washed in TBS and then developed using a LiCor Odyssey DLx system at 680 nm or 800 nm depending on the secondary antibody used (LiCor, UK). Primary and secondary antibodies that were used are detailed in Table 2-6.

Relative intensity of each protein of interest (POI) was determined and normalised to either ß-Actin or ß-Tubulin loading control depending on the POI size (kDa). Relative intensities of POI in ischaemic and non-ischaemic hemispheres were then normalised to intensities in cerebral hemispheres from sham-operated mice.

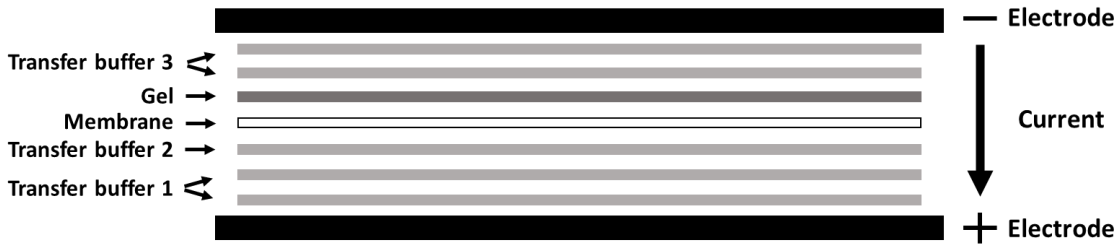

Figure 2-8. Schematic showing the layers of blotting paper sheets (light grey), transfer buffers, gel (dark grey), and membrane (white) for the transfer of proteins to a PVDF membrane by semi-dry electroblotting.

Target	Concentration	Species	Ab Type	Manufacturer	Catalogue No.
DDAH1	1:1,000	Rabbit	Primary	NSJ Bioreagents	R32437
DDAH2	1:500	Rabbit	Primary	Abcam	ab180599
PRMT1	1:500	Rabbit	Primary	Merck	07-404
PRMT4 (CARM1)	1:500	Rabbit	Primary	Abcam	ab245467
PRMT8	1:1,000	Rabbit	Primary	Merck	ABS517
ß-Actin	1:5,000	Mouse	Primary	Cell Signalling	3700S
B-Tubulin	1:5,000	Rabbit	Primary	Abcam	Ab6046
IRDye 800CW	1:10,000	Donkey anti-rabbit	Secondary	LiCor	926-32213
IgG AlexaFluor 680	1:10,000	Rabbit anti-mouse	Secondary	ThermoFisher	A-21065

Table 2-6. Primary and secondary antibodies for western blotting.

2.4 Histology

2.4.1 Sectioning FFPE thoracic aorta, common carotid, and middle cerebral artery rings

Thoracic aorta, CCA, and MCA were incubated in 70% EtOH for 24-hours followed by fixing in 4% PFA for a further 24-hours prior to paraffin embedding. Embedded tissues were sectioned at 5 (MCA) and 10 µm (thoracic aorta and CCA) using a Leica microtome (Leica Biosystems, UK). Sections were baked onto silane-coated slides at 55°C overnight.

2.4.2 Picrosirius red and elastin van Gieson staining of thoracic aorta, common carotid, and middle cerebral artery sections

Sections of thoracic aorta, CCA and MCA vessels from mice were deparaffinised and rehydrated using xylene, decreasing concentrations of ethanol (100% and 70%), and two washes of dH2O. Sections were stained for collagen using picrosirius red (0.1% direct red 80, 0.1% fast green FCF, 1.3% saturated aqueous picric acid) or elastin using elastin van Gieson (ab150667, Abcam, UK) stains. Stained thoracic aorta, CCA, and MCA sections (5 sections per mouse) were imaged using an Olympus BX41 Light Microscope (Olympus Life Science, UK), and then analysed using ImageJ Image Processing and Analysis software (NIH, US). Collagen content was quantified in the red channel followed by threshold

analysis of the total vessel wall area, whereas elastin content was quantified using a black and white threshold analysis of the media area of the vessel wall.

2.5 Statistical Analysis

All analyses were performed using GraphPad Prism version 9.1.0 (GraphPad Software Inc., US). $P<0.05$ was considered statistically significant. Group (n) numbers and statistical tests used to analyse data sets are indicated in the methods section and figure legends of the results chapters.

Parametric data are expressed as mean ± SEM and were analysed using a paired t-test, unpaired t-test with Welch's correction, one-way ANOVA with Tukey's post hoc test, one-way ANOVA with Dunnett's post hoc test, Brown-Forsythe ANOVA with Dunnet's T3 multiple comparisons test, a mixed-effects ANOVA with Tukey's multiple comparisons test or Holm- Šídák's multiple comparisons test, two-way ANOVA with Tukey's post hoc test, two-way repeated measures ANOVA with Šídák's multiple comparisons test, or simple linear regression and correlation. Multivariate analysis of RNA samples by RNA-seq was performed by Dr Graham Hamilton at Glasgow Polyomics, University of Glasgow.

Non-parametric data (e.g., nest building activity and mNSS) are expressed as median and were analysed using either a Wilcoxon matched pairs test, Mann Whitney U test, Friedman test with Dunn's multiple comparisons test, or Kruskal-Wallis with Dunn's multiple comparisons test.

Chapter 3 Establishing a clinically relevant model of transient middle cerebral artery occlusion in mice

3.1 Introduction

Survivable, acute ischaemic strokes in humans are typically small in size, ranging from 28-80 mm^3 (or 4-14% of the hemisphere) (Brott *et al.*, 1989; Carmichael, 2005). However, modelling ischaemic stroke pathophysiology and outcomes experimentally is challenging in stroke research. This is partially explained by the heterogenous nature of the disease in humans and is influenced by the presence of co-morbidities and numerous other modifiable and non-modifiable risk factors (Kuriakose and Xiao, 2020). Additionally, commonly used rodent models of ischaemic stroke often lack the complex pathophysiological features of stroke, such as ischaemia-reperfusion injury. Importantly, the findings from translational pre-clinical stroke studies have not been reproduced in human clinical trials, which led to the conceptualisation of the Stroke Therapy Academic Industry Roundtable to improve the quality of pre-clinical studies (Stroke Therapy Academic Industry Roundtable (STAIR), 1999). Thus, there is a large translational gap and researchers must take great consideration in selecting an experimental model of ischaemic stroke for the translation of findings into humans.

There are numerous experimental models of ischaemic stroke, including the photothrombotic, embolic, ET-1, and middle cerebral artery occlusion (MCAo) models (Macrae, 2011; Sommer, 2017). The strengths and weaknesses of these models vary vastly and there is no single option that has been identified as the perfect experimental model. Notably, however, >50% of ischaemic stroke cases occur as a result of occlusion of the MCA, and spontaneous or therapeutic recanalization is often associated with improved patient outcomes (Ng *et al.*, 2007; Rha and Saver, 2007). Therefore, the transient MCAo (tMCAo) model has become a widely used model by researchers. This method uses a silicon-coated monofilament that is inserted into the internal carotid artery (ICA) and advanced to the origin of the MCA at the circle of Willis to occlude blood flow for a chosen duration. Advantages of the tMCAo model include easily modifiable occlusion periods of cerebral blood flow (CBF) to the territory supplied by the MCA, as well as the ability to simulate recanalisation therapy and the opportunity to study a secondary complication known as reperfusion injury (Macrae, 2011). For example, Engel and colleagues compared 30- and 60-minutes of tMCAo in mice and demonstrated that significantly larger infarcts developed in the 60-minute group compared to 30-minutes (Engel *et al.*, 2011). Researchers can also simulate malignant strokes by permanently occluding the origin of the MCA by keeping the filament in place, known as the permanent MCAo (pMCAo) model. Notably, the choice of mouse strains have been shown to influence stroke outcomes in pre-clinical studies using the tMCAo model (Barone *et al.*, 1993; Hara *et al.*, 1996; Fujii *et al.*, 1997; Keum and Marchuk, 2009), and it was previously reported that the C57BL6/J mouse strain that is commonly used in studies using the tMCAo model often form an incomplete circle of Willis and typically lack one or both of the posterior communicating

arteries (Fujii *et al.*, 1997; Kitagawa *et al.*, 1998). These considerations therefore highlight further the complexity of translational stroke research. However, although the tMCAo model does not involve blockage of a cerebral blood vessel with a thrombus, this model allows varying severities of focal cerebral ischaemia-reperfusion to be easily achieved in a reproducible and high-throughput manner in rodents.

Ischaemic stroke is a leading cause of disability in humans; and neurological assessments (e.g. NIH stroke scale [NIHSS]) are often the primary outcome assessment used for diagnosing ischaemic stroke in patients (Chalos *et al.*, 2020). Neurological and functional deficits can also be measured in rodent models of stroke, and it is therefore important to measure changes of neurological outcomes in experimental stroke models with the aim of identifying mechanisms involved and treatments which may improve or prevent neurological impairments in patients suffering from ischaemic stroke. There are a plethora of behavioural tests and composite assessment scores available for rodent stroke studies, however, selecting an appropriate test can be challenging. Wild type, young and healthy mice typically present with symmetrical behaviours, whereas behaviours present asymmetrically in rodents after tMCAo (Phipps, 1991; Li *et al.*, 2004; Schallert, 2006; Schaar, Brenneman and Savitz, 2010). There are a number of tests which aim to interrogate the impairments based on the degrees of asymmetry, including the foot fault, cylinder, adhesive removal, and forelimb grip strength tests. Furthermore, composite tests such as the 5-point Bederson scale and modified neurological severity score (mNSS) can be used to further assess functional impairments (Schaar, Brenneman and Savitz, 2010). Consequently, the choice of experimental stroke model and subsequent neurological tests must be carefully considered by researchers.

In this study, we aimed to compare the impact of different durations of tMCAo on the extent of ischaemic brain injury, with the goal of establishing a clinically relevant model (4-14% of the hemisphere) of focal cerebral ischaemia in male C57BL6/J mice without exceeding the ethical severity limits stipulated in our Home Office Project Licence. Establishing a clinically relevant model will allow us to test for pathological mechanisms and causal links associated with ischaemic stroke pathogenesis. Additionally, a range of neurological and functional tests to assess neurological and functional outcomes were evaluated. It is hypothesised that the extent of ischaemic brain injury, and neurological and functional deficits in mice will worsen with increased duration of tMCAo.

3.2 Materials and methods

3.2.1 Animals

In this chapter, a total of 41 male C57BL6/J mice (8-12 weeks of age) were used. Total group sizes were n=9 for the 50- and 60-minute tMCAo groups, n=11 for the 65-minute tMCAo group, and n=4 for the 70-minute tMCAo group, however, nine mice were excluded from the study (50-minute tMCAo n=2, 60-minute tMCAo n=1, 65-minute tMCAo n=3, 70-minute tMCAo n=3). These exclusions occurred when: 1) there was inadequate reduction of rCBF (<70%) after induction of ischaemia, or insufficient reperfusion (<80%) within 10-minutes of filament withdrawal; 2) technical complications arose during surgery (e.g. loss of filament integrity, inaccurate rCBF measurement as a result of a loose laser-doppler flowmetry probe, or >0.2 mL blood loss); or 3) mice needed to be culled due to a clinical severity score prior to the scientific end-point of the study (day 3 post-stroke induction).

3.2.2 Assessment of stroke outcomes after different durations of tMCAo

Previously in our lab, 30- and 40-minutes of tMCAo were compared in mice (using isoflurane anaesthesia), however, neither duration presented with clinically relevant sized ischaemic brain injuries nor neurological deficits (data not shown). In this study, mice were subjected to tMCAo for 50-, 60-, 65-, or 70-minutes using a monofilament, as described in section 2.1.2 of General Methods, followed by withdrawal of the filament to allow for reperfusion. Sham-operated surgeries were also performed as described in section 2.1.2 in General Methods.

Neurological and functional outcomes were assessed on stroke and sham-operated mice on day 1 and 3 post-surgery, whereas 65-minute stroke mice were also subjected to neurological and functional testing pre-surgery (baseline). The tests performed included the modified neurological severity score (mNSS), nest building activity test, foot fault test, and cylinder test as described in section 2.1.5 of General Methods. Body weights were measured pre-surgery and every day thereafter until the scientific end-point on day 3 post-surgery.

On day 3 following stroke induction or sham surgery, mice were euthanised by a rising concentration of CO_2 (Schedule 1 of the Act). Brains from all stroke mice were collected followed by cryosectioning as described in section 2.1.3 of General Methods. The semi-quantification of TUNEL-positive cells was assessed in the infarct core and peri-infarct regions of brain sections from 65-minute tMCAo mice only, as described in section 2.1.13 of General methods.

3.2.3 Statistical analysis

All datasets were analysed with GraphPad Prism 9 (GraphPad Software, USA). $P<0.05$ was considered statistically significant, and group numbers are indicated in the corresponding figure legends.

Parametric data is expressed as mean ± SEM. This includes infarct and oedema volumes, forelimb asymmetry tests (cylinder and foot fault tests), and the semi-quantification of TUNEL-positive cells. The following statistical tests were used:

- Paired t-tests were used for the comparisons of forelimb asymmetry at day 1 and day 3 post-stroke for mice in each group, and pre-post analysis of forelimb asymmetry tests of 65-minute tMCAo mice between day 1 and day 3, and the semi-quantification of TUNEL-positive cells between the infarct core and peri-infarct tissue regions of 65-minute tMCAo mice.
- A one-way ANOVA with Dunnett's post hoc test was used for comparing infarct and oedema volumes between 50-, 60-, and 65-minute groups, and weight loss between groups between pre-stroke and the study end-point on day 3.
- A one-way ANOVA with Tukey's multiple comparisons post hoc test was used for comparing forelimb asymmetry at day 1 and day 3 between groups.
- A one-way ANOVA with Tukey's multiple comparisons post hoc test was used for comparing pre-tMCAo, day 1, and day 3 post-tMCAo forelimb asymmetry tests of mice in the 65-minute group.
- A Brown-Forsythe ANOVA with Dunnett's post hoc test was used for comparing % net weight loss between groups by day 3.
- A simple linear regression and correlation was used for determining correlations between infarct or oedema volumes against net weight loss on day 3 post-stroke.

Non-parametric data is expressed as median. This includes the nest building activity and mNSS neurological tests. The following statistical tests were used:

- A Kruskal-Wallis multiple comparisons test was used to compare pre- and post-surgery nesting between mice in all groups, and mNSS scores at day 1 and day 3 between mice in all groups.
- A Friedman test with Dunn's multiple comparisons post hoc test was used to compare matched pre-stroke, day 1, or day 3 mNSS scores of mice after 65-minute tMCAo.
- A Wilcoxon matched pairs test was used to compare mNSS scores of mice in all groups between day 1 and day 3 post-surgery, and for comparing pre- and post-surgery nest building activity of mice in all groups.
- A Mann-Whitney U test was used to compare nest building activity of sham and 65-minute tMCAo mice post-surgery.

3.3 Results

Male C57BL6/J mice were subjected to sham surgery or 50-, 60-, 65-, or 70-minutes of tMCAo followed by 3 days of reperfusion. The time period of anaesthesia for sham mice was time-matched with the 65-minute group. All mice experienced a ≥70% drop in regional cerebral blood flow (rCBF) following filament insertion and a ≥80% restoration of rCBF 10 minutes after filament withdrawal, whereas rCBF was unchanged in all sham mice (Figure 3-1).

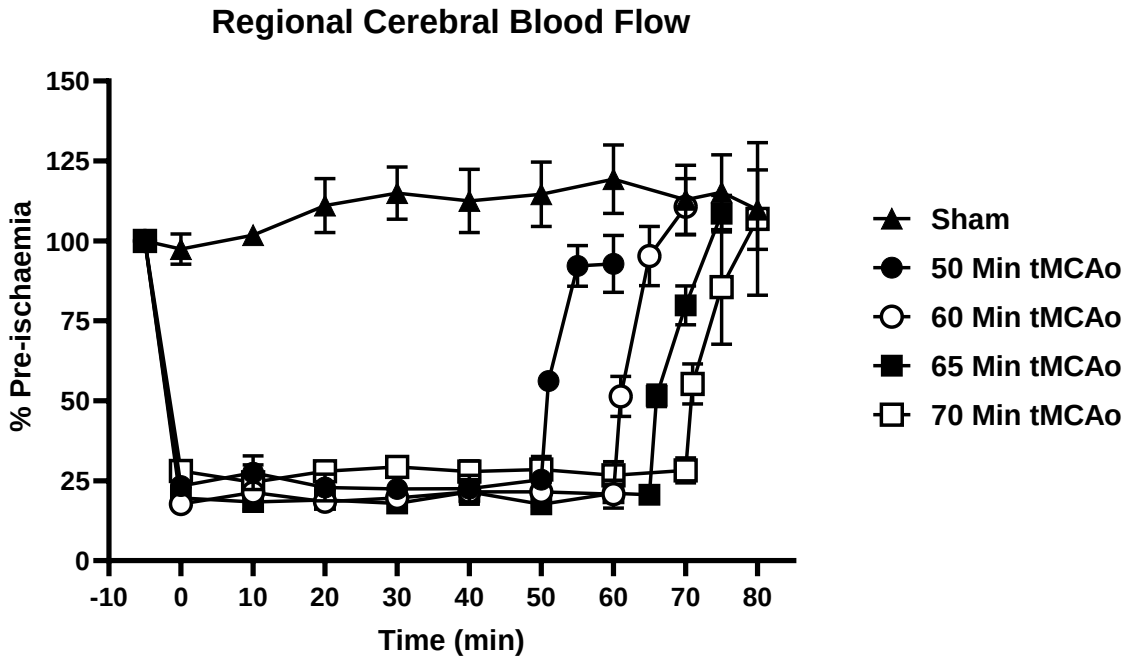

Figure 3-1. Regional cerebral blood flow (rCBF) of mice after different durations of transient middle cerebral artery occlusion (tMCAo) or sham surgery. Animals were subjected to 50-, 60-, 65-, or 70-minutes of tMCAo followed by 3 days of reperfusion. Mice experienced a ≥70% drop in rCBF after filament insertion and a ≥80% restoration of rCBF within the first 10-minutes after filament withdrawal. Data presented as mean ± SEM; sham, 50-, 60-, 65-minutes tMCAo, n=8; 70-minutes tMCAo, n=4. No statistical test was used.

3.3.1 65-minutes of tMCAo produces significantly larger infarcts compared to 50- and 60-minutes, whereas 70-minutes exceeded the ethical severity limits

50- or 60-minutes of tMCAo produced comparable and relatively small infarcts (total infarct volumes: 50-minutes, 11.8±2 mm^3 (6.2%); 60-minutes, 15.1±2 mm^3 (7.9%), $P>0.05$). 65-minutes of tMCAo produced significantly larger infarcts compared to 50- but not 60-minutes of tMCAo (29.3±6 mm^3 (16.4%), $P<0.05$, Figure 3-2A-C). However, there were no statistical differences in oedema volume between all three groups (50-minutes, 6.4±1 mm^3; 60-minutes, 7.9±3 mm^3; 65-minutes, 12.9±4 mm^3, Figure 3-2D). Mice subjected to 70-minutes of tMCAo exceeded the ethical severity limits of the model (as set out in our Home Office Project Licence) and as a result did not reach the scientific endpoint (n=3

were euthanised on day 2 post-stroke, n=1 reached day 3 post stroke and is demarcated with a #). Therefore, the 70-minute group was not included in the statistical comparisons in this dataset and were excluded from the remainder of the study (Figure 3-2B-D).

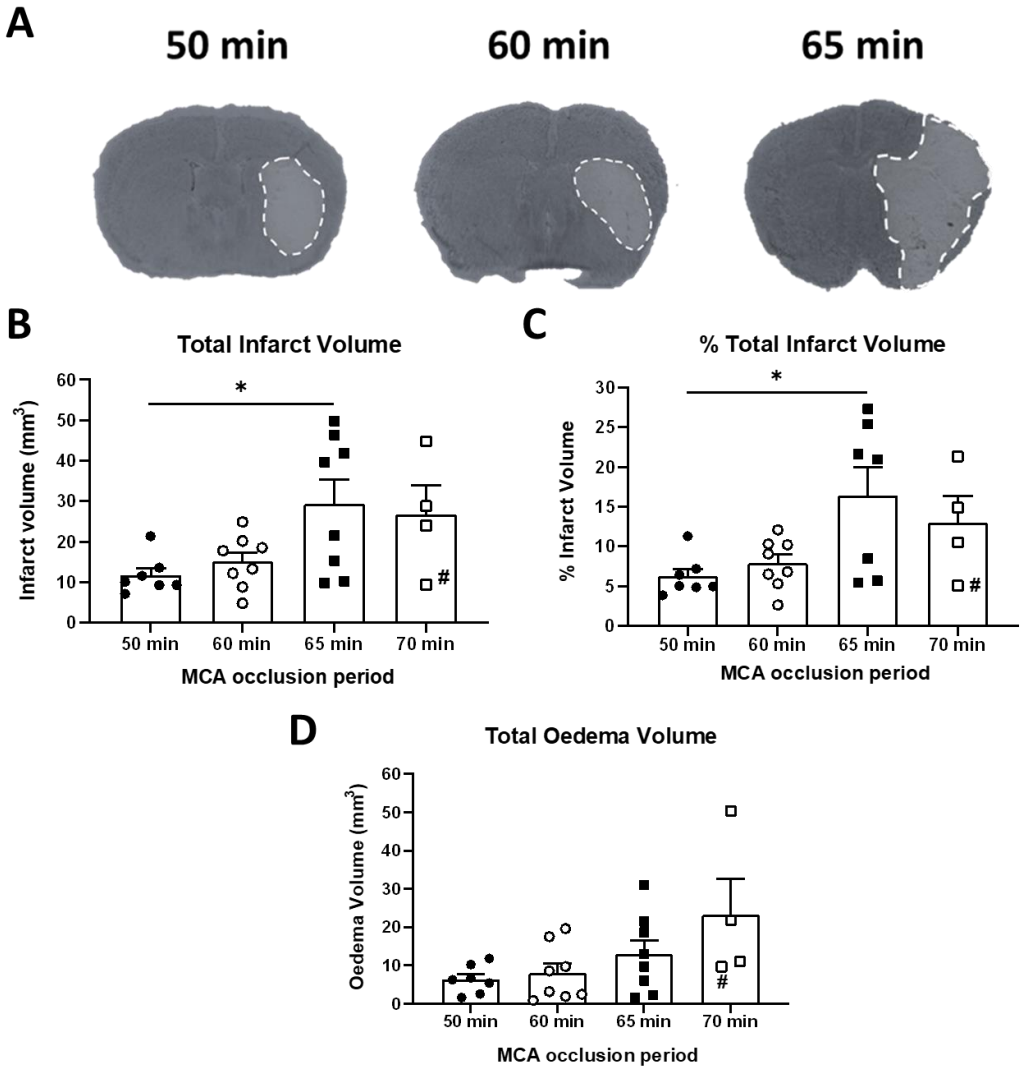

Figure 3-2. Total infarct and oedema volumes after different durations of transient middle cerebral artery occlusion (tMCAo) in mice. Representative images of mouse brain sections after 50-, 60-, and 65-minutes of tMCAo (**A**). Sections from each group were assessed for total infarct volume (**B**), % total infarct volume relative to non-ischaemic hemisphere volume (**C**), and total oedema volume of ischaemic hemisphere relative to non-ischaemic hemisphere (**D**). Data presented as mean ± SEM, 50-minutes tMCAo n=7; 60- and 65-minutes tMCAo n=8, 70-minutes tMCAo (day 2) n=3, 70-minutes tMCAo (day 3; #) n=1, *P<0.05, one-way ANOVA with Dunnett's post hoc test.

3.3.2 65-minutes of tMCAo produces larger cortical infarcts compared to 50-, and 60-minutes, whereas sub-cortical infarcts are comparable between all groups

There was a trend that mice exposed to 65-minute tMCAo group developed larger cortical infarcts compared to mice who underwent 50- or 60-minutes of tMCAo (65-minutes, 19.1±6 mm^3 vs 50-minutes, 2.4±1 mm^3 and 60-minutes, 4.9±2 mm^3; P>0.05), whereas sub-cortical infarcts were comparable between groups (Figure 3-3).

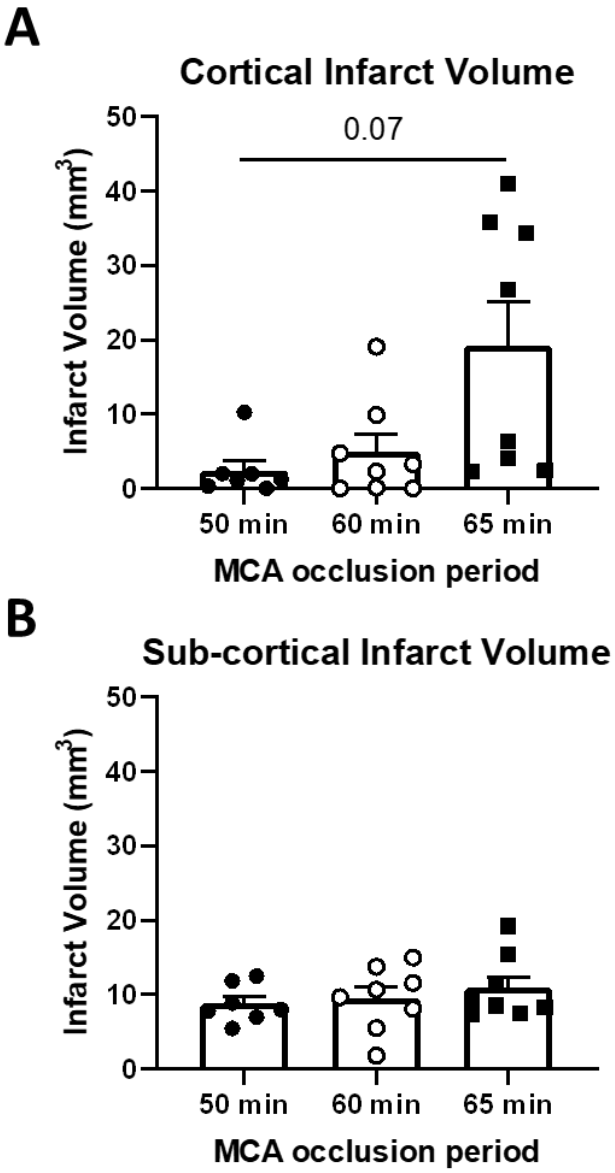

Figure 3-3. Cortical and sub-cortical infarct volumes of mice after different durations of transient middle cerebral artery occlusion (tMCAo). Sections from each group were analysed for infarct volumes in cortical (**A**) and sub-cortical (**B**) brain regions. Data presented as mean ± SEM, 50-minutes, n=7; 60- and 65-minutes, n=8, P>0.05, one-way ANOVA with Dunnett's post hoc test.

3.3.3 Establishing behavioural tests for measuring differences in neurological outcomes after increasing durations of focal cerebral ischaemia in mice

When assessing neurological and functional outcomes, we found that nest building activity scores were significantly lower in mice after 60- or 65-minutes of tMCAo but not 50-minutes tMCAo compared to their nest building activity scores pre-stroke and compared with sham mice post-surgery (Figure 3-4A). With respect to mNSS scores, mice after 65-minutes of tMCAo scored significantly higher on day 1 and 3 post-stroke compared to sham mice post-surgery, whereas mice after 50- and 60-minutes tMCAo only scored higher on day 3 (Figure 3-4B). For all tMCAO groups, there were no significant differences between forelimb asymmetry values (cylinder and foot fault tests, Figure 3-4C-D) measured on day

1 or day 3 post-stroke compared with values measured from sham mice post-surgery. Furthermore, apart from the foot fault asymmetry scores of mice exposed to 65-minutes of tMCAo (Figure 3-4D, $P<0.05$), there were no significant differences between values on day 1 vs day 3 within each of the tMCAo groups (Figure 3-4C-D).

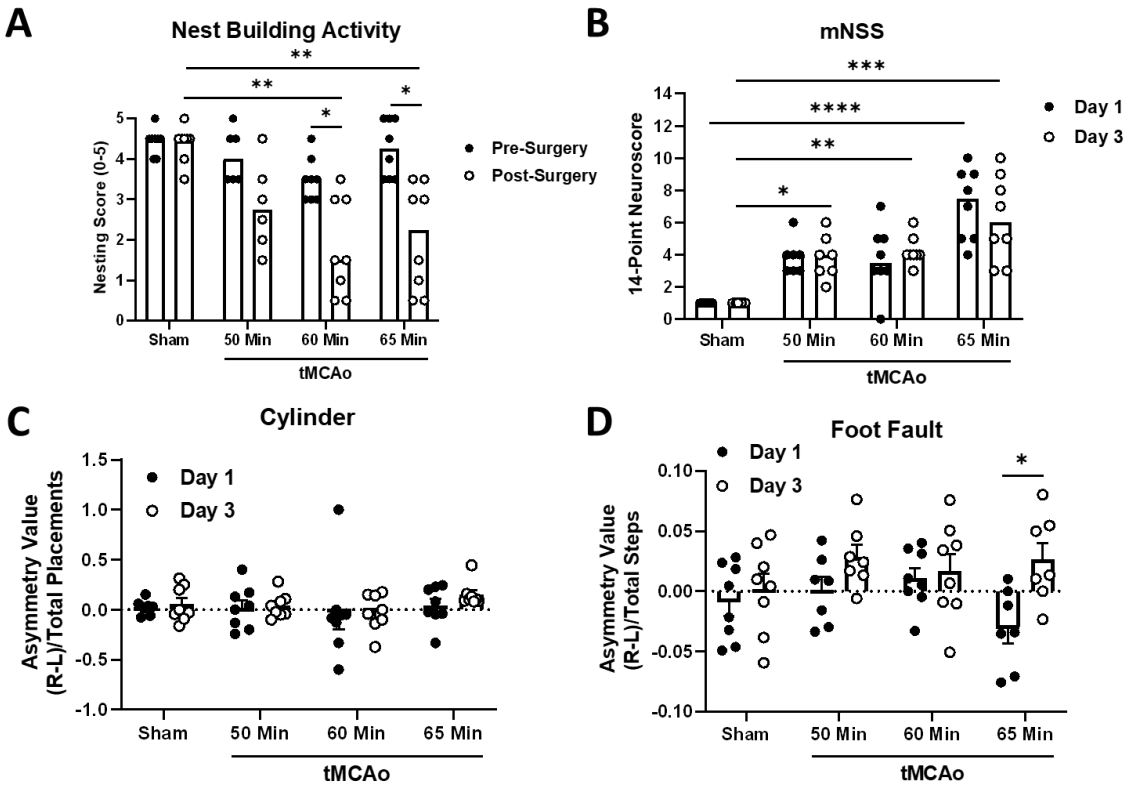

Figure 3-4. Neurological and functional outcomes of mice after different durations of transient middle cerebral artery occlusion (tMCAo) or sham surgery. Nest building activity (**A**) was assessed in stroke and sham mice pre-surgery and on day 2 post-surgery, whereas the modified neurological severity score (mNSS; **B**) and forelimb asymmetry tests [cylinder (**C**), and foot fault (**D**)] were performed on day 1 and day 3 post-surgery. Nest building activity data presented as median, n=7-8, **P*<0.05, ***P*<0.01, Kruskal-Wallis multiple comparisons post hoc test (between the sham and tMCAo groups both pre- and post-surgery), Wilcoxon matched pairs test (pre- vs post-stroke in each group); mNSS data presented as median, n=7-8, **P*<0.05, ***P*<0.01, ****P*<0.001, *****P*<0.0001, Kruskal-Wallis multiple comparisons test (day 1 and day 3 scores between groups), Wilcoxon matched pairs test (day 1 vs day 3 scores in each group). Cylinder and foot fault test data presented as mean ± SEM, n=7-8, **P*<0.05, one-way ANOVA with Tukey's post hoc test (asymmetry scores between sham and tMCAo groups on both day 1 and 3 post-surgery), paired t-test (comparison between day 1 and day 3 post-surgery for all groups).

3.3.4 Mice after 65-minutes of tMCAo display neurological impairment and exhibit significantly reduced nest building activity compared to sham mice post-surgery

Next, we assessed neurological and functional outcomes in mice after 65-minutes tMCAo compared to pre-stroke measurements. As previously mentioned, mice after 65-minutes tMCAo displayed significantly reduced nest building activity compared to pre-stroke levels and compared to sham mice post-surgery (Figure 3-5A). With regards to mNSS score, mice after 65-minutes tMCAo scored significantly higher at day 1 but not day 3 compared to

pre-stroke scores (Figure 3-5B). There were no differences with respect to forelimb asymmetry (cylinder and foot fault tests) at day 1 and day 3 post-stroke compared to pre-stroke levels, however, pre-post analysis (normalisation of day 1 and day 3 measurements to pre-stroke measurements) showed that forelimb asymmetry assessed using the foot fault test was significantly greater on day 1 compared to day 3 post-stroke (Figure 3-5C-D).

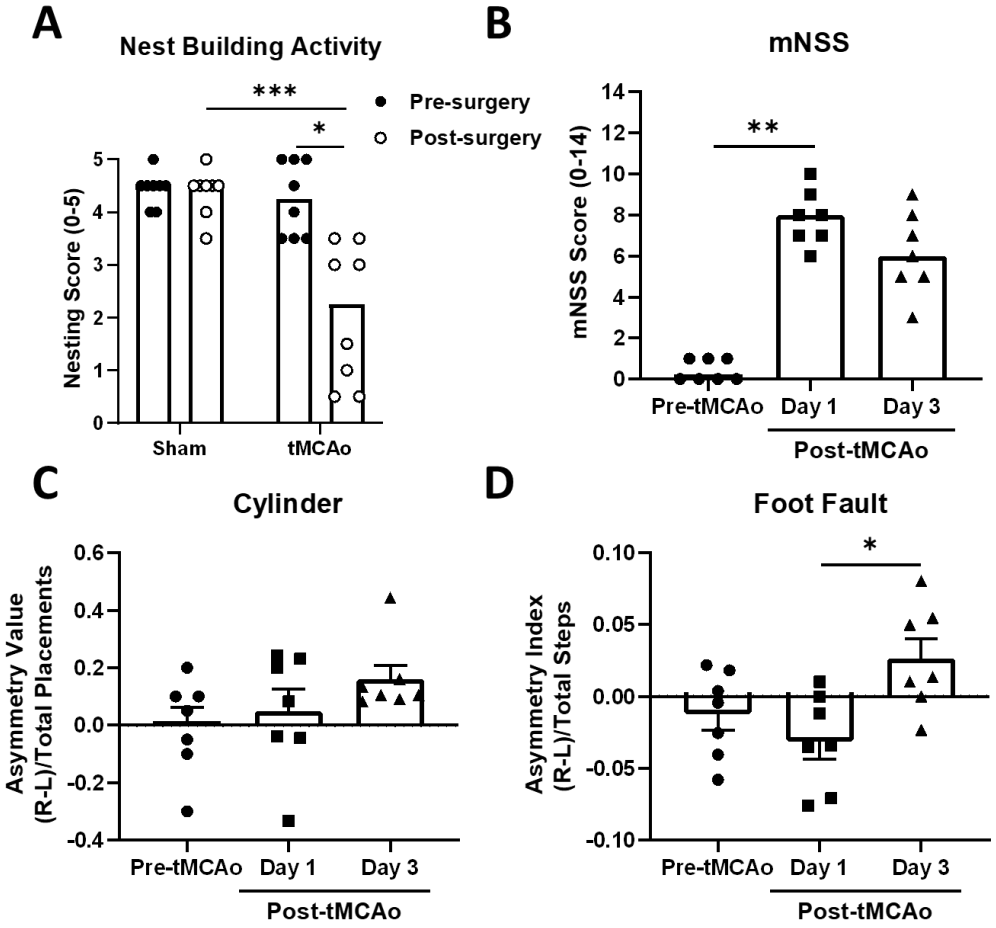

Figure 3-5. Neurological and functional assessments of mice after 65-minutes of transient middle cerebral artery occlusion (tMCAo) or sham surgery. Nest building activity (**A**) was assessed pre- and post-surgery in mice after 65-minutes of tMCAo and in mice after sham surgery. The modified neurological severity score (mNSS; **B**) and forelimb asymmetry tests [cylinder (**C**) and foot fault tests (**D**)] were also assessed prior to and on day 1 and day 3 after 65-minutes of tMCAo. Nest building activity data presented as median, n=7, **P*<0.05, ****P*<0.001, Mann-Whitney U test (comparison between groups both pre- and post-surgery), Wilcoxon matched pairs test (pre- vs post-surgery within each group); mNSS data presented as median, n=7, ***P*<0.01, Friedman test with Dunn's multiple comparisons (comparison of paired pre-stroke and post-stroke [day 1 and day 3] scores); repeated measures one-way ANOVA with Tukey's multiple comparisons test (comparison of paired pre-stroke and post-stroke [day 1 and day 3] asymmetry values).

3.3.5 Semi-quantification of TUNEL-positive cells in the infarct core and peri-infarct of 65-minute tMCAo mice

In addition to measuring infarct and oedema volumes, we semi-quantified the number of TUNEL-positive cells per mm^2 in the infarct core and peri-infarct brain tissue regions in

mice on day 3 after 65-minutes of tMCAo. We found that the number of TUNEL-positive cells was significantly greater in the infarct core compared to the peri-infarct (core 0.6±0.06 vs peri-infarct 0.3±0.02 cells/mm^2; *P*<0.01; Figure 3-6).

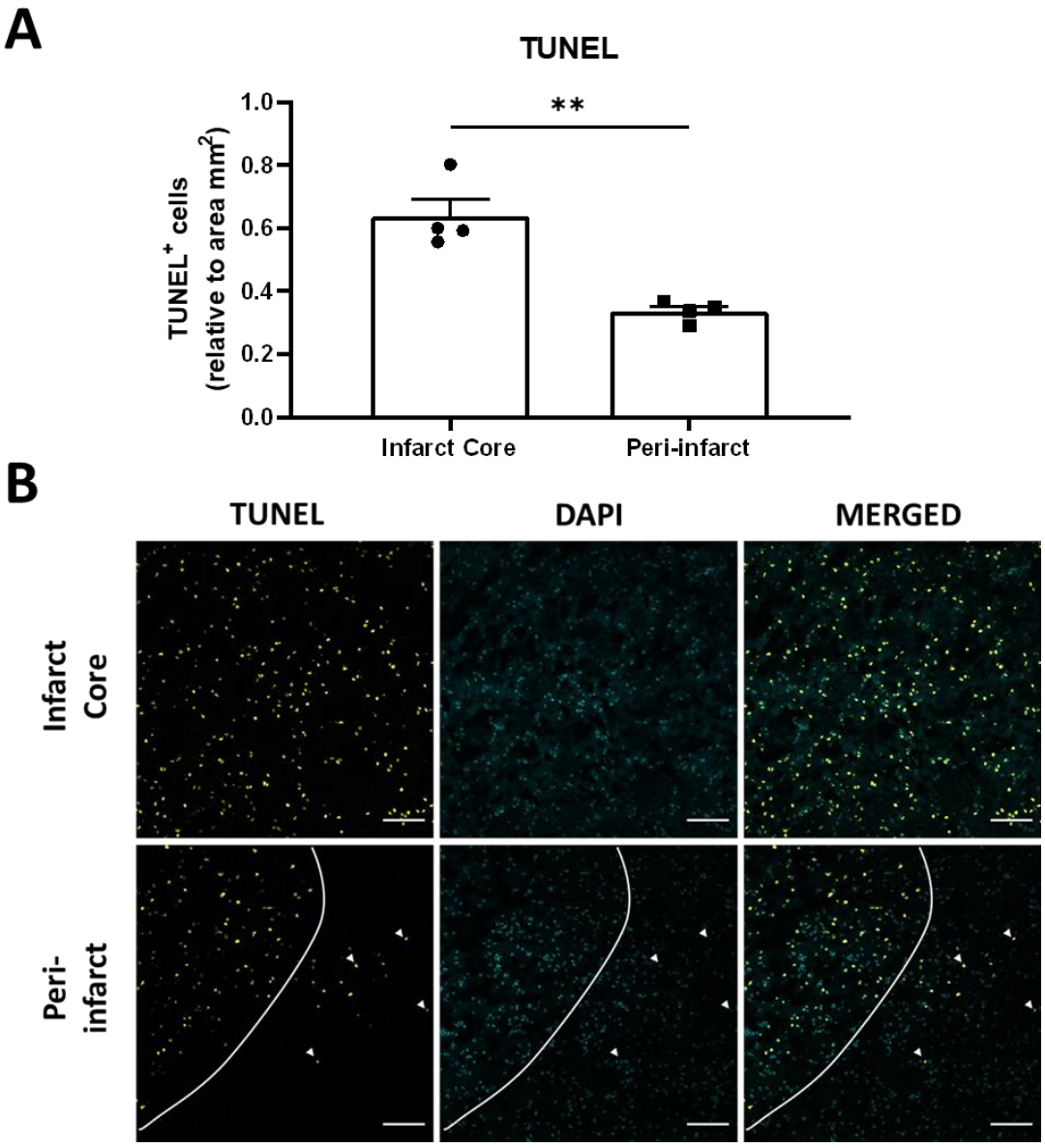

Figure 3-6. Cell death in the infarct core and peri-infarct regions in mice after 65-minutes transient middle cerebral artery occlusion (tMCAo). Representative images of the infarct core and peri-infarct regions of brains from mice after 65-minutes tMCAo (**B**; bottom). White lines denote the border between infarct core and peri-infarct tissue, white arrow heads denote TUNEL-positive cells in the peri-infarct tissue. Also shown is the semi-quantification of TUNEL-positive cells per mm^2 in infarct core and peri-infarct regions (**A**) and were quantified using the Cell Counter tool on ImageJ analysis software. Scale bars are 100 µm. Data presented as mean ± SEM, n=4, ***P*<0.01, paired t-test.

3.3.6 tMCAo mice experience greater weight loss compared to sham mice, and weight loss positively correlated with infarct and oedema volumes

Body weights were measured prior to stroke or sham surgery, and daily after surgery until the scientific endpoint (Figure 3-7A). On day 3 after post-surgery, % net body weight loss was significantly greater in 50-, 60-, and 65-minute groups compared to sham control

mice (sham, 2.4±0.5; 50-minutes, 7.6±1.1; 60-minutes, 14.1±1.8; 65-minutes, 11.2±1.4 %; *P*<0.05). To determine if there is a relationship between infarct and oedema volumes and % net body weight loss, a simple linear regression and correlation was performed using data from mice in all tMCAo groups. We found that there was a weak positive correlation between infarct (R^2 = 0.225, *P*<0.05) or oedema (R^2 = 0.284, *P*<0.01) volumes and % net body weight loss (Figure 3-7C-D).

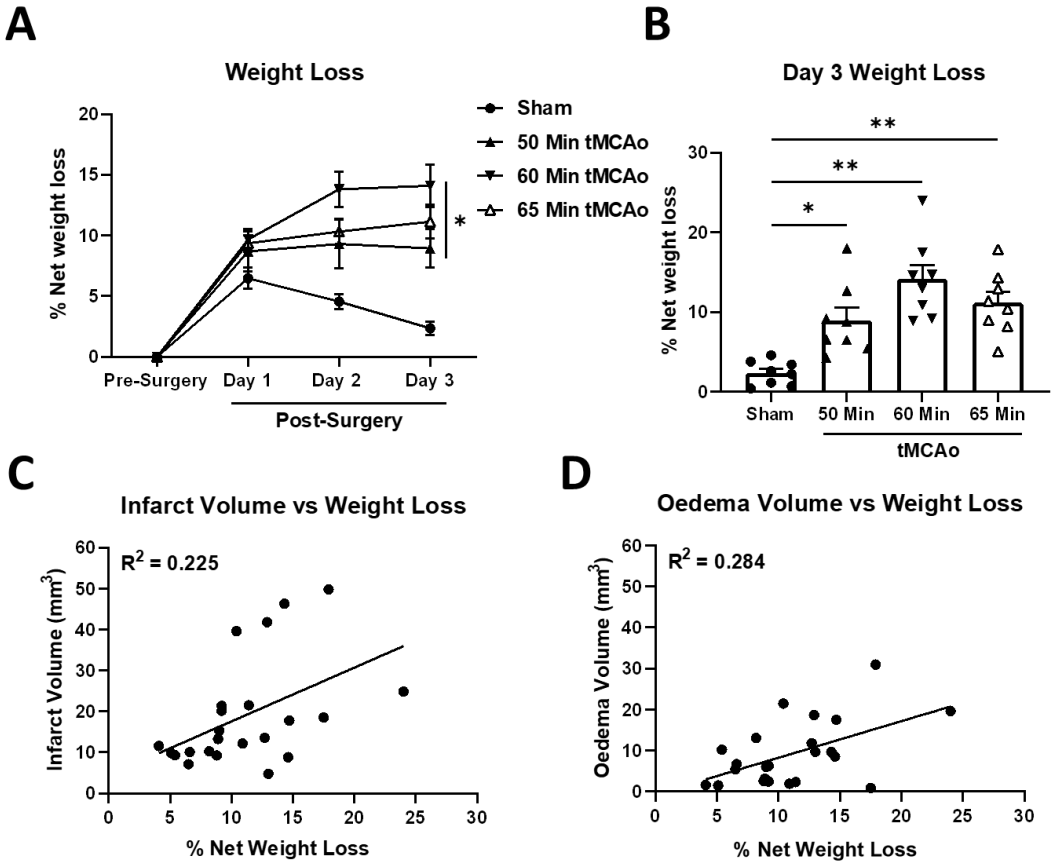

Figure 3-7. Net body weight loss of mice following transient middle cerebral artery occlusion (tMCAo) or sham surgery and the relationship between infarct and oedema volumes and net body weight loss. Mice were subjected to 50-, 60-, or 65-minutes tMCAo and allowed to recover for 3 days. Body weights were measured prior to and every day post-surgery until the scientific end-point and expressed as % net weight loss relative to pre-surgery weights (**A**). % weight loss on day 3 post-surgery (**B**). Scatter plots showing the relationship between infarct or oedema volumes and % net weight loss (**C-D**). Weight loss data presented as mean ± SEM, n=7-8, **P*<0.05, two-way ANOVA with Tukey's multiple comparisons post hoc test; day 3 weight loss data presented as mean ± SEM, n=7-8, **P*<0.05, ***P*<0.01, Brown-Forsythe and Welch ANOVA with Dunnett's T3 multiple comparisons post hoc test; infarct and oedema correlation data, n=23, **P*<0.05, ***P*<0.01, simple linear regression and correlation.

3.4 Discussion

In this study, I aimed to identify an appropriate duration of tMCAo in mice to achieve clinically relevant stroke outcomes without exceeding the ethical severity limits as stipulated by our Home Office Project Licence. Mice were subjected to 50-, 60-, or 65-minutes of tMCAo or sham surgery and then histological (infarct, oedema, and apoptosis) and neurological outcomes were assessed. The key finding of this study is that 65-minutes of tMCAo produced infarct sizes that were comparable to those typically found in human stroke, which spanned both cortical and sub-cortical brain regions. Furthermore, mice undergoing 65-minutes tMCAo exhibited neurological and functional deficits measured by a range of behavioural tests, and their severities did not reach the ethical severity limits of the Home Office Project Licence.

As mentioned previously, survivable human strokes are typically small, ranging from 28–80 mm^3, or equating to approximately 4–14% of the ischaemic hemisphere (Carmichael, 2005). Therefore, to improve the translation of findings from experimental stroke research, a key challenge for researchers is to identify a suitable model, and in the case of the tMCAo model, an appropriate duration which produced infarcts and associated functional deficits that are comparable to that found in human strokes. Furthermore, this is made even more complicated by the clear need to adhere to the ethical severity limits stipulated in the relevant ethical approvals for studies using pre-clinical stroke models. Historically our laboratory generated reproducible and clinically relevant sized infarcts in C57BL6/J mice (30- to 40-minutes tMCAo) using ketamine and xylazine as anaesthetic agents (Jackman *et al.*, 2009; Broughton *et al.*, 2013, 2014; Ku *et al.*, 2016). However, inhaled anaesthetic agents such as isoflurane are the preferred method of administering general anaesthesia in pre-clinical research (Percie du Sert *et al.*, 2017). Notably, however, several studies have shown that isoflurane exerts neuroprotective properties in experimental models of ischaemic stroke (Kawaguchi, Furuya and Patel, 2005; Y. Zhou *et al.*, 2010; Zhang *et al.*, 2010; Jiang *et al.*, 2017). Indeed, in our initial pilot work, we found that mice after 40-minutes tMCAo under anaesthesia with isoflurane exhibited very small infarcts (6±2.5 mm^3; section 8.6 of Appendix) compared with infarct sizes in our published studies where the MCA was occluded for approximately 30-minutes under anaesthesia with injectables (Jackman *et al.*, 2009; Broughton *et al.*, 2013, 2014; Ku *et al.*, 2016). Therefore, in this study we measured infarct and oedema volumes in mice after longer durations of tMCAo (50-, 60-, and 65-minutes) under anaesthesia with isoflurane. Additionally, we also assessed outcomes in mice after 70-minutes of tMCAo, however, a large portion (75%) of these mice exceeded the ethical severity limits and as a result, data collected from these animals was excluded from statistical comparisons, and experiments using this occlusion period were discontinued. As one might predict, we found that total infarct volumes were significantly larger in mice after 65-minutes tMCAo

which were comparable in size to human strokes (approximately 28 mm^3 or 16% of hemisphere) compared to mice after 50- and 60-minutes tMCAo. This effect is largely explained by larger infarct volumes in the cortical tissue in the 65-minute tMCAo group, whereas sub-cortical infarct volumes were comparable in all groups. Furthermore, using TUNEL staining, which fluorescently labels DNA breaks of apoptotic nuclei, I found that the number of TUNEL-positive cells in the peri-infarct region was significantly lower compared to the infarct core region of brains from 65-minute tMCAo mice. Therefore, this duration of tMCAo produces a peri-infarct which will allow for the testing of neuroprotective agents. Interestingly, we observed that the variability was greater in the 65-minute group (SEM: 5.9 mm^3) compared with the shorter durations of tMCAo (SEM: 50-minutes, 1.8 mm^3; 60-minutes, 2.3 mm^3), and in fact there appeared to be two distinct populations in the 65-minute tMCAo group. This could be explained by differences in the recruitment of collateral vessels or by technical differences (e.g., clamp time during insertion of a filament into the external carotid arteries) within the 65-minute group. However, one might predict that these factors would similarly influence variability of infarct size in the shorter tMCAo groups. Interestingly, we observed a noticeable but non-significant difference in infarct size in mice after 60- versus 65-minutes of tMCAo. Many studies have reported significantly larger infarcts after long durations of tMCAo (~60-minutes) compared to shorter durations (≤30-minutes) (McColl *et al.*, 2004; Engel *et al.*, 2011), however, another study documented that a difference of between 10- and 15-minutes of tMCAo determined whether mice exhibited detectable infarcts (Pedrono *et al.*, 2010). Therefore, whilst there is only a difference in occlusion period of 5-minutes between these two groups, this short additional time appears to significantly worsen stroke outcomes, at least in half of the cohort of animals that underwent 65-minutes of tMCAo.

Another key aim of this study was to evaluate neurological and functional outcomes in mice after the different durations of tMCAo. There are a plethora of tests which can evaluate different cognitive or functional behaviours, and selecting appropriate tests that are capable of detecting deficits after tMCAo in mice is paramount. Nest building is an innate behaviour of rodents and is important for shelter, reproduction, and heat conservation (Deacon, 2006). Additionally, nest building is commonly used as an indicator of general health and wellbeing (Gaskill *et al.*, 2013), as well as depressive-like behaviours (Haley *et al.*, 2020), which can easily be studied in rodent models of neurological disease such as ischaemic stroke. For example, a recent study reported nest building to be a reproducible and long-term test for evaluating stroke outcomes in mice, and impairment of nest building activity was proportional to duration of tMCAo (Yuan *et al.*, 2018). In this study, we similarly found that nest building activity was significantly impaired after 60- and 65-minutes of tMCAo, and there was a non-significant trend for

nest building to be impaired in mice after 50-minutes tMCAo. Another test that was evaluated was the mNSS test which is a composite scoring system for rodents after cerebral ischaemia (maximum 14 for mice, 18 for rats). It is often used by researchers to assess stroke severity and neurological impairments by combining a series of comprehensive motor, sensory, reflex, and balance tests (Schaar, Brenneman and Savitz, 2010; Ruan and Yao, 2020). Correspondingly, a recent study demonstrated that mNSS scores in mice increased in relation to infarct size after tMCAo (Bieber *et al.*, 2019). We have shown here that mice in all stroke groups scored significantly higher on day 1 post-stroke compared to sham mice, and that mice after 65-minutes tMCAo also scored significantly higher on day 3 post-stroke compared to sham mice. Therefore, the mNSS test can detect neurological and functional deficits in our clinically relevant mouse model of ischaemic stroke. In addition to the nest building and mNSS tests, we evaluated forelimb asymmetry using the cylinder and foot fault tests. A common consequence of ischaemic stroke in humans and rodents is the asymmetrical function of the arms or forelimbs, respectively. The cylinder test measures spontaneous forepaw placements on the wall of a transparent cylinder, and mice will display asymmetrical use of the forepaws towards the unaffected forelimb. An advantage of the cylinder test is its ease of use and objective scoring, as well as a lack of required pre-training. However, inter-animal forepaw bias can be high and therefore baseline measurements are recommended for all animals (Schaar, Brenneman and Savitz, 2010). In this study we found that the cylinder test did not detect any forelimb asymmetries in mice from any of the MCAo groups between day 1 and 3 post-surgery and compared to sham control mice. It is conceivable that performing the test during the animals' 12-hour light cycle influenced their explorative behaviour. Indeed, rodents are nocturnal animals, and it is therefore recommended that the test be performed during the dark cycle (Schaar, Brenneman and Savitz, 2010). Alternatively, it is conceivable that this test is not sensitive enough to detect deficits after tMCAo, however, a previous study detected significant forelimb asymmetries in mice up to day 15 after 90-minutes of tMCAo (Li *et al.*, 2004). An advantage of the foot fault test is that deficits can be observed in both short and long-term rodent models of stroke without requiring pre-training. Also, numerous studies have demonstrated increased forelimb asymmetry toward the stroke-affected forelimb in rodent models of stroke (Zhang *et al.*, 2002; Liu *et al.*, 2014; Ruan and Yao, 2020). Here, we found that mice after 65-minutes tMCAo display significant forelimb asymmetry on day 1 compared to day 3 but not pre-stroke, whereas no asymmetries were observed in all other groups. One potential explanation for this is the presence of larger cortical infarcts in the 65-minute tMCAo group relative to the 50- and 60-minute tMCAo groups where cortical infarcts were either not present or were very small in size. Indeed, the somatosensory and motor brain regions are located in the cortex of the brain and

therefore it is likely that deficits would only be observed in animals with infarcts affecting those brain regions (Barth, Jones and Schallert, 1990; Schaar, Brenneman and Savitz, 2010). Given that sub-cortical infarcts were similar between all groups, it is recommended that tests which evaluate neurological impairments of sub-cortical brain regions are used in future studies.

Weight loss commonly occurs after ischaemic stroke in rodents (Springer *et al.*, 2014; Haley *et al.*, 2017, 2020) and humans (Doehner *et al.*, 2013; Scherbakov *et al.*, 2019) and is characterised by global tissue wasting of muscle and fat at least in the acute phase post-stroke (Scherbakov, Dirnagl and Doehner, 2011). The mechanisms which underpin weight loss following ischaemic stroke remain unclear, however, some but not all researchers have proposed that it may arise from systemic pathophysiological mechanisms that are triggered by ischaemic brain injury. Most importantly, weight loss appears to be an important outcome measure in patients after stroke (FOOD Trial Collaboration, 2003; Jönsson *et al.*, 2008; Scherbakov, Dirnagl and Doehner, 2011). Notably, however, there are conflicting reports as to whether a relationship exists between ischaemic brain injury (infarct size) and net weight loss following experimental stroke (Scherbakov, Dirnagl and Doehner, 2011; Cai *et al.*, 2015; Haley *et al.*, 2017, 2020). In the present study we found that mice who underwent tMCAo (50-, 60-, 65-, and 70-minutes) exhibited greater weight loss compared to sham control mice. Mice subjected to 70-minutes of tMCAo exceeded the ethical severity limits of the study (≥20% net weight loss on or before day 3) and were therefore excluded from comparisons. Notably, we found a weak but significant correlation between both infarct and oedema volumes and weight loss in mice post-tMCAo, indicating that weight loss in rodents post-stroke is another important outcome measure to report. Nevertheless, the biological explanations for the positive correlation between weight loss and infarct or oedema volumes are unknown and thus, further investigation is needed to elucidate the mechanisms which may be responsible for the weight loss that was observed in our tMCAo mice.

It is worth highlighting the usefulness of mouse models in pre-clinical research. The vast similarities between the human and mouse genomes are well established, and translational mouse studies are considered to be a more ethically acceptable option for pre-clinical stroke studies which encompass a need of high throughput and cost-efficiency. Additionally, an advantage of using the inbred C57BL6/J mouse strain is they should be genetically identical and can be easily genetically modified. As such, the C57BL6/J mouse is becoming the most widely published mouse strain in pre-clinical research (Bryant, 2011). Thus, an advantage of this study is the use of C57BL6/J mice, which are a robust and highly characterised mouse model in pre-clinical studies of cerebral ischaemia-reperfusion. However, a key limitation of the work presented in this chapter is that tMCAo was induced in young, healthy male mice, which does not truly reflect the heterogenous

nature of human stroke. Indeed, stroke pathophysiology in humans is highly complex and is influenced by numerous cardiovascular risk factors and comorbidities such as age and hypertension. Additionally, there are well established sex differences in ischaemic stroke. For example, it was shown that young female C57BL6/J mice have smaller infarcts compared to their male counterparts (Nowak and Mulligan, 2019), which is consistent with the neuroprotective and vasoprotective effects of the female sex hormone oestrogen (Zhang *et al.*, 1998; Hurn and Brass, 2003; Lisabeth and Bushnell, 2012). Thus, investigating stroke using models that incorporate comorbidities, and performed in both sexes, would improve clinical translation of experimental findings. Another limitation of the present study is the lack of the formation of an embolus or thrombus to induce cerebral ischaemia-reperfusion using the tMCAo model. For example, the photothrombotic, embolic clot, and thromboembolic clot models of ischaemic stroke mimic human stroke more closely compared to tMCAo, which also allow for the testing of rtPA and other thrombolytic agents in combination with neuroprotective agents (Macrae, 2011; Liu *et al.*, 2017). In contrast, the photothrombotic model is limited by the lack of recruitment of collateral blood vessels and most importantly the formation of an ischaemic penumbra which is the primary focus point of neuroprotective stroke research (Liu *et al.*, 2017; Uzdensky, 2018). Moreover, the embolic and thromboembolic models exhibit poor reproducibility due to the risk of multifocal ischaemia and high variability in the location and size of the infarct (Macrae, 2011). Notably, over 50% of all ischaemic stroke cases occur as a result of occlusion of the MCA, thus, models that can achieve reproducible strokes in the territory supplied by the MCA are regarded as clinically relevant models (Ng *et al.*, 2007). As such, the distal MCAo (dMCAo) model is performed in the MCA territory which involves the ligation or coagulation of a distal branch of the MCA, however, it only yields reproducible cortical infarcts when combined with temporary bilateral occlusion of both CCAs (Chen *et al.*, 1986; Wayman *et al.*, 2016). Furthermore, permanent ligation or coagulation of the distal branch does not adequately mimic the majority of ischaemic stroke cases, and the global ischaemia achieved by the bilateral CCA ligation does not commonly occur in humans. As a result, the tMCAo model adequately mimics the majority of strokes via simulation of spontaneous reperfusion by withdrawal of the filament, which was shown to occur in 42-77% of stroke patients (Baird *et al.*, 1994; Jørgensen *et al.*, 1994; Bowler *et al.*, 1998). Moreover, reperfusion injury is a common secondary complication after stroke which can also be mimicked by tMCAo. Thus, the tMCAo model is an easily modifiable procedure whereby the severity of stroke outcomes can be altered easily by changing the duration of ischaemia, thereby supporting the use of the tMCAo model in this study.

In summary, we have demonstrated that stroke outcomes worsen with increased durations of ischaemia in mice. Additionally, we established that a duration of 65-minutes tMCAo

produces infarct volumes of approximately 28 mm^3 (16%) and is accompanied by detectable neurological and functional deficits in mice. Therefore, we have successfully achieved a clinically relevant model of ischaemic stroke in mice.

Chapter 4 Examining the roles of the ADMA-DDAH1 pathway in ischaemic stroke pathogenesis

4.1 Introduction

In the brain, nitric oxide (NO) is synthesised by the NO synthase (NOS) enzymes, neuronal NOS (nNOS; neurons), inducible NOS (iNOS; numerous cell types including immune cells), and endothelial NOS (eNOS; endothelial cells). It is well documented that NO has a vast number of functions in the brain, which is largely determined by the cellular source and the concentration of NO (Forstermann and Sessa, 2012). For example, neurons and endothelial cells produce relatively low levels of NO for long-term potentiation during synaptic transmission and for regulating vascular tone and cerebral blood flow, respectively. In contrast, larger amounts of NO are produced by iNOS when immune cells and other cell types become activated during immune responses to injury or infection. However, NO has dual roles after ischaemic stroke. High concentrations of nNOS- and iNOS-derived NO exacerbate ischaemic injury in the hyperacute and chronic stages, whereas eNOS-derived NO is considered protective during all stages of stroke by promoting cerebral blood flow, angiogenesis, and neurogenesis (Chen *et al.*, 2017).

The methylarginines asymmetric dimethylarginine (ADMA), N_G-monomethyl L-arginine (L-NMMA), and symmetric dimethylarginine (SDMA) are methylated derivatives of the semi-essential amino acid L-arginine produced by the protein arginine methyltransferase (PRMT) enzymes. Both ADMA and L-NMMA are produced by the type I PRMTs and are released into the cytosol following proteolysis. Importantly, these methylarginines are endogenous inhibitors of NOS and can therefore exert significant effects in the brain, whereas SDMA is produced by the type II PRMTs and does not inhibit NOS (Couto e Silva *et al.*, 2020). ADMA is found at significantly higher concentrations in plasma and tissues compared to L-NMMA and is therefore considered the most important methylarginine (Leone *et al.*, 1992). Additionally, the dimethylarginine dimethylaminohydrolase (DDAH) 1 and 2 enzymes are responsible for metabolising approximately 80% of ADMA.

In ischaemic stroke patients, ADMA levels are elevated in the cerebrospinal fluid (Brouns *et al.*, 2009). However, the mechanism responsible for elevated ADMA after ischaemic stroke is unclear. One potential mechanism responsible for elevated ADMA is by increased activity or expression of the type I PRMT enzymes followed by the increased release of ADMA following proteolysis. Examples of type I PRMTs expressed in the brain are PRMT1, PRMT2, PRMT4 (CARM1), and PRMT8. Alternatively, ADMA levels may accumulate in the ischaemic brain as a consequence of decreased DDAH activity or expression. Importantly, it is well documented that both type I PRMT and DDAH enzyme activities are modulated by oxidative stress and inflammation, both of which are key pathological features of ischaemic stroke (Wu *et al.*, 2020). For example, it was shown that gene expression of type I PRMTs and ADMA levels were increased in human endothelial cells in response to native and oxidised LDL, an effect that was blocked by co-treatment with an antioxidant drug (Bӧger *et al.*, 2000). On the other hand, the DDAH enzymes are at risk of impaired

activity due to the presence of a reactive cysteine residue in the active site and may be vulnerable to oxidative and nitrosative stress. For example, one study showed that DDAH was inhibited by S-nitrosylation after treatment with NO donors (Leiper *et al.*, 2002), whereas another study reported that the decreased DDAH activity and accumulation of ADMA found in endothelial cells cultured with high glucose was reversed by antioxidants (Lin *et al.*, 2002). These concepts are further supported by a study which showed that the antioxidative drug Probucol markedly attenuated the inhibitory effect of oxidative stress on endothelial DDAH activity, and also significantly inhibited the elevation of PRMT1 expression in endothelial cells exposed to oxidative stress (Jiang *et al.*, 2006). Taken together, these findings suggest that increased ADMA levels after ischaemic stroke may result from increased type I PRMT activity and/or reduced DDAH activity through oxidative stress.

Causal roles for elevated ADMA levels have been established in cardiovascular disease, including hypertension, cardiac disease, and atherosclerosis (Achan *et al.*, 2003; Jacobi *et al.*, 2010). Elevated ADMA levels are also associated with increased risk of stroke and worse patient outcomes (Yoo and Lee, 2001; Wanby *et al.*, 2006; Mamatha *et al.*, 2011; Worthmann *et al.*, 2011; Appel *et al.*, 2018). Furthermore, loss-of-function DDAH1 polymorphisms are associated with increased risk of ischaemic stroke (Ding *et al.*, 2010) as well as delayed cerebral ischaemia after subarachnoid haemorrhage (SAH) (Hannemann *et al.*, 2020). However, there is a lack of evidence showing causality between ADMA, DDAH1, and ischaemic brain injury. To date, only a small number of studies have tested for a causal role of the ADMA-DDAH1 pathway in ischaemic stroke. One study investigated the effect of overexpressing human DDAH1 on stroke outcome in mice and found no differences in ischaemic brain injury between transgenic and control animals (Leypoldt *et al.*, 2009). However, neither DDAH1 activity nor brain ADMA levels were elevated in these animals. Other studies have reported that global deletion of DDAH1 worsens stroke outcomes in rats, however, there were numerous confounding factors observed in these studies (Zhao *et al.*, 2021, 2022). For example, mean arterial blood pressure was elevated at baseline and post-stroke in DDAH1 knockout rats, and the extent of cerebral hypoperfusion following stroke induction was significantly greater in these animals compared to control rats. As previously mentioned, eNOS-derived NO plays a protective role in ischaemic stroke. Importantly, exogenous ADMA was shown to increase cerebrovascular tone and impair cerebral artery function of rat basilar arteries by disrupting eNOS-NO signalling (Faraci, Brian and Heistad, 1995). Also, ADMA infusion was shown to reduce cerebral perfusion while increasing arterial stiffness in healthy humans (Kielstein *et al.*, 2006). Therefore, taken together, we hypothesise that elevated ADMA levels worsen ischaemic brain injury and functional impairment by disrupting crucial eNOS-derived NO signalling in cerebral arteries.

The aims of this study were first to explore the mechanisms responsible for elevated ADMA levels after ischaemic stroke in mice by examining the effect of cerebral ischaemia-reperfusion on expression levels of type I PRMT and DDAH enzymes in mice, and in human cerebral microvascular endothelial cells exposed to ischaemia-like conditions *in vitro*. Secondly, using the selective DDAH1 inhibitor, L-257, we examined the effect of elevated ADMA levels on ischaemic stroke outcomes in mice after cerebral ischaemia-reperfusion, which included ischaemic brain injury, apoptosis, and neurological and functional impairment.

4.2 Materials and methods

4.2.1 Animals

In this chapter, a total of 120 male C57BL6/J mice (8-15 weeks of age) were used, including 40 for determining changes of DDAH and PRMT protein expression at 24- and 72-hours post-ischaemia or sham surgery, 16 for quantifying methylarginine levels after vehicle or L-257 treatment, 22 for measuring haemodynamics using tail cuff plethysmography or radiotelemetry, 18 for vascular function studies, and 24 for examining ischaemic stroke outcome after vehicle or L-257 treatment. However, 4 mice (n=2 each for vehicle- and L-257-treated groups) were excluded from the assessment of ischaemic stroke outcomes, and the reasons for exclusions are described later in this chapter.

4.2.2 Determining the effect of tMCAo on protein expression levels of DDAH and PRMT enzymes

4.2.2.1 Transient MCAo

Mice were subjected to tMCAo for 65-minutes using a monofilament, as described in section 2.1.2 of General Methods. Following either 24 or 72 hours of reperfusion, mice were euthanised by a rising concentration of CO_2 (Schedule 1 of the Act), followed by removal of the brains and their storage at -80°C. Sham-operated mice were exposed to the same duration of anaesthesia as tMCAo mice and were allowed to recover for 24- or 72-hours.

4.2.2.2 Protein extraction from frozen tMCAo- and sham-operated mouse brain hemispheres

Details of the protocol for protein extraction of mouse brain tissue are described in section 2.3.4 in General Methods.

4.2.2.3 Western blotting

Western blotting was used to measure changes of protein expression in the ischaemic mouse brain hemispheres compared to non-ischaemic brain hemispheres and sham-operated control brain hemispheres. Details of the experimental conditions are described in section 2.3.5 in General Methods. In brief, sham, ischaemic, and non-ischaemic hemisphere protein lysates were tested for differences of DDAH1, DDAH2, PRMT1, PRMT4 (CARM1), and PRMT8 protein expression.

4.2.3 Measuring the effect of oxygen-glucose deprivation on cerebral endothelial mRNA expression levels of DDAH and PRMT enzymes

4.2.3.1 Culture of hCMEC/D3 cells with EndoGRO™-MV complete media

The culture of hCMEC/D3 cells is described in section 2.2.2 of General Methods.

4.2.3.2 Oxygen-glucose deprivation of human cerebral microvascular endothelial cells (hCMEC/D3)

Oxygen-glucose deprivation (OGD) experiments were performed on hCMEC/D3 cells to mimic ischaemia-like conditions. In brief, hCMEC/D3 cells were cultured to confluence in T75 flasks. 48-hours post-confluence, cells were washed twice with PBS and replaced with OGD media (DMEM without FBS and D-Glucose, ThermoFisher, UK). Cells were transferred to a humidified hypoxic chamber maintained at 37°C and pre-equilibrated with an OGD gas mixture (95% N_2, 5% CO_2; Biospherix, US). hCMEC/D3 cells were incubated in an OGD environment for 6- or 24-hours. O_2 levels were maintained at 0.2-0.5% for the duration of the experiment using a digital oxygen controller (Biospherix, US). Time-controlled normoxic controls were run alongside each experiment by incubating hCMEC/D3 cells for the same duration of time as the OGD time-point in glucose-containing, serum-free DMEM media (37°C in a humidified 5% CO_2 atmosphere).

4.2.3.3 RNA extraction and cDNA synthesis

OGD and normoxic hCMEC/D3 cell pellets were resuspended in 1 mL Qiazol™ lysis reagent and lysed using a P1000 pipette and pipette tip (Qiagen, US). RNA was extracted and purified, and cDNA was synthesised as detailed in sections 2.3.1 and 2.3.2 in General Methods, respectively.

4.2.3.4 RT-qPCR of cerebral endothelial mRNA after oxygen-glucose deprivation

Quantification of cerebral endothelial DDAH1, DDAH2, PRMT1 and PRMT4 mRNA by RT-qPCR was performed as described in section 2.3.3 in General Methods. GAPDH was used as the reference housekeeping gene. Relative mRNA expression of each gene was compared between OGD and normoxic control samples for each duration of OGD.

4.2.4 Measurement of brain and plasma dimethylarginine levels in naïve mice following treatment with the selective DDAH1 inhibitor L-257

Details of the measurement of mouse brain and plasma ADMA and SDMA levels are described in section 2.1.8 in General Methods. In brief, 16 naïve male C57BL6/J mice (8 weeks old) were treated with either vehicle (saline, n=8) or L-257 (30 mg/kg; n=8) followed by collection of brain and plasma samples. Methylarginines were extracted from samples in extraction solvent prior to separation and quantification of ADMA and SDMA by HPLC-MS, using the labelled amino acid isotope ADMA-d7 as an internal standard. Known concentrations of ADMA and SDMA standards were also used as controls.

4.2.5 Assessment of haemodynamics in naïve mice following treatment with the DDAH1 inhibitor L-257

ADMA rapidly accumulates in plasma and tissues *in vivo* after L-257 treatment, and elevated plasma ADMA levels have been shown to play a causal role in hypertension (Achan *et al.*, 2003). It is well established that high blood pressure or hypertension is a

major risk factor ischaemic stroke, and changes in blood pressure can exacerbate ischaemic brain injury (Lattanzi, Brigo and Silvestrini, 2019). Therefore, prior to examining the effect of L-257 on stroke outcomes, it was important to first verify that the chosen dose of L-257 does not modulate cardiovascular haemodynamics.

4.2.5.1 Tail Cuff Plethysmography

Vehicle (saline i.p.) or L-257 (30 mg/kg i.p.) treatments were randomised for each mouse as previously described and administered 1.5 hours before measurements were collected each day, allowing mice to acclimatise after injections. This is because stress experienced by mice from injections and handling can influence blood pressure and heart rate values. Systolic and diastolic blood pressure, and heart rate were recorded using a BP-2000 Blood Pressure Analysis System™ (Visitech Systems Inc., US), as described in section 2.1.7 of General Methods. Miss Erika Trabold and I were blinded to treatments of all mice during measurements and analyses. Blinding was achieved by concealing the treatments administered to each mouse and the mouse ID during analysis.

4.2.5.2 Radiotelemetry

Mice were randomised to treatments prior to the study as previously described. Baseline recordings were taken for 24-hours before daily treatment with either vehicle (saline, i.p.) or L-257 (30 mg/kg, i.p.) and then recordings were taken for 4 days. Treatments were administered at the same time each morning for consistent recordings. Both systolic and diastolic blood pressure, heart rate, and activity levels were recorded for the duration of the study using a PC-C10 radiotelemetry probe (DSI PhysioTel, US), as described in section 2.1.6 in General Methods. Dr Alexandra Riddell and I were blinded to the treatments of all mice during measurements and analyses. Blinding was achieved by concealing the treatments administered to each mouse and the mouse ID during analysis.

4.2.6 Effect of DDAH1 inhibition by L-257 on middle cerebral and common carotid artery eNOS-NO function

To validate the consequences of accumulated ADMA on eNOS-NO signalling after DDAH1 inhibition, endothelium-dependent and -independent vasoreactivity was assessed in MCA and CCA vessels. Thus, MCAs and CCAs were collected as described in section 2.1.9 in General Methods and mounted on either perfusion (MCA) or wire myograph (CCA) systems, respectively, as described in sections 2.1.11 and 2.1.10 in General Methods.

Vessels were randomised to the following treatments using the random list generator www.random.org/lists: vehicle (dH_2O), L-257 (100 μM), or ADMA (100 μM), and were pre-incubated with treatments for 30-minutes. Vessels were then pre-constricted with the thromboxane A2 mimetic U46619 (10^{-9} to 10^{-8} M) followed by cumulative response curves to ACh (muscarinic agonist for eNOS-NO; 10^{-10} to $3x10^{-5}$ M) or SNP (NO donor molecule; 10^{-10} to $3x10^{-5}$ M). The vasodilator responses of MCA vessels were presented as % diameter

change, whereas vasorelaxation responses of CCA vessels were presented as % relaxation of total U46619 pre-contraction. Half-maximal effective concentration ($logEC_{50}$) and maximum relaxation responses (R_{max}) were also calculated for all vessels and compared in each group using an unpaired t-test with Welch's post hoc test.

4.2.7 Effect of DDAH1 inhibition by L-257 on outcomes after transient middle cerebral artery occlusion (tMCAo)

Focal cerebral ischaemia was induced by tMCAo in the right hemisphere in mice for 65 minutes using an intraluminal filament placed at the origin of the right MCA, as described in section 2.1.2 of General Methods. Vehicle (saline) and L-257 (30 mg/kg) treatments were administered by i.p. injection 1-hour before induction of ischaemia and every 24-hours until the study end-point for a maximum of three injections for each mouse. Neurological and functional outcomes were assessed at baseline and days 1, 2, and 3 post-ischaemia, as described in section 2.1.5 of General Methods. In brief, all tests were performed prior to induction of ischaemia, whereas the modified neurological severity score, foot fault, and cylinder tests were performed on days 1 and 3 post-stroke, and the forelimb grip strength and nest building activity tests were performed at day 2 post-stroke (Figure 4-1). Body weights were measured pre-stroke and then every day thereafter until the study endpoint.

Analyses for the study included determining infarct and oedema volume as well as the semi-quantification of TUNEL-positive apoptotic cells in the infarct core and peri-infarct tissue. In brief, brains were isolated from mice on day 3 post-stroke before being slow-frozen over liquid nitrogen. Frozen brains were embedded in OCT for cryosectioning, as described in section 2.1.3 of General Methods. Thionin staining was used to delineate the infarct, and total, cortical, and sub-cortical infarct and oedema volumes were evaluated as described in section 2.1.4 of General Methods. Semi-quantification of TUNEL-positive cells was assessed in the infarct core and peri-infarct regions of frozen brain sections from vehicle- and L-257-treated mice, as described in section 2.1.13 of General Methods.

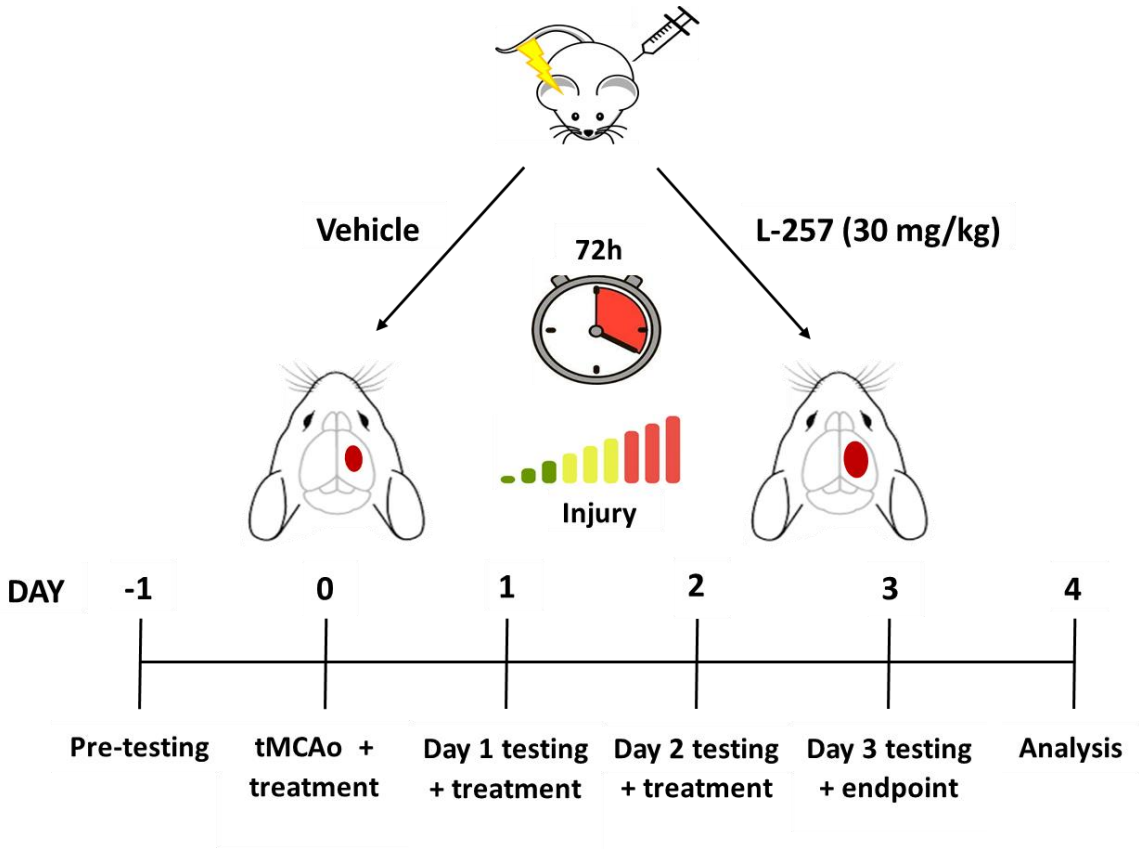

Figure 4-1. Schematic illustrating the schedule of vehicle or L-257 treatments, neurological tests, and study endpoint.

4.2.8 Power Calculations

Statistical powers for the L-257 stroke study was calculated using G* Power statistical power calculation software (Heinrich Heine University, Germany). In brief, pilot data in our lab showed that L-257 significantly increased infarct size compared to vehicle controls after mild cerebral ischaemia (40-minutes tMCAo, section 8.6 of Appendix), and thus we also expected worse outcomes in L-257-treated mice after 65-minutes tMCAo. Therefore, it was estimated that the minimal animals required were n=14 per group using the mean and SD infarct volume data from the 65-minute tMCAo group in Chapter 3 ($\alpha = 0.05$, power = 0.8 [$\beta = 0.2$], effect size = 1.14, two-tailed effect) to detect a minimum difference of 65% infarct size between vehicle- and L-257-treated mice.

4.2.9 Statistical Analysis

All datasets were analysed with GraphPad Prism 9 (GraphPad Software, USA). $P<0.05$ was considered statistically significant. Group numbers are indicated in the corresponding figure legends.

Parametric data is expressed as mean ± SEM. This includes gene and protein expression, quantification of brain and plasma methylarginine levels, measurement of mouse haemodynamics, cerebral endothelial and arterial function, changes of rCBF after tMCAo, acute ischaemic brain injury and neurological outcomes after tMCAo (% torn nestlet,

forelimb asymmetry tests [cylinder and foot fault], forelimb grip strength), and the semi-quantification of TUNEL-positive cells after tMCAo. The following statistical tests were used:

- Paired t-tests were used for gene expression data by RT-qPCR, and comparisons of forelimb asymmetry (cylinder and foot fault tests) between day 1 and day 3 in each treatment group post-stroke.
- Unpaired t-tests with Welch's correction were used for the quantification of methylarginine levels, maximal vascular function responses of MCA and CCA, and infarct and oedema volumes of vehicle- and L-257-treated mice post-stroke, comparisons of forelimb asymmetry between treatment groups at day 1 and day 3 post-stroke, and pre-post analysis of forelimb asymmetry in each treatment group.
- A one-way repeated measures ANOVA with Tukey's post hoc test was used for all Western blotting data.
- A two-way repeated measures ANOVA with Šídák's multiple comparisons test was used for comparing haemodynamics of vehicle- and L-257-treated mice using tail cuff plethysmography and radiotelemetry, endothelial-dependent and endothelial-independent vascular reactivity of MCA and CCA, and % weight loss in mice post-stroke, % torn nest building material, and forelimb grip strength.
- A two-way ANOVA with Tukey's post hoc test was used to compare TUNEL-positive cells in the infarct core and peri-infarct brain regions.

Non-parametric data is expressed as median. This includes the nest building activity and mNSS tests. The following statistical tests were used:

- A Wilcoxon matched pairs test as used to compare nest building activity post-stroke to baseline of mice in each treatment group.
- A Friedman test with Dunn's multiple comparisons test was used to measure changes of mNSS score of mice in each treatment group.
- A Mann-Whitney U test was used to compare nest building scores between treatment groups, as well as to compare mNSS scores between vehicle- and L-257-treated mice on day 1 and day 3 post-stroke.

4.3 Results

4.3.1 DDAH and PRMT protein expression appears to be unchanged 24- and 72-hours after tMCAo in mice

It is well documented that DDAH1 and 2 are expressed in the brain, meanwhile numerous type I PRMTs are also expressed. Importantly, PRMT1 is ubiquitously expressed and is responsible for nearly 85% of all PRMT activity (Tang *et al.*, 2000), whereas PRMT8 was shown to be exclusively expressed in neurons (Lee *et al.*, 2005). PRMT4 (CARM1) is also expressed in the brain, and it was previously reported that expression was increased after myocardial infarction in mice (Wang *et al.*, 2019). Therefore, using western blotting, the effects of cerebral ischaemia-reperfusion on DDAH1, DDAH2, PRMT1, PRMT4, and PRMT8 protein expression levels were assessed at 24- and 72-hours post-stroke in mice. Expression of both DDAH isoforms were unchanged at 24-hours post-stroke in the ischaemic and non-ischaemic hemispheres compared to sham control samples, whereas expression levels of both isoforms appeared to be significantly increased in the ischaemic hemispheres at 72-hours post stroke (Figure 4-2A-B). Expression of type I PRMTs was also unchanged at 24-hours post-stroke, whereas expression levels of PRMT4 and 8, but not PRMT1, were significantly increased at 72-hours post-stroke (Figure 4-3). Notably, however, we subsequently found that expression levels of ß-Actin (loading control for all proteins except PRMT1) were significantly lower in the ischaemic hemispheres at 72-hours post-stroke compared with non-ischaemic hemispheres and sham controls (Figure 4-4). Therefore, in subsequent experiments, we used ß-Tubulin as the loading control (which is unaltered at 72-hours post-stroke), and found that expression levels of DDAH1 and 2, and PRMT4 and 8 were unchanged in the ischaemic hemispheres at 72-hours post-stroke. Full blots showing antibody selectivity and comparisons of proteins of interest to ß-Tubulin at 72-hours post-stroke are shown in section 8.4 and section 8.2 of the Appendix, respectively, whereas the lack of an effect of cerebral ischaemia-reperfusion on ß-Tubulin after 72-hours is shown in section 8.3 of the Appendix.

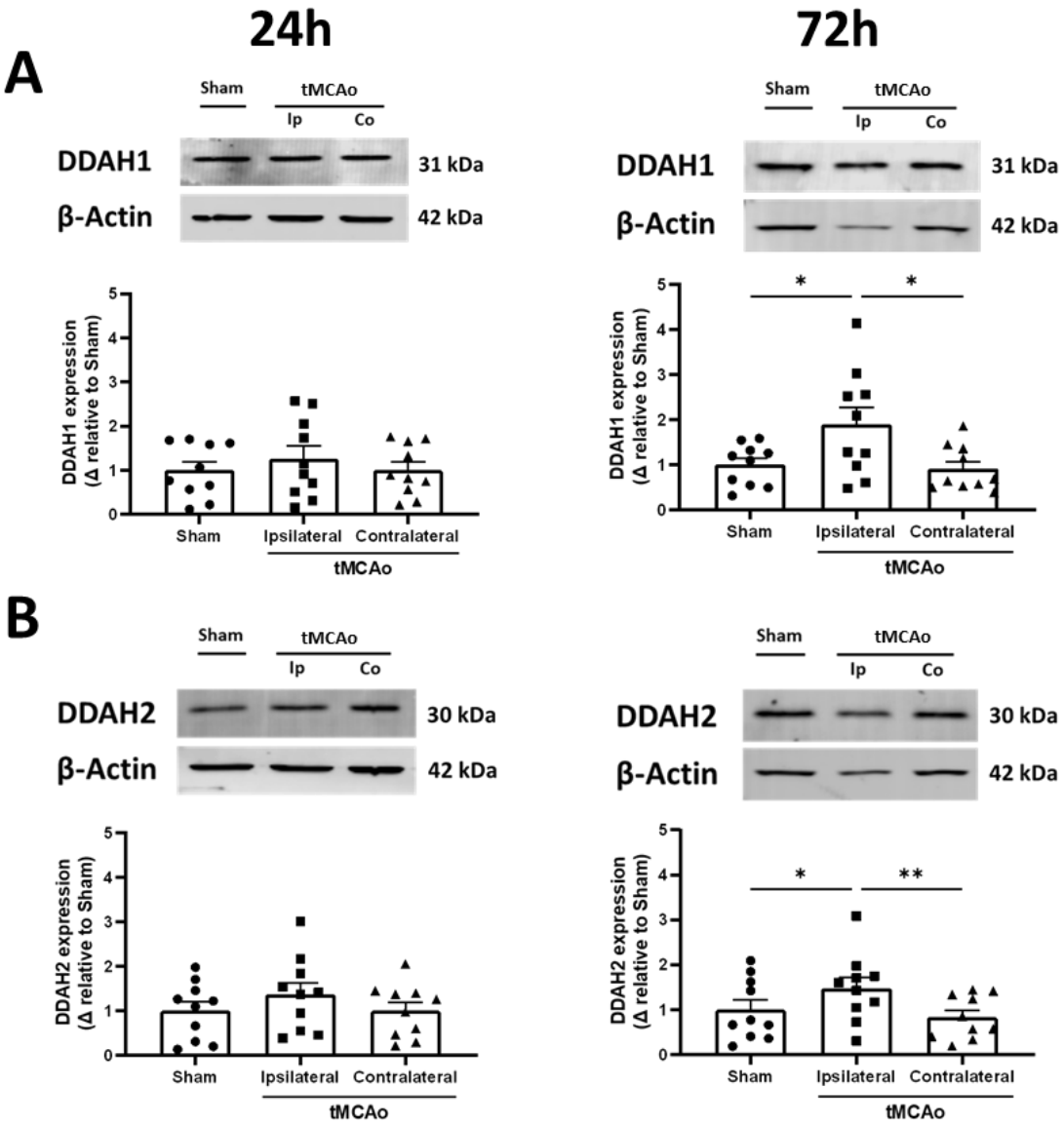

Figure 4-2. Effect of cerebral ischaemia on DDAH protein expression in mouse brain tissue at 24- and 72-hours after transient middle cerebral artery occlusion (tMCAo) or sham surgery. Representative Western blots showing protein expression of DDAH1 (**A**) and DDAH2 (**B**) in the ischaemic (ipsilateral), non-ischaemic (contralateral), or sham control hemisphere tissues at 24- and 72-hours post-surgery (top). Also shown is a summary of immunoreactive band intensities (bottom). Values are expressed as relative intensity normalised to ß-Actin (loading control) intensity. Data presented as mean ± SEM, n=10, **P*<0.05, ***P*<0.01, one-way ANOVA with Tukey's multiple comparisons post hoc test.

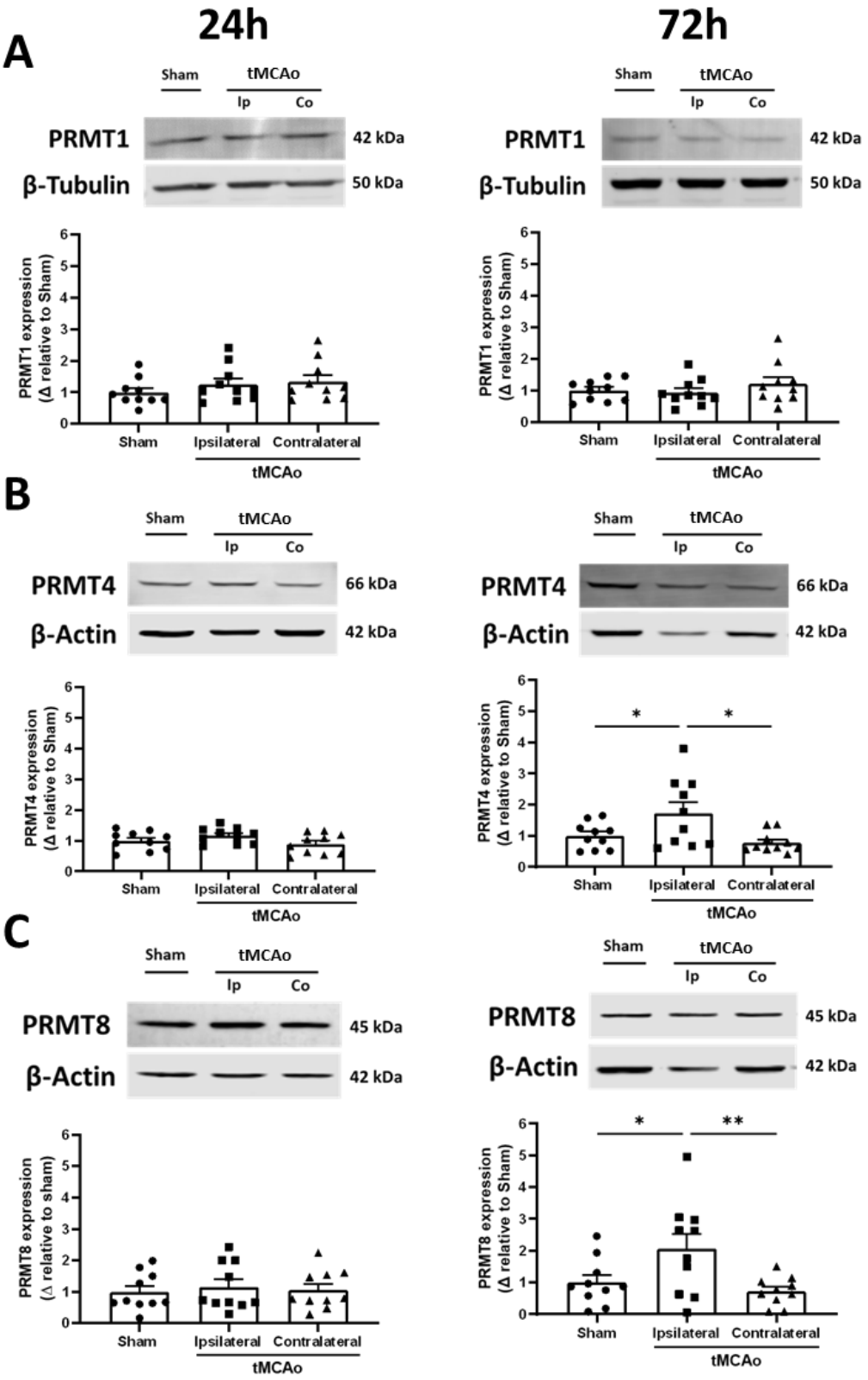

Figure 4-3. Effect of cerebral ischaemia on type I PRMT protein expression in mouse brain tissue at 24- and 72-hours after transient middle cerebral artery occlusion (tMCAo) or sham surgery. Representative Western blots showing protein expression of PRMT1 (**A**), PRMT4 (**B**), and PRMT8 (**C**) in the ischaemic (ipsilateral), non-ischaemic (contralateral), or sham control hemisphere tissues at 24- and 72-hours post-surgery (top). Also shown is a summary of immunoreactive band intensities (bottom). Values are expressed as relative intensity normalised to ß-Actin or ß-Tubulin intensity (loading controls). Data presented as mean ± SEM, n=10, **P*<0.05, ***P*<0.01, one-way ANOVA with Tukey's multiple comparisons post hoc test.

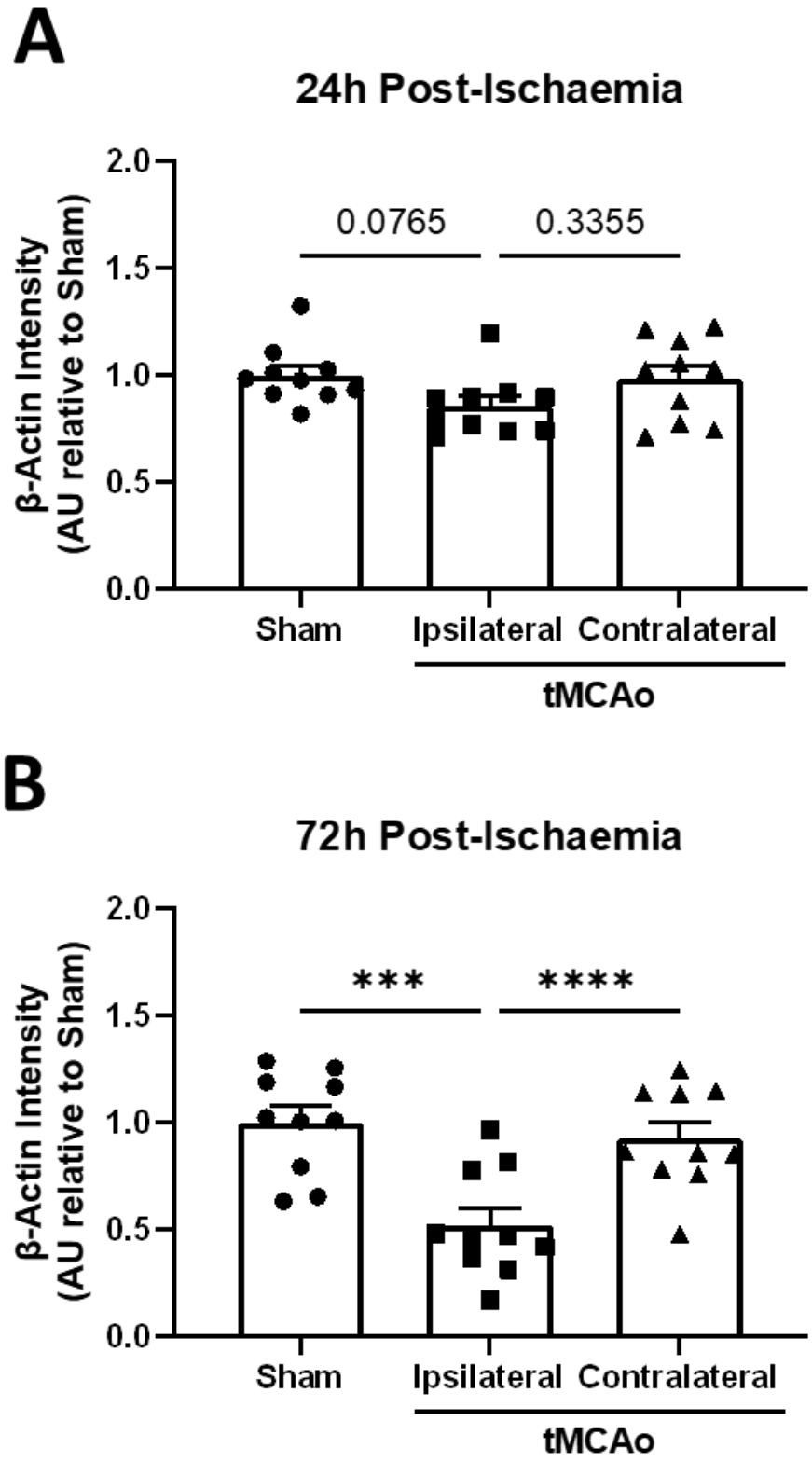

Figure 4-4. Effect of cerebral ischaemia on protein expression levels of the loading control ß-Actin in mouse brain tissue at 24- and 72-hours after transient middle cerebral artery occlusion or sham surgery. Relative intensities for the loading control ß-Actin. An average was taken for total ß-Actin band intensity for each sample across the DDAH1, DDAH2, PRMT4, and PRMT8 blots in the 24- and 72-hour assessments. ß-Actin averages were normalised and expressed relative to the sham mean at 24- (**A**) and 72-hours (**B**) post-stroke. Data presented as mean ± SEM, n=10, ***P<0.001 ****P<0.0001, one-way ANOVA with Tukey's multiple comparisons post hoc test.

4.3.2 DDAH and PRMT4 mRNA expression is elevated in human cerebral endothelial cells after 24 hours of oxygen-glucose deprivation

RNA was isolated from hypoxic and normoxic hCMEC/D3 cells followed by conversion to cDNA templates. Gene expression was then measured for DDAH1, DDAH2, PRMT1 and PRMT4 using SYBR Green RT-qPCR. A summary of hCMEC/D3 gene expression data after 6- and 24-hours of oxygen-glucose deprivation (OGD) are described in Table 4-1 and Table 4-2. After 6 hours of OGD, there were no transcriptional differences of all four genes compared to normoxic controls (Figure 4-5A-D). Conversely, 24-hours of OGD significantly increased mRNA expression of both DDAH isoforms compared to normoxic controls (Figure 4-6A-B; $P<0.05$). Although statistical significances were not achieved, our data also suggests a trend for PRMT4 mRNA expression to be increased after 24-hours of OGD compared to normoxic controls, while the same duration of OGD did not affect PRMT1 expression levels (Figure 4-6C-D). It is important to highlight that Ct values >35 typically reflect low or no mRNA template present in a sample. In this study, the mean Ct values for PRMT4 in both durations of OGD exceeded 35 cycles, thus whilst there was a trend for increased PRMT4 mRNA levels in response to OGD, it is likely that mRNA expression is negligible and therefore the significance of this increase is questionable (Table 4-1 and Table 4-2). Similarly, the Ct values for DDAH2 after 24 hours of OGD are between 30 and 35, which also raises questions over the biological significance of the increase in DDAH2 in Figure 4-6.

Gene	**Normoxic**				**OGD**			
	Ct Mean	**SD**	**SEM**	***n***	**Ct Mean**	**SD**	**SEM**	***n***
Ddah1	31.20	3.18	1.3	6	31.61	2.9	1.2	6
Ddah2	25.28	0.95	0.6	3	25.53	0.29	0.2	3
Prmt1	19.41	0.69	0.3	6	19.51	0.69	0.3	6
Prmt4	35.18	1.50	0.6	6	34.67	1.80	0.7	6
Gapdh	18.50	0.93	0.4	6	18.72	1.19	0.5	6

Table 4-1. Descriptive statistics of cycle threshold (Ct) data for 6-hour normoxic and oxygen-glucose deprivation (OGD) mRNA samples from hCMEC/D3 cells. Average Ct values, standard deviation (SD), standard error (SEM), and number of biological replicates (n) are shown. Due to insufficient amounts of samples, measurement of DDAH2 mRNA was limited to n=3.

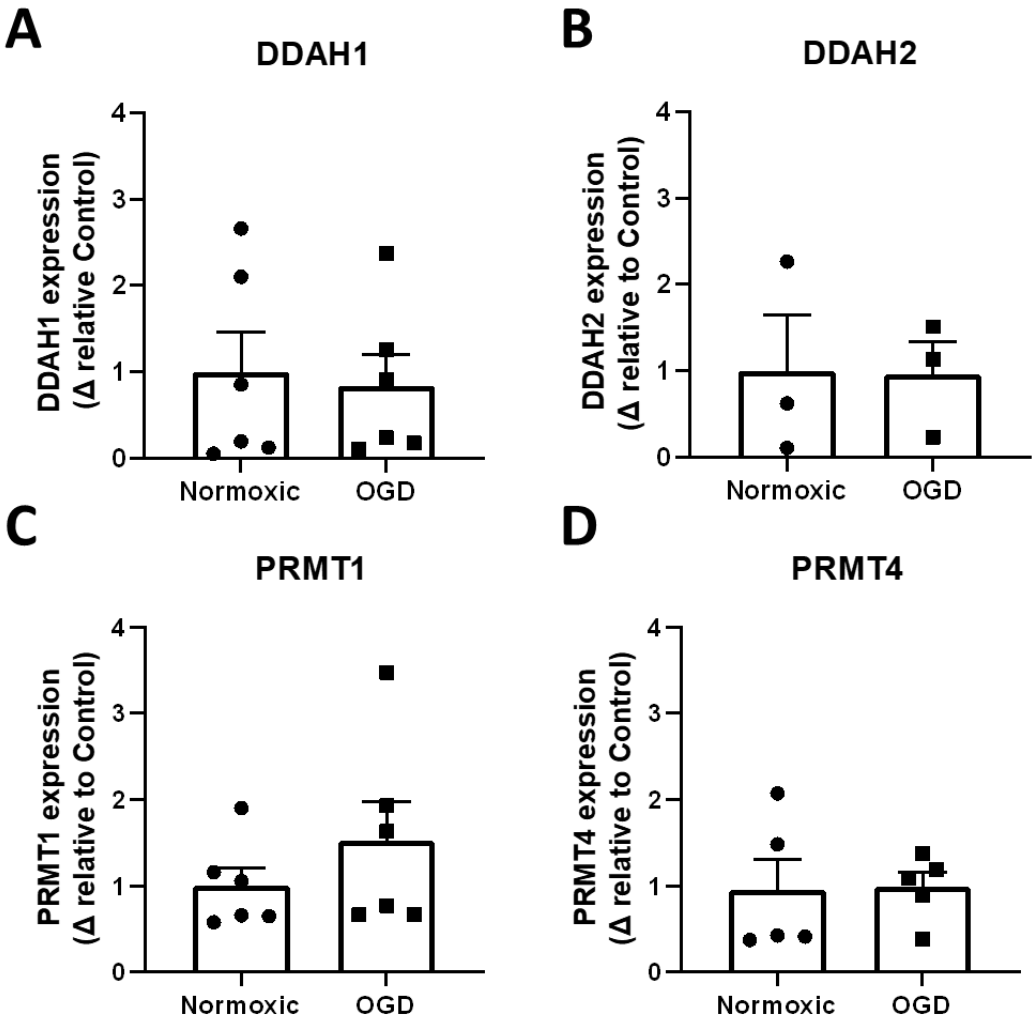

Figure 4-5. Effect of 6-hours of oxygen-glucose deprivation (OGD) on mRNA expression of DDAH1, DDAH2, PRMT1, and PRMT4 in hCMEC/D3 cells. RNA isolated from hCMEC/D3 cells exposed to 6-hours of OGD or normoxic conditions were compared for DDAH1 (**A**), DDAH2 (**B**), PRMT1 (**C**), and PRMT4 (**D**) by SYBR Green RT-qPCR. Data presented as mean ± SEM, n=3-6, *P*>0.05, paired t-test.

Gene	Normoxic				OGD			
	Ct Mean	SD	SEM	*n*	Ct Mean	SD	SEM	*n*
Ddah1	24.72	1.18	0.5	6	25.54	0.74	0.3	6
Ddah2	31.66	0.76	0.4	3	32.46	0.37	0.2	3
Prmt1	21.38	0.95	0.4	6	22.69	0.6	0.3	6
Prmt4	35.47	1.4	0.6	6	35.52	0.36	0.2	6
Gapdh	18.29	1.06	0.43	6	19.64	1.22	0.5	6

Table 4-2. Descriptive statistics of cycle threshold (Ct) data for 24-hour normoxic and oxygen-glucose deprivation (OGD) mRNA samples from hCMEC/D3 cells. Average Ct values, standard deviation (SD), standard error (SEM), and number of biological replicates (n) are shown. Due to insufficient amounts of samples, measurement of DDAH2 mRNA was limited to n=3.

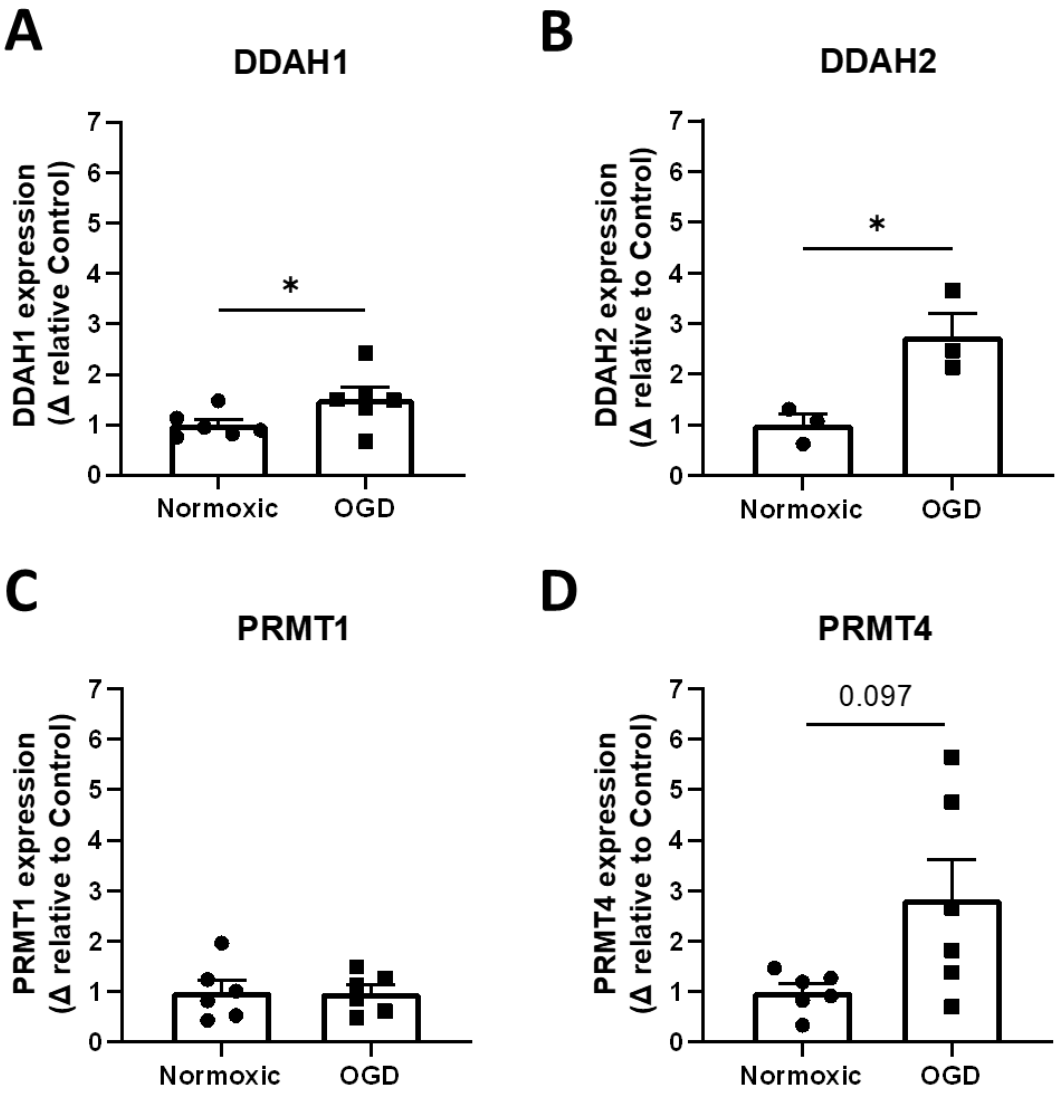

Figure 4-6. Effect of 24-hours of oxygen-glucose deprivation (OGD) on mRNA expression of DDAH1, DDAH2, PRMT1, and PRMT4 in hCMEC/D3 cells. RNA isolated from hCMEC/D3 cells exposed to 24-hours of OGD or normoxic conditions were compared for DDAH1 (**A**), DDAH2 (**B**), PRMT1 (**C**), and PRMT4 (**D**) by SYBR Green RT-qPCR. Data presented as mean ± SEM, n=3-6, **P*<0.05, paired t-test.

4.3.3 Systemic administration of the selective DDAH1 inhibitor, L-257, increases brain ADMA levels in naïve mice

Nandi *et al*. (2012) previously showed that intravenous administration of L-257 (ranging from 3-30 mg/kg) in Sprague-Dawley rats significantly increases circulating plasma ADMA levels compared to vehicle-treated controls (Nandi *et al.*, 2012). However, whether ADMA levels are altered in mouse brain after intraperitoneal injection of L-257 (30 mg/kg) remains unclear. Therefore, we measured ADMA and SDMA levels in brain and plasma from naïve C57BL6/J mice treated with either vehicle or L-257 using HPLC-MS. There was a trend for ADMA levels to be increased in the brain (L-257, 0.41±0.02 nmol/g vs vehicle, 0.35±0.02 nmol/g) and plasma (L-257, 1.62±0.2 µmol/L vs vehicle, 1.23±0.1 µmol/L) of mice treated with L-257 compared with vehicle-treated controls (Figure 4-7A). In contrast, SDMA levels in both brain and plasma were similar between the treatment groups (Figure 4-7B).

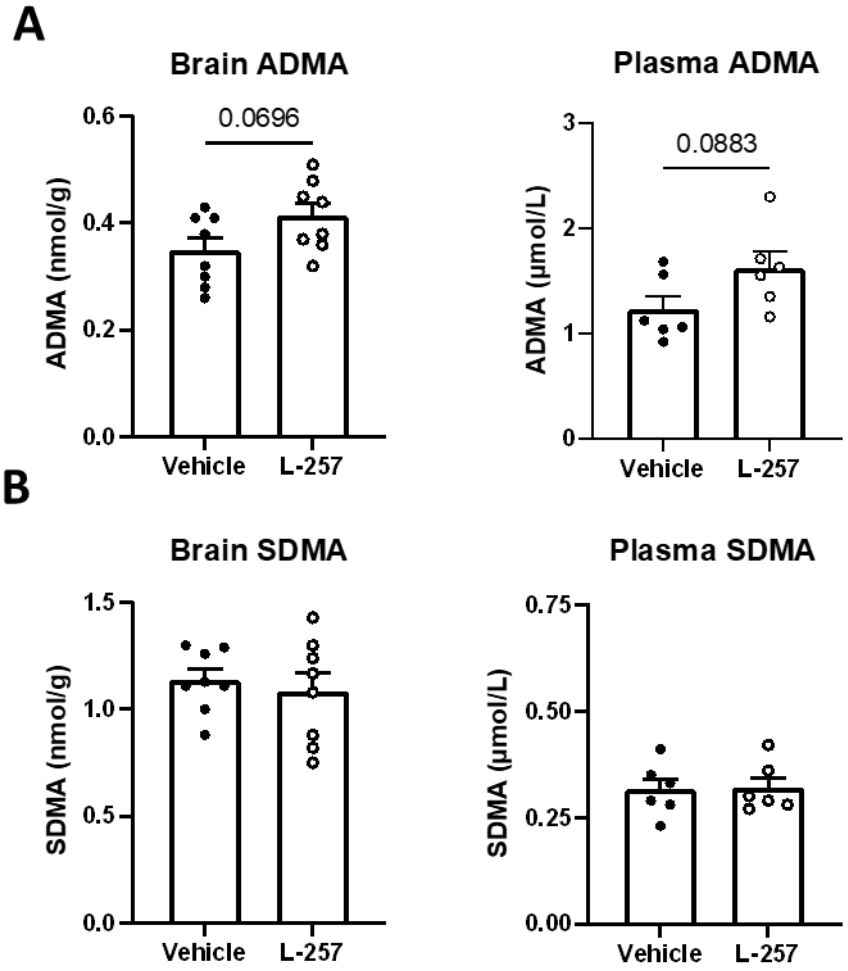

Figure 4-7. Effects of pharmacological inhibition of DDAH1 on mouse brain and plasma methylarginine levels. Naïve mice were injected intraperitoneally with vehicle (saline) or L-257 (30 mg/kg), and brains and plasma were collected 1.5 hours later. Methylarginines were extracted from samples in extraction solvent and ADMA (**A**) and SDMA (**B**) levels were quantified using HPLC-MS. Data presented as mean ± SEM, n=6-8, *P*>0.05, unpaired t-test with Welch's correction.

4.3.4 L-257 treatment does not alter cardiovascular haemodynamics

Using tail cuff plethysmography, we observed no differences in systolic and diastolic pressures, or heart rates between vehicle- and L-257-treated mice. Additionally, there were no changes in systolic and diastolic pressures, or heart rates within each group post-treatment compared to pre-treatment (Figure 4-8A-C; $P>0.05$). There were also no differences in either systolic (post-treatment, 118.6±6.4 vs pre-treatment, 119.8±3.9 mmHg) or diastolic (post-treatment, 64.3±4.7 vs pre-treatment, 63.7±3.6 mmHg) pressures in L-257-treated mice on Day 3 compared to pre-treatment (Day 0; Figure 4-8D; $P>0.05$).

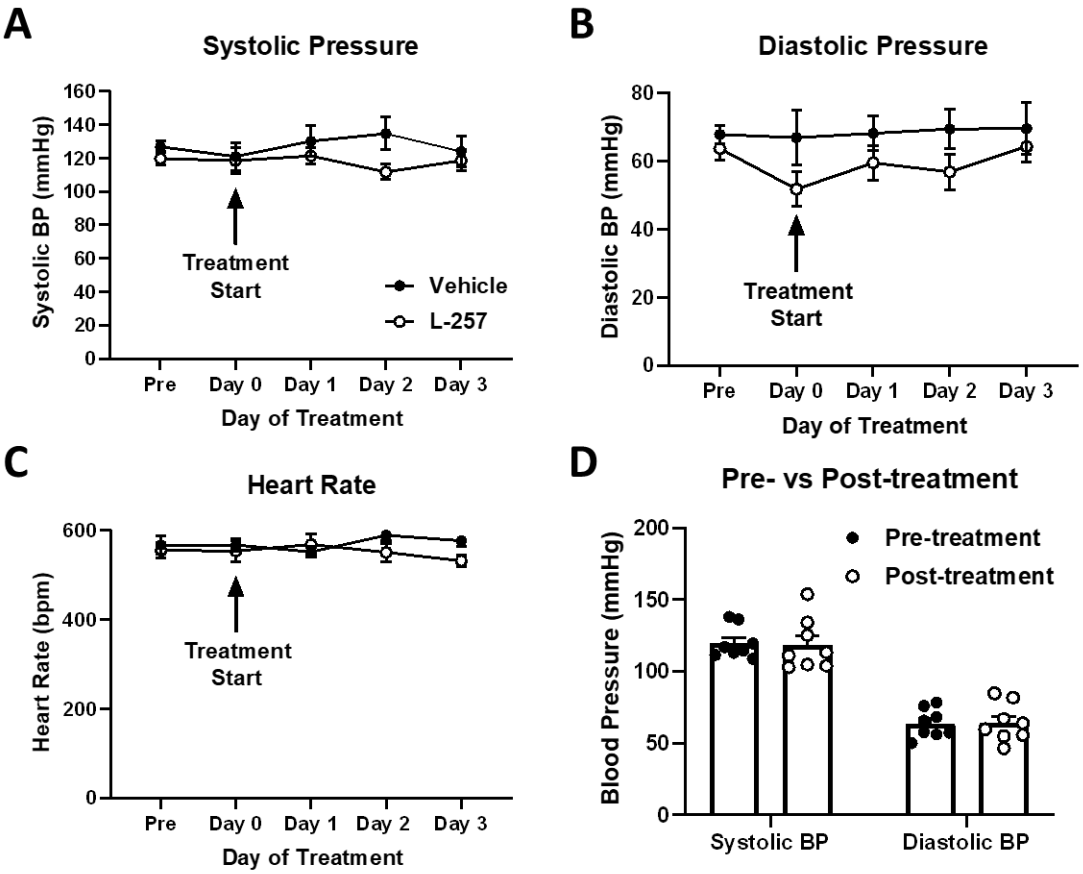

Figure 4-8. Effect of vehicle- and L-257-treatment on haemodynamics in mice as measured by tail cuff plethysmography. Baseline systolic pressure, diastolic pressure, and heart rate readings were taken from all mice before being treated with either vehicle or L-257 for 3 days (**A-C**). Measurements were taken at the same time each day after treatments were administered. Baseline systolic and diastolic pressure of L-257-treated mice were compared to measurements taken on day 3 (**D**). Data presented as mean ± SEM, n=8, $P>0.05$, a paired t-test was used for comparisons of pre- and post-treatment blood pressures, and a two-way ANOVA with repeated measures and Šídák's multiple comparisons test was used for comparing differences in systolic pressure, diastolic pressure, and heart rate between treatment groups from baseline (pre) and day 3.

Next, we examined the effect of systemic administration of L-257 on cardiovascular haemodynamics using radiotelemetry. Similarly, there were no statistical differences between L-257-treated and control mice with respect to systolic and diastolic pressures, and there were no changes in blood pressures throughout the treatment regime in both groups (Figure 4-9A-B; $P>0.05$). Similar to our findings using tail cuff plethysmography, neither systolic nor diastolic pressures in L-257-treated mice were changed on day 4 of measurement compared to pre-treatment (Figure 4-9C; $P>0.05$). Activity levels were similar between groups during both day and night cycles and therefore did not influence haemodynamic measurements (Figure 4-9D; $P>0.05$). Interestingly, L-257-treated mice displayed lower heart rate before and after treatment compared to vehicle control mice, however, there were no changes in heart rate of L-257-treated mice on day 4 compared to pre-treatment (Figure 4-9E-F).

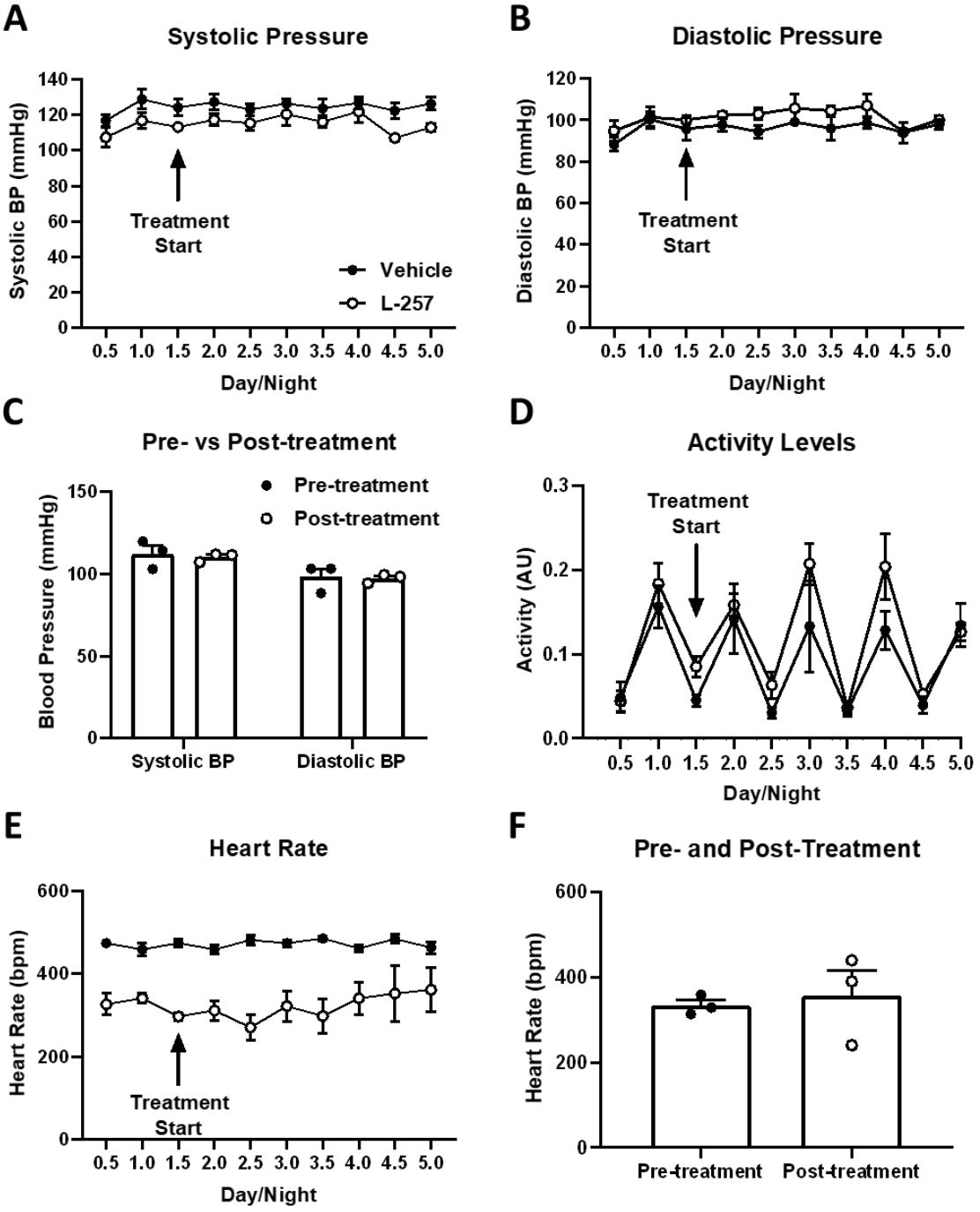

Figure 4-9. Effect of vehicle- or L-257-treatment on cardiovascular haemodynamics in naïve mice as measured by radiotelemetry. Systolic (**A**) and diastolic (**B**) pressure, activity levels (**D**), and heart rates (**E**) were measured at baseline and for 4 days following the first treatment. Pre- and post-treatment systolic and diastolic pressures (**C**), and heart rates (**F**) within the L-257 group were also compared. Day cycles are shown as decimals whereas night cycles are shown as whole numbers. Data presented as mean ± SEM, n=3, $P>0.05$, two-way ANOVA with repeated measures and Šídák's multiple comparisons test (**A, B, D**), or paired t-test (**C, F**).

4.3.5 DDAH1 inhibition impairs endothelial function of middle cerebral and common carotid arteries in an endothelial-dependent manner

Baseline diameters of MCA were similar between treatment groups (vehicle, 109.5±4.2 vs L-257, 115.8±4.5 μm, $P>0.05$). Data describing the integrity of the vessels, pre-constriction levels, R_{max}, and $logEC_{50}$ values for these experiments are shown in Table 4-3 and Table 4-4. Treatment of mouse MCA with L-257 markedly impaired total endothelium-dependent vasodilator responses to acetylcholine compared to vessels treated with vehicle (Figure 4-10A, $P<0.05$, two-way repeated measures ANOVA with Šídák's multiple comparisons test; R_{max}: L-257 36.4±7% vs vehicle 74.5±8%, $P<0.05$, unpaired t-test). Furthermore, L-257 inhibited NO-dependent vasodilation of MCA to a similar degree of that achieved by exogenous ADMA (Figure 4-10B, $P<0.05$, two-way repeated measures ANOVA with Šídák's multiple comparisons test; R_{max}: ADMA, 49.4±8% vs vehicle, 78.9±4%, $P<0.05$, unpaired t-test).

Treatment	**Acetylcholine**			**Acetylcholine**		
Group	**Vehicle**	**L-257**	***n***	**Vehicle**	**ADMA**	***n***
Baseline Diameter (μm)	109.5±4	115.8±5	4	114.3±7	110.7±2	3
KPSS (% Diameter change)	-67.1±4	-62.5±5	3	-68.5±2	-68.1±2	2-3
Pre-constriction to U46619 (% KPSS)	-47.8±3	-50.6±4	4	-53.6±5	-47.1±2	3

Table 4-3. Middle cerebral artery vessel integrity values that were used in acetylcholine-induced response curves. Maximum contractile responses to high potassium physiological salt solution (KPSS; % diameter change); and U46619 pre-constriction levels (% of baseline diameter) prior to commencing cumulative concentration-response curves. Data presented as mean ± SEM, where n is number of animals. There were no differences between treatment groups with all parameters, $P>0.05$, unpaired t-test.

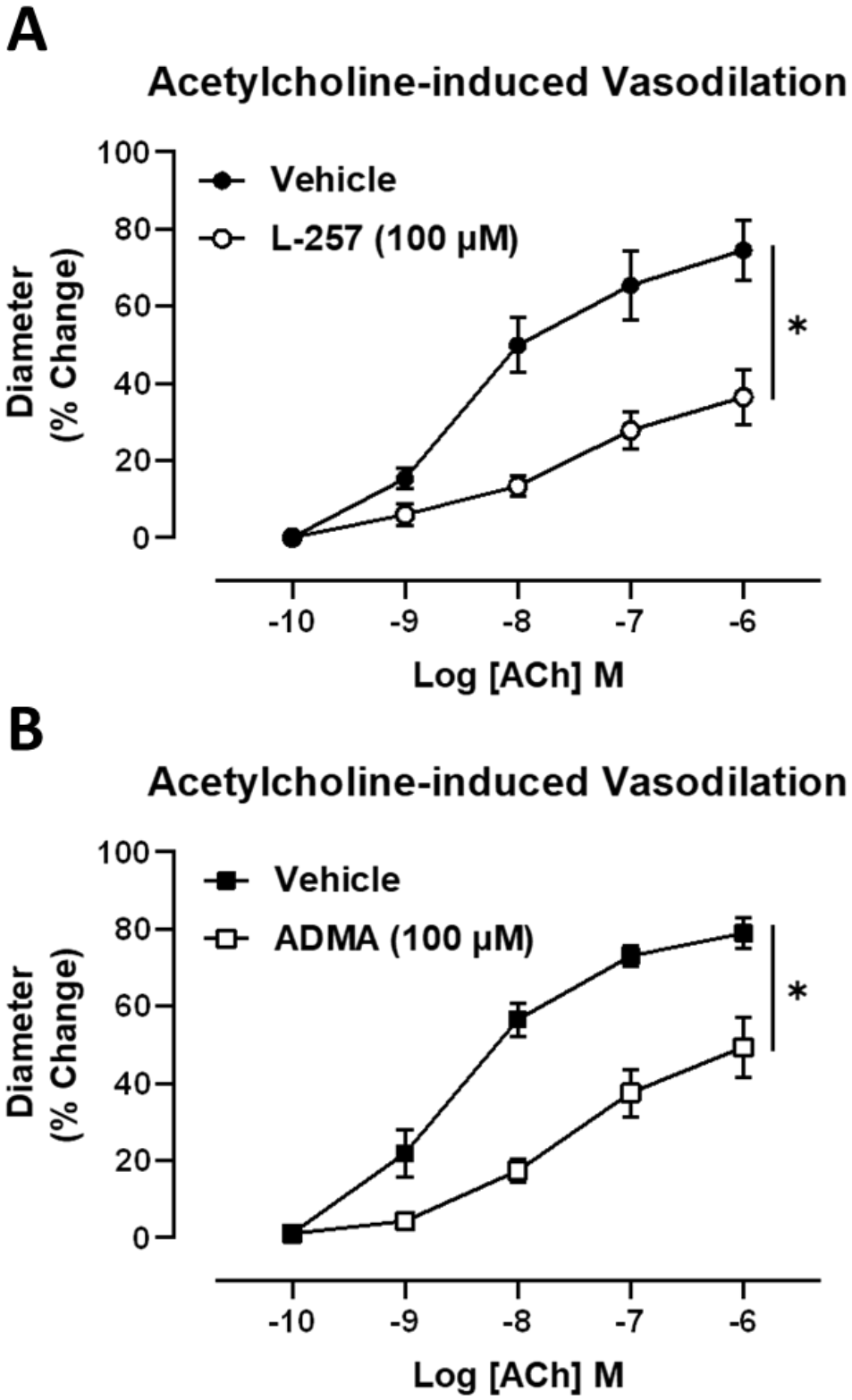

Figure 4-10. Acetylcholine-induced vasodilator responses of mouse middle cerebral arteries treated with vehicle, L-257 (100 µM), or exogenous ADMA (100 µM). Cumulative concentration-response curves showing vasodilation responses to acetylcholine (10^{-10} to 10^{-6} M) in isolated middle cerebral arteries treated with either vehicle (water) or L-257 (100 µM; **A**). Also shown are responses to acetylcholine in vessels treated with either vehicle (water) or ADMA (100 µM; **B**). Results are expressed as % change in intraluminal diameter. Data presented as mean ± SEM, n=3-4, **P*<0.05, repeated measures two-way ANOVA with Šídák's multiple comparisons test.

Treatment	Acetylcholine			Acetylcholine		
Groups	**Vehicle**	**L-257**	***n***	**Vehicle**	**ADMA**	***n***
R_{max} (% Pre-constriction to U46619)	74.5±8	36.4±7	4	78.9±4	49.4±8	3
R_{max} *P* Value	*P = 0.011			*P = 0.043		
$logEC_{50}$	-8.4±0.1	-7.7±0.3	3-4	-8.7±0.3	-7.5±0.04	3
$logEC_{50}$ *P* Value	P = 0.15			*P = 0.044		

Table 4-4. Summary of middle cerebral artery responses treated with either vehicle, L-257 (100 µM), or ADMA (100 µM). Maximal relaxation responses (R_{max}) and half-maximal effect concentration ($logEC_{50}$) values of cumulative concentration-response curves to acetylcholine in middle cerebral arteries treated with either vehicle (water), L-257 (100 µM), or exogenous ADMA (100 µM). Values are given as mean ± SEM, where n is number of animals. *P<0.05, unpaired t-test with Welch's correction.

Next, we assessed the effect of DDAH1 inhibition by L-257 on acetylcholine- and sodium nitroprusside-induced vasorelaxation responses of CCA. Data describing the integrity of the vessels, pre-constriction levels, R_{max}, and $logEC_{50}$ values are shown Table 4-5 and Table 4-6. Similar to MCA, treatment of mouse CCA with L-257 markedly impaired vasorelaxation responses to cumulative concentrations of acetylcholine compared to vehicle controls (Figure 4-11A; P<0.05, two-way repeated measures ANOVA with Šídák's multiple comparisons test). Additionally, there was a trend for L-257 treatment to impair maximal relaxation (R_{max}) responses to acetylcholine, however, there were no statistical differences with respect to $logEC_{50}$ values between treatments (Table 4-6). Treatment of CCA with L-257 had no significant effect on vasorelaxation responses to nitroprusside compared to vehicle controls (Figure 4-11B, P>0.05, two-way repeated measures ANOVA with Šídák's multiple comparisons test). Furthermore, vasorelaxation responses of CCA treated with L-257 to acetylcholine and nitroprusside were comparable to CCA treated with suprapathophysiological concentrations of exogenous ADMA (100 µM; section 8.5 in Appendix).

Treatment	Acetylcholine			Nitroprusside		
Group	**Vehicle**	**L-257**	***n***	**Vehicle**	**L-257**	***n***
KPSS (mN)	1.7±0.2	1.9±0.3	7	1.5±0.2	1.4±0.2	5
Endothelial Function (%)	112.9±6	112.3±13.3	7	61.5±13	91.3±7	5
Pre-constriction to U46619 (% KPSS)	57.4±6	54.4±2	7	56.2±7	51.8±4	5

Table 4-5. Common carotid artery vessel integrity values that were used in acetylcholine-induced and nitroprusside-induced response curves. Maximum contractile responses to high potassium physiological salt solution (KPSS; mN); endothelial function of common carotid arteries assessed by measuring maximal relaxation response to acetylcholine (% of U46619-induced tone); and U46619 pre-constriction levels (% of KPSS) prior to commencing cumulative concentration-response curves. Values are given as mean ± SEM, where n is number of animals. There were no differences between treatment groups with all parameters, P>0.05, unpaired t-test.

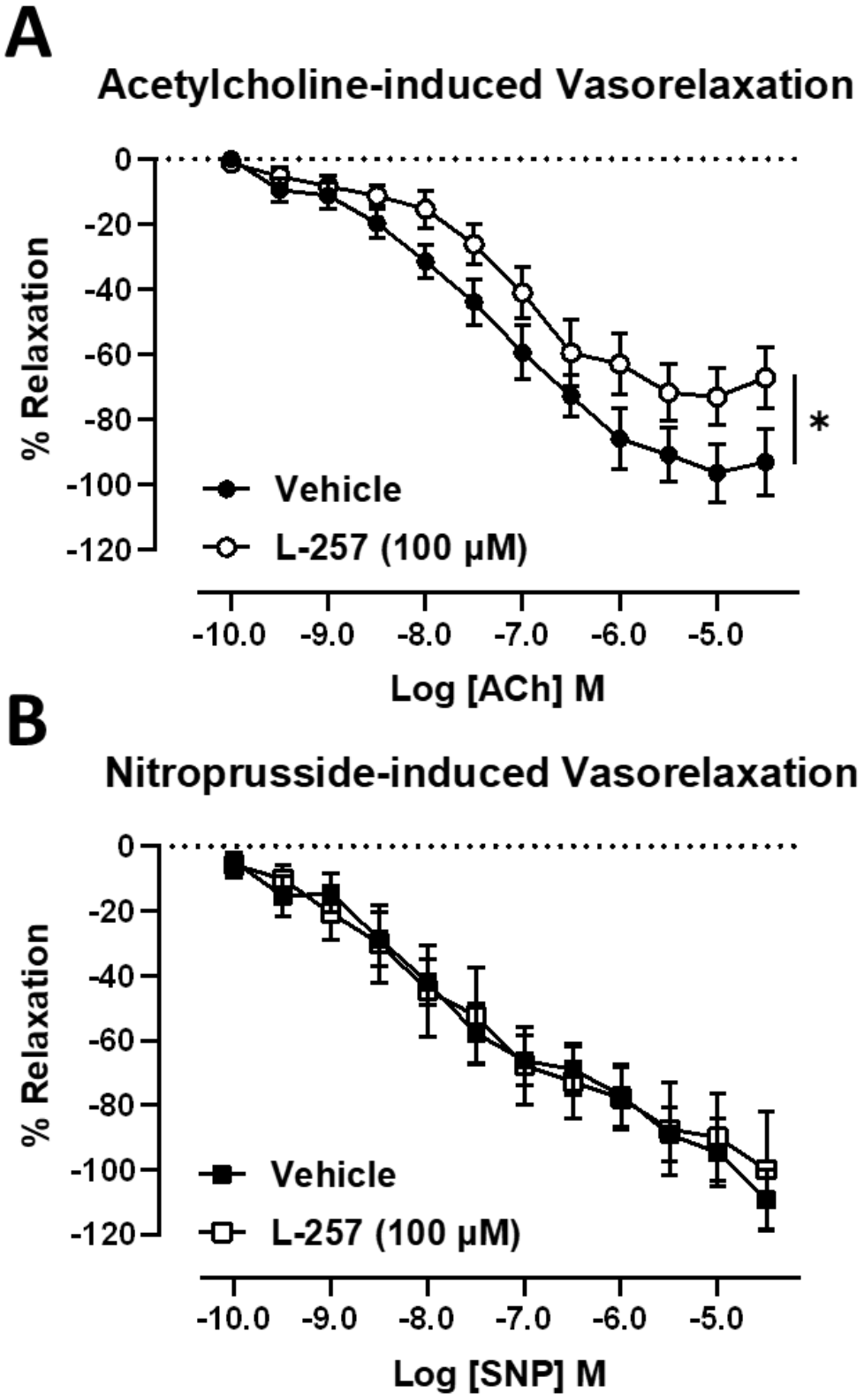

Figure 4-11. Acetylcholine- and nitroprusside-induced responses of common carotid arteries pre-treated with either vehicle or L-257 (100 µM). Cumulative concentration-response curves showing vasorelaxation responses to acetylcholine (10^{-10} to $3x10^{-5}$ M; **A**) and sodium nitroprusside (10^{-10} to $3x10^{-5}$ M; **B**) in isolated common carotid arteries treated with either vehicle (water) or L-257 (100 µM). Results are expressed as % relaxation of U46619 pre-constriction. Data presented as mean ± SEM, n=3-7, **P*<0.05, two-way ANOVA with repeated measures and Šídák's multiple comparisons test.

Treatment	Acetylcholine			Nitroprusside		
Groups	**Vehicle**	**L-257**	***n***	**Vehicle**	**L-257**	***n***
R_{max} (% Pre-constriction to U46619)	-93.1±10	-67.2±9	7	-109±9	-99.6±18	5
R_{max} *P* Value	*P* = 0.086			*P* = 0.67		
$logEC_{50}$	-7.4±0.2	-7.1±0.1	7	-7.6±0.6	-7.9±1	3-5
$logEC_{50}$ *P* Value	*P* = 0.28			*P* = 0.85		

Table 4-6. Summary of common carotid artery responses in vehicle or L-257-treated vessels. Maximal relaxation responses (R_{max}) and half-maximal effect concentration ($logEC_{50}$) values of cumulative concentration-response curves to acetylcholine and nitroprusside in vehicle- and L-257-treated common carotid arteries. Values are given as mean ± SEM, where n is number of animals. *P*>0.05, unpaired t-test with Welch's correction.

4.3.6 DDAH1 inhibition does not worsen injury, infarct distribution, or neurological outcome in mice following 65-minutes of tMCAo

Following the insertion of the monofilament, rCBF was reduced by approximately 70% or greater, and restored by a minimum of 80% within 10-minutes of filament withdrawal, to a similar extent in both treatment groups (Figure 12). There were no mortalities in either group, however, 2/13 (15%) of vehicle-treated mice were culled prior to the scientific endpoint as they exceeded the clinical severity limits. One mouse was excluded from the vehicle-treated group due to inadequate reperfusion (~38%) within 10-minutes of filament withdrawal, and two mice were excluded from the L-257-treated group where one had a CCA clamp time greater than 5-minutes, and the other did not develop a visible infarct. One mouse was excluded from the rCBF data of the vehicle-treated group, and two mice were excluded from the rCBF data of the L-257-treated group due to a loose laser-doppler probe during each surgery. However, these mice met our additional criteria for correct filament placement at the MCA origin (resistance of the filament at the estimated distance for insertion) and each mouse developed an infarct that did not correlate with an insufficient reduction of rCBF or inadequate reperfusion.

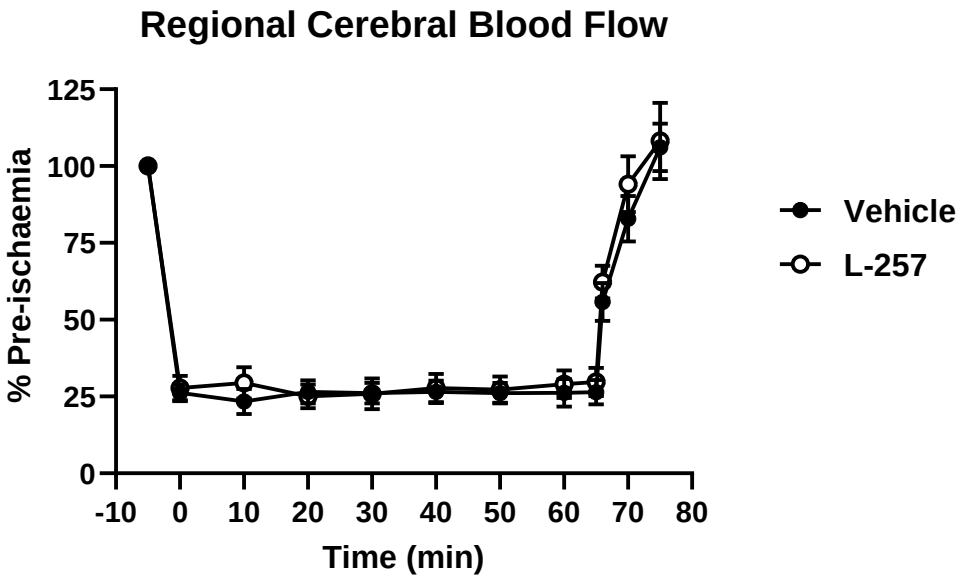

Figure 4-12. Regional cerebral blood flow of vehicle- and L-257-treated mice during 65-minutes of tMCAo and 10-minutes reperfusion. A reduction of ≥70% and ≥80% restoration of blood flow was required for mice in each treatment group. Data presented as mean ± SEM, n=9 per group. No statistical test was used.

Treatment of mice with L-257 (30 mg/kg) had no statistically significant effect on total infarct (L-257, 18.1±4 vs vehicle, 19.7±2 mm^3; *P*>0.05), or oedema (L-257, 10.8±3 vs vehicle, 7.1±1 mm^3; *P*>0.05) volumes compared to mice treated with vehicle (Figure 4-13A-D). Consistent with our infarct data, there were also no differences in the extent of weight loss on day 3 between treatment groups (Figure 4-13E). Furthermore, no statistically significant evidence of differences between treatment groups was found with respect to cortical and sub-cortical infarct and oedema volumes (Figure 4-14), or the distribution of total, cortical, and sub-cortical infarcts relative to Bregma (Figure 4-15).

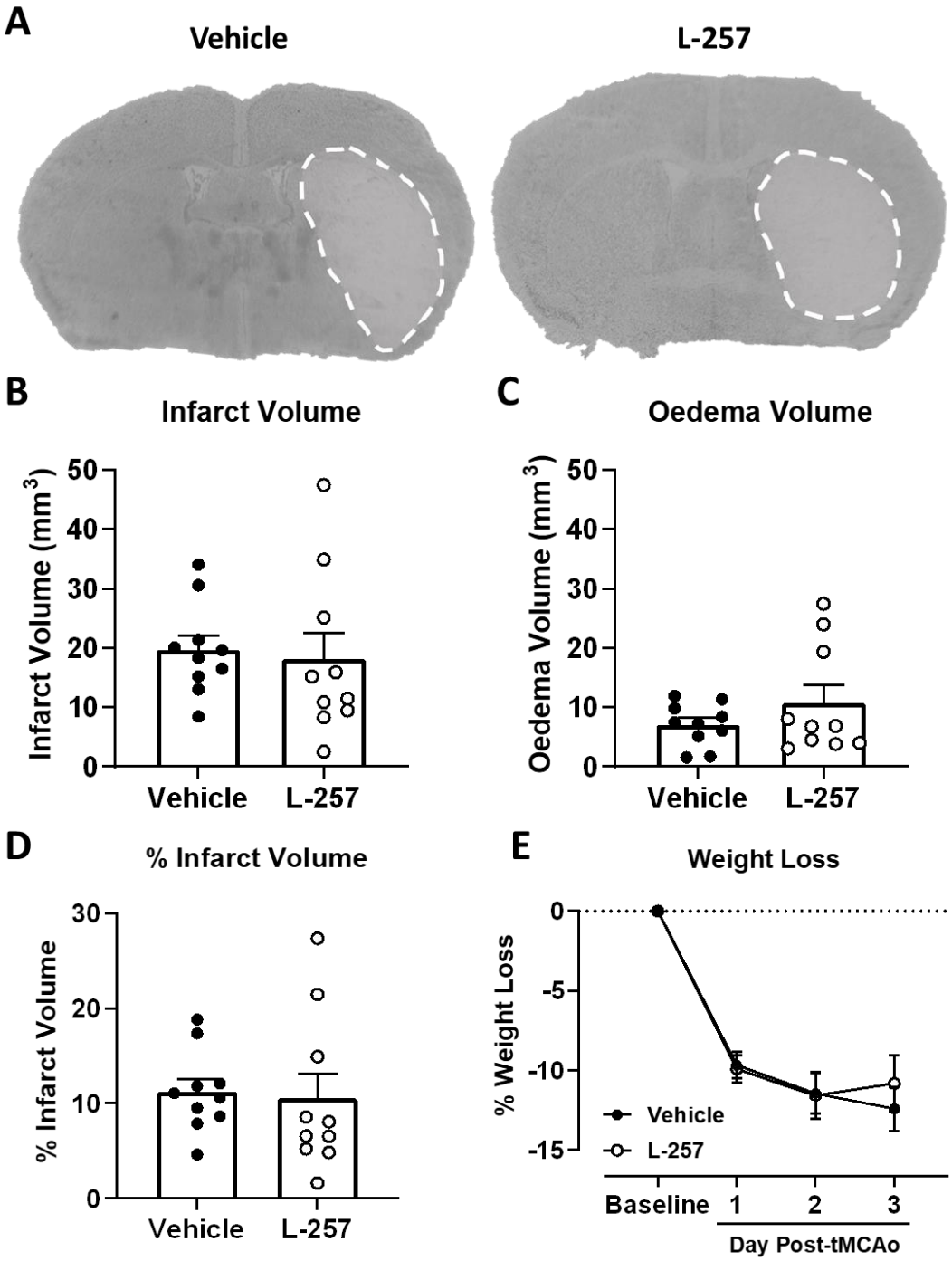

Figure 4-13. Infarct and oedema volumes, and weight loss of vehicle- or L-257-treated mice following 65-minutes of transient middle cerebral artery occlusion (tMCAo). Representative images of vehicle- and L-257-treated mouse brain sections (**A**). Mouse brain sections in both groups were assessed for total infarct (**B**) and oedema volume (**C**) on day 3 post-stroke. Percent infarct volume was also expressed relative to non-ischaemic hemisphere volume (**D**). Weight loss was measured at baseline and each day from stroke onset for a total of 3 days (**E**). Data presented as mean ± SEM, n=10, $P>0.05$, an unpaired t-test with Welch's post hoc test was used for comparisons of infarct or oedema volumes, whereas a two-way repeated measures ANOVA with Šídák's multiple comparisons test was used for comparisons of percent weight loss.

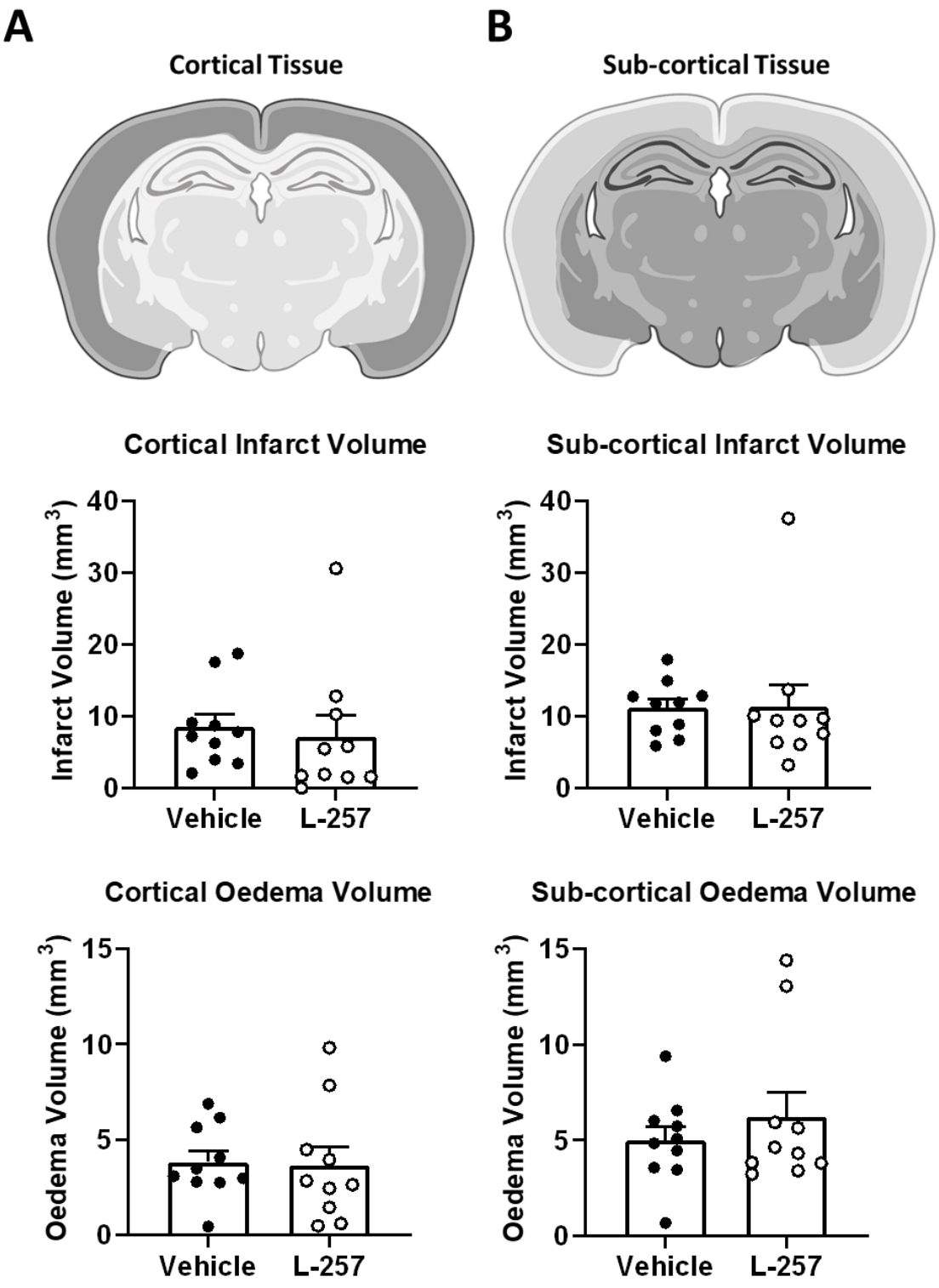

Figure 4-14. Cortical and sub-cortical infarct and oedema volumes of vehicle- and L-257-treated mice following 65-minutes of transient middle cerebral artery occlusion. Infarct and oedema volumes were measured in cortical (**A**) or sub-cortical (**B**) brain regions which are highlighted in dark grey in the representative images. Data presented as mean ± SEM, n=10, *P*>0.05, unpaired t-test with Welch's correction. Cortical vs Sub-cortical reference images were created with BioRender.com.

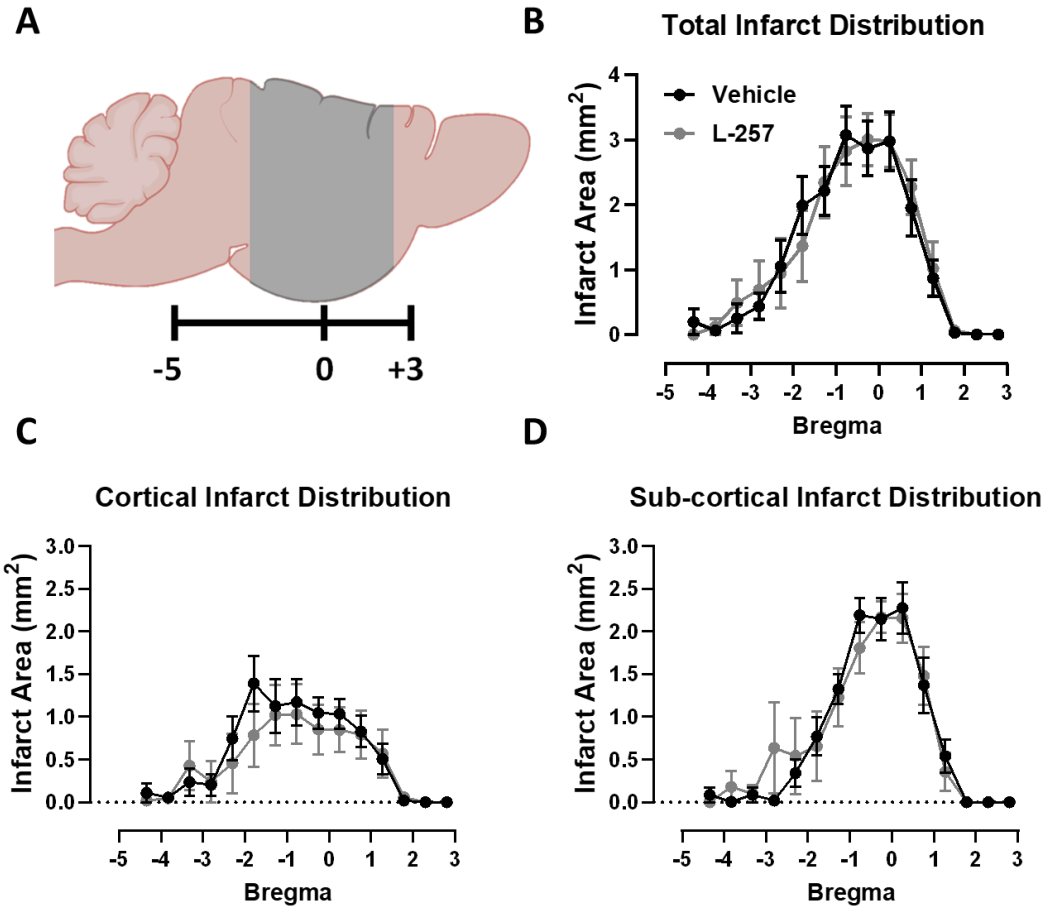

Figure 4-15. Differential infarct area distribution relative to Bregma of vehicle- and L-257-treated C57BL6/J mice following 65-minutes of transient middle cerebral artery occlusion (tMCAo). Thionin stained brain sections were collected between +3 anterior and -5 posterior relative to Bregma, spanning the typical region of infarct formation in this mouse model of tMCAo and is highlighted in grey (**A**). Total (**B**), cortical (**C**), and sub-cortical (**D**) infarct distribution of infarct area (mm^2) was plotted against the Bregma coordinates. Data presented as mean ± SEM, n=10, no statistical test was used. Bregma reference image was made with BioRender.com.

When assessing neurological and functional outcomes, no statistically significant evidence of differences was found between vehicle and L-257-treated mice post-stroke with respect to nest building activity, forelimb asymmetry (cylinder and foot fault tests), mNSS, or forelimb grip strength (Figure 4-16A-F). For example, both treatment groups displayed significantly reduced but comparable forelimb grip strength post-stroke (Figure 4-16F; L-257: pre-stroke, 103.5±6 vs post-stroke, 65.4±6 g, $P<0.05$; vehicle: pre-stroke, 109.2±6 vs post-stroke, 64.7±5 g, $P<0.05$). The same observation was made with nest building activity of mice in both groups. Moreover, significantly higher mNSS scores were observed on day 1 post-stroke in both treatment groups, whereas only vehicle-treated mice produced significantly higher scores on day 3 post-stroke. However, there were no statistical differences of mNSS scores between treatment groups on day 1 or day 3 post-stroke (Figure 4-16E).

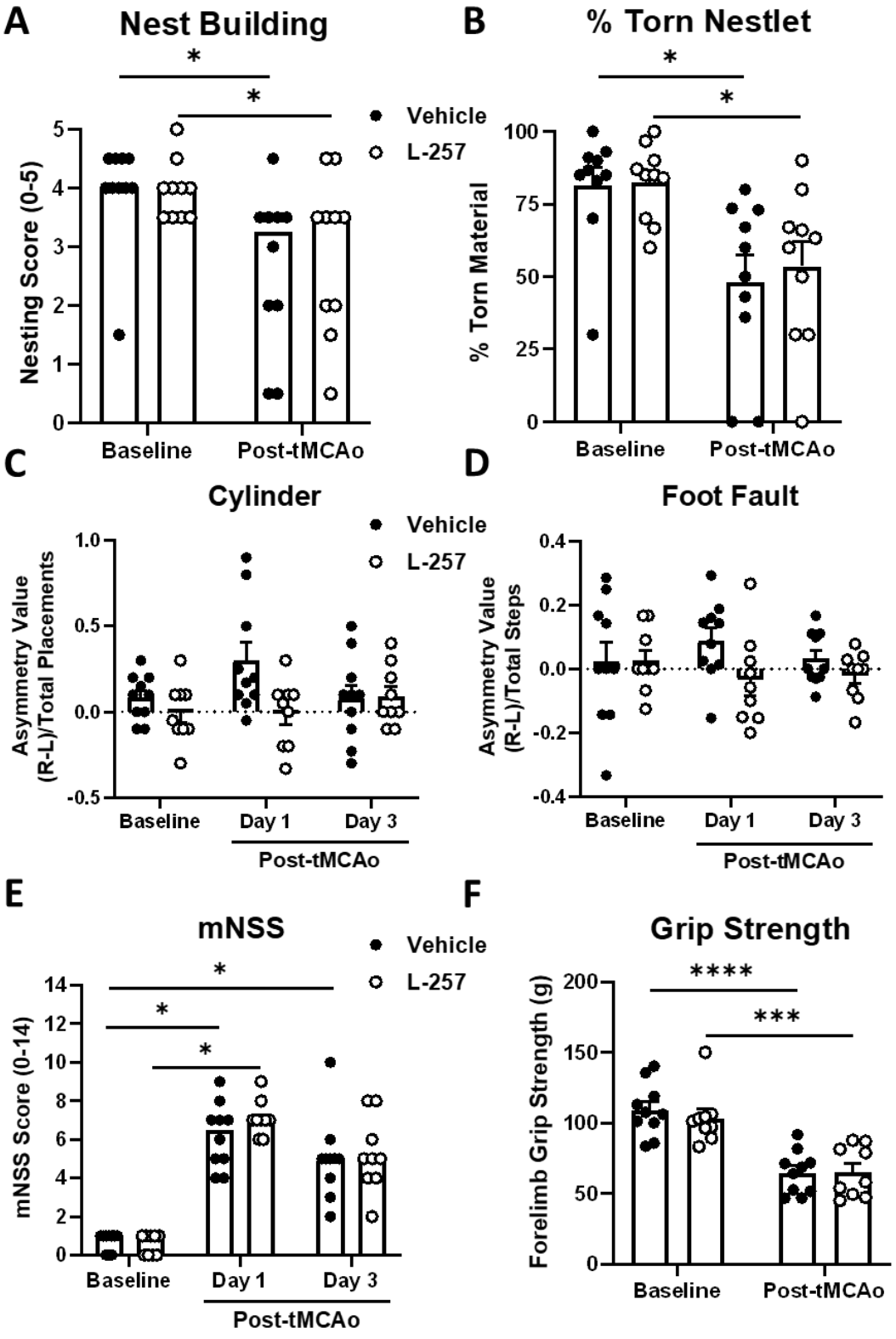
A
Nest Building
Nesting Score (0-5)
Vehicle
L-257
Baseline
Post-tMCAo
B
% Torn Nestlet
% Torn Material
C
Cylinder
Asymmetry Value (R-L)/Total Placements
Baseline
Day 1
Day 3
Post-tMCAo
D
Foot Fault
Asymmetry Value (R-L)/Total Steps
E
mNSS
mNSS Score (0-14)
F
Grip Strength
Forelimb Grip Strength (g)

Figure 4-16. Effect of DDAH1 inhibition using L-257 on neurological and functional outcomes after 65-minutes of transient middle cerebral artery occlusion (tMCAo) in mice. Baseline functional and neurological tests were performed in all mice prior to 65-minutes of tMCAo and treatment with either vehicle (saline) or L-257 (30 mg/kg) for 3 days. Tests were repeated on all mice on either day 1, 2, or 3 post-stroke, including the nest building activity test (**A-B**; day 2), forelimb grip strength test (**F**; day 2), cylinder and foot fault tests of forelimb asymmetry (**C-D**; day 1 and day 3), modified neurological severity score (**E**; day 1 and day 3). Nest building data presented as median, n=10, **P*<0.05, Wilcoxon matched pairs tests (pre- vs post-stroke) and Mann Whitney U tests (vehicle vs L-257), % torn nestlet data presented as mean ± SEM, n=10, **P*<0.05, paired t tests (pre- vs post-stroke) and unpaired t-tests (vehicle vs L-257), forelimb asymmetry test data presented as mean ± SEM, n=9-10, *P*>0.05, two-way repeated measures ANOVA with Šídák's multiple comparisons tests (baseline vs day 1 vs day 3; and vehicle vs L-257) and pre-post correction analysis was performed on day 1 and day 3 for both tests using unpaired t-tests (vehicle vs L-257), mNSS data presented as median, n=10, **P*<0.05, Friedman tests with multiple comparisons (baseline vs day 1 vs day 3) and unpaired t-tests (vehicle vs L-257), forelimb grip strength data presented as mean ± SEM, n=10, ****P*<0.001, *****P*<0.0001, two-way repeated measures ANOVA with Šídák's multiple comparisons tests.

4.3.7 DDAH1 inhibition does not alter apoptosis after 65-minutes of tMCAo in mice

Next, we examined the number of apoptotic cells in the infarct core and peri-infarct tissue regions in vehicle- and L-257-treated mice on day 3 post-stroke. As expected, the number of TUNEL-positive cells were greater in the infarct core compared to peri-infarct tissue in both treatment groups, however, treatment with L-257 (30 mg/kg) in mice had no significant effect on the number of TUNEL-positive cells in either tissue region relative to vehicle-treated mice (Figure 4-17A-B; Core: L-257, 0.73±0.07 vs Vehicle, 0.66±0.08 cells/mm^2; Peri-infarct: L-257, 0.15±0.02 vs Vehicle, 0.17±0.04 cells/mm^2).

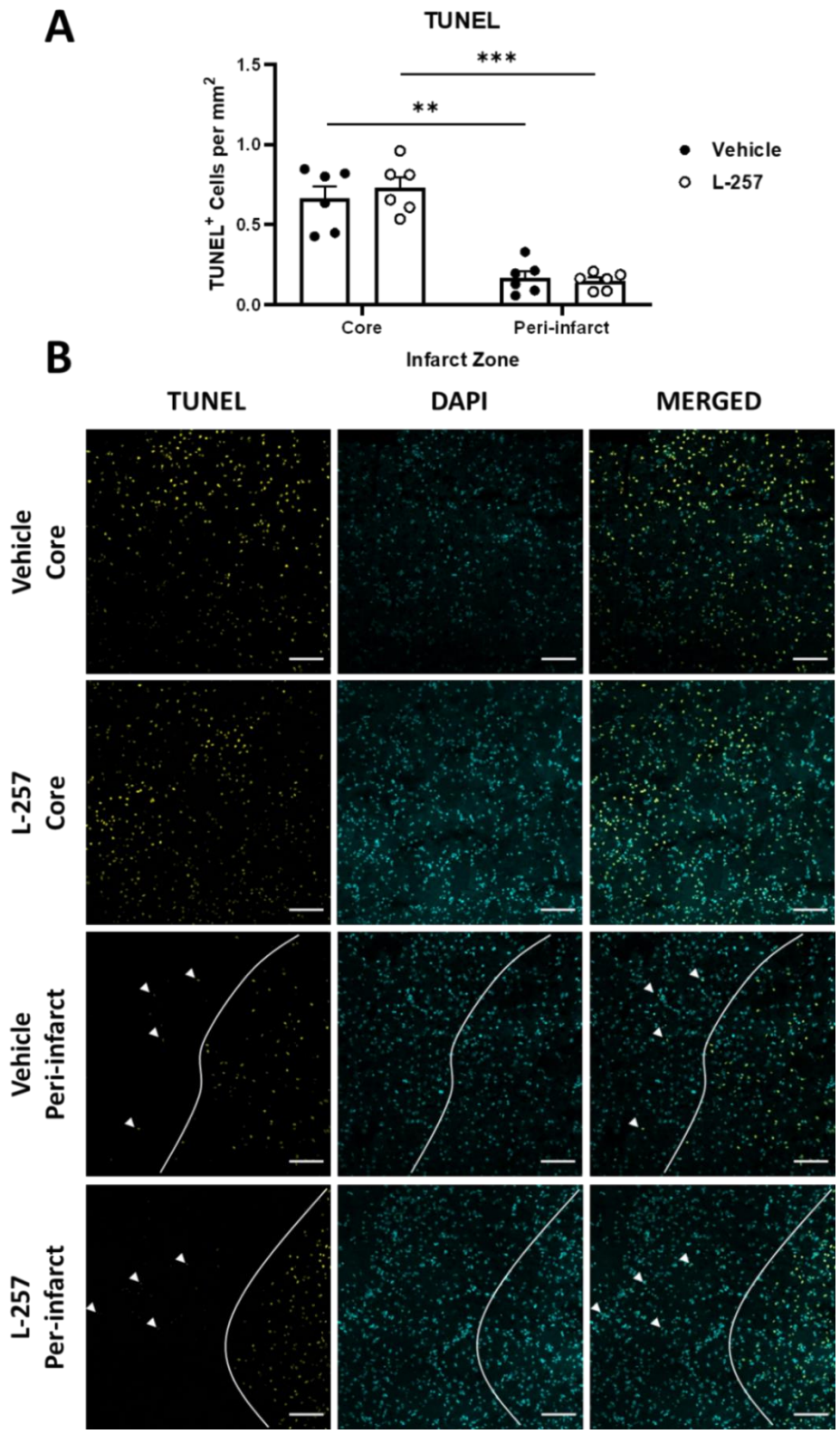

Figure 4-17. Effect of DDAH1 inhibition on apoptotic cell death in the infarct core and peri-infarct after 65-minutes of transient middle cerebral artery occlusion (tMCAo) in mice. Representative images of the infarct core and peri-infarct tissue regions of vehicle- and L-257-treated mice following 65-minutes tMCAo (**B**; bottom). Also shown is the semi-quantification of TUNEL-positive cells per mm^2 of each infarct tissue region of mice in both treatment groups (**A**). TUNEL-positive cells were quantified in the infarct core and peri-infarct regions using the Cell Counter tool on ImageJ analysis software and expressed relative to area (mm^2). Scale bars 100 µm. Data presented as mean ± SEM, n=6, $^{**}P<0.01$, $^{***}P<0.001$, paired t-test (core vs peri-infarct), unpaired t-test with Welch's correction (L-257 vs vehicle).

4.4 Discussion

One aim of this study was to determine the mechanisms that contribute to elevated ADMA levels post-stroke, which prior to this study was not clear. Using Western blotting and RT-qPCR, we showed that DDAH and type I PRMT protein and mRNA expression was unchanged after focal cerebral ischaemia in mice or oxygen-glucose deprivation in human cerebral microvascular endothelial cells. These findings suggest that altered expression of either DDAH isoform or the type I PRMTs evaluated in this study do not contribute to the increased ADMA levels following ischaemic stroke. A second aim of this study was to test the hypothesis that elevated ADMA levels following the inhibition of DDAH1 worsens ischaemic brain injury and functional and neurological outcomes by disrupting eNOS-NO signalling. We found that DDAH1 inhibition using the selective inhibitor L-257 disrupts eNOS-derived NO signalling in intracranial and extracranial cerebral arteries *in vitro*, presumably through the accumulation of ADMA, and increases brain ADMA levels *in vivo* without altering cardiovascular haemodynamics. Importantly, however, the major new finding was that DDAH1 inhibition in mice had no effect on the extent of ischaemic brain injury or neurological outcomes following cerebral ischaemia-perfusion. Taken together, these findings indicate that although DDAH1 appears to be a key regulator of cerebral eNOS-NO signalling, elevated ADMA levels following DDAH1 inhibition does not influence stroke outcomes in mice.

In healthy humans, plasma ADMA concentrations are approximately 0.5±0.1 μmol/L (Horowitz and Heresztyn, 2007), and concentrations of ADMA in plasma and CSF are significantly increased in ischaemic stroke patients compared to controls (Brouns *et al.*, 2009; Worthmann *et al.*, 2011). However, the mechanisms which underpin these changes after stroke are unclear. As mentioned previously, one potential mechanism is the increased expression or activity of the type I PRMTs that are responsible for methylating protein arginine residues, leading to increased ADMA release during proteolysis. Another potential mechanism is reduced metabolism of ADMA by the DDAH enzymes, also due to altered expression or activity of these enzymes. It is well established that oxidative and nitrosative stress are major contributors to injury during ischaemic stroke pathogenesis (Moskowitz, Lo and Iadecola, 2010; De Silva *et al.*, 2011), both of which were shown to be increased during the first two days in stroke patients after admission compared to both healthy and high-risk controls (Dogan *et al.*, 2018). Importantly, studies have demonstrated that expression or activity of both type I PRMTs and the DDAH enzymes are modulated by oxidative and nitrosative stress (Bӧger *et al.*, 2000; Leiper *et al.*, 2002; Sydow and Münzel, 2003). We therefore aimed to evaluate the effects of cerebral ischaemia-reperfusion on type I PRMT and DDAH expression in the mouse brain. Using Western blotting, we showed that there were no differences in type I PRMT or DDAH expression at 24-hours post-stroke. However, there was a significant increase in PRMT4

and 8, and DDAH1 and 2 at 72-hours post-stroke, whereas there were no differences in expression levels of PRMT1. Notably, however, we found that expression levels of ß-Actin, the loading control for PRMT4 and 8, and both DDAH isoforms were significantly decreased in the ischaemic hemisphere compared to non-ischaemic and sham control hemispheres at 72-hours post-stroke. Consistent with our findings, numerous studies have also reported modulated ß-Actin expression levels in pre-clinical models of cerebral ischaemia. For example, one study demonstrated that ß-Actin mRNA was significantly increased 7 days after subarachnoid haemorrhage in dogs (Aihara *et al.*, 2008), whereas another study demonstrated that expression of several common loading control proteins, including ß-Actin, were significantly reduced in bEnd.3 cells after 2.5-hours of OGD (Comajoan *et al.*, 2018). Thus, ß-Actin appears to be downregulated in response to cerebral ischaemia-reperfusion and is therefore an unsuitable loading control for investigations of protein expression in ischaemic mouse brain tissue using Western blotting (Goasdoue *et al.*, 2016). Due to similarities in molecular weight between PRMT1 and ß-Actin, ß-Tubulin was used as the loading control for PRMT1 experiments, and importantly, expression levels of ß-Tubulin were unchanged at 72-hours post-stroke (section 8.3 of Appendix). Consequently, in our subsequent experiments we analysed protein expression levels of PRMT4 and 8, and DDAH1 and 2 at 72-hours after cerebral ischaemia-reperfusion using ß-Tubulin and found that there were no differences in expression levels of all proteins of interest (section 8.2 of Appendix). Therefore, it is unlikely that changes in type I PRMT or DDAH protein expression are responsible for elevated ADMA levels following stroke.

As discussed earlier, eNOS-NO is important for cerebrovascular homeostasis and is protective during ischaemic stroke. Elevated ADMA after stroke may disrupt crucial eNOS-NO signalling, however, whether ADMA levels are altered within the cerebral endothelium post-stroke, and the mechanisms which underpin these potential changes are unknown. Therefore, we aimed to evaluate changes of type I PRMT and DDAH mRNA expression in cultured human cerebral microvascular endothelial cells (hCMEC/D3) after exposure to ischaemia-like conditions *in vitro* (OGD). Using RT-qPCR, we found that mRNA expression of both DDAH isoforms was increased in hCMEC/D3 cells after 24- but not 6-hours of OGD compared to normoxic controls. We observed no differences of PRMT1 mRNA expression, whereas there was a trend for increased mRNA expression of PRMT4 (CARM1; P=0.097). PRMT8 is expressed exclusively in neurons and therefore was not assessed. It is important to note, however, that the cycle threshold values for our PRMT4 data exceeded 35 in both normoxic and OGD conditions, suggesting that the levels of PRMT4 mRNA were negligible, raising questions about the biological relevance of increased PRMT4 expression in cells exposed to OGD. Furthermore, the use of immortalised hCMEC/D3 cells raises concerns whether the changes of DDAH expression after 24-hours OGD can be considered as reliable and representative of changes of gene expression in *in vivo* models. Taken together, our

Western blotting data indicate that neither DDAH1 and 2 nor any type I PRMT under investigation were altered after cerebral ischaemia in whole brain tissue, however, increased mRNA expression after 24-hours OGD raises the possibility that DDAH1 and 2 may be upregulated in cerebral endothelial cells after ischaemic stroke. It is clear therefore that further research is needed to explore the mechanisms responsible for increased ADMA levels following stroke. For instance, future studies using primary cerebral microvascular endothelial cells from mice and exposing them to ischaemia-like conditions are needed to confirm our findings using an immortalised cerebral endothelial cell line. It is important to also consider that the activities of the type I PRMTs and DDAH enzymes may be altered following stroke independently of protein expression levels. Additionally, increased proteolysis after ischaemic brain injury is likely to contribute to increased ADMA levels independently of changes in synthesis or metabolism by the PRMTs or DDAH enzymes, respectively. Lastly, although PRMT8 is exclusively expressed in neurons, other type I PRMTs (namely PRMT2, 3, and 6) are also expressed in the brain, and therefore alterations in the expression or activity of these isoforms may also contribute to increased ADMA levels following stroke.

To test whether elevated ADMA levels worsen stroke outcomes in mice, we used the selective DDAH1 inhibitor, L-257, to increase endogenous ADMA levels. It was previously shown that intravenous administration of L-257 (30 mg/kg) to rats significantly increased plasma ADMA levels by ~78% (Nandi *et al.*, 2012). Additionally, ADMA levels in CSF and plasma were previously shown to be increased in stroke patients compared to controls by approximately 31% and 20%, respectively (Brouns *et al.*, 2009; Worthmann *et al.*, 2011). Prior to this study, however, it remained unclear whether intraperitoneal administration of L-257 similarly increases plasma and more importantly brain ADMA levels in mice. Using HPLC-MS we found that L-257 led to a 17% and 32% increase in brain and plasma ADMA levels, respectively, without affecting levels of the stereoisomer SDMA which is not metabolised by DDAH1. However, the effect of L-257 on both brain and plasma ADMA levels failed to reach statistical significance. Using pilot data, *a priori* power calculations predicted that an n=6 was required for both groups in order to detect a minimum difference of 25%. However, *post hoc* power calculations now indicate that n=11 and n=18 is required for statistical powering for plasma and brain methylarginine levels, respectively. Therefore, additional experiments are needed to verify that L-257 administration to mice significantly increases ADMA levels in the brain. Indeed, the relative increases in plasma but not brain ADMA levels are comparable to those reported in studies showing a significant association between CSF (~31% increase vs healthy controls) and plasma (~20% increase vs healthy controls) ADMA levels and outcomes in stroke patients. Given it is well documented that elevated ADMA levels can increase arterial blood pressure through disruption of eNOS-NO, and that acute elevations in blood

pressure are positively associated with increased brain injury and worse outcome after ischaemic stroke (Pistoia *et al.*, 2016), we next evaluated the effect of DDAH1 inhibition using 30 mg/kg L-257 on cardiovascular haemodynamics in naïve mice. Using two approaches – tail-cuff plethysmography and radiotelemetry, we demonstrated that arterial blood pressures were comparable between vehicle and L-257-treated mice. Additionally, systolic, and diastolic pressures of L-257-treated mice were unchanged on day 3 of treatments relative to their baseline measurements. Interestingly, however, the cohort of L-257-treated mice had lower heart rates compared to vehicle-treated mice, however, it is important to highlight that there were no differences between heart rates at baseline compared with after the course of L-257 treatments.

Previous studies have shown that exogenous ADMA impairs eNOS-NO signalling in cerebral vessels from both rodents and humans (Faraci, Brian and Heistad, 1995; Segarra *et al.*, 1999), and that overexpression of DDAH1 enhances eNOS-NO signalling and prevents the inhibitory effects of ADMA on eNOS-NO signalling in carotid or cerebral arteries (Dayoub *et al.*, 2008; Rodionov *et al.*, 2010; Torondel *et al.*, 2010). However, direct evidence showing the functional importance of DDAH1 for maintaining eNOS-NO signalling in cerebral arteries is lacking. Furthermore, although a previous study showed that inhibition of DDAH1 with a structural isomer of L-257 (L-291, differing only by the inclusion of a hydroxyl group) impairs eNOS-NO signalling in peripheral vessels by increasing endogenous ADMA levels (Leiper *et al.*, 2007), no study has similarly tested whether DDAH1 inhibition by L-257 similarly impairs eNOS-NO signalling in cerebral arteries. Therefore, prior to examining the effect of DDAH1 inhibition by L-257 on stroke outcomes, we used small vessel myography to examine the effect of L-257 on eNOS-NO-dependent dilator responses of intracranial (middle cerebral) and extracranial (common carotid) cerebral arteries. We found that inhibition of DDAH1 with L-257 markedly impaired dilator responses to acetylcholine in both vessel types without affecting endothelial-independent dilator responses of carotid arteries to NO donor sodium nitroprusside. Additionally, the inhibitory effect of L-257 on dilator responses of middle cerebral arteries was comparable to that achieved by exogenous ADMA. Collectively, these experiments not only validate that L-257 impairs eNOS-NO signalling in cerebral vessels, most likely through the accumulation of ADMA, but also demonstrate for the first time the functional importance of DDAH1 in maintaining eNOS-NO signalling in cerebral arteries.

As mentioned previously, there is a lack of evidence showing a causal relationship between elevated ADMA and stroke outcomes. Therefore, having established that L-257 administration *in vivo* appears to increase brain and plasma ADMA levels without affecting cardiovascular haemodynamics, and that L-257 inhibits eNOS-NO signalling in cerebral vessels *in vitro*, we next assessed the effect of DDAH1 inhibition on stroke outcomes in

mice following 65-minutes transient middle cerebral artery occlusion. As discussed in Chapter 3, this occlusion period was chosen because it presented clinically relevant stroke outcomes (approximately 4-14% or 28-80 mm^3 infarct volume, (Carmichael, 2005)) as well as detectable neurological and functional deficits. We found that there was no difference between vehicle and L-257-treated mice with respect to infarct and oedema volumes, or apoptosis on day 3 post-stroke, and there were there no differences in neurological and functional outcomes between treatment groups. These findings suggest that elevated ADMA levels resulting from DDAH1 inhibition does not influence outcomes in this model of stroke. Notably, *a priori* power calculations indicated an n=14 per group would be required to see a 65% increase in infarct volume after L-257 treatment compared to controls. However, there was no obvious trend that stroke outcomes were increased in L-257-treated mice at n=10 and thus it is unlikely that a difference would emerge by increasing each group to the predicted statistical powering. An important consideration is the relatively short half-life of L-257 in plasma (approximately 2 hours, personal communication by Professor Leiper). It is likely that by 12-hours post-stroke, the levels of L-257 in the circulation and possibly the brain will have decreased significantly. Notably, however, the pathological effects of accumulated ADMA on eNOS-NO and other NOS isoforms may be sustained beyond this duration. As discussed above, we found that L-257 resulted in a 17% increase in brain ADMA levels in naïve mice, which was comparable to the relative change in ADMA levels in the plasma but not the CSF of stroke patients who experienced worse outcomes, and therefore the increased ADMA levels following L-257 treatment may be insufficient to significantly disrupt eNOS-NO and subsequently stroke outcomes. However, previous pilot experiments in our laboratory have shown that infarct volumes were significantly increased in mice treated with L-257 after a shorter and milder tMCAo duration of 40-minutes (section 8.6 of Appendix). Therefore, it appears unlikely that the lack of effect of L-257 on stroke outcomes in this study can be explained by the short half-life and thus bioavailability of L-257, or an inadequate increase in brain ADMA levels.

Our central hypothesis was that elevated ADMA levels will disrupt the protective effects of eNOS-NO, thereby worsening stroke outcomes. Indeed, previous studies have reported that eNOS-deficient mice produce larger infarcts compared to control mice after tMCAo (Huang *et al.*, 1996; Cui *et al.*, 2013). In contrast, it is well established that nNOS- and iNOS-derived NO is toxic during stroke, contributing to nitrosative stress and exacerbated cell death. For example, studies have shown that mice deficient in nNOS or iNOS exhibit reduced ischaemic injury compared to control mice after tMCAo (Huang *et al.*, 1994; Iadecola *et al.*, 1997). Additionally, studies using nNOS and iNOS inhibitors similarly demonstrate the deleterious effects of NO derived from nNOS and iNOS during stroke (Nagafuji *et al.*, 1995; Zhang *et al.*, 1996; Zhang and Iadecola, 1998; L. Zhou *et al.*, 2010;

Li *et al.*, 2022). Thus, it is likely that the deleterious contributions of nNOS- and iNOS-NO to stroke outcomes may be more pronounced in severe ischaemia models compared to milder ischaemia models. We therefore propose that in our initial pilot stroke studies where DDAH1 inhibition worsened outcomes in mice who underwent a relatively short 40-minute occlusion period, the contributions of the toxic effects of nNOS-NO and iNOS-NO on stroke outcome could be less pronounced than in mice in the present study who have undergone a longer 65-minute occlusion period. As such, in the mice undergoing milder 40-minute tMCAo, the deleterious effects of elevated ADMA on outcomes may largely relate to the inhibition of protective eNOS-NO signalling, whereas in the mice undergoing a more moderate-severe 65-minute tMCAo, the lack of effect of elevated ADMA on outcomes may relate to the inhibition of both the protective and toxic effects of the different NOS isoforms. Therefore, although speculative at present, the impact of elevated ADMA on stroke outcomes may ultimately be dependent on the initial stroke severity and resultant relative contributions of the NOS isoforms.

In summary, we have provided evidence that although inhibition of DDAH1 markedly impairs eNOS-NO signalling in cerebral vessels, the accumulation of ADMA after DDAH1 inhibition has no effect on stroke outcomes in mice, including ischaemic brain injury and neurological and functional deficits. As discussed, future studies are required to examine whether the impact of ADMA on stroke outcomes is ultimately dependent on stroke severity and the opposing contributions of eNOS vs nNOS/iNOS to ischaemic brain injury. Such studies should allow us to definitively test whether ADMA plays a causal role in ischaemic stroke pathogenesis.

Chapter 5 Investigating the importance of endothelial DDAH1 in regulating cerebral artery function and in ischaemic stroke pathogenesis

5.1 Introduction

The cerebral endothelium plays a crucial role in maintaining vascular homeostasis in the cerebral circulation. Furthermore, it constitutes a key structural component of the blood-brain barrier, characterised by an array of tight junctions, which together with neighbouring cell types (neurons, astrocytes, microglia, pericytes) form the neurovascular unit (NVU) (Iadecola, 2017). Central to the roles of the cerebral endothelium is the synthesis of nitric oxide (NO) by endothelial NO synthase (eNOS) which occurs in response to numerous stimuli. Cerebral eNOS-NO is important for the regulation of resting vascular tone and cerebral blood flow (CBF), furthermore it influences BBB permeability, inhibits vascular remodelling, and contributes to angiogenesis (Faraci, 2011). Notably, however, it is widely accepted that cerebral endothelial dysfunction, characterised by reduced eNOS-NO bioavailability, is associated with all major cardiovascular risk factors (Grover-Páez and Zavalza-Gómez, 2009), and contributes to cerebral small vessel disease, and increases the risk of stroke (Quick *et al.*, 2021). For example, studies have demonstrated that eNOS deficiency in mice leads to spontaneous cerebral infarction (Tan *et al.*, 2015) and also worsens ischaemic stroke outcomes (Huang *et al.*, 1996). Furthermore, there is substantial clinical evidence indicating that endothelial dysfunction contributes to the pathogenesis of cerebrovascular disease, including stroke (Zimmermann, Wimmer and Haberl, 2004; Chan *et al.*, 2008; Cao *et al.*, 2020; Sashindranath and Nandurkar, 2021). Thus, it is likely that mechanisms which disrupt eNOS-NO may contribute to ischaemic stroke pathogenesis and result in worse stroke outcomes in humans.

Asymmetric dimethylarginine (ADMA) is an endogenous inhibitor of eNOS-NO signalling and therefore can exert profound pathological effects on the cerebral circulation. The dimethylarginine dimethylaminohydrolase (DDAH) enzymes are responsible for approximately 80% of ADMA clearance, of which DDAH1 was recently reported to be expressed in numerous cell types within the brain, including cerebral endothelial cells (Kozlova *et al.*, 2022). Exogenous ADMA was previously shown to impair NO-dependent vasorelaxation of human middle cerebral arteries (MCA) (Segarra *et al.*, 1999), and ADMA infusion was also shown to significantly reduce cerebral perfusion as well as increase cerebral arterial stiffness in healthy humans (Kielstein *et al.*, 2006). Studies have shown that DDAH1 overexpression in mice protects against the pathological effects of ADMA-induced cerebral vascular dysfunction (Dayoub *et al.*, 2008; Zhao *et al.*, 2021), however, no such studies have directly demonstrated the importance of DDAH1 for regulating eNOS-NO signalling in the cerebral circulation. Importantly, in the context of ischaemic stroke, elevated ADMA levels are associated with increased stroke risk (Wanby *et al.*, 2006) and worse stroke outcomes (Worthmann *et al.*, 2011). Furthermore, a loss-of-function (-396 4N deletion-insertion) polymorphism in the promoter region of the DDAH1 gene is significantly associated with increased risk of ischaemic stroke (Ding *et al.*, 2010).

Additionally, the rs233112 DDAH1 single nucleotide polymorphism significantly increases the risk of delayed cerebral ischaemia after subarachnoid haemorrhage (Hannemann *et al.*, 2020). Collectively, this work suggests that DDAH1 in the cerebral endothelium is a functionally important regulator of eNOS-NO and thus stoke outcomes by controlling intracellular ADMA levels.

The aims of this study were first to evaluate the functional importance of endothelial DDAH1 for regulating eNOS-NO signalling by examining the impact of endothelial-specific DDAH1 knockout on endothelial and vascular smooth muscle function in mouse cerebral and carotid arteries. Secondly, we examined the importance of endothelial DDAH1 for outcomes after ischaemic stroke by evaluating the impact of endothelial-specific DDAH1 knockout on ischaemic brain injury, apoptosis, and neurological and functional impairments in mice after cerebral ischaemia-reperfusion.

5.2 Materials and methods

5.2.1 Animals

In this chapter, a total of 77 male and 49 female mice (8-15 weeks of age) were used, including 12 DDAH1$^{En-/-}$ (6 male, 6 female) and 12 DDAH1$^{fl/fl}$ (6 male, 6 female) mice for measuring haemodynamics using tail cuff plethysmography, 26 DDAH1$^{En-/-}$ (11 male, 15 female), 29 DDAH1$^{fl/fl}$ (15 male, 14 female), and 9 male C57BL6/J mice for vascular function studies, 4 female DDAH1$^{En-/-}$ and 4 female DDAH1$^{fl/fl}$ mice for the histological assessment of arterial stiffness, 7 male DDAH1$^{En-/-}$ and 7 male DDAH1$^{fl/fl}$ mice for evaluating differentially expressed genes by RNAseq, 9 male DDAH1$^{En-/-}$ and 7 male DDAH1$^{fl/fl}$ mice for studying ischaemic stroke outcomes. However, 1 male DDAH1$^{En-/-}$ mouse and 2 male DDAH1$^{fl/fl}$ mice were excluded from the groups used for evaluating ischaemic stroke outcomes, and the reasons for exclusions are described later in this chapter.

5.2.2 Assessment of endothelial-specific DDAH1 knockout on cardiovascular haemodynamics in mice using tail cuff plethysmography

Systolic and diastolic pressures, and heart rates of male and female DDAH1$^{En-/-}$ and DDAH1$^{fl/fl}$ mice were recorded using a BP-2000 Blood Pressure Analysis System™ (Visitech Systems Inc., US), as described in section 2.1.7 in General Methods. Dr Alexandra Riddell performed blood pressure measurements whereas the experimental design and analysis was performed by me.

5.2.3 Effect of endothelial-specific DDAH1 knockout on eNOS-NO function in middle cerebral arteries, common carotid arteries, mesenteric arteries and thoracic aorta

To evaluate the importance of endothelial DDAH1 for regulating eNOS-NO signalling, endothelium-dependent and -independent vasoreactivity was assessed in MCA, CCA, mesenteric arteries and thoracic aortae of both male and female DDAH1$^{En-/-}$ and DDAH1$^{fl/fl}$ mice. Thus, vessels were collected as described in section 2.1.9 in General Methods and mounted in perfusion (MCA) or wire (CCA, mesenteric artery, thoracic aorta) myograph systems as described in sections 2.1.11 and 2.1.10 in General Methods, respectively.

Vessels were randomly allocated to the following cumulative concentration response curves using the random list generator www.random.org/lists: acetylcholine (10^{-10} to $3x10^{-5}$ M), nitroprusside (10^{-10} to $3x10^{-5}$ M), phenylephrine (10^{-10} to $3x10^{-5}$ M), or U46619 (10^{-10} to $3x10^{-6}$ M). For vasodilation (MCA) and vasorelaxation (CCA, mesenteric artery, thoracic aorta) curves, vessels were pre-contracted using the thromboxane A2 mimetic U46619 (10^{-9} – 10^{-8} M). Vessels for contraction curves (CCA) were allowed to equilibrate at baseline for 15-minutes before performing concentration response curves. Vasodilation responses of MCA are presented as % diameter change, whereas vasorelaxation responses

of CCA, mesenteric arteries and thoracic aortae are presented as % relaxation of U46619 pre-contraction. Contractile responses of CCA were presented as isometric force (mN). Half-maximal effective concentration ($logEC_{50}$) and maximum relaxation/contraction responses (R_{max}/C_{max}) were calculated for all vessels.

5.2.4 Evaluation of collagen and elastin content in middle cerebral and common carotid arteries from endothelial-specific DDAH1 knockout mice

MCA and CCA from female $DDAH1^{En-/-}$ and $DDAH1^{fl/fl}$ control mice were isolated as described in section 2.1.9 in General Methods, embedded in paraffin and sectioned as described in section 2.4.1 in General Methods. Collagen and elastin composition of arterial sections were evaluated using picrosirius red and elastin van Gieson staining, respectively, as described in section 2.4.2 in General Methods. A total of 5 sections of MCA and CCA from each mouse were analysed and an average was taken for each vessel type. Images were analysed using ImageJ Image Processing and Analysis Software (NIH, US).

5.2.5 Evaluation of differentially expressed genes in cerebral microvessels from endothelial-specific DDAH1 knockout and floxed control mice

Cerebral microvessel enriched pellets were isolated from naïve or tMCAo male $DDAH1^{En-/-}$ and $DDAH1^{fl/fl}$ mice as described in section 2.1.12 in General Methods. RNA was extracted from microvessel pellets from each mouse and quantified as described in section 2.3.1 in General Methods, followed by storage at -80°C. A schematic of the RNA-seq study workflow is shown in Figure 5-1. All samples were assessed for integrity and purity followed by RNA-sequencing (RNA-seq) by the Next-Generation Sequencing (NGS) team at Glasgow Polyomics. Bulk RNA-seq was performed using poly-A selection, 2x 100 base pairs, and 35 million reads on purified RNA samples. Data analysis was performed by Dr Graham Hamilton at Glasgow Polyomics, whereas data interpretations were performed by Graham and me.

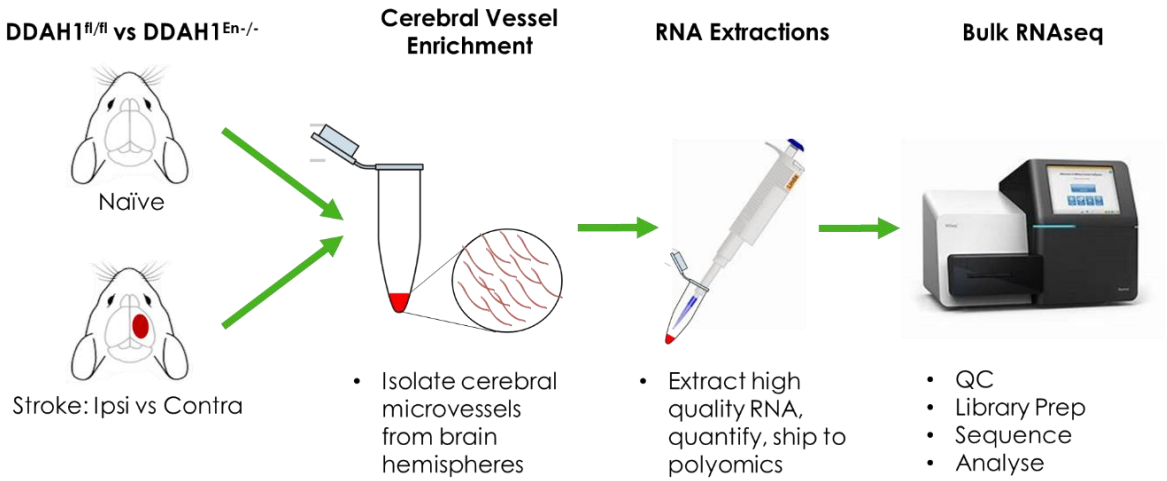

Figure 5-1. Schematic of the RNA-seq study workflow. Mouse brain microvessels were isolated from the hemispheres of naïve or tMCAo male DDAH1$^{En-/-}$ and DDAH1$^{fl/fl}$ mice. Purified RNA was extracted from vessel enriched preparations prior to quality control, library prep and sequencing by the Glasgow Polyomics NGS team.

5.2.6 Effect of endothelial-specific DDAH1 knockout on outcomes after tMCAo

Focal cerebral ischaemia was induced in DDAH1$^{En-/-}$ and DDAH1$^{fl/fl}$ control mice by tMCAo for 50-minutes followed by reperfusion as described in section 2.1.2 of General Methods. In Chapter 3, we showed that 65-minutes tMCAo in C57BL6/J mice produced clinically relevant stroke outcomes. However, in our pilot studies using DDAH1$^{En-/-}$ and DDAH1$^{fl/fl}$ mice we found that this duration of tMCAo resulted in the mice exceeding the ethical severity limits of our Home Office Project Licence, with a large proportion of the mice being culled before the scientific endpoint of the study. Therefore, in this chapter we reduced the occlusion period to 50-minutes. Neurological and functional outcomes were assessed at baseline and post-stroke, as described in section 2.1.5 of General Methods. In brief, all tests were performed prior to induction of ischaemia. The modified neurological severity score, foot fault, and cylinder tests were performed on days 1 and 3 post-stroke, whereas the forelimb grip strength and nest building activity tests were performed on day 2 post-stroke (Figure 5-2). Body weights were measured pre-stroke and then every day thereafter until the study endpoint.

Analyses for the study included determining infarct and oedema volumes as well as the semi-quantification of TUNEL-positive apoptotic cells in the infarct core and peri-infarct tissue. In brief, brains were isolated from mice at 72-hours post-stroke before being slow-frozen over liquid nitrogen. Frozen brains were embedded in OCT for cryosectioning, as described in section 2.1.3 of General Methods. Thionin staining was used to delineate the infarct, and total, cortical, and sub-cortical infarct and oedema volumes were evaluated as described in section 2.1.4 of General Methods. Semi-quantification of TUNEL-positive cells was assessed in the infarct core and peri-infarct regions of frozen brain sections from DDAH1$^{En-/-}$ and DDAH1$^{fl/fl}$ mice, as described in section 2.1.13 of General Methods.

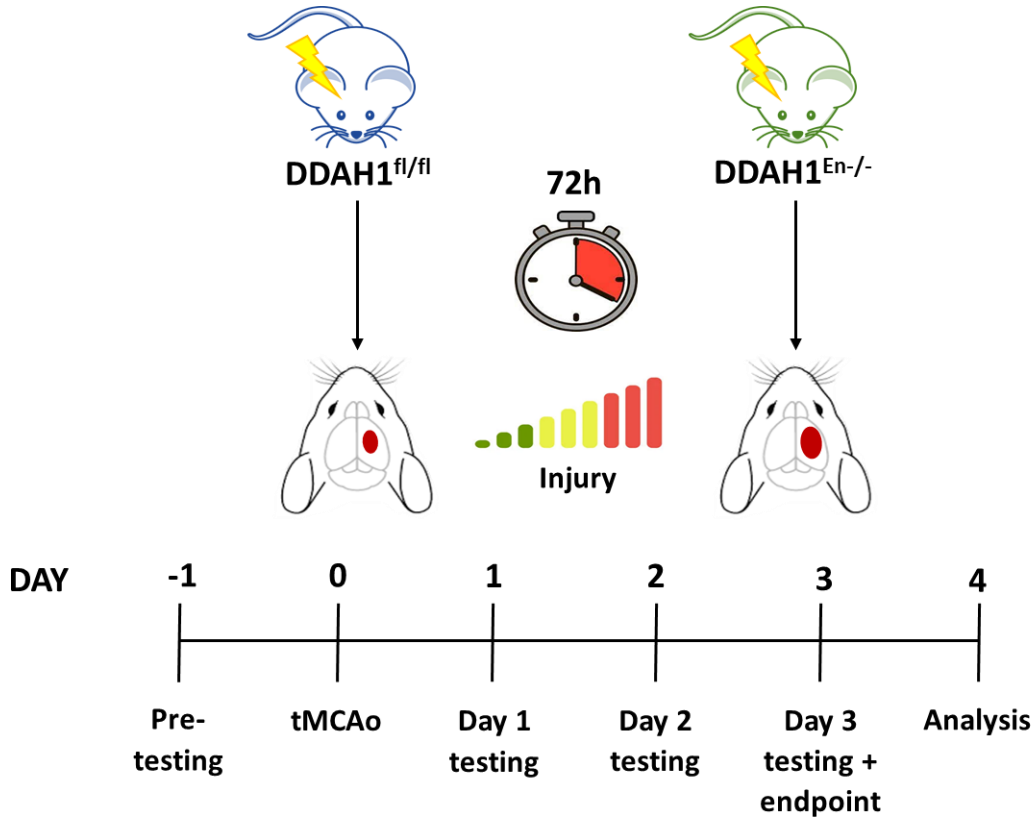

Figure 5-2. Schematic illustrating the groups, neurological tests, and study endpoint.

5.2.7 Power Calculations

Statistical powers for the transgenic DDAH1 stroke study were calculated using G* Power statistical power calculation software (Heinrich Heine University, Germany). In brief, pilot data from our lab showed that the selective DDAH1 inhibitor L-257 significantly increased infarct size compared to vehicle controls after mild cerebral ischaemia (40-minutes tMCAo, section 8.6 of Appendix), and thus we also expected worse outcomes in DDAH1$^{En-/-}$ mice compared to DDAH1$^{fl/fl}$ controls after 50-minutes tMCAo. Therefore, it was estimated that the minimal animals required were n=12 per group using the mean and SD infarct volume data from the 50-minute tMCAo group in Chapter 3 ($\alpha = 0.05$, Power = 0.8 [$\beta = 0.2$], effect size = 1.26, two-tailed effect) to detect a minimum difference of 50% infarct size between DDAH1$^{fl/fl}$ and DDAH1$^{En-/-}$ mice.

5.2.8 Statistical Analysis

All datasets were analysed with GraphPad Prism 9 (GraphPad Software, USA). $P<0.05$ was considered statistically significant. Group numbers are indicated in the corresponding figure legends.

Parametric data is expressed as mean ± SEM. This includes measurement of cardiovascular haemodynamics using tail cuff plethysmography, vascular function (cerebral and systemic vessels), quantification of collagen and elastin content in MCA and CCA, changes in rCBF after tMCAo, infarct and oedema volumes and neurological outcomes after tMCAo (% torn

nestlet, forelimb asymmetry tests [cylinder and foot fault], forelimb grip strength), and the semi-quantification of TUNEL-positive cells after tMCAo. The following statistical tests were used:

- Paired t-tests were used for comparisons of forelimb asymmetry (cylinder and foot fault tests) between day 1 and 3 in each group post-stroke.
- Unpaired t-tests with Welch's correction were used for comparisons of collagen and elastin content of cerebral arteries, half-maximal effective concentration ($logEC_{50}$) and maximal dilator or contractile responses (R_{max}/C_{max}) of cerebral and peripheral vessels, infarct and oedema volumes post-stroke, comparisons of forelimb asymmetry between groups on day 1 and 3 post-stroke, and pre-post analysis of forelimb asymmetry in each group.
- A two-way repeated measures ANOVA with Šídák's multiple comparisons test was used for comparing cardiovascular haemodynamics, endothelial-dependent and endothelial-independent vascular reactivity of MCA, CCA, mesentery, and aorta, % weight loss in mice post-stroke, % torn nest building material, and forelimb grip strength.
- A two-way ANOVA with Tukey's post hoc test was used to compare TUNEL-positive cells in the infarct core and peri-infarct brain regions.
- Multivariate analysis of RNA samples from isolated $DDAH1^{En-/-}$ and $DDAH1^{fl/fl}$ cerebral microvessels by RNAseq was performed by Graham Hamilton at Glasgow Polyomics, University of Glasgow. An adjusted *p*-value of $P<0.1$ was considered statistically significant.

Non-parametric data is expressed as median. This includes the nest building activity and mNSS tests. The following statistical tests were used:

- A Wilcoxon matched pairs test as used to compare nest building activity post-stroke to baseline of mice in each group.
- A Friedman test with Dunn's multiple comparisons test was used to measure changes of mNSS score of mice in each group.
- A Mann Whitney U test was used to compare nest building scores between groups, as well as to compare mNSS scores between $DDAH1^{En-/-}$ and $DDAH1^{fl/fl}$ mice on day 1 and 3 post-stroke.

5.3 Results

5.3.1 Endothelial-specific DDAH1 knockout does not alter cardiovascular haemodynamics

A previous study has shown that endothelial-specific DDAH1 knockout has no effect on cardiovascular haemodynamics in male mice (Dowsett *et al.*, 2015). However, it is unknown whether DDAH1 deletion similarly has no effect in female mice. Therefore, we firstly evaluated whether cardiovascular haemodynamics are altered in male and female DDAH1$^{En-/-}$ and DDAH1$^{fl/fl}$ mice using tail cuff plethysmography. We found that there were no statistical differences in systolic or diastolic blood pressures, or heart rates between genotypes for both male and female mice in each group (Figure 5-3). For example, systolic blood pressures were comparable between genotypes of male (DDAH1$^{fl/fl}$, 114.9±2 vs DDAH1$^{En-/-}$, 110.4±1 mmHg) and female (DDAH1$^{fl/fl}$, 118.2±2 vs DDAH1$^{En-/-}$, 120.3±1 mmHg) mice.

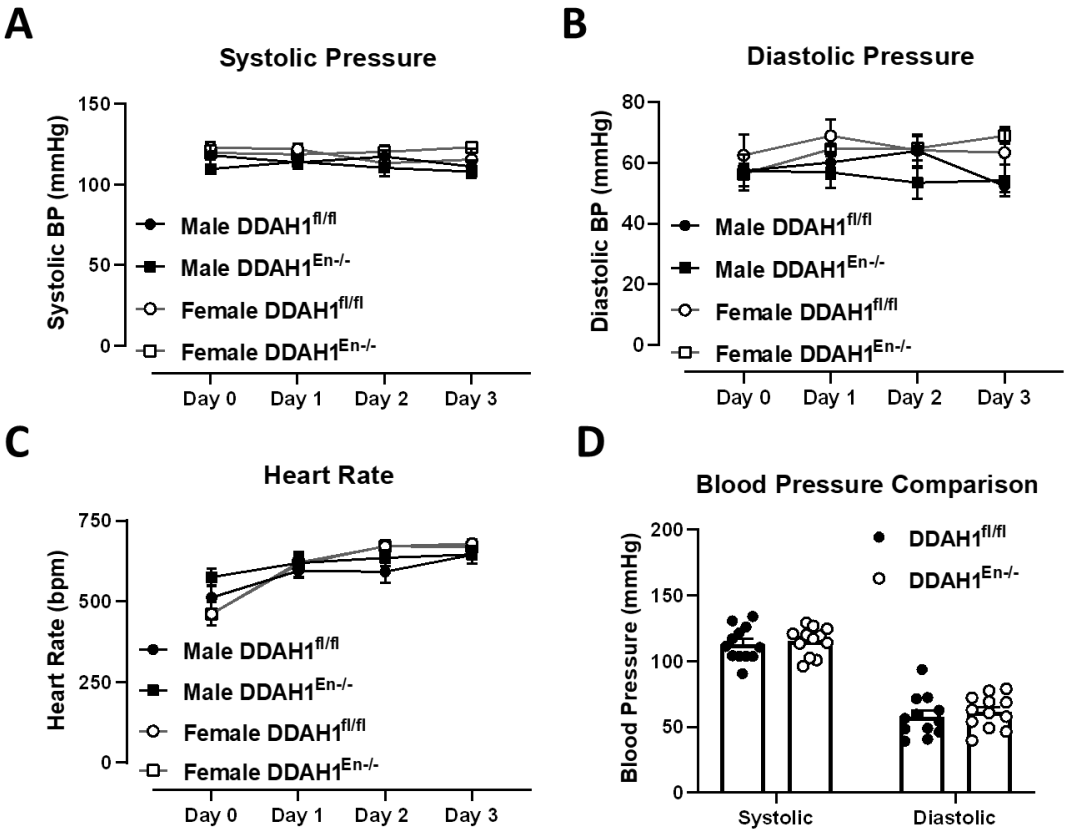

Figure 5-3. Effect of endothelial-specific DDAH1 knockout on haemodynamics in mice by tail cuff plethysmography. Systolic pressure, diastolic pressure, and heart rate readings were taken from male and female DDAH1$^{fl/fl}$ and DDAH1$^{En-/-}$ mice for 4 days (**A-C**). Measurements were taken at the same time each day, and mean blood pressures of each mouse for each of the 4 days was compared between genotypes (mixed sex; **D**). Data presented as mean ± SEM, n=8, P>0.05, a paired t-test was used for comparisons of heart rate between day 0 and day 3 in each group, and a two-way ANOVA with repeated measures and Šídák's multiple comparisons test was used for comparing differences of systolic pressure, diastolic pressure, and heart rate between groups.

5.3.2 Vascular function of cerebral but not systemic arteries is impaired in endothelial-specific DDAH1 knockout mice

Baseline diameters of MCA were comparable between groups ($DDAH1^{En-/-}$, 131.7±2 vs $DDAH1^{fl/fl}$, 125±4 µm; *P*>0.05, unpaired t-test). Data describing the integrity of the vessels and R_{max} and $logEC_{50}$ values for cumulative concentration response curves are shown in Table 5-1 and Table 5-2, respectively. Notably, maximal KPSS contractile responses of MCA from $DDAH1^{En-/-}$ mice were significantly lower compared to $DDAH1^{fl/fl}$ controls, and the level of U46619 pre-contractile responses (prior to acetylcholine and nitroprusside curves) were significantly higher in $DDAH1^{En-/-}$ mice compared to controls (Table 5-1; ACh, *P*<0.05; SNP, *P*>0.05). There was a trend for acetylcholine-induced vasodilator responses of MCA from $DDAH1^{En-/-}$ mice (mixed sex, n=3-4) to be impaired compared to MCA from control mice, however, this difference failed to reach statistical significance (Figure 5-4A). Similarly, there were no statistical differences between genotypes with respect to maximal relaxation (R_{max}) or half-maximal effect concentrations ($logEC_{50}$) responses to acetylcholine. For vasodilator responses to nitroprusside, the data comprises of only n=2 and therefore no statistical analyses were performed. However, the data so far suggests no obvious differences in nitroprusside-induced vasodilator responses of MCA between $DDAH1^{En-/-}$ and $DDAH1^{fl/fl}$ controls (Figure 5-4B).

Acetylcholine			
	Mixed sex $DDAH1^{fl/fl}$	**Mixed sex $DDAH1^{En-/-}$**	***n***
Baseline Diameter (µm)	131.7±2	125±4	3-4
KPSS (% diameter change)	-64.2±2	-47.1±5*	
Pre-contractile to U46619 (% KPSS)	44.2±5	61.4±3*	
Pre-contractile to U46619 (% Baseline Diameter)	28.8±3	28±1	
Nitroprusside			
	Male $DDAH1^{fl/fl}$	**Male $DDAH1^{En-/-}$**	***n***
Baseline Diameter (µm)	135; 130	125; 135	2
KPSS (% diameter change)	-64.3; -61.5	-44.0; -51.9	
Pre-contractile to U46619 (% KPSS)	33.3; 43.8	49.1; -35.7	
Pre-contractile to U46619 (% Baseline Diameter)	23.1; 26.9	21.6; 20.0	

Table 5-1. Middle cerebral artery integrity values of vessels that were used in acetylcholine-induced and nitroprusside-induced response curves. Maximum contractile responses of middle cerebral arteries to high potassium physiological salt solution (KPSS; % diameter change); and U46619 pre-contraction levels (% KPSS and % baseline diameter) prior to commencing cumulative concentration-response curves. Data presented as mean ± SEM (acetylcholine) or individual values for experiment 1 and 2 (nitroprusside), where *n* is number of animals. There were statistically significant differences between $DDAH1^{En-/-}$ and $DDAH1^{fl/fl}$ for KPSS and U46619 pre-contraction levels (%KPSS) prior to acetylcholine curves, *P<0.05, unpaired t-test with Welch's correction. No statistical tests were performed on nitroprusside data.

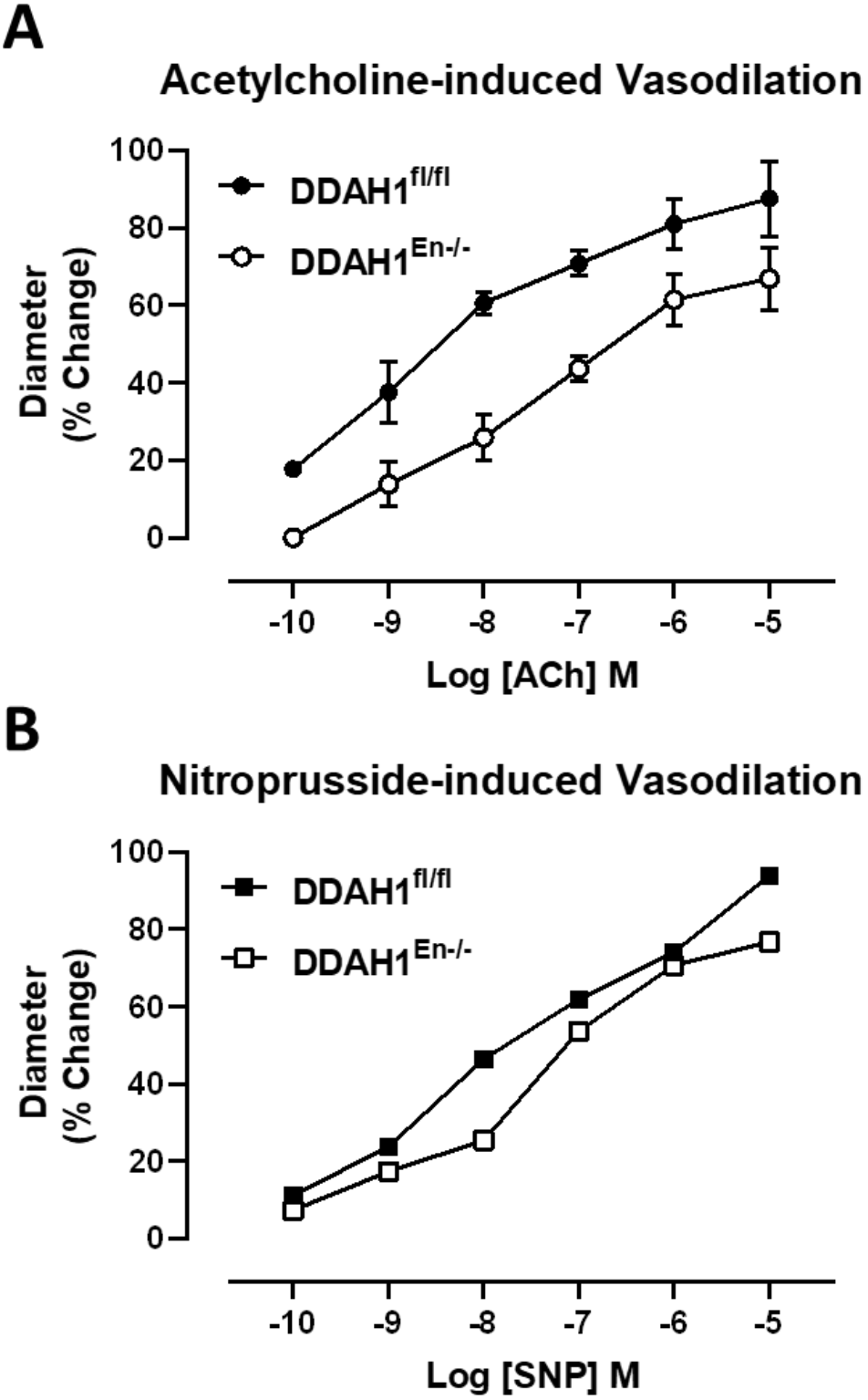

.

Figure 5-4. Acetylcholine-induced and nitroprusside-induced vasodilator responses of middle cerebral arteries from endothelial-specific DDAH1 knockout (DDAH1$^{En-/-}$) and control (DDAH1$^{fl/fl}$) mice. Cumulative concentration response curves to acetylcholine (10^{-10} to $3x10^{-6}$ M; male DDAH1$^{En-/-}$, n=3; female DDAH1$^{En-/-}$, n=1; male DDAH1$^{fl/fl}$, n=2; female DDAH1$^{fl/fl}$, n=1; **A**) or sodium nitroprusside (10^{-10} to $3x10^{-6}$ M; male DDAH1$^{En-/-}$ and DDAH1$^{fl/fl}$, n=2; **B**) in isolated middle cerebral arteries. Data presented as mean ± SEM, n=4 (acetylcholine data), $P>0.05$, two-way ANOVA with repeated measures and Šídák's multiple comparisons test. No statistical tests were performed on nitroprusside data.

Acetylcholine			
	Mixed sex DDAH1$^{fl/fl}$	**Mixed sex DDAH1$^{En-/-}$**	***n***
R_{max} (% diameter change to U46619)	87.6±10	66.9±8	3-4
R_{max} *P* Value	*P* = 0.17		
$logEC_{50}$	-7.7; -9.1	-7.5±0.2	2-3
$logEC_{50}$ *P* Value	N/A		
Nitroprusside			
	Male DDAH1$^{fl/fl}$	**Male DDAH1$^{En-/-}$**	***n***
R_{max} (% diameter change to U46619)	93.3; 94.3	81.5; 72.0	2
R_{max} *P* Value	N/A		
$logEC_{50}$	-6.7; ND	-7; ND	1
$logEC_{50}$ *P* Value	N/A		

Table 5-2. Summary of responses of middle cerebral arteries from endothelial-specific DDAH1 knockout (DDAH1$^{En-/-}$) and control (DDAH1$^{fl/fl}$) mice. Maximal relaxation responses (R_{max}) and half-maximal effect concentration ($logEC_{50}$) values of cumulative concentration-response curves to acetylcholine or nitroprusside. Data presented as mean ± SEM (acetylcholine) or as individual values (nitroprusside), where n is number of animals. P>0.05, unpaired t-tests with Welch's correction. No statistical tests were performed on nitroprusside data. ND: not determined.

Next, we evaluated the effect of endothelial-specific DDAH1 knockout on acetylcholine- and nitroprusside-induced vasorelaxation responses, as well as phenylephrine- and U46619-induced vasocontraction responses of CCA rings from both male and female mice. Vessel integrity, R_{max}, and $logEC_{50}$ values for cumulative concentration response curves are described in Table 5-3, Table 5-4, Table 5-5, and Table 5-6. Acetylcholine-induced vasorelaxation of CCA rings from male or female DDAH1$^{En-/-}$ mice were significantly impaired compared to DDAH1$^{fl/fl}$ controls (Figure 5-5A, Table 5-4). In contrast, nitroprusside-induced vasorelaxation response of CCA rings from male or female DDAH1$^{En-/-}$ mice were comparable to their respective DDAH1$^{fl/fl}$ controls, however, a modest, non-significant trend for impaired vasorelaxation was observed in CCA rings from male DDAH1$^{En-/-}$ (Figure 5-5B, Table 5-4). Interestingly, vasocontraction responses to phenylephrine or U46619 of CCA rings from male DDAH1$^{En-/-}$ mice were markedly impaired compared to DDAH1$^{fl/fl}$ controls, whereas there was only a non-significant trend for contractile responses to phenylephrine to be impaired in CCA rings from female DDAH1$^{En-/-}$ mice (Figure 5-6).

Acetylcholine						
	Male DDAH1$^{fl/fl}$	Male DDAH1$^{En-/-}$	*n*	Female DDAH1$^{fl/fl}$	Female DDAH1$^{En-/-}$	*n*
KPSS (mN)	1.2±0.4	2.3±0.2	4-6	2.9±0.9	2.7±0.5	4-6
Endothelial Function (%)	112.7±11	106.7±9	4-6	117.8±12	111.8±7	
Pre-contraction to U46619 (% KPSS)	55.7±4	51.2±3	4-6	61.6±9	53.2±5	
Nitroprusside						
	Male DDAH1$^{fl/fl}$	**Male DDAH1$^{En-/-}$**	***n***	**Female DDAH1$^{fl/fl}$**	**Female DDAH1$^{En-/-}$**	***n***
KPSS (mN)	1.6±0.3	1.9±0.2	5-6	2.4±0.2	2.5±0.5	5-6
Endothelial Function (%)	94.4±17	91.5±4	5-6	89.4±14	69.4±13	
Pre-contraction to U46619 (% KPSS)	51.2±5	47.3±3	5-6	52.5±3	58.2±6	

Table 5-3. Common carotid artery vessel integrity values that were used in acetylcholine-induced and nitroprusside-induced response curves. Maximum contractile responses to high potassium physiological salt solution (KPSS; mN); endothelial integrity which was assessed by measuring maximal relaxation responses to 10^{-6} M acetylcholine (% of U46619-induced tone); and U46619 pre-contraction levels (% of KPSS) prior to commencing cumulative concentration-response curves. Data presented as mean ± SEM, where n is number of animals. There were no statistical differences between genotypes for all parameters, $P>0.05$, unpaired t-test.

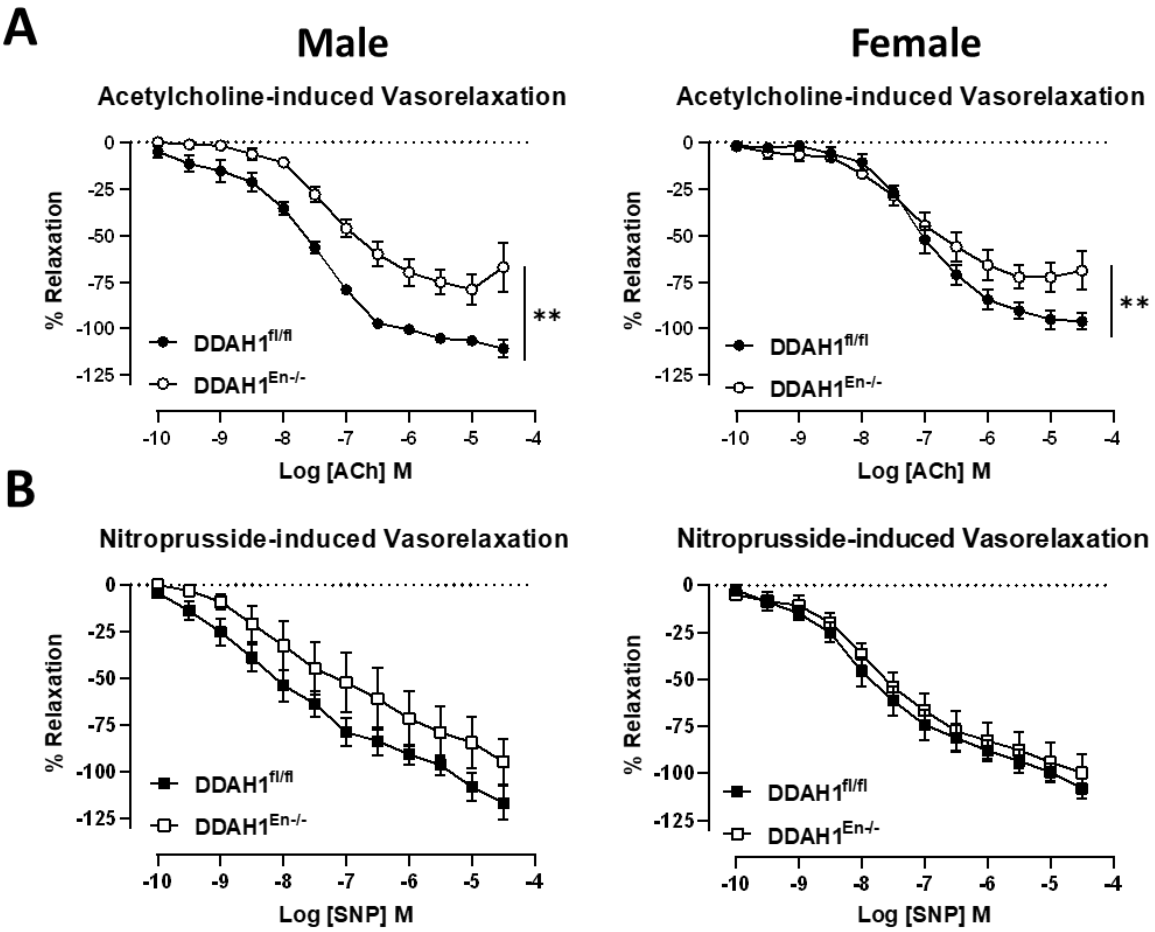

Figure 5-5. Acetylcholine-induced and nitroprusside-induced responses of common carotid arteries from endothelial-specific DDAH1 knockout (DDAH1$^{En-/-}$) and control (DDAH1$^{fl/fl}$) mice. Cumulative concentration response curves of CCA rings from male and female mice to acetylcholine (10^{-10} to $3x10^{-5}$ M; **A**) or sodium nitroprusside (10^{-10} to $3x10^{-5}$ M; **B**). Data presented as mean ± SEM, n=4-6, ***P*<0.01, two-way ANOVA with repeated measures and Šídák's multiple comparisons test.

	Acetylcholine					
	Male DDAH1$^{fl/fl}$	**Male DDAH1$^{En-/-}$**	***n***	**Female DDAH1$^{fl/fl}$**	**Female DDAH1$^{En-/-}$**	***n***
R_{max} (% Pre-contraction to U46619)	-110.7±5	-66.9±13	4-6	-94.8±4	-69.04±10	5-6
R_{max} *P* Value	**P* = 0.0211			*P* = 0.0523		
$logEC_{50}$	-7.49±0.05	-7.32±0.1	4-6	-7.03±0.07	-7.23±0.2	4-6
$logEC_{50}$ *P* Value	*P* = 0.276			*P* = 0.319		
	Nitroprusside					
	Male DDAH1$^{fl/fl}$	**Male DDAH1$^{En-/-}$**	***n***	**Female DDAH1$^{fl/fl}$**	**Female DDAH1$^{En-/-}$**	***n***
R_{max} (% Pre-contraction to U46619)	-116.7±9	-94.6±12	5-6	-108±5	-99.7±10	5
R_{max} *P* Value	*P* = 0.179			*P* = 0.481		
$logEC_{50}$	-7.53±1.2	-7.31±0.6	3-5	-7.87±0.2	-7.46±0.2	5
$logEC_{50}$ *P* Value	*P* = 0.879			*P* = 0.168		

Table 5-4. Summary of vasorelaxation responses of common carotid arteries from endothelial-specific DDAH1 knockout (DDAH1$^{En-/-}$) and control (DDAH1$^{fl/fl}$) mice. Maximal relaxation responses (R_{max}) and half-maximal effect concentration ($logEC_{50}$) values of cumulative concentration-response curves to acetylcholine or nitroprusside. Data presented as mean ± SEM, where n is number of animals. **P*<0.05, unpaired t-tests with Welch's correction.

	Phenylephrine					
	Male DDAH1$^{fl/fl}$	**Male DDAH1$^{En-/-}$**	***n***	**Female DDAH1$^{fl/fl}$**	**Female DDAH1$^{En-/-}$**	***n***
KPSS (mN)	2.06±0.3	1.5±0.2	4	1.49±0.4	1.52±0.2	4-5
Endothelial Function (%)	87.3±8	121±12	4	100±13	108±20	
	U46619					
	Male DDAH1$^{fl/fl}$	**Male DDAH1$^{En-/-}$**	***n***	**Female DDAH1$^{fl/fl}$**	**Female DDAH1$^{En-/-}$**	***n***
KPSS (mN)	2.01±0.08	1.6±0.5	4	1.4±0.4	1.2±0.3	5
Endothelial Function (%)	108.8±9	99.8±9	4	93.4±19	89.2±6	

Table 5-5. Common carotid artery vessel integrity values that were used in phenylephrine-induced and U46619-induced response curves. Maximum contractile responses to high potassium physiological salt solution (KPSS; mN); and endothelial integrity which was assessed by measuring maximal relaxation responses to 10-6 M acetylcholine (% of U46619-induced tone); and pre-contraction levels prior to commencing cumulative concentration-response curves. Data presented as mean ± SEM, where *n* is number of animals. There were no differences between genotypes for all parameters, *P*>0.05, unpaired t-test with Welch's correction.

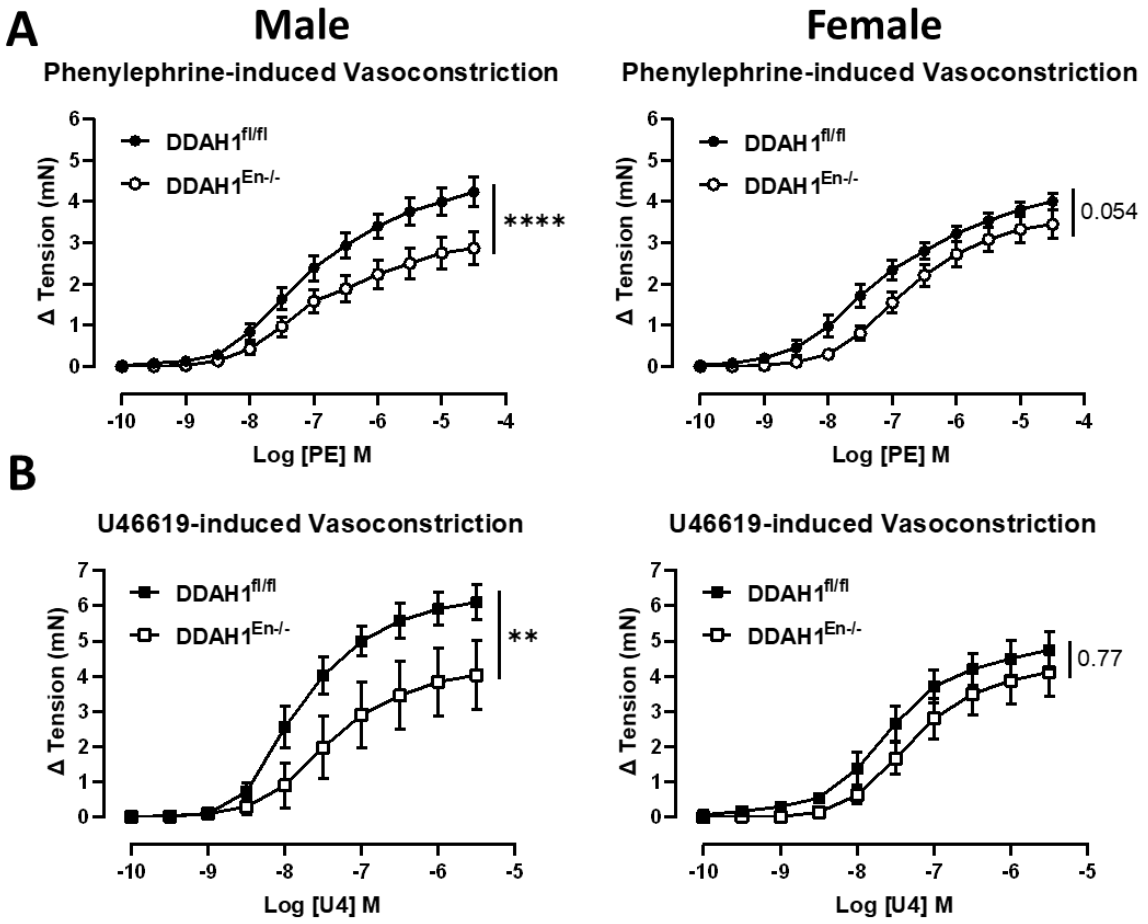

Figure 5-6. Phenylephrine-induced and U46619-induced contractile responses of common carotid arteries from endothelial-specific DDAH1 knockout (DDAH1$^{En-/-}$) and control (DDAH1$^{fl/fl}$) mice. Cumulative concentration response curves of CCA rings from male (left) and female (right) mice to phenylephrine (10^{-10} to $3x10^{-5}$ M; **A**) or U46619 (10^{-10} to $3x10^{-6}$ M; **B**). Data presented as mean ± SEM, n=4-6, ***P*<0.01, *****P*<0.0001 two-way ANOVA with repeated measures and Šídák's multiple comparisons test.

	Phenylephrine					
	Male DDAH1$^{fl/fl}$	**Male DDAH1$^{En-/-}$**	***n***	**Female DDAH1$^{fl/fl}$**	**Female DDAH1$^{En-/-}$**	***n***
C_{max} (mN)	4.2±0.4	2.9±0.4	4	4.01±0.2	3.5±0.3	4
C_{max} *P* Value	**P* = 0.0445			*P* = 0.224		
$logEC_{50}$	-7.2±0.2	-7.02±0.1	4	-7.3±0.2	-6.8±0.07	4
$logEC_{50}$ *P* Value	*P* = 0.501			*P* = 0.122		
	U46619					
	Male DDAH1$^{fl/fl}$	**Male DDAH1$^{En-/-}$**	***n***	**Female DDAH1$^{fl/fl}$**	**Female DDAH1$^{En-/-}$**	***n***
C_{max} (mN)	6.1±0.5	4.04±1	4	4.8±0.5	4.1±0.7	4
C_{max} *P* Value	*P* = 0.126			*P* = 0.499		
$logEC_{50}$	-7.8±0.1	-7.3±0.2	4	-7.6±0.1	-7.3±0.08	4
$logEC_{50}$ *P* Value	*P* = 0.122			*P* = 0.0818		

Table 5-6. Summary of common carotid artery responses from endothelial-specific DDAH1 knockout (DDAH1$^{En-/-}$) and control (DDAH1$^{fl/fl}$) mice. Maximal contraction responses (C_{max}) and half-maximal effect concentration ($logEC_{50}$) values of cumulative concentration-response curves to phenylephrine or U46619. Data presented as mean ± SEM, where n is number of animals. **P*<0.05, unpaired t-tests with Welch's correction.

To examine whether endothelial-specific DDAH1 knockout also impairs endothelial function of systemic arteries that are of similar size to CCA (CCA: 300 μm vs 1st order mesenteric artery: 200 μm diameter), we evaluated acetylcholine- and nitroprusside-induced vasorelaxation responses of mesenteric arteries from DDAH1$^{En-/-}$ (mixed sex, n=2 for each sex) and DDAH1$^{fl/fl}$ (mixed sex, n=2 for each sex) mice. Vessel integrity, R_{max}, and $logEC_{50}$ values for cumulative concentration response are described in Table 5-7 and Table 5-8. In contrast to our findings with MCA and CCA, we found that there were no differences in vasorelaxation responses to acetylcholine or nitroprusside in mesenteric arteries from DDAH1$^{En-/-}$ mice compared to DDAH1$^{fl/fl}$ controls (Figure 5-7).

	Acetylcholine			**Nitroprusside**		
	Mixed sex DDAH1$^{fl/fl}$	**Mixed sex DDAH1$^{En-/-}$**	***n***	**Mixed sex DDAH1$^{fl/fl}$**	**Mixed sex DDAH1$^{En-/-}$**	***n***
KPSS (mN)	4.9±1.4	4.2±1.1	4	4.8±1.2	2.9±0.7	4
Endothelial Function (%)	89.9±3	95.2±7		93.3±3	72.4±8	
Pre-contraction to U46619 (% KPSS)	53.4±7	52.5±2		50.9±7	51.6±5	

Table 5-7. Mesenteric artery integrity values that were used in acetylcholine-induced and nitroprusside-induced response curves. Maximum contractile responses to high potassium physiological salt solution (KPSS; mN); and endothelial integrity which was assessed by measuring maximal relaxation responses to 10^{-6} M acetylcholine (% of U46619-induced tone); and pre-contraction levels prior to commencing cumulative concentration-response curves. Data presented as mean ± SEM, where n is number of animals. There were no differences between genotypes for all parameters, $P>0.05$, unpaired t-test with Welch's correction.

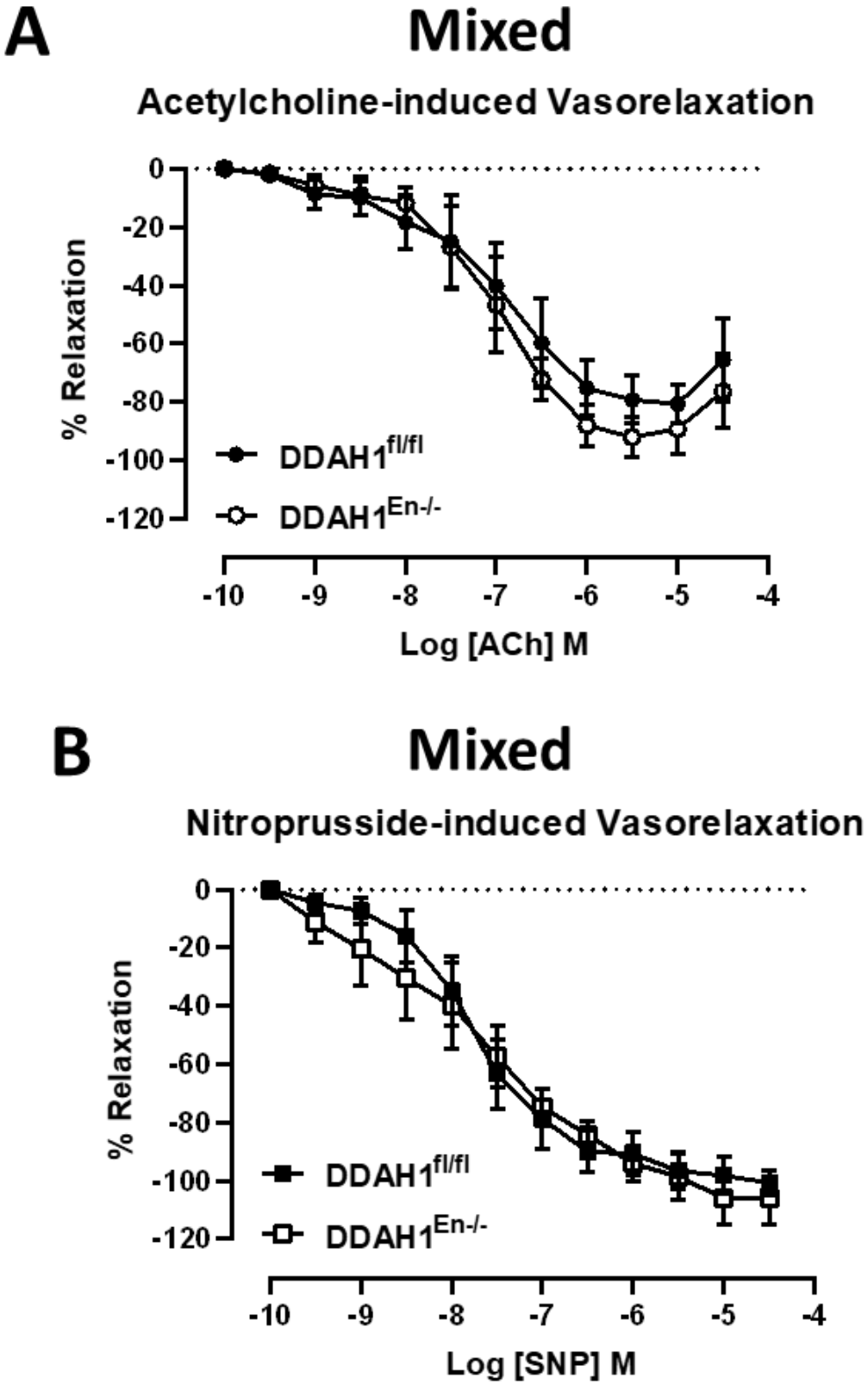

Figure 5-7. Acetylcholine-induced and nitroprusside-induced responses of mesenteric arteries from endothelial-specific DDAH1 knockout (DDAH1$^{En-/-}$) or control (DDAH1$^{fl/fl}$) mice. Cumulative concentration response curves of mesenteric artery rings from mixed sex (male: n=2, female: n=2) mice to acetylcholine (10^{-10} to $3x10^{-5}$ M; **A**) or sodium nitroprusside (10^{-10} to $3x10^{-5}$ M; **B**). Data presented as mean ± SEM, n=4, *P*>0.05, two-way ANOVA with repeated measures and Šídák's multiple comparisons test.

	Acetylcholine			Nitroprusside		
	Mixed sex DDAH1$^{fl/fl}$	**Mixed sex DDAH1$^{En-/-}$**	***n***	**Mixed sex DDAH1$^{fl/fl}$**	**Mixed sex DDAH1$^{En-/-}$**	***n***
R_{max} (% Pre-contraction to U46619)	-65.6±14	-76.3±13	4	-100.8±4	-106±9	4
R_{max} *P* Value	*P* = 0.595			*P* = 0.633		
logEC_{50}	-7.01±0.3	-7.06±0.2	4	-7.7±0.2	-7.4±0.4	3-4
logEC_{50} *P* Value	*P* = 0.908			*P* = 0.555		

Table 5-8. Summary of mesenteric artery responses from endothelial-specific DDAH1 knockout (DDAH1$^{En-/-}$) and control (DDAH1$^{fl/fl}$) mice. Maximal relaxation responses (R_{max}) and half-maximal effect concentration (logEC_{50}) values of cumulative concentration-response curves to acetylcholine and nitroprusside. Data presented as mean ± SEM, where n is number of animals. *P*>0.05, unpaired t-tests with Welch's correction.

Next, we evaluated the effect of endothelial-specific DDAH1 knockout on acetylcholine- and nitroprusside-induced vasorelaxation responses of thoracic aortae from DDAH1$^{En-/-}$ and DDAH1$^{fl/fl}$ mice (mixed sex). Vessel integrity, R_{max}, and logEC_{50} values for cumulative concentration response curves are described in Table 5-9 and Table 5-10, whereas the same data for thoracic aorta rings from C57BL6/J mice and incubated with either vehicle or L-257 are described in Table 5-11 and Table 5-12. Similar to our findings with mesenteric arteries, there were no differences in acetylcholine or nitroprusside relaxation responses of thoracic aorta rings between DDAH1$^{En-/-}$ and DDAH1$^{fl/fl}$ mice (Figure 5-8, Table 5-10). Importantly, however, we found that selective DDAH1 inhibition with L-257 markedly impaired acetylcholine-induced relaxation responses of thoracic aorta rings from C57BL6/J mice without affecting responses to nitroprusside (Figure 5-9, Table 5-12). Therefore, this data suggests that DDAH1 expressed in vascular smooth muscle rather than in the endothelium is crucial for maintaining eNOS-NO signalling in systemic arteries, whereas endothelial DDAH1 may be more important in cerebral arteries.

	Acetylcholine			Nitroprusside		
	Mixed sex DDAH1$^{fl/fl}$	**Mixed sex DDAH1$^{En-/-}$**	***n***	**Mixed sex DDAH1$^{fl/fl}$**	**Mixed sex DDAH1$^{En-/-}$**	***n***
KPSS (mN)	7.7±0.5	6.3±0.4	8	6.5±0.4	4.5±0.4	7-11
Endothelial Function (%)	66.2±6	60.3±3	8	42.4±4	38.8±4	
Pre-contraction to U46619 (% KPSS)	47±3	53.8±3	8	45.4±2	54.6±5	

Table 5-9. Thoracic aorta vessel integrity values from endothelial-specific knockout (DDAH1$^{En-/-}$) and control (DDAH1$^{fl/fl}$) mice that were used in acetylcholine- or nitroprusside-induced response curves. Maximum contractile responses to high potassium physiological salt solution (KPSS; mN); and endothelial integrity which was assessed by measuring maximal relaxation responses to 10^{-6} M acetylcholine (% of U46619-induced tone); and pre-contraction levels prior to commencing cumulative concentration-response curves. Data presented as mean ± SEM, where *n* is number of animals. There were no differences between genotypes for all parameters, *P*>0.05, unpaired t-test with Welch's correction.

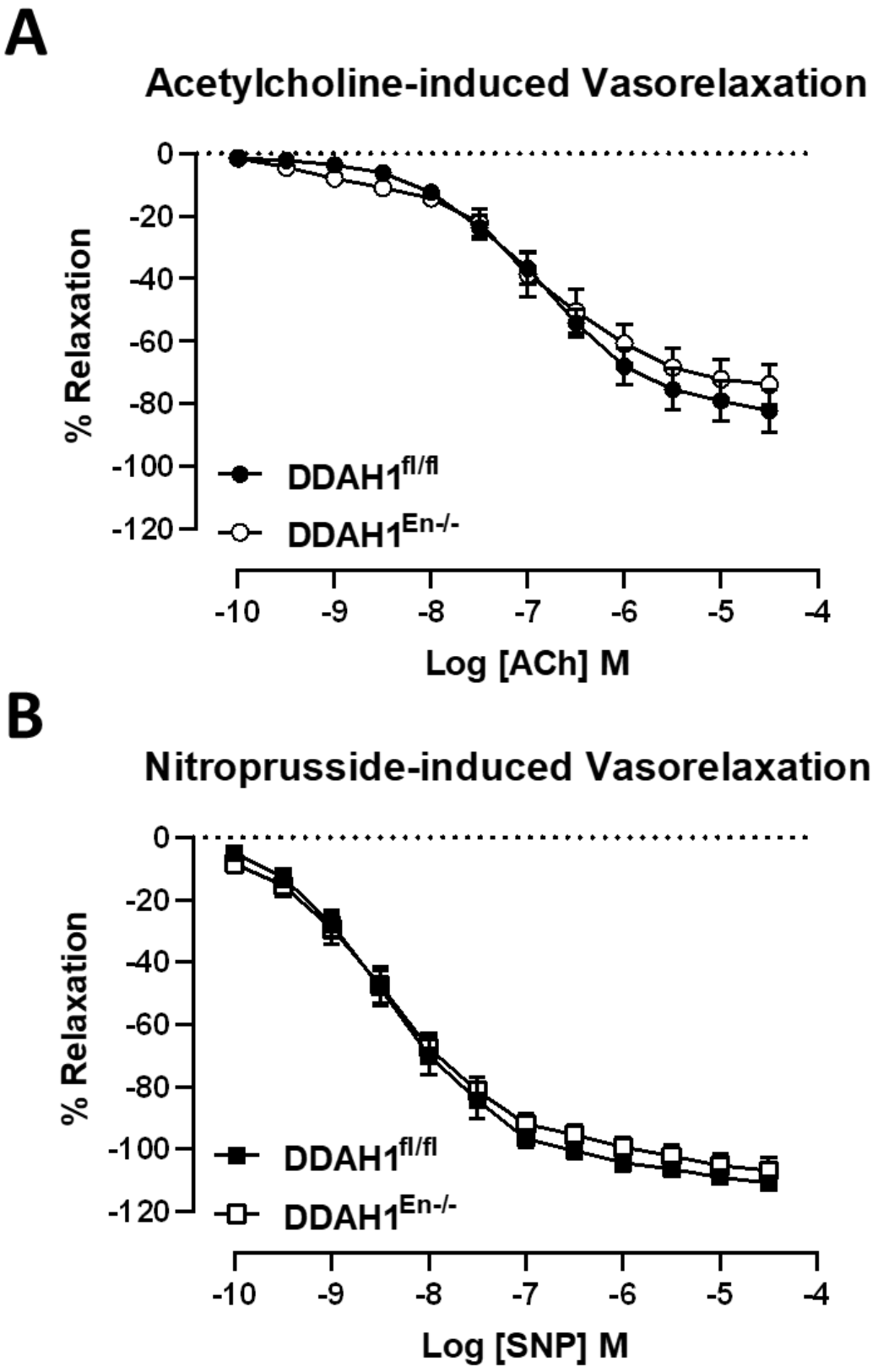

Figure 5-8. Acetylcholine-induced and nitroprusside-induced responses of thoracic aortae from endothelial-specific DDAH1 knockout (DDAH1$^{En-/-}$) or control (DDAH1$^{fl/fl}$) mice. Cumulative concentration response curves of thoracic aorta rings from mixed sex (DDAH1$^{fl/fl}$: male, n=3-5 and female, n=4 vs DDAH1$^{En-/-}$: male, n= 3-5 and female, n= 5-6) mice to acetylcholine (10^{-10} to $3x10^{-5}$ M; **A**) or sodium nitroprusside (10^{-10} to $3x10^{-5}$ M; **B**). Data presented as mean ± SEM, n=7-11, *P*>0.05, two-way ANOVA with repeated measures and Šídák's multiple comparisons test.

	Acetylcholine			Nitroprusside		
	Mixed sex DDAH1$^{fl/fl}$	**Mixed sex DDAH1$^{En-/-}$**	***n***	**Mixed sex DDAH1$^{fl/fl}$**	**Mixed sex DDAH1$^{En-/-}$**	***n***
R_{max} (% Pre-contraction to U46619)	-82.1±7	-73.9±7	8	-110.9±2	-106.9±4	10-11
R_{max} *P* Value	*P* = 0.395			*P* = 0.409		
logEC_{50}	-6.9±0.1	-6.9±0.2	8	-8.4±0.1	-8.4±0.2	10-11
logEC_{50} *P* Value	*P* = 0.935			*P* = 0.963		

Table 5-10. Summary of thoracic aorta responses from endothelial-specific DDAH1 knockout (DDAH1$^{En-/-}$) or control (DDAH1$^{fl/fl}$) mice. Maximal relaxation responses (R_{max}) and half-maximal effect concentration (logEC_{50}) values of cumulative concentration-response curves to acetylcholine or nitroprusside. Data presented as mean ± SEM, where *n* is number of animals. *P*>0.05, unpaired t-tests with Welch's correction.

	Acetylcholine			Nitroprusside		
	Male + Vehicle	**Male + L-257**	***n***	**Male + Vehicle**	**Male + L-257**	***n***
KPSS (mN)	8.3±2	*4.7±1	4	4.2±0.7	4.1±0.8	3-5
Endothelial Function (%)	48.1±8	50.7±7	3-4	52.4±9	51.6±5	
Pre-contraction to U46619 (% KPSS)	52.2±7	60.8±8	4	41.3±1	47.8±4	

Table 5-11. Thoracic aorta vessel integrity values that were used in acetylcholine-induced and nitroprusside-induced response curves and treated with vehicle or L-257 (100 µM). Maximum contractile responses to high potassium physiological salt solution (KPSS; mN); and endothelial integrity which was assessed by measuring maximal relaxation responses to 10^{-6} M acetylcholine (% of U46619-induced tone); and pre-contraction levels prior to commencing cumulative concentration-response curves. Data presented as mean ± SEM, where *n* is number of animals. There were no differences between treatment groups for all parameters except for KPSS responses in vessels used for acetylcholine-induced response curves, *P<0.05, unpaired t-test with Welch's correction.

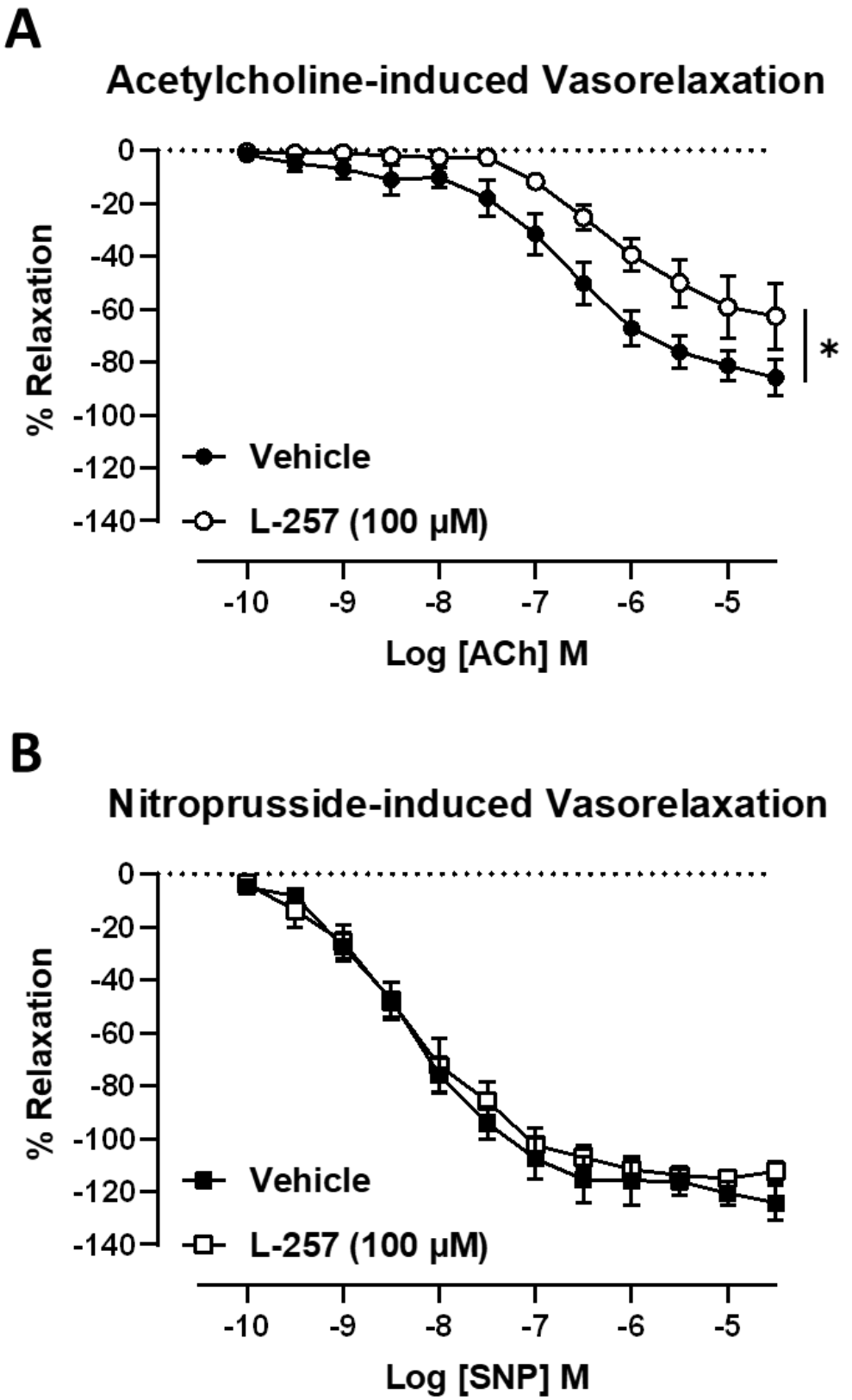

Figure 5-9. Acetylcholine- and nitroprusside-induced responses of mouse thoracic aortas treated with vehicle (water) or L-257 (100 µM). Cumulative concentration-response curves showing vasodilation responses to acetylcholine (10^{-10} to $3x10^{-5}$ M; **A**) or sodium nitroprusside (10^{-10} to $3x10^{-5}$ M; **B**). Results are expressed as % change in intraluminal diameter. Data presented as mean ± SEM, n=3-4, **P*<0.05, two-way ANOVA with repeated measures and Šídák's multiple comparisons test.

	Acetylcholine			Nitroprusside		
	Male + Vehicle	**Male + L-257**	***n***	**Male + Vehicle**	**Male + L-257**	***n***
R_{max} (% Pre-contraction to U46619)	-85.9±7	-62.7±13	4	-124.3±7	-112.4±4	4-5
R_{max} *P* Value	*P* = 0.172			*P* = 0.177		
$logEC_{50}$	-6.6±0.2	-6.2±0.2	4	-8.3±0.1	-8.3±0.2	4-5
$logEC_{50}$ *P* Value	*P* = 0.196			*P* = 0.997		

Table 5-12. Summary of male C57BL6/J thoracic aorta responses in vehicle or L-257 treated vessels. Maximal relaxation responses (R_{max}) and half-maximal effect concentration ($logEC_{50}$) values of cumulative concentration-response curves to acetylcholine and nitroprusside in vehicle- and L-257-treated thoracic aortas. Data presented as mean ± SEM, where n is number of animals. *P*>0.05, unpaired t-tests with Welch's correction.

5.3.3 Middle cerebral and common carotid arteries from female endothelial-specific DDAH1 knockout ($DDAH1^{En-/-}$) mice do not display evidence of altered collagen or elastin content

Our data examining relaxation responses of CCA to nitroprusside and subsequent contractile responses suggest altered or impaired vascular smooth muscle function and/or vascular stiffness in mice lacking endothelial DDAH1, albeit predominating in male mice. Therefore, we next examined whether these functional abnormalities are associated with altered collagen and/or elastin content in MCA and CCA. Due to time constraints and availability of mice we were only able to perform these experiments in female $DDAH1^{En-/-}$ and $DDAH1^{fl/fl}$ control mice. Using picrosirius red or elastin van Gieson staining, we found no significant differences in collagen or elastin staining between genotypes in both vessel types (Figure 5-10 and Figure 5-11), which potentially aligns with our finding that CCA from female $DDAH1^{En-/-}$ display less pronounced functional abnormalities of the vascular smooth muscle.

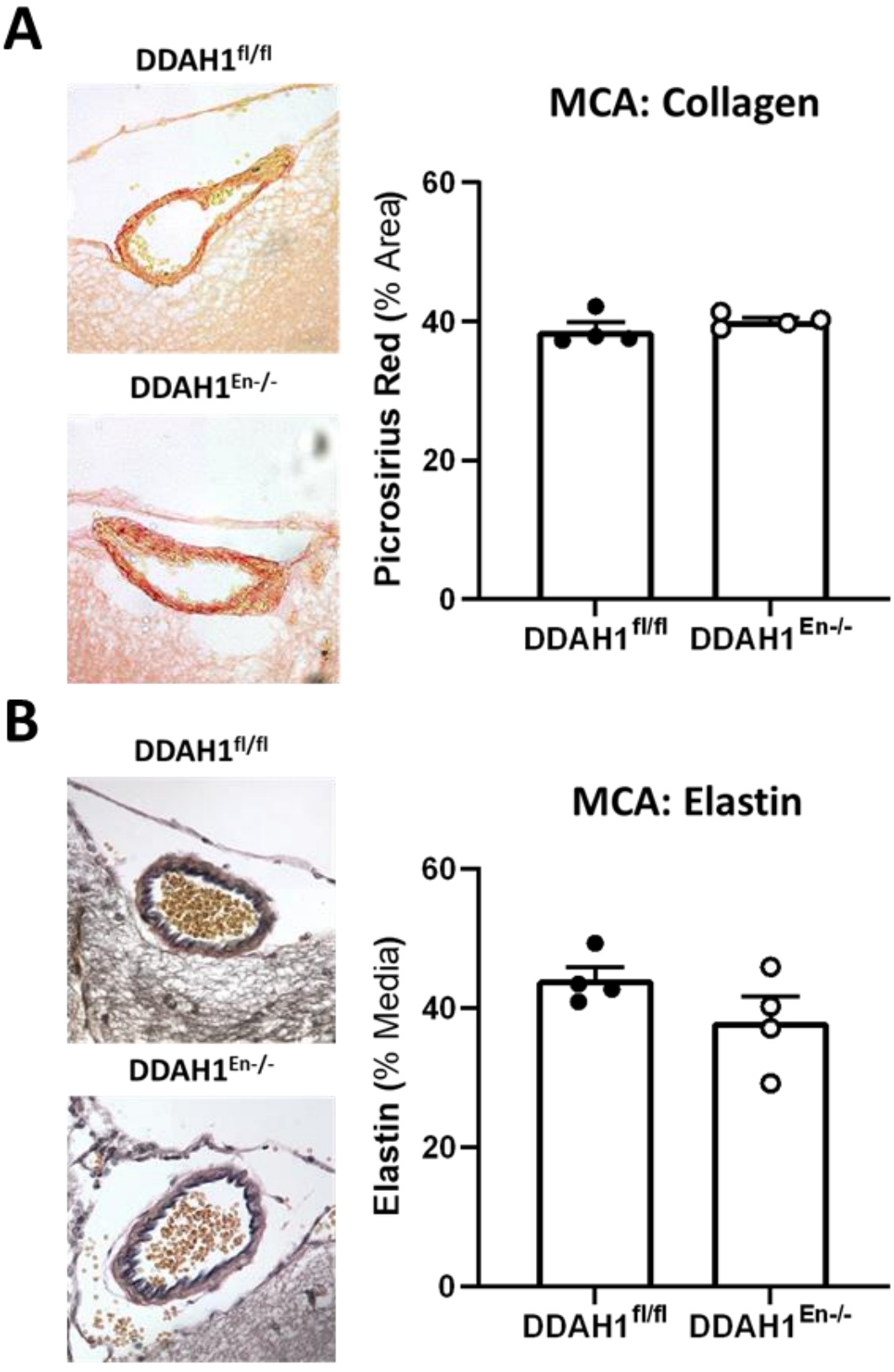

Figure 5-10. Effect of endothelial-specific DDAH1 knockout on collagen and elastin content in middle cerebral artery rings in mice. Representative images (left) of sections of middle cerebral arteries from female DDAH1$^{En-/-}$ and DDAH1$^{fl/fl}$ mice stained with picrosirius red (**A**, collagen) and elastin van Gieson (**B**, elastin). Also shown is a summary of mean collagen and elastin content (right) from five sections per mouse. Data presented as mean ± SEM, n=4, *P*>0.05, unpaired t-tests with Welch's correction.

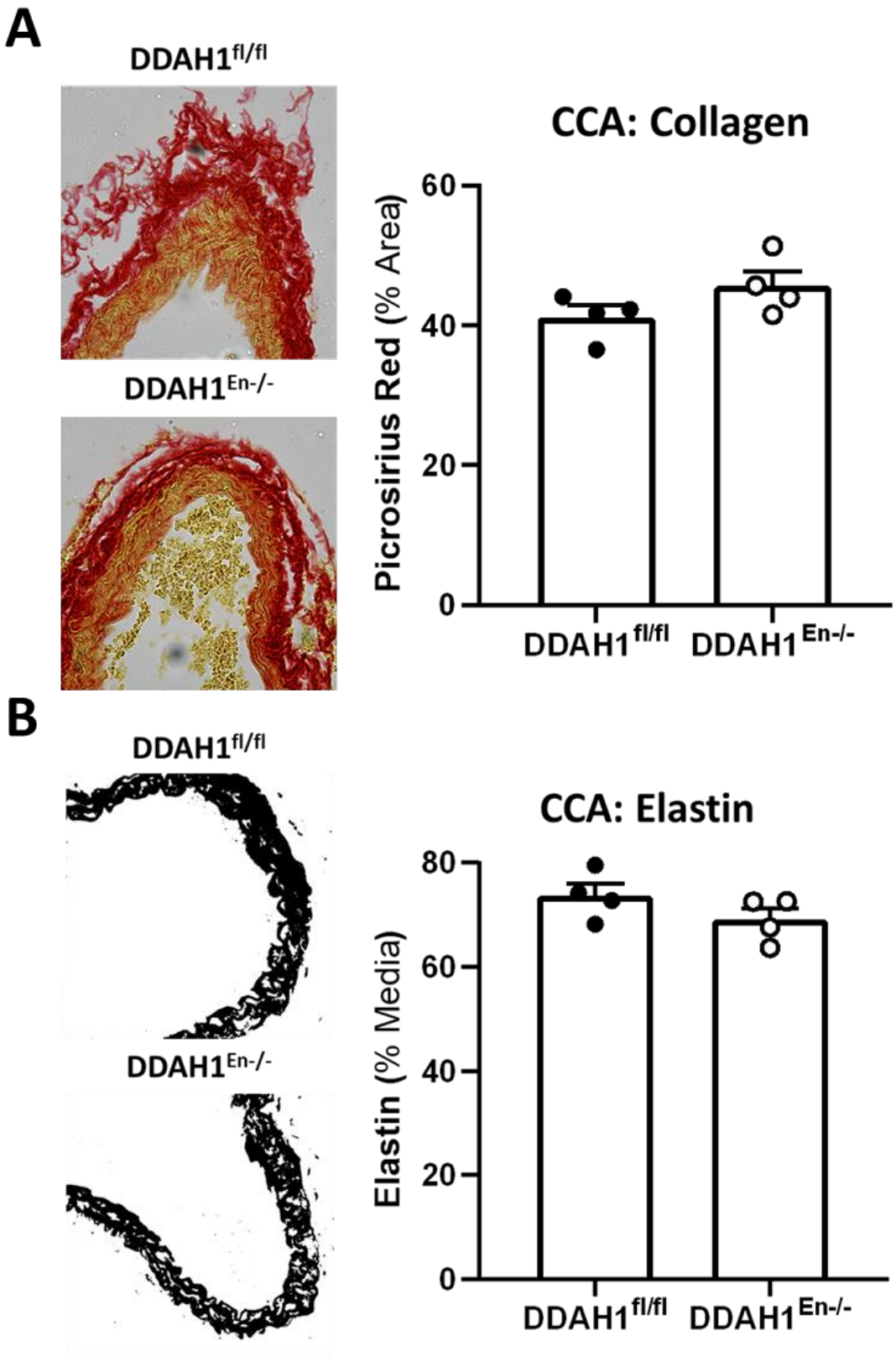

Figure 5-11. Effect of endothelial-specific DDAH1 knockout on collagen and elastin content in common carotid artery rings in mice. Representative images (left) of sections of common carotid arteries from female DDAH1$^{En-/-}$ and DDAH1$^{fl/fl}$ mice stained with picrosirius red (**A**, collagen) and elastin van Gieson (**B**, elastin). Also shown is a summary of mean collagen and elastin content (right) from five sections per mouse. Data presented as mean ± SEM, n=4, *P*>0.05, unpaired t-tests with Welch's correction.

5.3.4 Assessing differentially expressed genes in cerebral microvessels of naïve endothelial-specific DDAH1 knockout mice and after 40-minutes tMCAo

To further explore the importance of endothelial DDAH1 for regulating cerebral artery function, we next evaluated differentially expressed genes (DEGs) in cerebral microvessels from DDAH1$^{En-/-}$ and DDAH1$^{fl/fl}$ control mice using bulk RNA-seq. Sample groups and the groups that were compared in this study are described in Table 5-13 and Table 5-14. Unsupervised cluster analysis of the transcriptome profiles showed no distinct clustering patterns for any group (Figure 5-12). Additionally, heat maps and plots of upregulated and downregulated genes are shown in Figure 5-13 and Figure 5-14. Notably, however, differential transcriptome analysis revealed no upregulated or downregulated genes in naïve (comparison 1) or ischaemic (comparison 2) DDAH1$^{En-/-}$ cerebral microvessels compared to the respective DDAH1$^{fl/fl}$ controls. Transcriptomic analysis of all other comparisons described in Table 5-14 (comparisons 3-6) are given in section 8.7 of the Appendix.

Group	Description	*n*
Group 1	Naïve DDAH1$^{fl/fl}$	4
Group 2	Naïve DDAH1$^{En-/-}$	4
Group 3	Stroke DDAH1$^{fl/fl}$, ipsilateral (ischaemic) hemisphere	3
Group 4	Stroke DDAH1$^{fl/fl}$, contralateral (non-ischaemic) hemisphere	3
Group 5	Stroke DDAH1$^{En-/-}$, ipsilateral (ischaemic) hemisphere	3
Group 6	Stroke DDAH1$^{En-/-}$, contralateral (non-ischaemic) hemisphere	3

Table 5-13. Details of the sample groups used for comparisons of differentially expressed genes by bulk RNA sequencing.

Comparison	Details
Comparison 1	Naïve DDAH1$^{fl/fl}$ *vs* naïve DDAH1$^{En-/-}$
Comparison 2	Stroke DDAH1$^{fl/fl}$ *vs* DDAH1$^{En-/-}$ ischaemic hemispheres
Comparison 3	Stroke DDAH1$^{fl/fl}$ ipsilateral *vs* contralateral hemisphere
Comparison 4	Stroke DDAH1$^{En-/-}$ ipsilateral *vs* contralateral hemisphere
Comparison 5	Naïve DDAH1$^{fl/fl}$ *vs* Stroke DDAH1$^{fl/fl}$ ipsilateral hemisphere
Comparison 6	Naïve DDAH1$^{En-/-}$ *vs* Stroke DDAH1$^{En-/-}$ ipsilateral hemisphere

Table 5-14. Details of the comparisons of differentially expressed genes by bulk RNA sequencing. Ipsilateral and contralateral hemispheres refer to the ischaemic and non-ischaemic hemispheres, respectively.

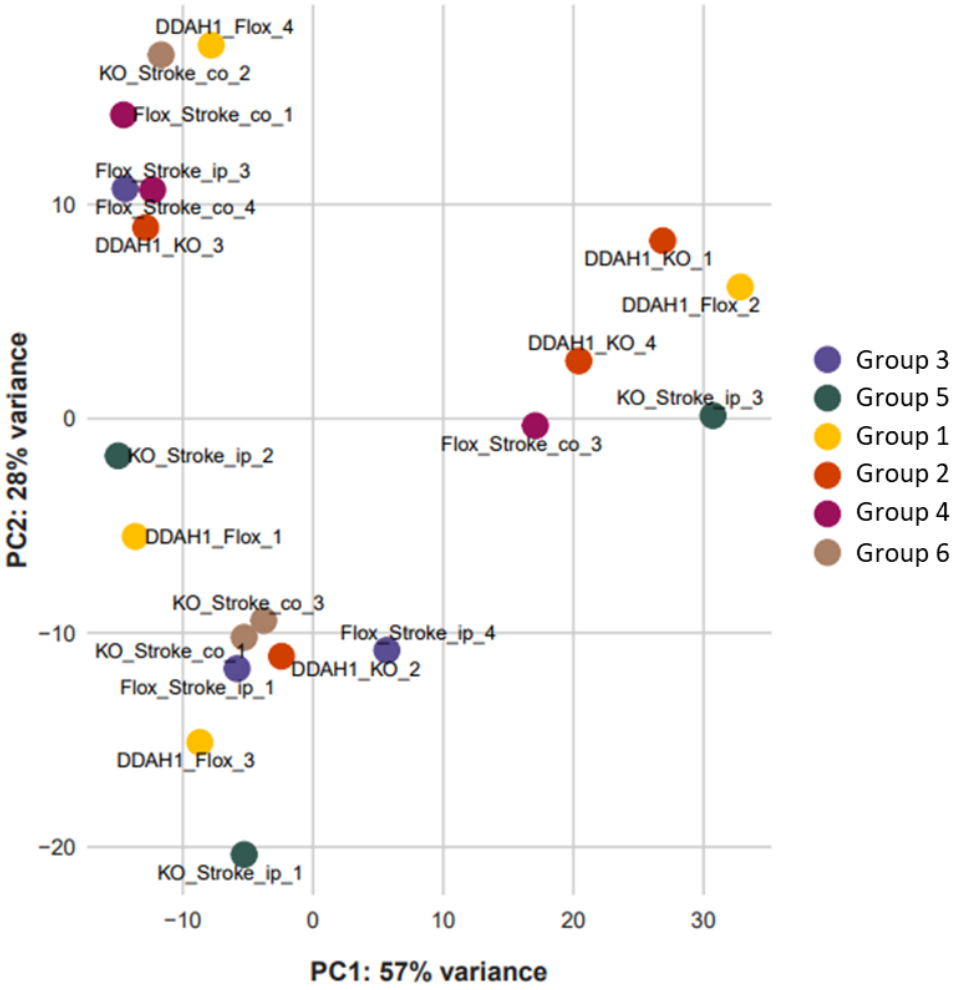

Figure 5-12. Principal component analysis of transcriptome cluster profiling of multidimensional association of data points in each group. Bulk RNAseq was performed on RNA isolated from cerebral microvessel enriched pellets from DDAH1$^{En-/-}$ and DDAH1$^{fl/fl}$ control mice. Mice in groups 3-6 were subjected to 40-minutes tMCAo. Microvessel isolations and RNA extractions were performed 24-hours after stroke induction. Cluster analysis of multidimensional scaling points of transcriptome profiles for each sample were plotted and the variance in each principal component was calculated.

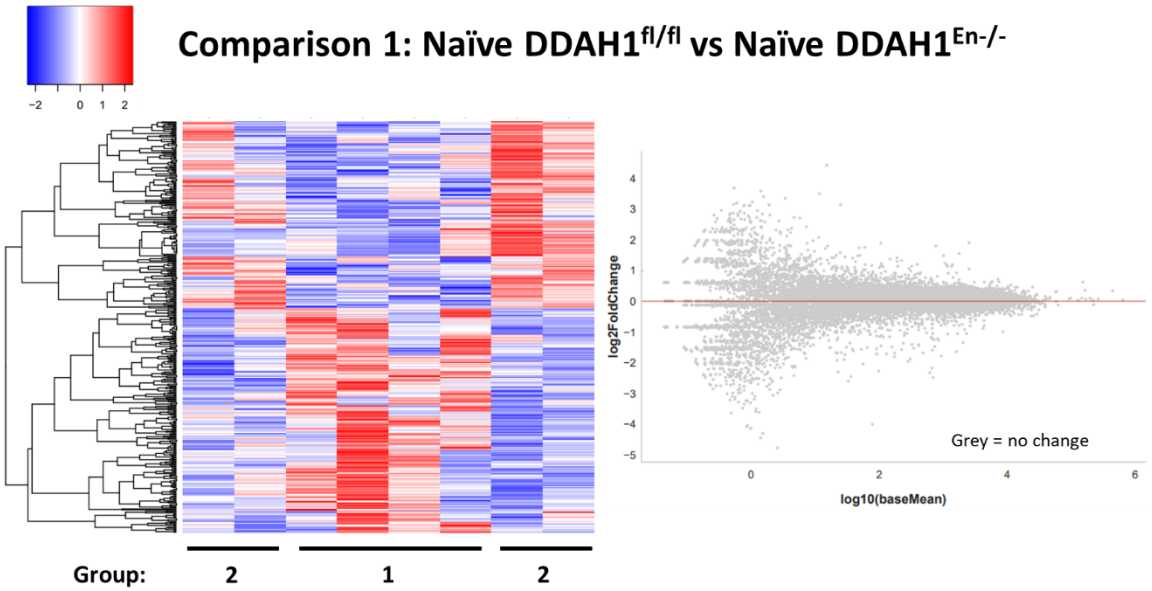

Figure 5-13. Heatmap and MA plot of transcriptome gene expressions in isolated cerebral microvessels from naïve endothelial-specific DDAH1 knockout (DDAH1$^{En-/-}$) and control (DDAH1$^{fl/fl}$) mice. A colour key indicating upregulated and downregulated genes in the heatmap (left) is shown in the top left-hand corner. Grey dots in the MA plot (right) indicate no change of expression between groups.

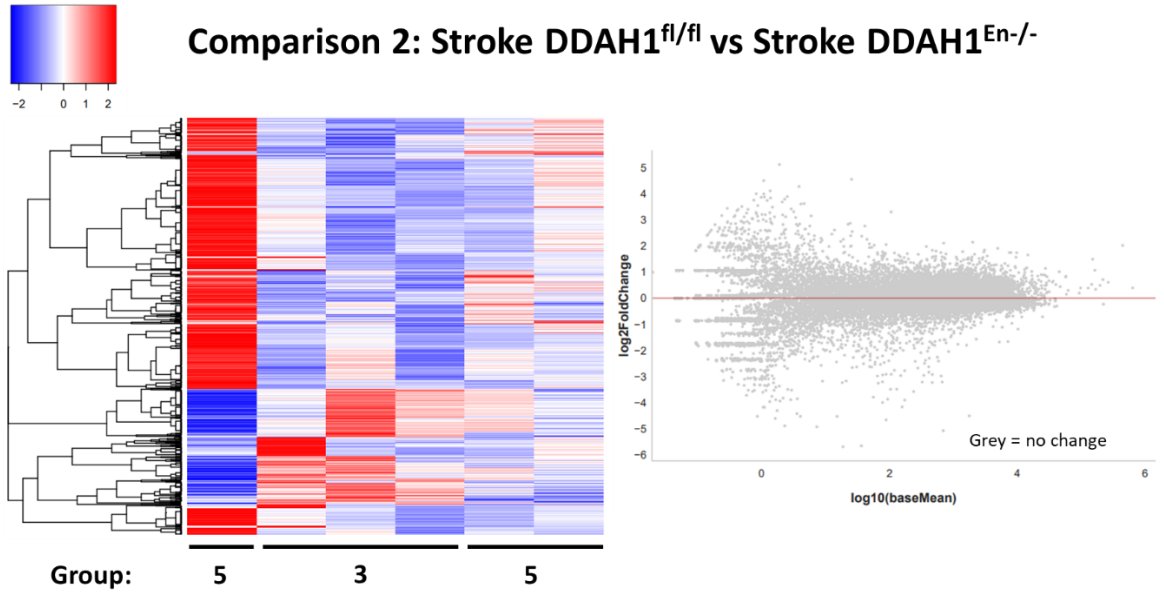

Figure 5-14. Heatmap and MA plot of transcriptome gene expressions in isolated cerebral microvessels from endothelial-specific DDAH1 knockout (DDAH1$^{En-/-}$) and control (DDAH1$^{fl/fl}$) mice after 40-minutes transient middle cerebral artery occlusion (tMCAo). Cerebral microvessel isolations and RNA extractions were performed 24-hours after stroke induction. A colour key indicating upregulated and downregulated genes in the heatmap (left) is shown in the top left-hand corner. Grey dots in the MA plot (right) indicate no change of expression between groups.

5.3.5 Endothelial-specific DDAH1 deletion does not worsen injury, infarct distribution, or neurological outcome in male mice following 50-minutes tMCAo

Due to technical challenges relating to the use of a new laser doppler, we adjusted our criteria for successful ischaemia and reperfusion (as described in section 2.1.2 of General Methods) to a ≥60% reduction of rCBF following filament insertion and a minimum of ≥50%

restoration of rCBF following filament withdrawal. Changes of rCBF during surgeries were comparable between genotypes (Figure 5-15). There were no mortalities in either group, however, 2/7 (29%) of DDAH1$^{fl/fl}$ control mice, and 1/9 (11%) of DDAH1$^{En-/-}$ mice were culled prior to the scientific endpoint as they exceeded the ethical severity limits. There were no exclusions from either group.

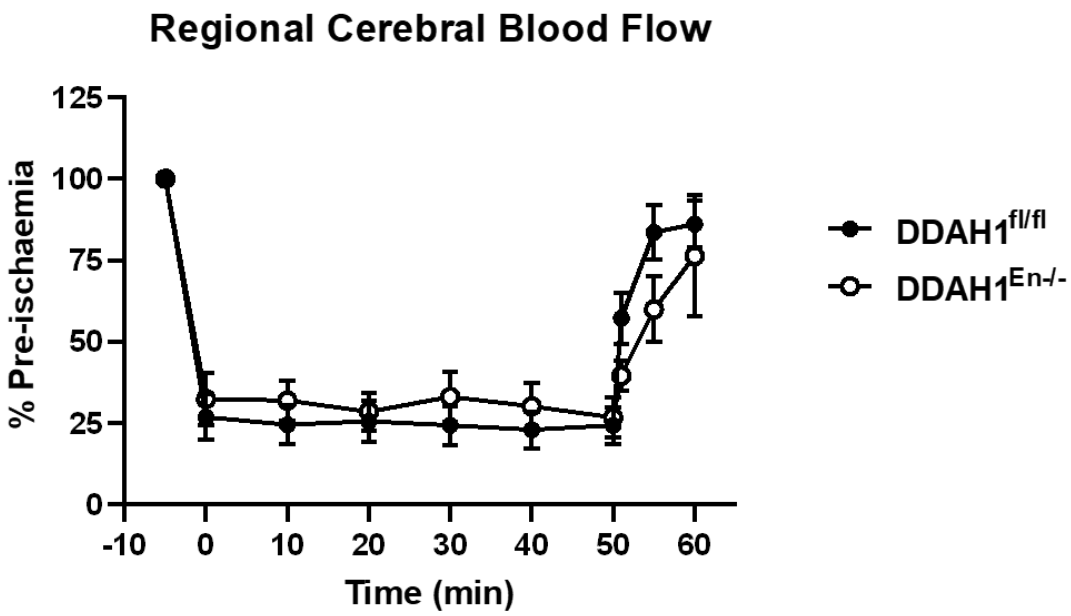

Figure 5-15. Regional cerebral blood flow of DDAH1$^{En-/-}$ and DDAH1$^{fl/fl}$ mice during 50-minutes of tMCAo and 10-minutes reperfusion. A reduction of ≥60% and ≥50% restoration of blood flow was required for mice in each group. Data presented as mean ± SEM, DDAH1$^{En-/-}$: n=5; DDAH1$^{fl/fl}$: n=7. No statistical test was performed.

Endothelial-specific DDAH1 deletion had no statistically significant effect on total infarct (DDAH1$^{En-/-}$, 16.0±4 vs DDAH1$^{fl/fl}$, 13.9±4mm^3; P>0.05), oedema (DDAH1$^{En-/-}$, 13.6±5 vs DDAH1$^{fl/fl}$, 12.9±3 mm^3; P>0.05), or % infarct volume compared to control mice (Figure 5-16A-D). Consistent with our infarct data and the potential correlation between infarct volume and the extent of weight loss described in Chapter 3, the extent of weight loss on day 3 post-stroke was similar between genotypes (Figure 5-16E). Furthermore, there was no statistically significant evidence of differences with respect to cortical and sub-cortical infarct and oedema volumes (Figure 5-17), and the distribution of total, cortical, and sub-cortical infarcts relative to Bregma (Figure 5-18).

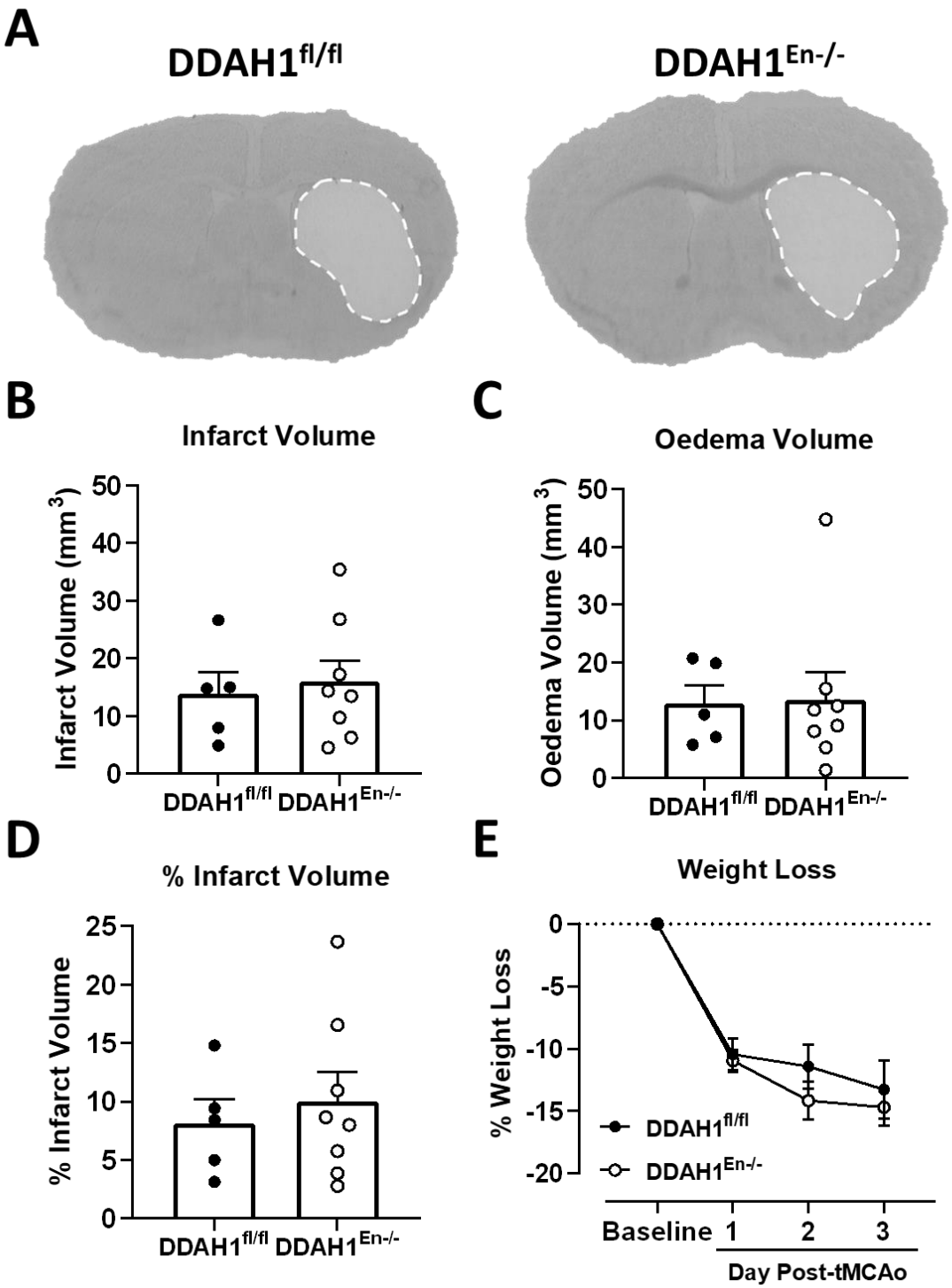

Figure 5-16. Infarct and oedema volumes, and weight loss of DDAH1$^{En-/-}$ and DDAH1$^{fl/fl}$ mice following 50-minutes of transient middle cerebral artery occlusion. Representative images of mouse brain sections (**A**). Mouse brain sections in both groups were assessed for total infarct (**B**) and oedema volume (**C**) 3 days post-stroke. Percent infarct volume was also expressed relative to non-ischaemic hemisphere volume (**D**). Weight loss was measured at baseline and each day from stroke onset for a total of 3 days (**E**). Data presented as mean ± SEM, n=5-8, *P*>0.05, an unpaired t-test with Welch's post hoc test was used for comparisons of infarct or oedema volumes, whereas a two-way ANOVA with repeated measures and Šídák's multiple comparisons test was used for comparisons of percent weight loss.

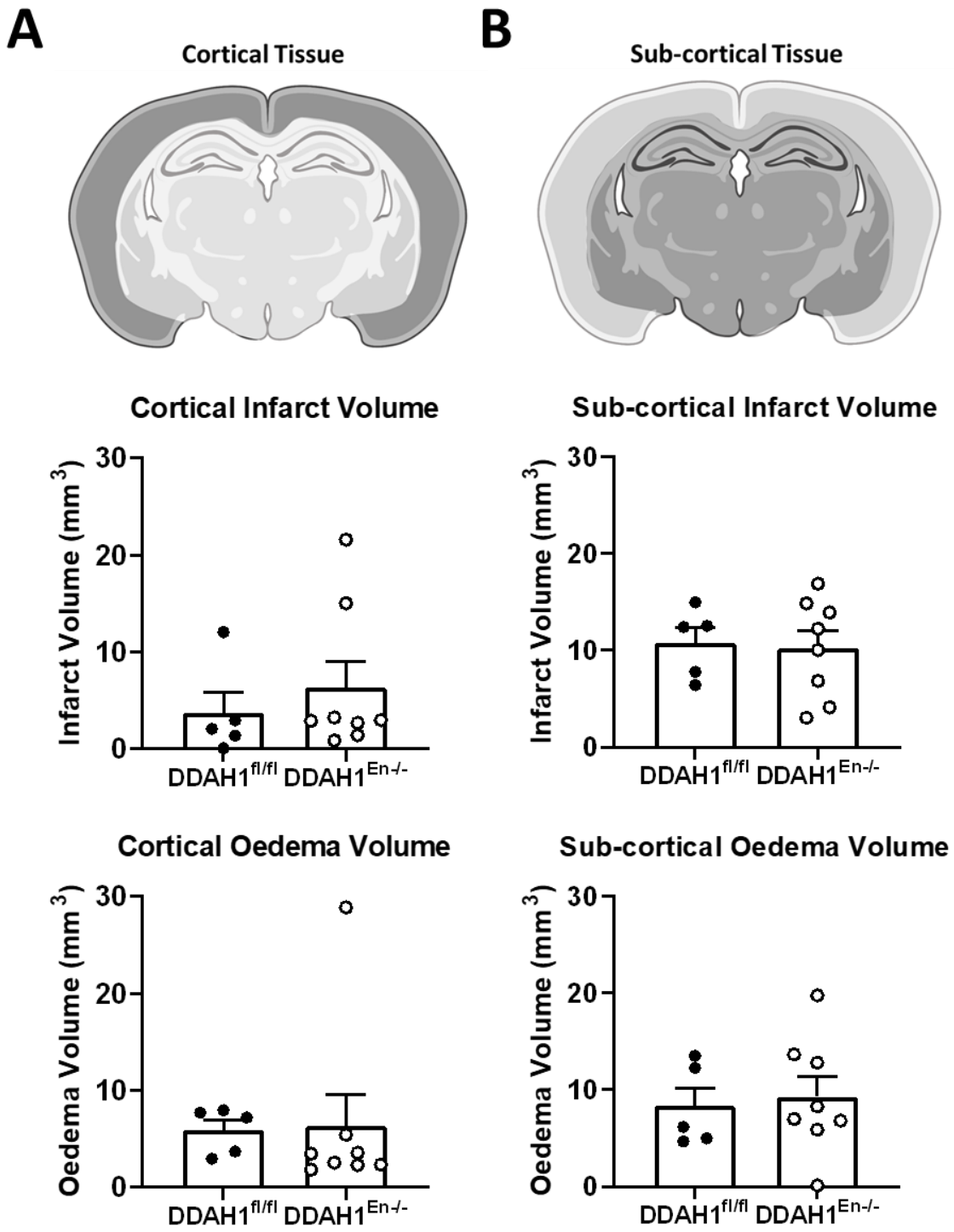

Figure 5-17. Cortical and sub-cortical infarct and oedema volumes of DDAH1$^{En-/-}$ and DDAH1$^{fl/fl}$ mice following 50-minutes of transient middle cerebral artery occlusion. Infarct and oedema volumes were measured in the cortical (**A**) or sub-cortical (**B**) brain regions which are highlighted in dark grey in the representative images. Data presented as mean ± SEM, n=5-8, *P*>0.05, unpaired t-test with Welch's correction. Cortical and sub-cortical reference images were created with BioRender.com.

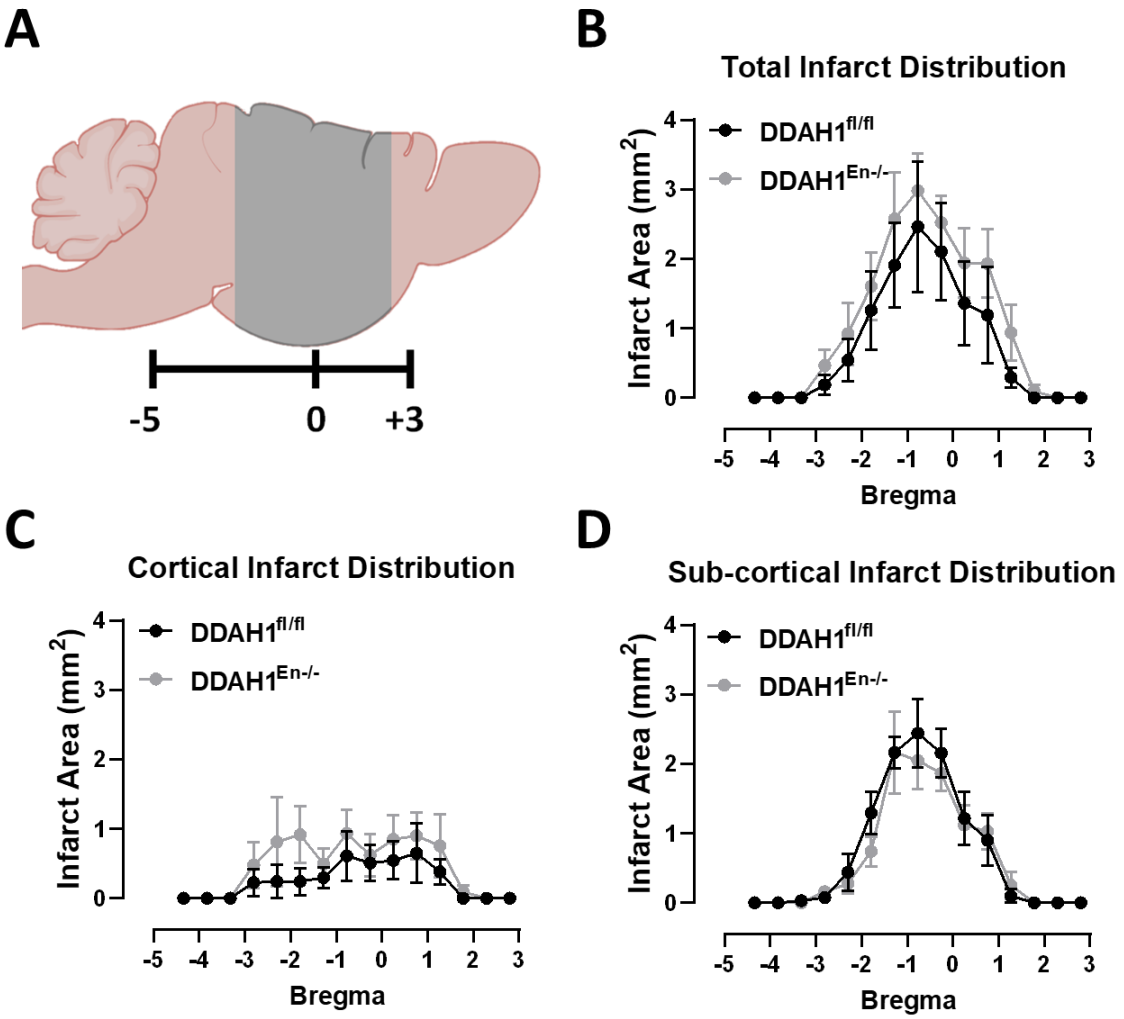

Figure 5-18. Differential infarct area distribution relative to Bregma of DDAH1$^{En-/-}$ and DDAH1$^{fl/fl}$ mice following 50-minutes transient middle cerebral artery occlusion. Thionin stained brain sections were collected between +3 anterior and -5 posterior relative to Bregma, spanning the typical region of infarct formation in this mouse model of tMCAo and is highlighted in grey (**A**). Total (**B**), cortical (**C**), and sub-cortical (**D**) infarct distribution of infarct area (mm^2) was plotted against the Bregma coordinates. Data presented as mean ± SEM, n=5-8, no statistical test was used. Bregma reference image was made with BioRender.com.

When assessing neurological and functional outcomes, no statistically significant evidence of differences was found between DDAH1$^{En-/-}$ and DDAH1$^{fl/fl}$ mice post-stroke with respect to nest building, forelimb asymmetry (cylinder and foot fault tests), mNSS, or forelimb grip strength (Figure 5-19A-F). For example, median mNSS scores on day 1 and day 3 post-stroke were comparable, and mice in both groups scored significantly higher on day 1 post-stroke compared to baseline (Figure 5-19E). The same observation was made for the forelimb grip strength test, however, DDAH1$^{En-/-}$ but not DDAH1$^{fl/fl}$ mice had significantly reduced grip strength post-stroke compared to baseline (Figure 5-19F). Consistent with the forelimb grip strength test, DDAH1$^{En-/-}$ mice displayed significant forelimb asymmetry in favour of the contralateral (affected) forelimb during the foot fault test on day 1 compared to day 3 post-stroke (Figure 5-19D). There were no differences during the

cylinder post-stroke compared to baseline in either group (Figure 5-19C). In contrast, a trend was observed for DDAH1$^{fl/fl}$ mice to exhibit reduced nest building activity at baseline compared to DDAH1$^{En-/-}$ mice (DDAH1$^{En-/-}$, median = 3.5 vs DDAH1$^{fl/fl}$, median = 1.0; *P*=0.0676).

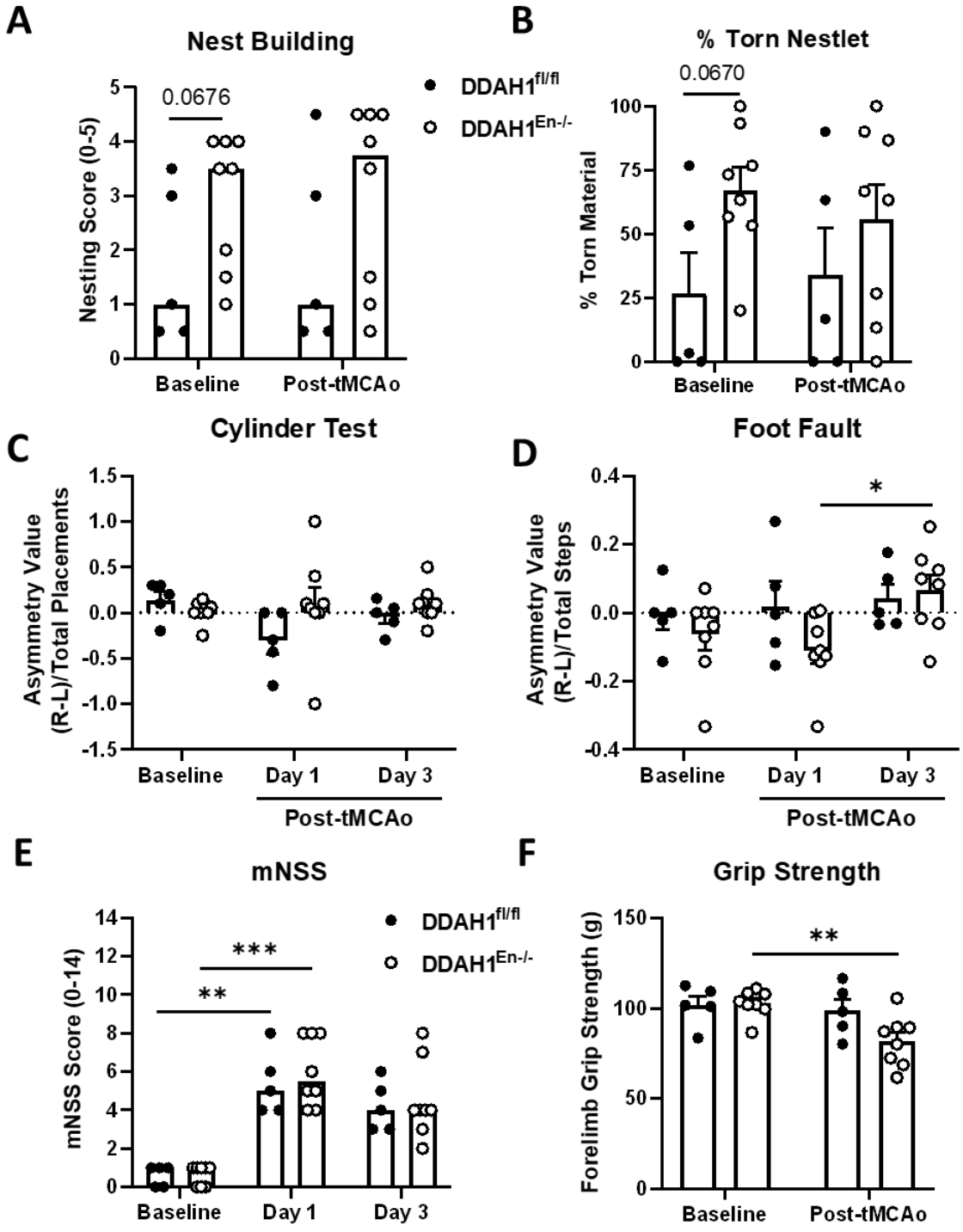

Figure 5-19. Effect of endothelial-specific DDAH1 deletion on neurological and functional outcomes after 50-minutes of transient middle cerebral artery occlusion. Baseline functional and neurological tests were performed prior to 50-minutes of tMCAo. Tests were repeated on day 1, 2, or 3 post-stroke, including the nest building activity test (**A-B**; day 2), forelimb grip strength test (**F**; day 2), cylinder and foot fault tests of forelimb asymmetry (**C-D**; day 1 and 3), modified neurological severity score (**E**; day 1 and 3). Nest building data presented as median, n=5-8, *P*>0.05, Wilcoxon matched pairs tests (pre- vs post-stroke) and Mann-Whitney U tests (DDAH1$^{fl/fl}$ vs DDAH1$^{En-/-}$), % torn nestlet data presented as mean ± SEM, n=5-8, *P*>0.05, paired t tests (pre- vs post-stroke) and unpaired t-tests (DDAH1$^{fl/fl}$ vs DDAH1$^{En-/-}$), forelimb asymmetry test data presented as mean ± SEM, n=5-8, **P*<0.05, two-way repeated measures ANOVA with Šídák's multiple comparisons tests (baseline vs day 1 vs day 3; DDAH1$^{fl/fl}$ vs DDAH1$^{En-/-}$) and pre-post correction analysis was performed at day 1 and day 3 for both tests using unpaired t-tests (DDAH1$^{fl/fl}$ vs DDAH1$^{En-/-}$), mNSS data presented as median, n=5-8, ***P*<0.01, ****P*<0.001, Friedman tests with multiple comparisons (baseline vs day 1 vs day 3) and unpaired t-tests (DDAH1$^{fl/fl}$ vs DDAH1$^{En-/-}$), forelimb grip strength data presented as mean ± SEM, n=5-8, ***P*<0.01, two-way repeated measures ANOVA with Šídák's multiple comparisons tests.

5.3.6 Endothelial-specific DDAH1 deletion does not alter apoptosis after 50-minutes of tMCAo in mice

Next, we examined the number of apoptotic cells in the infarct core and peri-infarct tissue regions in DDAH1$^{En-/-}$ and DDAH1$^{fl/fl}$ mice on day 3 post-stroke. Consistent with our findings in Chapter 4, the number of TUNEL-positive cells were greater in the infarct core compared to the peri-infarct in both groups, however, endothelial-specific DDAH1 knockout had no significant effect on the number of TUNEL-positive cells in either region compared to controls (Figure 5-20; DDAH1$^{En-/-}$: Core, 0.58±0.05 vs Peri-infarct, 0.16±0.02 cells/mm^2).

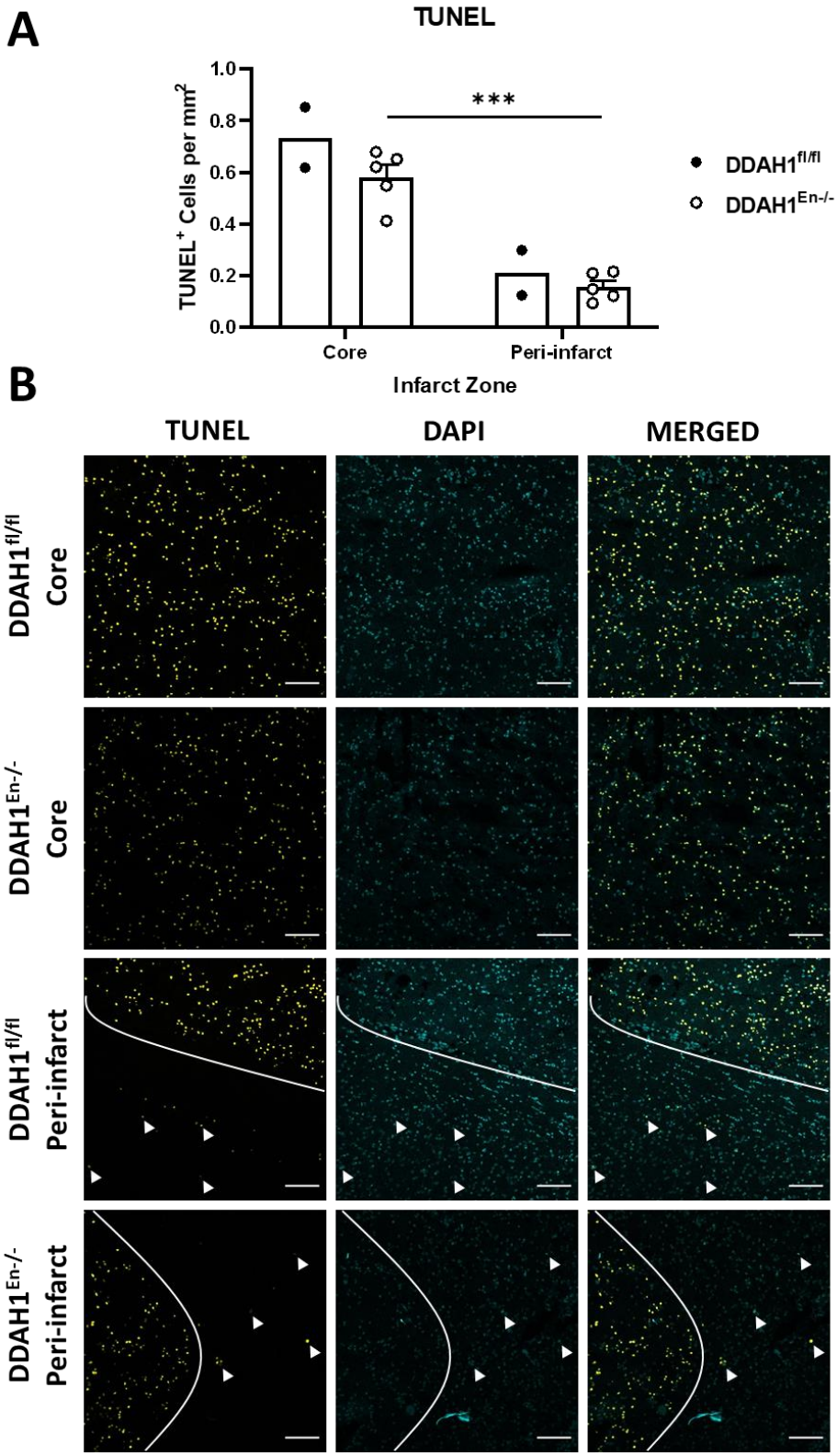

Figure 5-20. Effect of endothelial-specific DDAH1 knockout on apoptotic cell death in the infarct core and peri-infarct regions after 50-minutes of transient middle cerebral artery occlusion. Representative images of the infarct core and peri-infarct tissue regions of DDAH1$^{En-/-}$ and DDAH1$^{fl/fl}$ mice following 50-minutes tMCAo (**B**; bottom). Also shown is the semi-quantification of TUNEL-positive cells per mm^2 of each infarct tissue region of mice in both groups (**A**). TUNEL-positive cells were quantified in the ischaemic core and penumbral regions using the Cell Counter tool on ImageJ analysis software and expressed relative to area (mm^2). Scale bars 100 μm. Data presented as mean ± SEM, n=2-5, ***P<0.001, paired t-test (core vs peri-infarct). No statistical tests were performed on the DDAH1$^{fl/fl}$ group due to insufficient group sizes.

5.4 Discussion

One aim of this study was to establish the functional importance of endothelial DDAH1 in regulating eNOS-NO signalling in cerebral arteries, which prior to this study had not been examined. Firstly, we have shown that endothelial-specific DDAH1 knockout not only results in impaired eNOS-NO-dependent endothelial function of intracranial and extracranial cerebral arteries, but also vascular smooth muscle dysfunction that is characterised by hypocontractility to vasoconstrictors. In contrast, we found that endothelial-specific DDAH1 knockout had no effect on the endothelial function of systemic (thoracic aortae and mesenteric) arteries. Secondly, despite marked cerebrovascular abnormalities in endothelial-specific DDAH1 knockout mice, our data so far indicates that endothelial DDAH1 is not functionally important for ischaemic brain injury or neurological and functional outcomes after 50-minutes of tMCAo. Notably, however, we provide the first evidence that endothelial DDAH1 is a crucial regulator of cerebral eNOS-NO signalling and resultant endothelial and vascular smooth muscle function, likely though the metabolism of endothelial ADMA, without playing a critical role in brain injury or functional outcomes after ischaemic stroke.

In Chapter 4, we demonstrated the importance of DDAH1 as a regulator of eNOS-NO in cerebral arteries using the selective pharmacological DDAH1 inhibitor, L-257. Notably, however, our experiments using L-257 do not allow us to evaluate the importance of endothelial DDAH1 activity in isolation from DDAH1 activity that is also expressed in the vascular smooth muscle. Therefore, using small vessel myography, we evaluated the effect of endothelial-specific DDAH1 knockout ($DDAH1^{En-/-}$) on endothelial-NO-dependent and -independent vasodilator responses of intracranial (middle cerebral) and extracranial (common carotid) cerebral arteries. We found that endothelial-dependent vasodilation of middle cerebral arteries appeared to be impaired in vessels from $DDAH1^{En-/-}$ mice (mixed sex) compared to controls, however, these differences were not statistically significant which is likely due to small group sizes. Notably, however, we show for the first time that endothelial-specific DDAH1 knockout markedly impairs endothelial-dependent vasorelaxation responses of common carotid arteries from both male and female mice, which importantly occurred in the absence of altered cardiovascular haemodynamics as measured using tail cuff plethysmography. Additionally, although we observed no statistical differences in endothelial-independent vasorelaxation responses of carotid arteries from $DDAH1^{En-/-}$ mice of both sexes, there was a trend for impaired nitroprusside-induced relaxation responses of vessels from males. Interestingly, although we found that DDAH1 inhibition with L-257 markedly impaired eNOS-NO signalling in mouse thoracic aortae, endothelial-specific DDAH1 knockout had no effect on either endothelial-dependent or -independent relaxation responses of this systemic vessel type, which is consistent with previous findings (Dowsett *et al.*, 2015). However, although the carotid

arteries are like the thoracic aorta in that they are conduit vessels (for the cerebral circulation), they are much smaller in size and the ratio of vascular smooth muscle to endothelial cells is lower. Therefore, we next examined the effect of endothelial-specific DDAH1 knockout in first order mouse mesenteric arteries and showed no differences in endothelial-dependent or -independent vasorelaxation responses between genotypes. Collectively, this work provides the first evidence that endothelial DDAH1 may be critical for maintaining eNOS-NO signalling in cerebral but not systemic arteries.

As mentioned previously, we observed a trend for endothelial-independent vasorelaxation responses to be impaired in carotid arteries from male DDAH1$^{En-/-}$ mice, raising the possibility of impaired vascular smooth muscle signalling and/or vascular remodelling and stiffness. Thus, we next evaluated vasoconstrictor responses of carotid arteries from male and female DDAH1$^{En-/-}$ and DDAH1$^{fl/fl}$ mice to phenylephrine and the thromboxane A2 mimetic U46619. Consistent with vascular smooth muscle abnormalities, we found that the vasoconstriction responses of carotid arteries from male DDAH1$^{En-/-}$ mice were markedly impaired, whereas a non-significant trend for impaired responses to phenylephrine in vessels from female DDAH1$^{En-/-}$ mice was observed. Interestingly, eNOS-deficient mice were previously shown to have elevated systolic blood pressure and exhibited cerebral vascular remodelling (Baumbach, Sigmund and Faraci, 2004), whereas the mice in this study displayed signs of vascular abnormalities whilst being normotensive, which likely reflects our finding that endothelial DDAH1 is not functionally important in systemic arteries. It was previously reported that infusion of ADMA increases arterial stiffness and decreases cerebral blood flow in healthy humans (Kielstein *et al.*, 2006). Another study also demonstrated that arterial stiffness is an independent predictor of fatal stroke (Laurent *et al.*, 2003). Increased collagen crosslinking together with decreased elastin fibres in the vessel wall has been reported to be characteristic of arterial stiffening in the mouse aorta (Moore *et al.*, 2015). Here, we found no differences in collagen and elastin content in either middle cerebral and common carotid arteries from DDAH1$^{En-/-}$ and DDAH1$^{fl/fl}$ mice however, a major caveat of these experiments was that this work was performed only on female vessels. Therefore, further experiments are needed to measure collagen and elastin content in cerebral vessels from male DDAH1$^{En-/-}$ mice, where the vascular phenotype is more pronounced. Furthermore, a priority should also be to assess the passive mechanical wall properties of middle cerebral and common carotid arteries from DDAH1$^{En-/-}$ mice.

To further explore the importance of endothelial DDAH1 for cerebral arterial function, we used RNA-seq to explore differentially expressed genes (DEGs) in cerebral microvessel mRNA from male DDAH1$^{En-/-}$ and DDAH1$^{fl/fl}$ mice (naïve and after 40-minutes tMCAo). However, our transcriptomic analyses revealed no DEGs between male DDAH1$^{En-/-}$ and

DDAH1$^{fl/fl}$ mice in any of the comparisons performed, which included cerebral microvessels from naïve DDAH1$^{En-/-}$ and DDAH1$^{fl/fl}$ control mice, as well as cerebral microvessels from the ischaemic hemisphere of DDAH1$^{En-/-}$ and DDAH1$^{fl/fl}$ mice following 40-minutes tMCAo. Also, cluster analysis assessing the multidimensional variation of the data points was inconclusive and revealed no relationships between the transcriptome profiles within or between groups. One potential caveat of this work is the cellular purity of the cerebral microvessel RNA samples. For example, the separation and isolation of cerebral microvessels from the parenchyma may not yield purely vascular preparations, and it is likely that RNA from contaminating cells (e.g., astrocytic end feet) were present in the preparations which may have interfered with accurate measurements of any changes of the transcriptomes of cerebral endothelial cells or vascular smooth muscle cells/pericytes. Alternatively, the presence of multiple cell types (endothelial, vascular smooth muscle, and pericytes) in these preparations may not have been appropriate for adequately assessing DEGs in cerebral microvessels. Therefore, in hindsight this work should have been performed in isolated and cultured primary cerebral endothelial or vascular smooth muscle cells rather than whole vessel preparations. Another key consideration is that a previous study showed that single-cell transcriptomics analysis of cerebral endothelial cells revealed several distinct clusters of cerebral endothelial and associated cell types that correspond to different brain regions and vascular segments along the cerebral vascular tree (Vanlandewijck *et al.*, 2018; Kalucka *et al.*, 2020). Therefore, it is likely that our transcriptomic comparisons of cerebral microvessels preparations from whole cerebral hemispheres was not appropriate for identifying and comparing the transcriptome profiles and clusters between naïve or ischaemic DDAH1$^{En-/-}$ and DDAH1$^{fl/fl}$ mice. Thus, further transcriptomic experiments are required to further explore the importance of endothelial DDAH1 for cerebrovascular function, and to elucidate the mechanisms responsible for the vascular phenotype that we observed in cerebral vessels from male DDAH1$^{En-/-}$ mice.

Next, we examined the functional importance of endothelial DDAH1 for stroke outcomes by measuring brain injury and neurological and functional deficits in DDAH1$^{En-/-}$ and DDAH1$^{fl/fl}$ mice following cerebral ischaemia-reperfusion. Given that we found strong evidence of cerebrovascular abnormalities in male DDAH1$^{En-/-}$ mice, and that there are well documented protective actions of eNOS-NO after ischaemic stroke, we hypothesised that endothelial-specific DDAH1 knockout would worsen stroke outcomes. Contrary to this hypothesis, our data currently indicates there were no differences between DDAH1$^{En-/-}$ and DDAH1$^{fl/fl}$ mice with respect to infarct and oedema volumes, apoptosis, and neurological and functional outcomes after 50-minutes tMCAo. Also, we observed significantly reduced forelimb grip strength in DDAH1$^{En-/-}$ and not DDAH1$^{fl/fl}$ mice following stroke which may be indicative of worse functional outcomes, however, the insufficient

group sizes makes it difficult to verify this observation. Thus, these findings so far suggest that either: 1) endothelial DDAH1 is not functionally important during ischaemic stroke pathogenesis; 2) elevated ADMA levels following ischaemic stroke does not exacerbate the disruption of eNOS-NO signalling; or 3) elevated ADMA levels in cerebral endothelial cells alone does not sufficiently influence stroke outcomes. Interestingly, the presence of a hypocontractile vascular abnormality in the cerebral arteries from male DDAH1$^{En-/-}$ mice appeared to similarly have no effect on stroke. It may be that the vascular abnormalities in DDAH1$^{En-/-}$ mice are not sufficient to impact resting CBF and cerebral perfusion post-stroke. Importantly, these findings are consistent with our findings in Chapter 4 in that disruption of eNOS-NO by DDAH1 inhibition or knockout did not influence stroke outcomes in our model of cerebral ischaemia-reperfusion in mice. One limitation of the present study is the lack of complete group sizes (DDAH1$^{En-/-}$: n=8; DDAH1$^{fl/fl}$: n=5). *A priori* power calculations indicated a requirement of n=12 per group, thereby highlighting that both groups were underpowered relative to the predicted statistical powering. Nevertheless, at n=5-8 there does not appear to be a trend for worse stroke outcomes (ischaemic brain injury and neurological deficits) in DDAH1$^{En-/-}$ mice. Collectively, further experiments are required to truly evaluate the importance of cerebral endothelial DDAH1 for ischaemic stroke outcomes.

In summary, we have demonstrated for the first time that endothelial DDAH1 appears to play a crucial role in maintaining cerebral eNOS-NO signalling and thus, cerebral artery function. Interestingly, this discovery contrasts with previous evidence that endothelial DDAH1 does not appear to play a role in regulating eNOS-NO signalling in peripheral arteries. However, our data so far indicates that endothelial DDAH1 does not influence stroke outcomes, including ischaemic brain injury and neurological deficits in mice. As discussed, future experiments are needed to fully evaluate the functional importance of endothelial DDAH1 in ischaemic stroke pathogenesis.

Chapter 6 Investigating the roles of the ADMA-DDAH1 pathway in cerebral angiogenesis

6.1 Introduction

Cerebral angiogenesis refers to the formation of new blood vessels from existing cerebral microvessels, and it is mediated by numerous pro-angiogenic factors in the adult brain, such as vascular endothelial growth factor (VEGF). It is well established that VEGF expression is increased by hypoxia, and that angiogenesis is subsequently upregulated after cerebral ischaemia (Plate, 1999). Angiogenesis after ischaemic stroke is essential for brain recovery as it is associated with increased neurogenesis (the processes of forming new functional neurons from precursor cells) as well as altered synaptic plasticity (the increase of functional synaptic junctions between neural cells) (Font, Arboix and Krupinski, 2010). Importantly, cerebral angiogenesis was shown to be positively associated with patient outcomes after ischaemic stroke (Krupinski *et al.*, 1994). During angiogenesis, VEGF-A binds the VEGFR2 receptor on the endothelial cell membrane leading to activation of PI3K/Akt signalling and a resultant increase in the production of eNOS-derived nitric oxide (NO), which is known as a key mediator of VEGF-stimulated angiogenesis (Papapetropoulos *et al.*, 1997; Dimmeler, Fleming, *et al.*, 1999; Fiedler *et al.*, 2009). As mentioned previously, asymmetric dimethylarginine (ADMA) is an endogenous inhibitor of NO synthesis and elevated levels may therefore exert inhibitory effects on angiogenesis. Many studies have demonstrated that elevated ADMA disrupts the angiogenic activity of cultured endothelial cells derived from peripheral blood vessels as well as angiogenic responses in a rodent model of hindlimb ischaemia (Achan *et al.*, 2005; Wojciak-Stothard *et al.*, 2007; Fiedler *et al.*, 2009). It was also shown that endothelial-specific DDAH1 knockout functionally impairs the sprouting angiogenic activity of aortic rings (Dowsett *et al.*, 2015). Another study evaluating the effects of an inhibitor of DDAH1 (PD404182) on angiogenesis showed that human microvascular endothelial cells treated with L-257 also displayed reduced angiogenic activity (Ghebremariam, Erlanson and Cooke, 2014). It is therefore conceivable that elevated ADMA levels after ischaemic stroke, either by increased production by the PRMTs followed by proteolysis, or by DDAH1 dysfunction may impact the reparative angiogenic activity of cerebral vessels. However, no study has examined the roles of the ADMA-DDAH1 pathway in cerebral angiogenesis.

There are numerous experimental models of angiogenesis, each with a unique combination of advantages and disadvantages (Nowak-Sliwinska *et al.*, 2018). However, one of the most frequently used is the aortic ring assay of sprouting angiogenesis. In this study, we applied the aortic ring assay to evaluate the impact of the ADMA-DDAH1 pathway on the angiogenic activity of intracranial (middle cerebral) and extracranial (common carotid) cerebral arteries. It is hypothesised that elevated ADMA will impair the angiogenic activity of cerebral endothelial cells by disrupting eNOS-NO signalling. To explore the hypothesis, we firstly tested the efficacy of the aortic ring assay of angiogenesis for use on mouse cerebral vessels (MCA and CCA), and secondly evaluated

the impact of selective DDAH1 inhibition using L-257, or endothelial-specific DDAH1 knockout on the sprouting angiogenic activity of cerebral arteries.

6.2 Materials and methods

6.2.1 Animals

In this chapter, a total of 19 male C57BL6/J mice, 8 female DDAH1$^{fl/fl}$, 6 male DDAH1$^{En-/-}$, and 6 female DDAH1$^{En-/-}$ mice (8-15 weeks of age) were used for the vessel sprouting assay of angiogenesis. There were no exclusions from any group in this chapter. Male and female DDAH1$^{fl/fl}$ and DDAH1$^{En-/-}$ mice were generated as described in section 2.1.1 in General Methods. The thoracic aorta, left and right CCAs, and left and right MCAs were dissected from mice as described in section 2.1.9 in General Methods, and then placed in ice-cold PBS before being cut into ~1 mm long rings. Vessel rings were only excluded from analyses if the vessels were dead or failed to exhibit any signs of vascular remodelling of the vessel wall, cellular outgrowth from the vessel rings, or the sprouting angiogenic activity (formation of sprouts and branches).

6.2.2 *In vitro* vessel sprouting assay of angiogenesis and drug treatments

Vessel rings of C57BL6/J, DDAH1$^{fl/fl}$, and DDAH1$^{En-/-}$ mice were used in a vessel sprouting assay as described in section 2.2.3 in General Methods.

Vessel rings from male C57BL6/J mice were treated with either vehicle (sterile dH_2O), 0.5-100 μM ADMA (Merck, UK), or 100 μM L-257 (provided by Professor Leiper) every day. Fresh, serum-free OptiMEM media supplemented with 30 ng/mL VEGF and 1% Penicillin/Streptomycin was replaced every 2 days. All rings were assigned treatments at random using the random list generator www.random.org/lists and pharmacological treatments were blinded for all vessels during image analysis by concealing treatments vessel treatments in each experiment.

Analysis criteria for sprouting angiogenesis of vessel rings were: 1) all sprouts must visibly originate from or branch from another sprout originating from the vessel ring, 2) a branch point is where one sprout divides into two sprouts or a sprout extends from the side of an existing sprout; 3) sprouts can be characterised as large neovessel formations or thin wire-like structures; 4) when one sprout divides into two new branches, each new division counts as a new individual sprout, whereas branches arising from an existing sprout each count as a new individual sprout; 5) sprouts with no identifiable origin or connection to the vessel ring must not be counted; 6) sprouts must only be counted if visible in each plane, whereas branches in a new plane from a pre-existing sprout can be counted; 7) the total area of a vessel ring must always be quantified for normalisation of angiogenic sprouting characteristics. The number of sprouts was defined as the total number of all sprouts and branching sprouts originating from the vessel across all planes. The number of branch points was defined as the total number of branch points leading to one or more new sprouts from an existing sprout. The average sprout length was defined as the mean

sprout length across all sprouts quantified for each vessel ring. If sprouts and branch points did not meet the criteria above, the vessel ring was not included in the analysis.

6.2.3 Statistical Analysis

All analyses were performed using GraphPad Prism version 9.1.0 (GraphPad Software Inc., US). $P<0.05$ was considered statistically significant. Group numbers are indicated in the corresponding figure legends.

All data is expressed as mean ± SEM. This includes comparisons of number of sprouts, average sprout length, and number of branch points. The following statistical tests were used:

- A paired t-test was used to compare sprouting characteristics between MCA and CCA rings treated with L-257 or ADMA compared to vehicle controls.
- A one-way ANOVA with Dunnett's post hoc test was used to compare sprouting characteristics between aorta, CCA, or MCA rings.
- A mixed-effects ANOVA with Tukey's multiple comparisons test or Holm-Šídák's multiple comparisons test was used to compare sprouting of CCA rings treated with different concentrations of exogenous ADMA.
- A Brown-Forsythe and Welch ANOVA with Dunnett's T3 multiple comparisons test was used to compare sprouting angiogenesis of male and female $DDAH1^{En-/-}$ and female $DDAH1^{fl/fl}$ MCA, CCA, and thoracic aorta rings.

6.3 Results

6.3.1 Middle cerebral artery rings exhibit greater angiogenic activity compared to common carotid artery and thoracic aorta rings

The aortic ring assay of angiogenesis was originally designed for use on rat aortic rings in a collagen matrix, however, only one study has reported the adaptation of the technique for use with other vessel types (Stiffey-Wilusz *et al.*, 2001). We therefore adapted the aortic ring assay for MCA and CCA rings from male C57BL6/J mice and compared the angiogenic activity of each vessel type. The number of sprouts, average sprout length, and number of branch points were used as measures of VEGF-stimulated sprouting angiogenesis. The angiogenic sprouts produced by CCA and MCA rings in response to VEGF were comparable to aortic rings (Figure 6-1A). When normalised to vessel area (Table 6-1), MCA rings displayed significantly greater angiogenic activity compared to both aortic and CCA rings (Figure 6-1B-D).

Vessel Type	Vessel Area (mm^2)
Aorta	1.84±0.3
CCA	0.78±0.07
MCA	0.28±0.05

Table 6-1. Average area of thoracic aorta, common carotid artery, and middle cerebral artery rings. Vessels were imaged using an EVOX XL bright field microscope at 10X magnification. Vessel area was determined for every ring using ImageJ analysis software. Data presented as mean ± SEM.

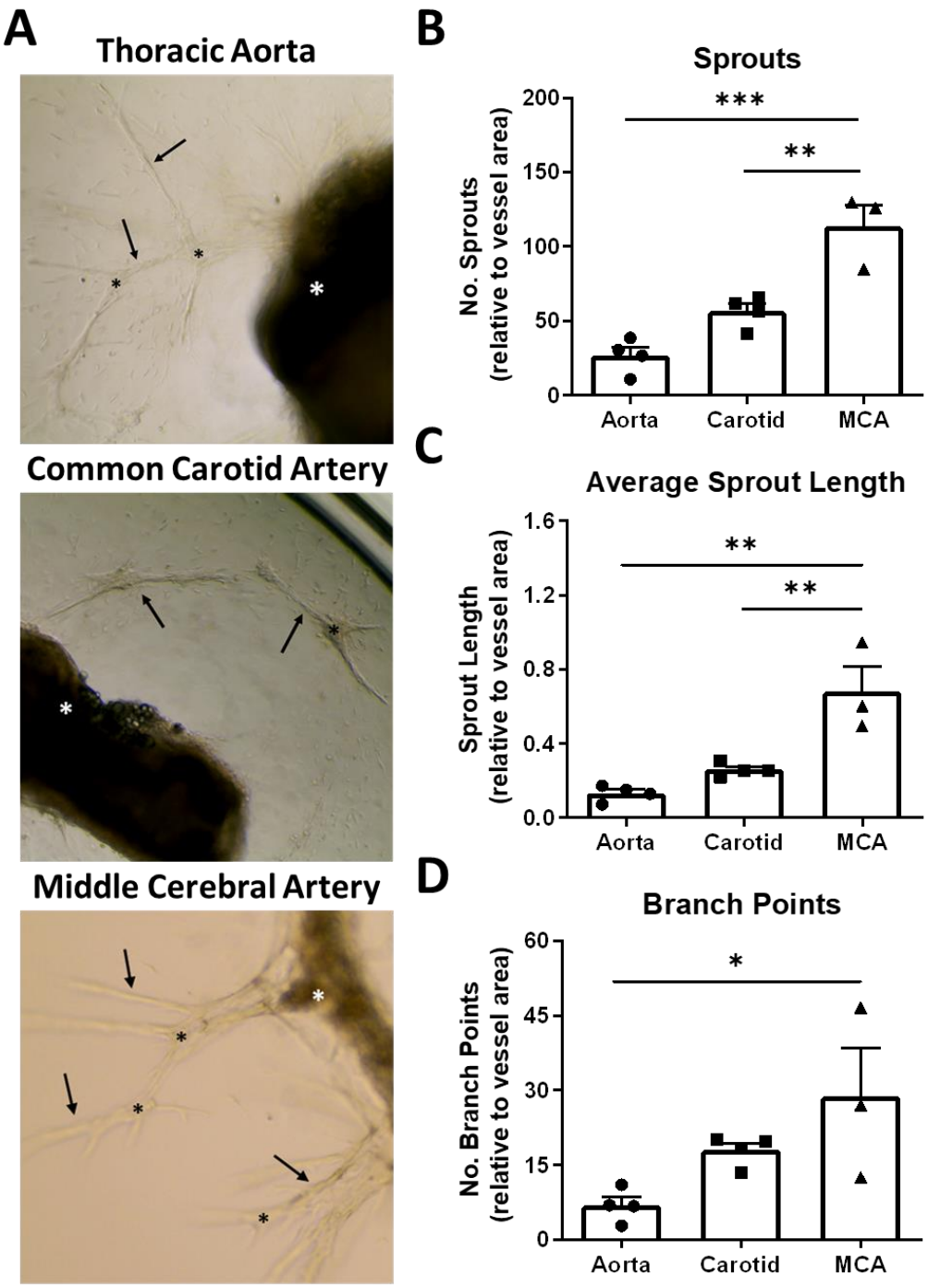

Figure 6-1. Comparison of sprouting angiogenic activity of thoracic aorta, common carotid, and middle cerebral artery rings. Representative images (**A**) of thoracic aorta, common carotid artery, and middle cerebral artery ring sprouting angiogenesis from male C57BL6/J mice. Vessel rings were treated with VEGF-containing media (30 ng/mL) and cultured for 7-10 days. Number of sprouts (**B**), average sprout length (**C**), and number of branch points (**D**) were quantified for all vessels and normalised to vessel area (mm^2). Arrows define sprouts, black asterisks define branch points, and white asterisks define the vessel ring. Images were taken at 10X magnification in bright field and then analysed using ImageJ Analysis software. Data presented as mean ± SEM, n=3-4, **P*<0.05, ***P*<0.01, ****P*<0.001, one-way ANOVA with Dunnett's post-hoc test.

6.3.2 Selective DDAH1 inhibition impairs VEGF-stimulated angiogenic activity of middle cerebral and common carotid artery rings

Both exogenously applied ADMA and L-257 treatment have been shown to impair the angiogenic activity of cultured endothelial cells from peripheral vessels (Fiedler *et al.*, 2009; Ghebremariam, Erlanson and Cooke, 2014). However, whether DDAH1 inhibition using L-257 similarly inhibits the angiogenic activity of the cerebral vessels is unknown. Indeed, the average sprout length and number of branch points of both MCA and CCA rings treated with L-257 (100 μM) were significantly reduced compared to vehicle controls, whereas CCA rings treated with L-257 also produced fewer sprouts (Figure 6-2 and Figure 6-3).

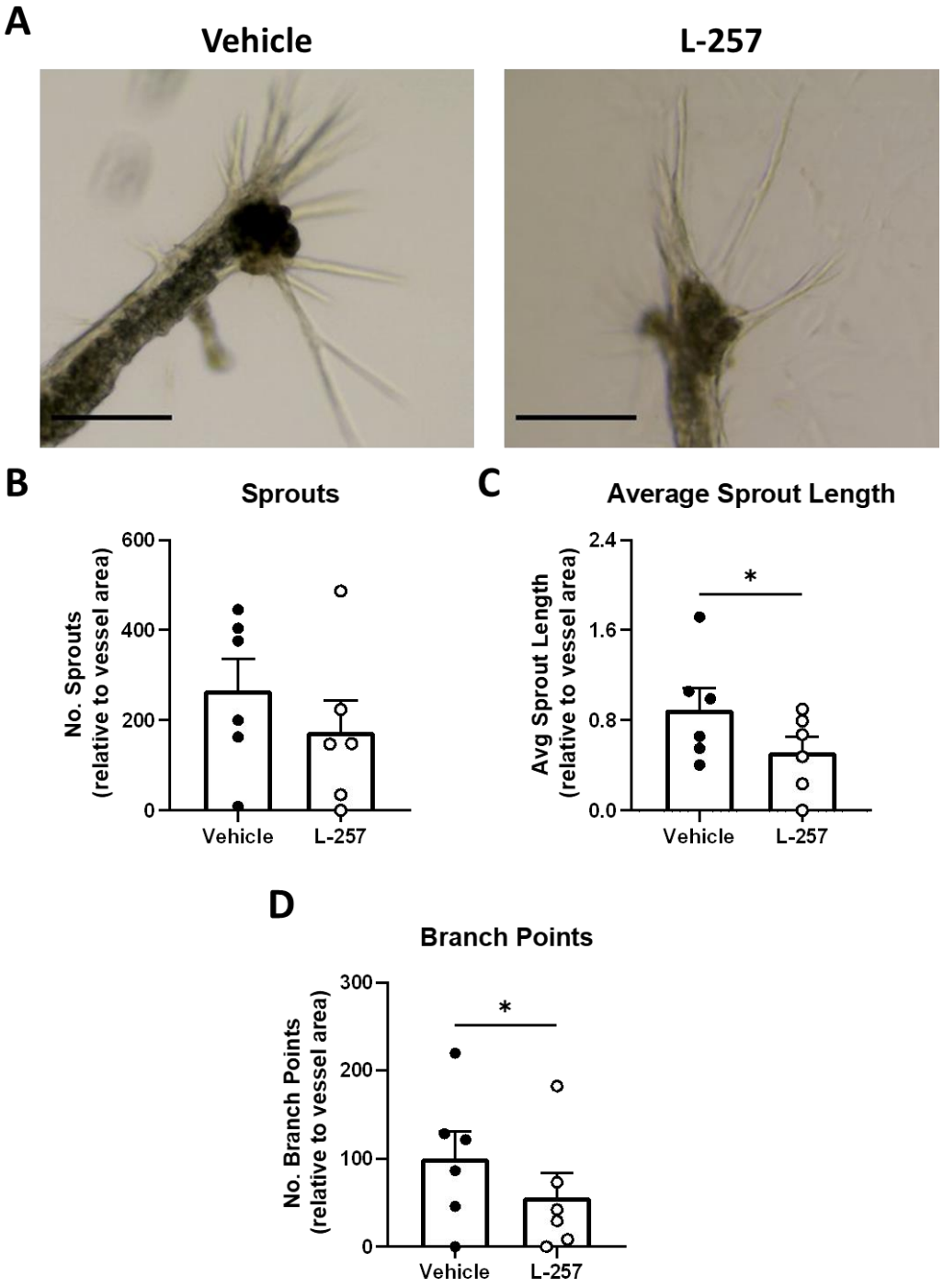

Figure 6-2. Effect of selective DDAH1 inhibition on sprouting angiogenic activity of mouse middle cerebral artery rings. Representative images (**A**) of middle cerebral artery rings from male C57BL6/J mice treated with either vehicle (sterile H_2O) or L-257 (100 μM). Vessel rings were treated with VEGF-containing media (30 ng/mL) and cultured for 10 days. Number of sprouts (**B**), average sprout length (**C**), and number of branch points (**D**) were quantified for all vessels and normalised to vessel area (mm^2). Images were taken at 10X magnification in bright field and then analysed using ImageJ analysis software. Data presented as mean ± SEM, n=6, **P*<0.05, paired t-tests. Scale bar 0.3 mm.

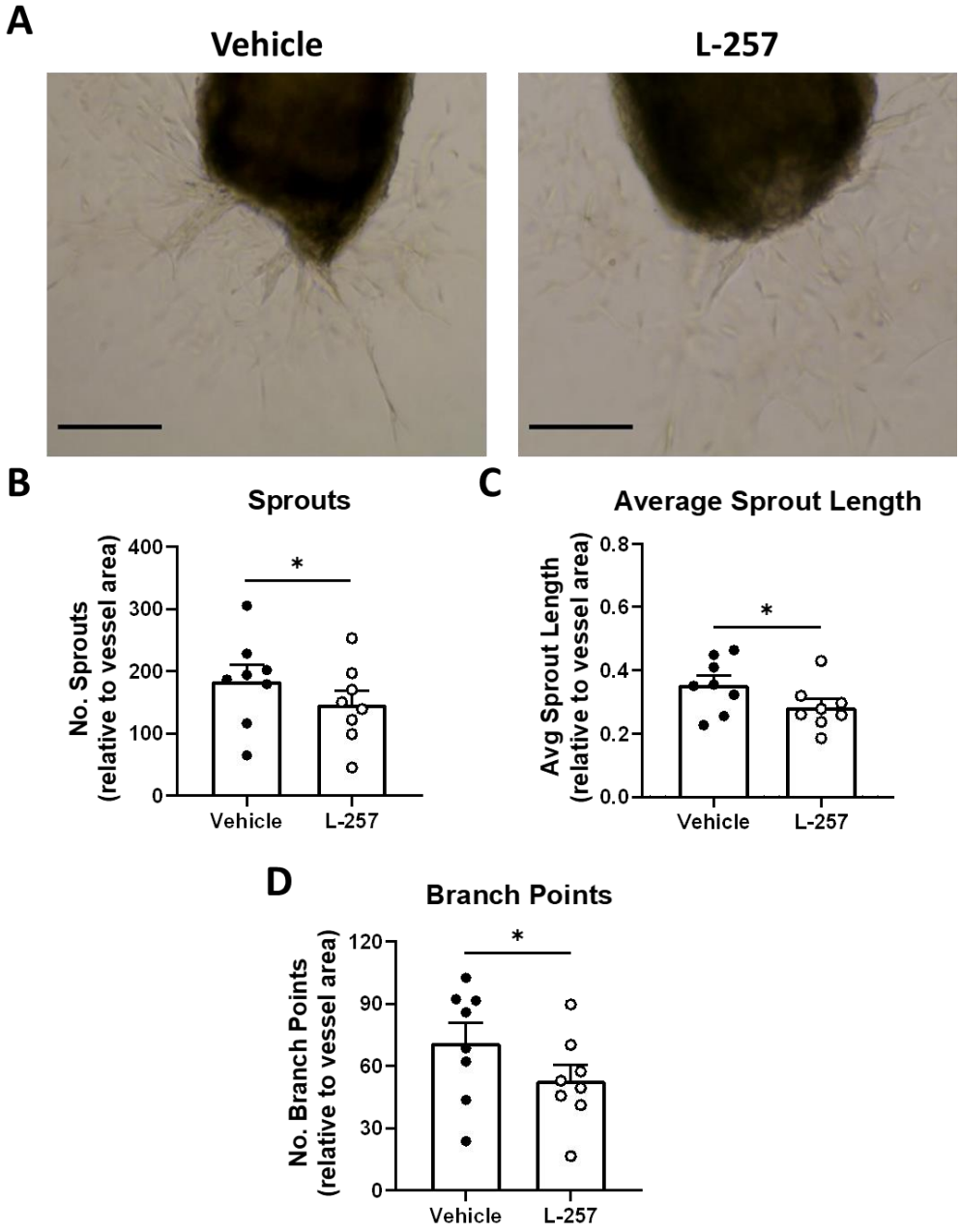

Figure 6-3. Effect of selective DDAH1 inhibition on the sprouting angiogenic activity of mouse common carotid artery rings. Representative images (**A**) of common carotid artery rings from male C57BL6/J mice treated with either vehicle (sterile H_2O) or L-257 (100 μM). Vessel rings were treated with VEGF-containing media (30 ng/mL) and cultured for 7 days. Number of sprouts (**B**), average sprout length (**C**), and number of branch points (**D**) were quantified for all vessels and normalised to vessel area (mm^2). Images were taken at 10X magnification in bright field and then analysed using ImageJ analysis software. Data presented as mean ± SEM, n=8, $P<0.05$, paired t-tests. Scale bar 0.3 mm.

To ascertain whether the effects of DDAH1 inhibition by L-257 treatment impairs angiogenesis via the inhibitory effects of ADMA on endothelial NO synthesis, we examined the effects of exogenous ADMA (0.5, 3, and 100 μM) on sprouting angiogenesis of CCA rings. CCA rings treated with 100 μM but not 0.5 and 3 μM ADMA produced significantly fewer sprouts and branch points compared to vehicle-treated rings, whereas average sprout length was comparable between treatments (Figure 6-4).

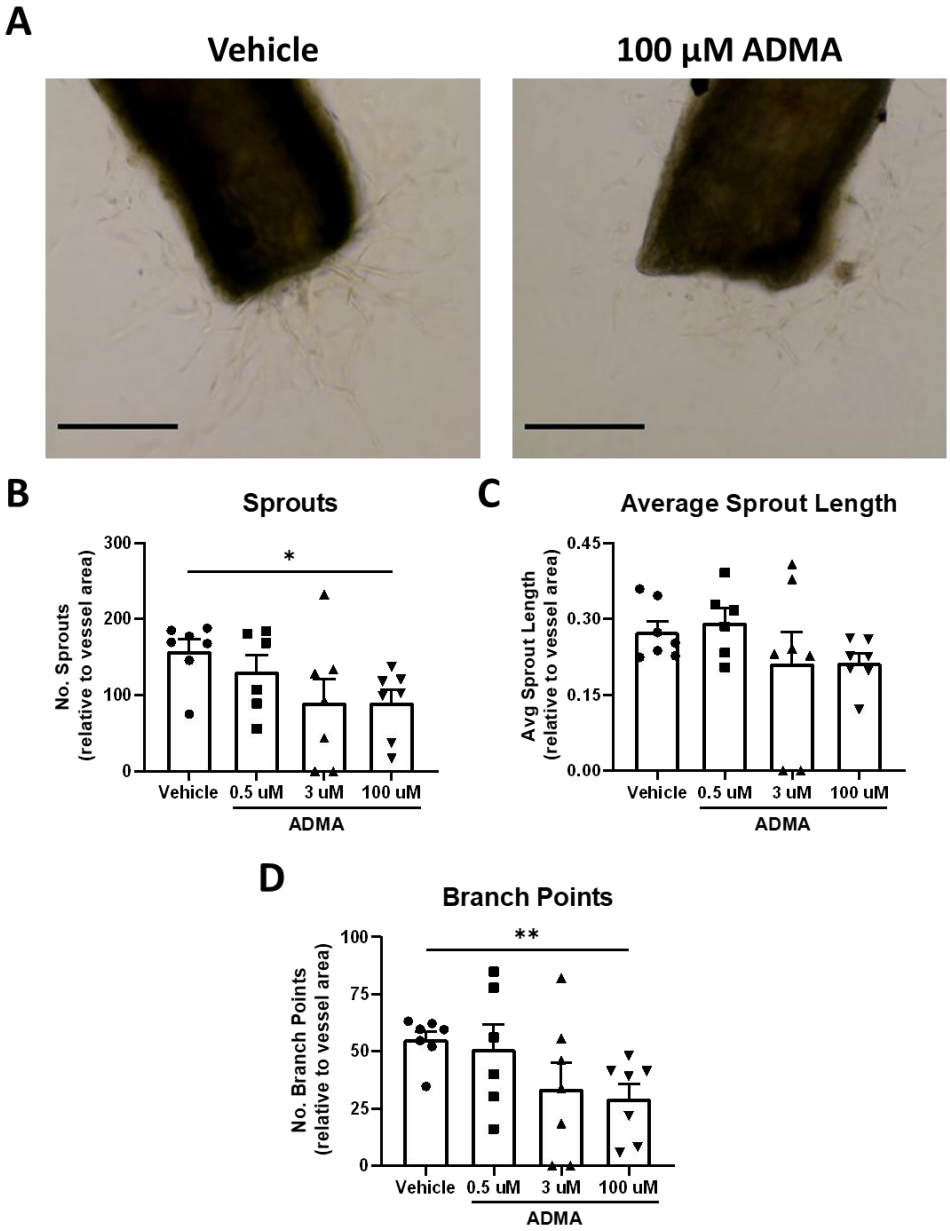

Figure 6-4. Effect of increasing concentrations of ADMA on sprouting angiogenic activity of common carotid artery rings. Representative images (**A**) of common carotid artery rings from male C57BL6/J mice treated with either vehicle (sterile H_2O) or ADMA (0.5, 3, and 100 µM). Vessel rings were treated with VEGF-containing media (30 ng/mL) and cultured for 7 days. Number of sprouts (**B**), average sprout length (**C**), and number of branch points (**D**) were quantified for all vessels and normalised to vessel area (mm^2). Images were taken at 10X magnification in bright field and then analysed using ImageJ analysis software. Data presented as mean ± SEM, n=6-7, **P*<0.05, ***P*<0.01, mixed-effects ANOVA with Tukey's multiple comparisons test or Holm-Sidak's multiple comparisons test. Scale bar 0.3 mm.

6.3.3 Endothelial-specific DDAH1 knockout significantly impairs angiogenic activity of middle cerebral arteries in a sex-dependent manner

Albeit not a direct assessment of sprouting angiogenesis in male endothelial-specific DDAH1 knockout mice, due to insufficient male $DDAH1^{fl/fl}$ mice being produced in litters after breeding we performed additional experiments using vessels from female $DDAH1^{fl/fl}$ mice to increase the group size before making comparisons of the sprouting angiogenic

activity of MCA and CCA rings from male DDAH1$^{En-/-}$ mice. MCA rings of male DDAH1$^{En-/-}$ (KO) mice produced significantly fewer sprouts and branch points compared to female DDAH1$^{fl/fl}$ (Flox) controls, whereas MCA from female DDAH1$^{En-/-}$ mice displayed comparable angiogenic activity to female DDAH1$^{fl/fl}$ controls (Figure 6-5). In contrast, the angiogenic activity (all endpoints) of CCA rings from male DDAH1$^{En-/-}$ mice was similar to CCA rings from female DDAH1$^{fl/fl}$ control mice, however, there was a trend for the number of sprouts and branch points to be reduced in CCA rings from female DDAH1$^{En-/-}$ mice compared to controls (Figure 6-6). Finally, the angiogenic activity in the thoracic aorta from male DDAH1$^{En-/-}$ mice was comparable to that of the thoracic aorta from female DDAH1$^{fl/fl}$ controls, whereas the number of sprouts and branch points were significantly reduced in thoracic aorta from female DDAH1$^{En-/-}$ mice compared with controls (Figure 6-7).

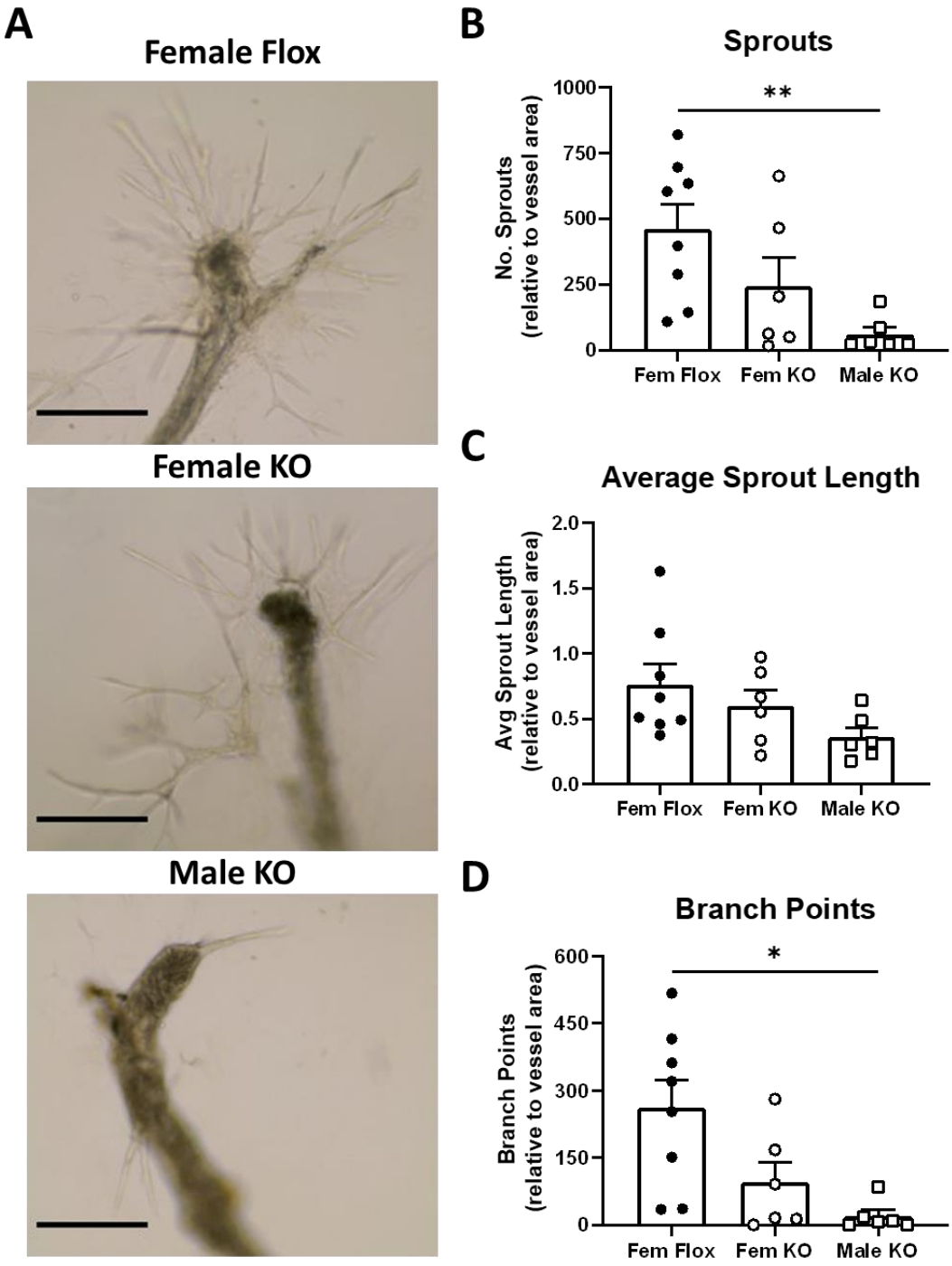

Figure 6-5. Effect of endothelial-specific DDAH1 knockout on the angiogenic activity of middle cerebral artery rings. Representative images (**A**) of middle cerebral artery rings from female DDAH1$^{fl/fl}$ (Fem Flox), female DDAH1$^{En-/-}$ (Fem KO), and male DDAH1$^{En-/-}$ (Male KO) mice. Vessel rings were treated with VEGF-containing media (30 ng/mL) and cultured for 10 days. Number of sprouts (**B**), average sprout length (**C**), and number of branch points (**D**) were quantified for all vessels and normalised to vessel area (mm^2). Images were taken at 10X magnification in bright field and then analysed using ImageJ analysis software. Data presented as mean ± SEM, n=6-8, *P<0.05, **P<0.01, Brown-Forsythe and Welch ANOVA with Dunnett's T3 multiple comparisons test. Scale bar 0.3 mm.

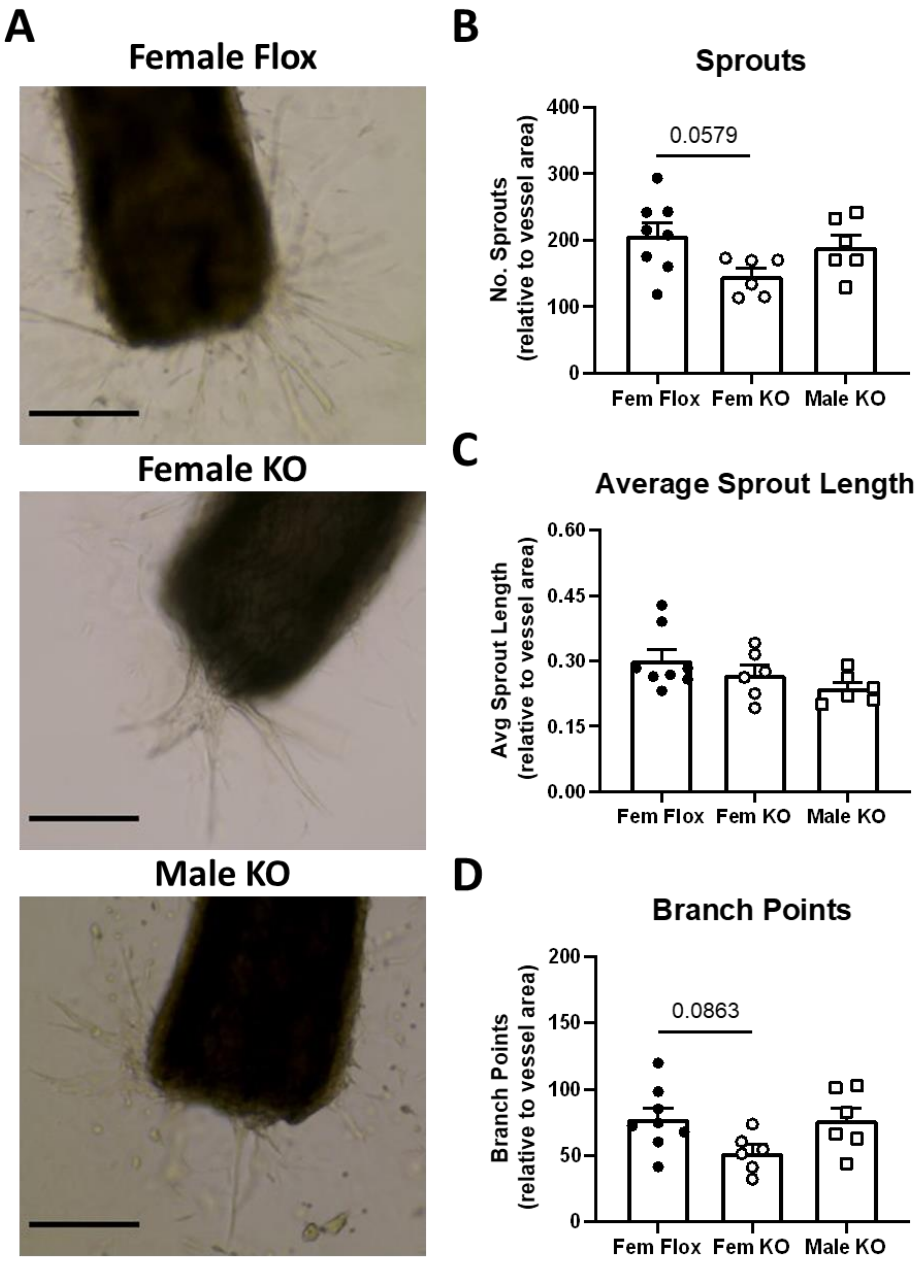

Figure 6-6. Effect of endothelial-specific DDAH1 knockout on the angiogenic activity of common carotid artery rings. Representative images (**A**) of common carotid artery rings from female DDAH1$^{fl/fl}$ (Fem Flox), female DDAH1$^{En-/-}$ (Fem KO), and male DDAH1$^{En-/-}$ (Male KO) mice. Vessel rings were treated with VEGF-containing media (30 ng/mL) and cultured for 7 days. Number of sprouts (**B**), average sprout length (**C**), and number of branch points (**D**) were quantified for all vessels and normalised to vessel area (mm^2). Images were taken at 10X magnification in bright field and then analysed using ImageJ analysis software. Data presented as mean ± SEM, n=6-8, Brown-Forsythe and Welch ANOVA with Dunnett's T3 multiple comparisons test. Scale bar 0.3 mm.

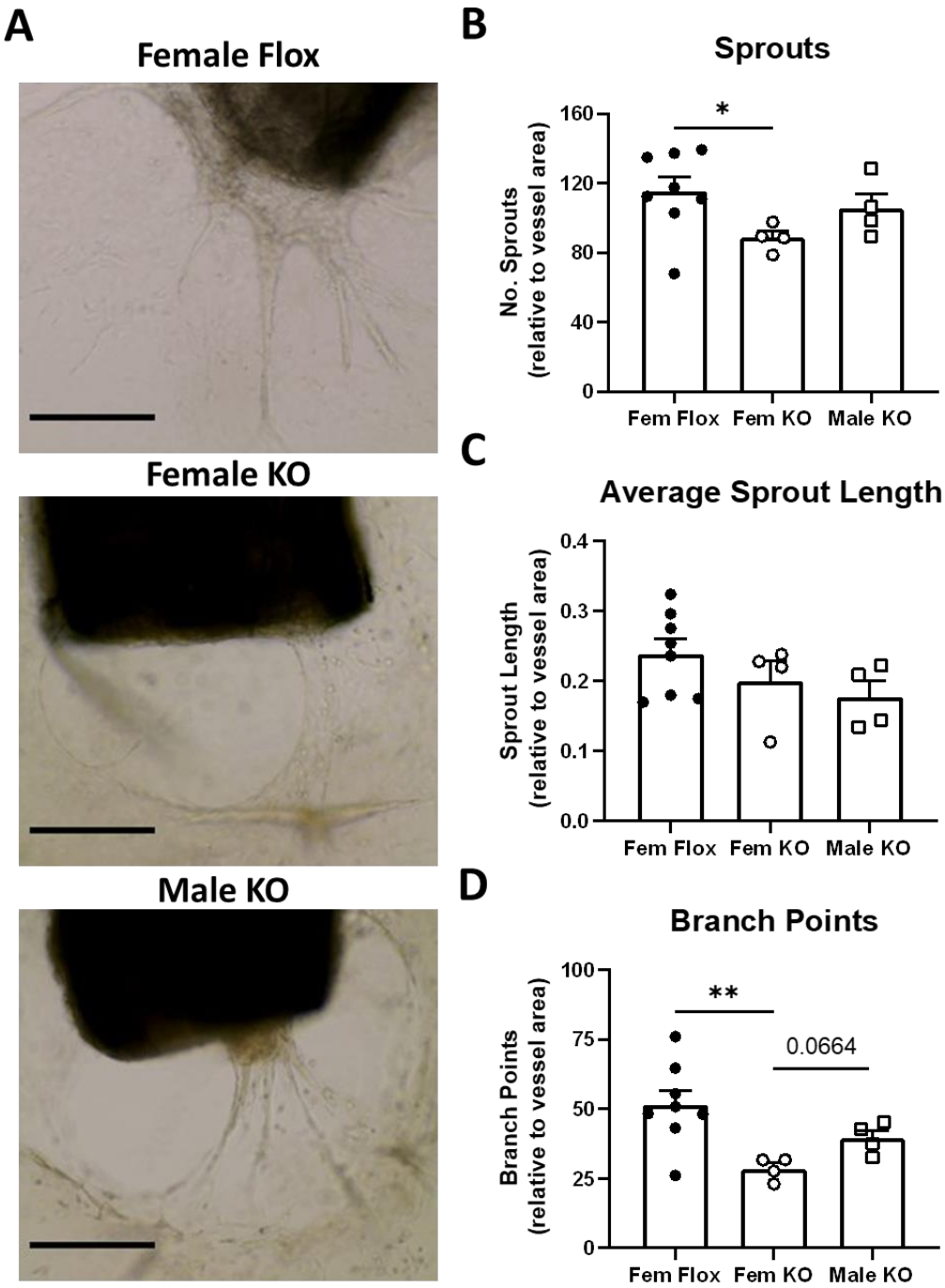

Figure 6-7. Effect of endothelial-specific DDAH1 knockout on the angiogenic activity of thoracic aorta rings. Representative images (**A**) of thoracic aorta rings from female DDAH1$^{fl/fl}$ (Fem Flox), female DDAH1$^{En-/-}$ (Fem KO), and male DDAH1$^{En-/-}$ (Male KO) mice. Vessel rings were treated with VEGF-containing media (30 ng/mL) and cultured for 7 days. Number of sprouts (**B**), average sprout length (**C**), and number of branch points (**D**) were quantified for all vessels and normalised to vessel area (mm^2). Images were taken at 10X magnification in bright field and then analysed using ImageJ analysis software. Data presented as mean ± SEM, n=4-8, *P<0.05, **P<0.01, Brown-Forsythe and Welch ANOVA with Dunnett's T3 multiple comparisons test. Scale bar 0.3 mm.

6.4 Discussion

In this chapter, we successfully established a vessel sprouting assay of angiogenesis using intracranial and extracranial mouse cerebral arteries. A key finding was that total vascular DDAH1 activity is an important regulator of sprouting angiogenesis in MCA and CCA rings, exhibiting similar outcomes as with vessels which were treated with suprapathophysiological concentrations of ADMA. Our data also suggests that endothelial DDAH1 is functionally important for the sprouting angiogenic activity of male but not female MCAs. Paradoxically, endothelial DDAH1 in CCA and thoracic aorta rings appeared to be important in female but not male vessels. However, these findings suggest that elevated ADMA levels following ischaemic stroke may negatively impact ischaemic stroke outcomes by disrupting reparative angiogenic processes and salvaging of the ischaemic penumbra.

As mentioned previously, there are numerous experimental assays for measuring angiogenesis, including tubule formation assay, cell migration assay, cell proliferation assay, fibrin bead assay, aortic ring assay, and so on (Nowak-Sliwinska *et al.*, 2018). The aortic ring assay has many advantages over most *in vitro* angiogenesis assays. For example, numerous vascular cell types are present which can release endogenous growth factors, the outgrowth of angiogenic sprouts are stimulated in response to injury by the dissection process thus first appearing at the dissected ends, and the vessel rings are embedded in a 3D matrix allowing for a more natural formation of angiogenic sprouts (Nicosia, 2009). In contrast, angiogenesis typically takes place in small vessels such as capillaries and therefore angiogenesis is an unnatural process for large artery rings. There is also a lack of shear stress from the absence of blood flow which may alter the bioavailability of NO and other pro-angiogenic factors, and it was previously reported that migrating immune cells in response to VEGF signals via the VEGFR1 receptor may exert anti-angiogenic effects which is a process that is otherwise missing during *in vitro* and *ex vivo* angiogenesis assays (Barleon *et al.*, 1996; Nowak-Sliwinska *et al.*, 2018). However, the aortic ring assay reflects the molecular mechanisms of angiogenesis closer than most *in vitro* techniques while remaining reproducible, cost effective, and easy to use. While the aortic ring assay is commonly used, to date there has been only one report of the technique being applied to another vessel type, and there have been no reports of the technique used for investigating cerebral angiogenesis (Stiffey-Wilusz *et al.*, 2001). Therefore, we sought to adapt the aortic ring assay for the use on mouse MCA and CCA rings, and showed that relative to vessel size, MCA rings appeared to display greater angiogenic activity compared to thoracic aorta and CCA rings. A greater angiogenic potential of MCA compared to other vessel types may therefore be reflective of the fact that angiogenesis is characteristic of smaller blood vessels.

Previous studies have demonstrated the functional importance of DDAH1 activity during NO-mediated angiogenesis of the systemic circulation (Achan *et al.*, 2005; Wojciak-Stothard *et al.*, 2007; Fiedler *et al.*, 2009). However, it remained unclear whether DDAH1 was equally important in cerebral angiogenesis. In chapter 4, we demonstrated that L-257 functionally impairs cerebral artery function by disrupting eNOS-NO signalling in MCAs and CCAs. In chapter 5, we similarly demonstrated the functional importance of endothelial-specific DDAH1 as a regulator of cerebral arterial eNOS-NO signalling in the same vessels. Our findings in the present study suggest that DDAH1 activity also appears to have an important role in sprouting angiogenesis of cerebral vessels, which is likely due to the regulation of levels of the endogenous eNOS inhibitor ADMA. Furthermore, exogenous ADMA also appeared to impair sprouting angiogenesis of CCA rings, however, there is a lack of mechanistic insight in this study to substantiate that the negative effects of ADMA on sprouting angiogenesis in cerebral vessels is due the inhibition of eNOS-NO signalling. For example, the ADMA-DDAH1 pathway was also shown to regulate the angiogenic activity of endothelial cells via modulation of the Rho GTPases which are important for endothelial cell motility (Wojciak-Stothard *et al.*, 2007; Fiedler *et al.*, 2009). Therefore, further studies should be performed to elucidate whether the effects of ADMA after DDAH1 inhibition or knockout impair sprouting angiogenesis of cerebral vessels by disrupting eNOS-NO signalling.

A major limitation of this study was the use of OptiMEM media, which contains the eNOS substrate L-arginine (L-Arg). L-Arg is therefore present in quantities which may compete with ADMA for eNOS, thereby influencing the angiogenic activity of the cultured cerebral vessels and influencing the subsequent findings. For example, a plethora of studies have demonstrated that exogenous L-Arg improves endothelial function via increased eNOS-NO signalling and by competing with ADMA (Böger *et al.*, 1997; Bode-Böger *et al.*, 2003; Achan *et al.*, 2005). Thus, studies evaluating the inhibitory effects of ADMA on eNOS-NO-dependent processes of cultured endothelial cells typically use L-Arg-free media (Fiedler *et al.*, 2009). Additionally, there are also concerns over the use of exogenous L-Arg in experiments for evaluating the inhibitory mechanisms of ADMA on endothelium-derived NO signalling. For example, the 'arginine paradox' refers to the concept that intracellular L-Arg levels already exceed the affinity for saturating eNOS, and that exogenous L-Arg would therefore yield no differences in outcomes (Bode-boger, Scalera and Ignarro, 2007; Dioguardi, 2011). However, Achan and colleagues reported that supplementation of L-Arg in a rodent model of hindlimb ischaemia improved angiogenesis in the affected tissue regions compared to controls (Achan *et al.*, 2005). Therefore, further experiments in the absence of L-Arg-containing media should be performed, followed by the use of exogenous L-Arg treatment to determine whether total vascular and endothelial DDAH1 is an

important regulator of cerebral angiogenesis, by controlling the inhibition of eNOS-NO by ADMA.

As mentioned previously, one advantage of the aortic ring assay of angiogenesis is the presence of other cell types, which may release growth factors thereby promoting the angiogenic response of the vessels to injury at the site of incision. However, sprouting angiogenesis typically occurs in the microvascular bed, and thus a major caveat of this technique is the presence of the vascular smooth muscle. Specifically, DDAH1 is expressed by both endothelial and vascular smooth muscle cells (Leiper and Nandi, 2011), and our findings using L-257 do not reveal the relative importance of DDAH1 activity from the vascular endothelium or smooth muscle during sprouting angiogenesis. Therefore, we next used endothelial-specific DDAH1 knockout mice to evaluate the importance of DDAH1 in the cerebral endothelium. Indeed, it was previously reported that endothelial-specific DDAH1 knockout impairs sprouting angiogenesis of mouse thoracic aorta rings (Dowsett *et al.*, 2015). Similarly, our findings also suggest that angiogenesis is disrupted in cerebral vessels of endothelial-specific knockout mice, implying that indeed endothelial DDAH1 activity is crucial for cerebral angiogenesis.

It is well documented that brain and plasma ADMA levels are increased after ischaemic stroke (Brouns *et al.*, 2009; Worthmann *et al.*, 2011). In the present study, we showed that the application of suprapathophysiological concentrations of ADMA (100 μM) markedly impaired the sprouting angiogenic activity of mouse common carotid arteries. These findings suggest that elevated ADMA levels after ischaemic stroke may exert significant inhibitory effects on cerebral angiogenesis that are otherwise important for brain repair and patient recovery. Furthermore, in combination with the findings that cerebral angiogenesis is also impaired after both DDAH1 inhibition and endothelial-specific knockout, it is conceivable that dysregulation of the ADMA-DDAH1 pathway after cerebral ischaemia-reperfusion may impact cerebral angiogenesis and the subsequent neurogenesis and synaptic plasticity (Font, Arboix and Krupinski, 2010), where the former is positively correlated with patient outcomes after ischaemic stroke (Krupinski *et al.*, 1994). However, the inhibitory mechanisms in this study that were responsible for impaired cerebral angiogenesis by elevated ADMA as well as whether there are differences in cerebral angiogenesis between males and females remain unclear. Thus, further studies are required to evaluate whether dysregulation of the ADMA-DDAH1 pathway impacts cerebral angiogenesis in a NO-dependent manner, whether sex differences in cerebral angiogenesis exist, and whether elevated ADMA levels after ischaemic stroke contributes to patient outcomes by disrupting restorative cerebral angiogenic processes.

In summary, we have provided the first evidence that total vascular and endothelial-specific DDAH1 is an important regulator of sprouting angiogenesis of cerebral arteries

and propose that elevated ADMA levels after ischaemic stroke may influence stroke outcomes by disrupting crucial restorative cerebral angiogenic processes. Notably, however, it is unknown whether the dysregulation of the ADMA-DDAH1 pathway affects cerebral angiogenesis by disrupting eNOS-NO signalling, or via other mechanisms. As discussed, further studies in the absence of extracellular L-Arg as well as performing co-treatments with exogenous L-Arg are required to elucidate whether the inhibitory effects of ADMA on cerebral angiogenesis are NO-dependent.

Chapter 7 General discussion

7.1 Summary of major findings

Overall, the findings presented in this thesis provide novel insight into the importance of the ADMA-DDAH1 pathway in the regulation of cerebral vascular function during health, and in the context of ischaemic stroke pathogenesis and potentially post-stroke angiogenesis. Specifically, the major findings are as follows:

Chapter 3: Establishing a clinically relevant model of transient middle cerebral artery occlusion in mice

The primary aim of the work presented in this chapter was to identify a tMCAo occlusion period that produces clinically relevant stroke outcomes in mice without exceeding the ethical severity limits outlined in our Home Office Project Licence. Specifically, we compared endpoint measures of stroke outcome – infarct size, neurological and functional deficits, net body weight loss – in mice after 50-, 60-, or 65-minutes tMCAo. The major finding of this chapter was that mice who underwent 65-minutes tMCAo exhibited infarct sizes that are comparable to infarct size typically observed in humans following survivable, acute ischaemic strokes (28-80 mm^3 or 4-14% of the hemisphere). Also, mice after 65-minutes tMCAo appeared to develop larger infarcts in the cortical tissue compared with mice exposed to shorter occlusion periods, whilst infarcts in the sub-cortical tissue were comparable between groups. In addition to infarct size, 65-minute tMCAo mice also presented with greater detectable neurological and functional deficits compared to mice following 50- and 60-minutes tMCAo using a combination of behavioural tests. Lastly, we found a weak but significant correlation between infarct or oedema volumes and net body weight loss in mice following tMCAo, indicating that weight loss in rodent models of ischaemic stroke may be an important endpoint measure. Taken together, these findings demonstrate that, in our hands, 65-minutes tMCAo is an ideal occlusion period for achieving clinically relevant stroke outcomes in mice.

Chapter 4: Examining the roles of the ADMA-DDAH1 pathway in ischaemic stroke pathogenesis

Using the selective pharmacological DDAH1 inhibitor L-257, the experiments in this chapter primarily aimed to evaluate whether elevated ADMA following DDAH1 inhibition worsens ischaemic stroke outcomes by impairing eNOS-NO signalling, with the objective of testing for a causal role for the ADMA-DDAH1 pathway. In this study, there are numerous major findings. Firstly, we found that selective DDAH1 inhibition using L-257 modestly but non-significantly increased brain and plasma ADMA levels after intraperitoneal administration in naïve mice, without influencing cardiovascular haemodynamics. Thus, we next tested whether elevated ADMA levels following DDAH1 inhibition disrupts crucial eNOS-NO signalling in middle cerebral and common carotid arteries. Correspondingly, the second major new finding of this thesis chapter was that inhibition of DDAH1 with L-257 markedly impaired NO-dependent dilator responses of

cerebral arteries *in vitro*, an effect that was comparable to the inhibitory effects of exogenous ADMA. Lastly, the third major finding of this study was that DDAH1 inhibition with L-257 had no effect on stroke outcomes (infarct and oedema volumes, apoptosis in infarct core and peri-infarct brain regions, neurological deficits, or body weight loss) in mice after 65-minutes tMCAo. These findings were surprising as our laboratory previously found that mice treated with L-257 following 40-minutes tMCAo (milder model of ischaemia) had significantly larger infarcts. Collectively, we have provided evidence that although DDAH1 inhibition markedly impairs eNOS-NO signalling in cerebral vessels, the accumulation of ADMA after DDAH1 inhibition has no effect on stroke outcomes in mice subjected to 65-minutes tMCAo, including ischaemic brain injury and neurological and functional deficits, suggesting that the ADMA-DDAH1 pathway is functionally important for cerebral artery function but it may not play a major role in ischaemic stroke pathogenesis.

Chapter 5: Investigating the importance of endothelial-specific DDAH1 in regulating cerebral artery function and in ischaemic stroke pathogenesis

Using endothelial-specific DDAH1 knockout mice, this chapter aimed to evaluate for the first time the functional importance of endothelial DDAH1 for regulating eNOS-NO signalling in cerebral arteries. Also, it examined the importance of endothelial DDAH1 for ischaemic stroke outcomes. There were three major findings in this chapter. Firstly, we have shown that endothelial-specific DDAH1 knockout not only results in impaired NO-dependent endothelial function of intracranial and extracranial cerebral arteries, but also vascular smooth muscle dysfunction that is characterised by hypocontractility to vasoconstrictors. In contrast, we found that endothelial-specific DDAH1 knockout had no effect on the endothelial function of systemic arteries (thoracic aortae and mesenteric). The third major finding was that despite the marked cerebrovascular abnormalities observed in endothelial-specific DDAH1 knockout mice, our data so far indicates that endothelial DDAH1 is not functionally important for ischaemic brain injury or neurological and functional outcomes after 50-minutes of tMCAo. Notably, however, we provide the first evidence that endothelial DDAH1 is critically important for regulating cerebral eNOS-NO signalling and thus cerebral artery function, likely through the metabolism of cerebral vascular ADMA.

Chapter 6: Investigating the roles of the ADMA-DDAH1 pathway in cerebral angiogenesis

The main aim of this thesis chapter was to examine the roles of the ADMA-DDAH1 pathway in cerebral angiogenesis. However, we first aimed to establish an assay of cerebral sprouting angiogenesis using intracranial and extracranial cerebral artery rings in a collagen matrix. We showed that middle cerebral and common carotid artery rings formed reproducible angiogenic sprouts in response to exogenous VEGF. The major finding in this chapter was that using the selective DDAH1 inhibitor, L-257, total vascular (i.e.,

endothelial, and smooth muscle) DDAH1 is an important regulator of sprouting angiogenesis in cerebral arteries, an effect which was similar to treatment with exogenous ADMA. A second major finding was that endothelial DDAH1 (using arteries from endothelial-specific DDAH1 knockout mice) is functionally important for the sprouting angiogenic activity of male but not female middle cerebral arteries. Paradoxically, the importance of endothelial DDAH1 for sprouting angiogenesis appeared to be important in female but not male common carotid and thoracic aorta rings. Notably, however, it remains unclear whether dysregulation of the ADMA-DDAH1 pathway affects cerebral angiogenesis by disrupting eNOS-NO signalling, or via other mechanisms.

7.2 Clinical perspectives of the ADMA-DDAH1 pathway in ischaemic stroke pathogenesis

7.2.1 Elevated ADMA and DDAH1 dysfunction in cerebral artery function, cerebrovascular risk, and ischaemic stroke

In Chapter 5, we found that in contrast to arteries of the peripheral circulation, endothelial DDAH1 was functionally important in cerebral arteries for regulating eNOS-NO signalling, and for regulating vascular smooth muscle function. These findings therefore indicate that endothelial DDAH1 in extracranial (e.g., carotid) and intracranial (e.g., middle cerebral) cerebral vessels plays a critical role in maintaining eNOS-NO signalling and thus vascular function, whereas in systemic vessels it does not appear to play a role. Furthermore, the data also suggests that in contrast to systemic arteries, cerebral endothelial cells may be a major source of ADMA. Consistent with this, using endothelial-specific DDAH1 knockout mice Dowsett and colleagues demonstrated that peripheral-derived endothelial cells are not a major source of ADMA (Dowsett *et al.*, 2015). It is conceivable that the inherent differences between endothelial cells of the cerebral and systemic circulations explain why DDAH1 is functionally more important in cerebral vessels. For example, cerebral endothelial cells from rats were shown to have a higher cytosolic mitochondrial content compared to endothelial cells from other vascular beds (Oldendorf, Cornford and Brown, 1977). As mentioned previously, increased generation of ROS and/or RNS can modulate the activity of the type I PRMT and DDAH enzymes (Böger *et al.*, 2000; Leiper *et al.*, 2002; Jiang *et al.*, 2006), thereby leading to increased production by PRMTs and/or reduced metabolism of ADMA by DDAHs. Importantly, rat and mouse cerebral vessels were shown to produce greater amounts of ROS under physiological conditions than peripheral vessels (Miller *et al.*, 2005, 2009), which may in turn result in greater ADMA production in cerebral vessels. Whilst speculative at present, it is postulated that cerebral endothelial cells may be more reliant on DDAH1 activity and/or expression to regulate intracellular ADMA levels. Another potential explanation is that cerebral endothelial cells may undergo greater or more rapid protein turnover (resulting in greater release of free ADMA into the cytosol following proteolysis) due to the high metabolic demands of cerebral endothelial cells required for the transport of

nutrients across the BBB (Grammas, Martinez and Miller, 2011). Future work is therefore required to examine if indeed cerebral endothelial cells produce more ADMA under physiological conditions than endothelial cells from other vascular beds, and if this is the case, studies are needed to explore the mechanisms responsible for this. Additionally, it may be insightful to compare the expression levels and/or activity of DDAH1 between cerebral and peripheral vascular beds.

Although we have given evidence of cerebrovascular abnormalities in endothelial-specific DDAH1 knockout mice *in vitro*, it remains unclear whether such abnormalities in turn result in altered cerebral perfusion *in vivo*, or whether such changes can influence brain health. Therefore, future studies are required to evaluate the importance of total vascular or endothelial DDAH1 for cerebral perfusion and overall brain health. One such approach for substantiating the importance of DDAH1 in regulating cerebral perfusion and brain health is by measuring changes of cerebral perfusion of mice treated with exogenous ADMA or L-257, as well as in endothelial-specific DDAH1 knockout mice using imaging techniques such as laser speckle contrast imaging. Nevertheless, in combination with the data presented in this thesis, there are several lines of evidence which indicate the importance of DDAH1 for maintaining cerebral perfusion and brain health. Firstly, as mentioned previously, a -396 4N del/ins loss-of-function DDAH1 polymorphism was shown to be associated with an increased risk of ischaemic stroke (Ding *et al.*, 2010). Furthermore, endothelial dysfunction underpins the deleterious consequences of virtually all cardiovascular risk factors on the brain (Sibal *et al.*, 2010), and endothelial dysfunction in the cerebral circulation contributes to numerous cerebrovascular diseases such as cerebral small vessel disease and ischaemic stroke (Faraci, 2011). Also, it is well documented that infusion of ADMA in healthy humans increases arterial stiffness whilst reducing cerebral perfusion (Kielstein *et al.*, 2006), and arterial stiffening is an independent predictor of fatal stroke in patients with essential hypertension (Laurent *et al.*, 2003). Thus, it appears likely that DDAH1 plays a critical functional role in maintaining cerebral perfusion and brain health. As such, it is conceivable that DDAH1 dysfunction and the resultant increase in circulating or cerebral vascular ADMA may have devastating consequences on the brain such as chronic cerebral hypoperfusion and the resultant increased susceptibility to ischaemic brain injury, as well as contributing to cerebral small vessel disease. Importantly, however, studies have shown that DDAH1 activity is decreased by oxidative stress (Leiper *et al.*, 2002; Jiang *et al.*, 2006), and whilst future work is needed, given oxidative stress is a common feature of vascular-related conditions these findings suggest that DDAH1 dysfunction may indeed be a common feature of cardiovascular risk factors. Notably, however, despite marked impairments of cerebral artery function, our data so far showed no differences in stroke outcomes in endothelial-specific DDAH1 knockout mice compared to controls. However, due to technical

challenges relating to the use of a new laser doppler, the criteria for successful ischaemia-reperfusion in Chapter 5 were adjusted compared to the criteria used in Chapters 3 and 4. As a result, this raises questions over the reliability of the focal cerebral ischaemia experienced by the mice in this study, which ultimately may have been inadequate for evaluating the importance of endothelial DDAH1 for ischaemic stroke outcomes in mice. Another key limitation of our tMCAo model was the use of young healthy male mice. Although we observed marked vascular dysfunction in mice lacking endothelial DDAH1, which as proposed may result in chronic hypoperfusion and increased susceptibility to ischaemic brain injury; it may be that such effects might only impact stroke outcomes in aged endothelial-specific DDAH1 knockout mice, or in mice with cardiovascular co-morbidities (e.g., hypertension). Thus, future studies using the same selection criteria used in Chapters 3 and 4, as well as using aged or co-morbid endothelial-specific DDAH1 mice are needed. Thus, our findings so far indicate that endothelial DDAH1 function is crucial for cerebrovascular health and homeostasis, however, its importance for cerebral perfusion and brain health, and ischaemic stroke outcomes remains to be determined.

Our data in Chapter 5 demonstrate a crucial role for endothelial DDAH1 in regulating both endothelial and vascular smooth muscle function of common carotid arteries. Although these vessels are not major contributors to total cerebral vascular resistance (unlike large cerebral arteries such as the middle cerebral artery), they are a major site of atherosclerosis (carotid artery disease; CAD) (Bir and Kelley, 2022), and CAD is a major risk factor for stroke (Rothwell, 2000). It is well documented that elevated ADMA levels play a causal role in the development of atherosclerosis and that DDAH1 is functionally important for the prevention and/or protection against atherosclerosis. For example, a study by Jacobi and colleagues demonstrated that plaque formation was reduced in the aortae of $ApoE^{-/-}$ mice overexpressing DDAH1 (Jacobi *et al.*, 2010). Furthermore, plasma levels of ADMA were shown to significantly correlate with carotid intima-media thickness in humans (Miyazaki *et al.*, 1999), which is a common measure of carotid atherosclerotic formation and CAD (Dowsett *et al.*, 2020). Endothelial dysfunction also plays an essential role in the development of atherosclerosis and eventually CAD (Medina-Leyte *et al.*, 2021). In addition, there is a wealth of evidence linking CAD and ischaemic stroke risk (O'Leary *et al.*, 1992; Bots *et al.*, 1997, 1999; Ebrahim *et al.*, 1999; Manolio *et al.*, 1999), and large-artery atherosclerosis is one of the major clinical subtypes of ischaemic stroke (Adams *et al.*, 1993). Taken together with our data in Chapter 5, it is conceivable that the accumulation of ADMA following DDAH1 dysfunction could predispose otherwise healthy individuals to the development of carotid artery endothelial dysfunction and carotid artery disease, and thus ischaemic stroke. One approach to testing for a causal role of the ADMA-DDAH1 pathway in CAD would be to evaluate carotid artery function, carotid artery atherosclerosis, and potentially stroke outcomes in endothelial-specific

DDAH1 knockout mice fed with an atherogenic diet. Furthermore, a study recently showed that basal plasma ADMA levels in rabbits are approximately 1 μM (Brinkmann *et al.*, 2015), whereas ADMA levels were previously shown to be 5 times higher (approximately 5 μM) in carotid endothelial cells from healthy rabbits (Masuda *et al.*, 1999). Thus, these findings support our notion that cerebral endothelial cells may generate more ADMA and as a result endothelial DDAH1 is functionally more important in the cerebral circulation. Lastly, DDAH1 polymorphisms were previously assessed in a human population with a history of atherosclerotic diseases – namely stroke and coronary heart disease (Ding *et al.*, 2010). Therefore, another approach to test for a causal role of DDAH1 in CAD is to test for DDAH1 polymorphisms in patients presenting with measures of carotid artery disease, such as carotid intima-media thickening and atherosclerotic plaque formation.

7.2.2 Impairment of cerebral angiogenesis following ischaemic stroke and long-term outcomes

Cerebral angiogenesis is essential for brain recovery in the chronic phase following ischaemic stroke and is associated with neurogenesis, neuronal plasticity (Font, Arboix and Krupinski, 2010). Furthermore, cerebral angiogenesis is positively associated with patient recovery and outcomes following stroke (Krupinski *et al.*, 1994). As previously mentioned, ADMA levels are elevated in the plasma and CSF of ischaemic stroke patients, and high plasma ADMA levels also correlated with unfavourable outcomes up to 90 days after stroke onset (Brouns *et al.*, 2009; Worthmann *et al.*, 2011). Numerous preclinical studies have previously reported that exogenous ADMA or DDAH1 dysfunction, as a result of pharmacological inhibition or genetic deletion, significantly impairs the angiogenic activity of peripheral arteries or endothelial cells thereof (Achan *et al.*, 2005; Wojciak-Stothard *et al.*, 2007; Fiedler *et al.*, 2009; Ghebremariam, Erlanson and Cooke, 2014; Dowsett *et al.*, 2015). It is proposed that the primary mechanism through which elevated ADMA and/or DDAH1 dysfunction impairs angiogenesis is through the inhibition of VEGF-dependent eNOS-NO signalling mechanisms (Wojciak-Stothard *et al.*, 2007; Fiedler *et al.*, 2009). In Chapter 6 we evaluated the angiogenic activity of intracranial and extracranial cerebral arteries from C57BL6/J mice treated with the selective DDAH1 inhibitor, or from $DDAH1^{En-/-}$ and $DDAH1^{fl/fl}$ control mice. Consistent with the aforementioned studies of peripheral vessels, we showed that either DDAH1 inhibition or genetic deletion markedly impaired the VEGF-stimulated angiogenic activity of cerebral vessels. Therefore, this work highlights that DDAH1 in endothelial cells is an important regulator of the angiogenic activity of the cerebral endothelium. Although studies are required to examine the role of the ADMA-DDAH1 pathway on cerebral angiogenesis *in vivo* after stroke, these *in vitro* findings suggest that elevated ADMA levels following ischaemic stroke may worsen long-term outcomes and impair the recovery of stroke patients. Indeed, increased brain and/or plasma ADMA levels may disrupt the angiogenic activity of cerebral endothelial cells in

peri-infarct regions after stroke, thereby attenuating the associated neurogenesis and neuronal plasticity that are important for brain recovery. As mentioned, more studies are needed to evaluate the impact of elevated ADMA and/or DDAH1 dysfunction on cerebral angiogenesis *in vivo*. In theory, clinical evaluation of this concept could be explored by evaluating cerebral angiogenesis post-stroke in patients with or without loss-of-function DDAH1 polymorphisms and/or higher plasma ADMA levels using imaging techniques such as magnetic resonance angiography (MRA) or high-resolution x-ray angiography (Simons *et al.*, 2015). Whilst such studies would be invasive and challenging, they would allow the evaluation of changes in cerebral perfusion and blood vessel density in the ischaemic penumbra in the weeks following ischaemic stroke onset. It would be hypothesised that patients with loss-of-function DDAH1 polymorphisms and/or higher plasma ADMA levels will exhibit lower blood vessel densities and reduced cerebral perfusion in the peri-infarct tissue compared to control patients, and this would correlate with worse clinical outcomes.

7.3 Future directions for investigating the importance of the ADMA-DDAH1 pathway in cerebrovascular health and disease

7.3.1 Potential dual roles of elevated ADMA following ischaemic stroke

Given the evidence that ADMA levels are elevated following stroke and are associated with worse stroke outcomes, a key focus of this thesis was to test for a causal relationship between elevated ADMA levels and ischaemic stroke pathogenesis. However, in Chapters 4 and 5, we found that neither DDAH1 inhibition nor genetic endothelial DDAH1 deletion influenced stroke outcomes. As mentioned, previous pilot work in our laboratory showed that mice treated with the selective DDAH1 inhibitor, L-257, had significantly larger infarcts compared to controls following a relatively short 40-minute duration of tMCAo (mild model of stroke; section 8.6 in Appendix). Thus, we hypothesised that elevated ADMA levels following DDAH1 inhibition disrupted crucial protective eNOS-NO signalling during ischaemic stroke pathogenesis, leading to worse stroke outcomes. However, as discussed in Chapter 4, we propose that the relative contributions of the impact of elevated ADMA on stroke outcomes may ultimately be dependent on stroke severity and the resultant contributions of the different NOS isoforms to ischaemic brain injury. Indeed, in mild stroke the deleterious contributions of nNOS- and iNOS-derived NO are likely to be less pronounced than the contributions of protective eNOS-derived NO. In contrast, in more severe stroke the toxic effects of nNOS and iNOS are likely to supersede the protective effects of eNOS-derived NO. Therefore, it is conceivable that elevated ADMA in the brain may have dual roles in ischaemic stroke pathogenesis that are dictated by the severity of ischaemia. Notably, however, there are many obstacles in selectively targeting nNOS and iNOS in experimental stroke to prove if indeed ADMA has dual roles. Studies have demonstrated that mice deficient in eNOS have larger infarcts after tMCAo

(Huang *et al.*, 1996; Cui *et al.*, 2013), whereas mice deficient in nNOS or iNOS have smaller infarcts (Huang *et al.*, 1994; Iadecola *et al.*, 1997). We therefore propose that by manipulating brain and plasma ADMA levels using L-257 treatments in mice in line with the known timings of nNOS or iNOS activation following stroke onset, followed by the assessment of the relevant stroke outcome measures, may enable us to determine if indeed ADMA has dual roles during ischaemic stroke. Indeed, it is well documented that nNOS becomes activated in the hyperacute phase post-stroke (Chen *et al.*, 2017), whereas iNOS appears to become activated from 12 hours after stroke which peaks on day 4 (Iadecola *et al.*, 1997). Therefore, we propose that a single bolus injection of L-257 administered up to 2 hours following the onset of cerebral ischaemia in mice may sufficiently increase ADMA levels to disrupt nNOS-NO signalling during excitotoxicity, and mice should be allowed to recover to 24 hours after ischaemia induction before evaluating infarct size. Alternatively, a course of L-257 treatments could be applied to stroke mice in line with iNOS activation (e.g., days 1-4) and mice allowed to recover to day 7 before evaluating infarct size.

7.4 Limitations of the study

7.4.1 Measuring neurological and functional deficits following ischaemic stroke in mice

In Chapter 3, we demonstrated that mice after 65-minutes of ischaemia produced larger cortical infarcts compared to shorter durations of tMCAo. Furthermore, mice in this cohort exhibited neurological and functional deficits using the foot fault test of forelimb asymmetry, which assesses sensorimotor function of cortical brain regions in rodents (Stroemer, Kent and Hulsebosch, 1995). In contrast, mice treated with vehicle or L-257 (Chapter 4), as well as DDAH1$^{En-/-}$ and DDAH1$^{fl/fl}$ mice which were subjected to 50-minutes tMCAo due to increased severity of the 65-minute model (Chapter 5), had smaller cortical infarcts compared to the cohort of mice in Chapter 3, and there were no detectable cortical-related neurological deficits as assessed by the cylinder and foot fault tests in both studies. Notably, however, sub-cortical infarct volumes were similar between all tMCAo mice in Chapters 3, 4, and 5 (approximately 10 mm^3). Therefore, this highlights the need for future studies which will include additional tests for assessing neurological outcomes which relate to sub-cortical and not cortical infarcts. For example, the skilled reaching and digital flexion test was used to assess neurological deficits in rats who experienced only sub-cortical infarcts following tMCAo, which showed that skilled reaching and digital flexion was severely impaired in the affected forepaws of tMCAo rats compared to controls (Gharbawie, Auer and Whishaw, 2006). Notably, skilled reaching is a clinically relevant test as it is analogous to human reaching tests used to assess deficits in patients following stroke (van Lieshout *et al.*, 2021). Another important consideration is the lack of consistent cortical infarcts across these studies, which highlights the inherent variability of this mouse model of focal cerebral ischaemia (tMCAo). Indeed,

despite all stroke surgeries being performed in the same environment and on animals of the same age, sex, genetic background, this study demonstrates that infarct size and neurological outcomes can vary considerably across cohorts of mice after tMCAo.

7.4.2 Validation of endothelial-specific DDAH1 knockout in cerebral endothelial cells and cerebral arteries

Dowsett and colleagues recently established the endothelial-specific DDAH1 knockout mouse line (C57BL6/J background) using the Cre-LoxP system (Dowsett *et al.*, 2015). Specifically, female mice possessing LoxP sites which flank exon 1 of the *DDAH1* gene were mated with heterozygous male mice expressing Cre recombinase under the endothelial *Tie2* promoter to achieve cell specificity. DDAH1 expression was detected in cortical neurons, hepatocytes, kidney cells, and in adipocytes, however, the authors only validated endothelial-specific DDAH1 knockout in peripheral artery endothelial cells (Dowsett *et al.*, 2015). Therefore, it was unclear whether endothelial-specific DDAH1 knockout was also achieved in cerebral endothelial cells and importantly whether DDAH1 expression was preserved in cerebral vascular smooth muscle cells. Considerable efforts were made to validate that DDAH1 knockout was achieved in cerebral endothelial cells from DDAH1$^{En-/-}$ mice, however, due to time constraints this work could not be completed for inclusion in this thesis. One might argue that the validation of an endothelial-specific DDAH1 knockout in cerebral endothelial cells was crucial for this study, however, our findings so far have demonstrated that carotids and middle cerebral arteries from endothelial-specific DDAH1 knockout mice display impaired eNOS-NO signalling, which given ADMA inhibits eNOS, provides functional evidence that DDAH1 has indeed been deleted from cerebral endothelial cells. Nevertheless, future studies should prioritise validating the endothelial-specific DDAH1 knockout in cerebral vessels, and determining whether DDAH1 deletion alters ADMA levels in cerebral endothelial cells and/or vessels.

7.4.3 Evaluating the mechanisms of impaired cerebral angiogenesis by ADMA and the 'L-Arginine paradox'

In Chapter 6, we evaluated the effects of DDAH1 inhibition (L-257) or endothelial-specific knockout (DDAH1$^{En-/-}$), on the sprouting angiogenic activity of mouse cerebral arteries. We found that elevated ADMA resulting from DDAH1 inhibition or endothelial-specific DDAH1 knockout impaired the sprouting angiogenic processes of intracranial and extracranial cerebral arteries. However, a major limitation of this study was the lack of mechanistic insight into the inhibitory effects of ADMA on sprouting angiogenesis of cerebral arteries. Previous studies have demonstrated that the inhibitory effects of ADMA on VEGF-stimulated angiogenesis of peripheral-derived endothelial cells can be reversed by supplementation with L-arginine or NO donors (Achan *et al.*, 2005; Wojciak-Stothard *et al.*, 2007; Fiedler *et al.*, 2009), indicating the effects of ADMA on angiogenesis are mediated through the inhibition of eNOS-NO signalling. Moreover, overexpression of

DDAH1 was also shown to prevent the inhibitory effects of ADMA on angiogenic processes (Achan *et al.*, 2005; Fiedler *et al.*, 2009). Whilst it appears likely that ADMA inhibits cerebral angiogenesis through similar mechanisms (i.e., inhibiting eNOS-NO), future studies are needed to prove this. Notably, however, it is curious that ADMA inhibited the angiogenic activity of cerebral vessels cultured in an arginine-rich environment. Indeed, one might predict that the L-arginine in the culture media may be at a sufficient concentration to outcompete ADMA for the eNOS binding site. The 'L-Arginine paradox' describes the phenomenon that exogenous L-arginine modulates NO-mediated biological effects despite the fact that the NOS enzymes are theoretically saturated with L-arginine (Dioguardi, 2011). Thus, it is surprising that exogenous or elevated ADMA has any biological effects at all given that cells are likely to be saturated with L-arginine that will compete for the active site of NOS. Importantly, however, exogenous L-arginine treatment has also been shown to induce the expression of the arginase enzymes which subsequently metabolises excess arginine levels (Grody *et al.*, 1989), indicating a potential mechanism by which researchers still observe effects of ADMA (or L-arginine supplementation) in an arginine-rich environment. This latter point notwithstanding, evaluating the effects of pharmacological DDAH1 inhibition or genetic knockout in arginine-free environments is critical for establishing the functional importance of the ADMA-DDAH1 pathway in cerebral angiogenesis and subsequently in ischaemic stroke outcomes. Lastly, we propose that the use of NO donor molecules (e.g., *S*-nitroso-*N*-acetyl-D,L-penicillamine [SNAP]), or activators of the NO signalling pathway (e.g., cGMP-dependent protein kinases) are the preferred tools for establishing whether the inhibitory effects of elevated ADMA after DDAH1 inhibition or genetic knockout are NO-dependent. Nevertheless, our vasoreactivity data suggests that DDAH1 is functionally more important in cerebral vessels compared to peripheral vessels. As such, it is conceivable that it may similarly have a more prominent role in regulating cerebral angiogenesis compared with angiogenesis in the peripheral circulation, and further studies are required to confirm this.

7.5 Conclusions

In conclusion, we have provided the first evidence that endothelial DDAH1 in the cerebral circulation is a functionally important regulator of eNOS-NO signalling and thus cerebral artery function. This is in contrast with the peripheral circulation where it is not an important regulator of eNOS-NO signalling or vascular function. We also found that elevated ADMA as a result of pharmacological DDAH1 inhibition or endothelial-specific DDAH1 knockout had no effect on ischaemic stroke outcomes. Thus, this data suggests that there is no causal relationship between elevated ADMA or DDAH1 dysfunction and ischaemic stroke pathogenesis. Lastly, we provide the first evidence that DDAH1 is also an important regulator of cerebral angiogenesis. We therefore propose that elevated

ADMA following ischaemic stroke may influence longer-term stroke outcomes by disrupting reparative cerebral angiogenic processes. Ultimately, the findings in this thesis highlight that DDAH1 is crucial for maintaining cerebrovascular homeostasis, and that DDAH1 dysfunction in the cerebral circulation may have important consequences for brain health and disease. Therefore, although more research is needed, this work may ultimately justify the identification of novel DDAH1 focussed therapies for cerebrovascular disease.

Chapter 8 Appendix

8.1 Example images of before and after the nest building test

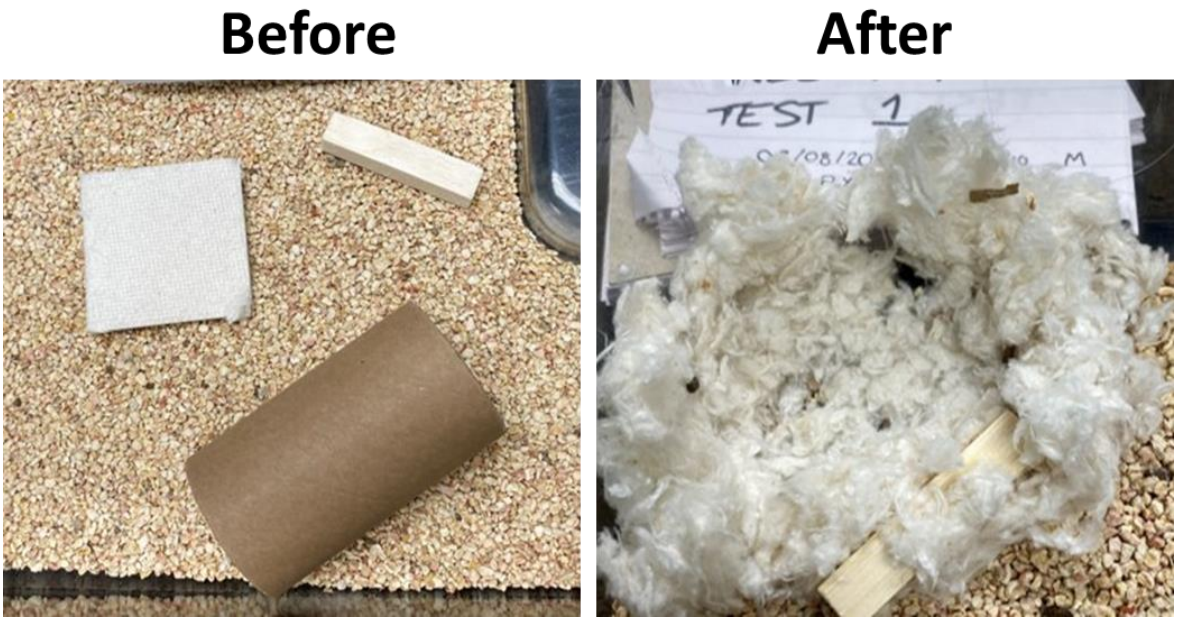

Figure 8-1. Example images of the nest building activity test. Mice were housed in a cage with minimal enrichment to encourage interaction with 3 g of nestlet material (left), and mice were given 24-hours before assessment of nest building activity (right). Untorn pieces weighing ≥0.1 g were collected, and total untorn weight was calculated after each test.

8.2 Cerebral ischaemia does not alter protein expression of DDAH1 and 2, and PRMT4 and 8

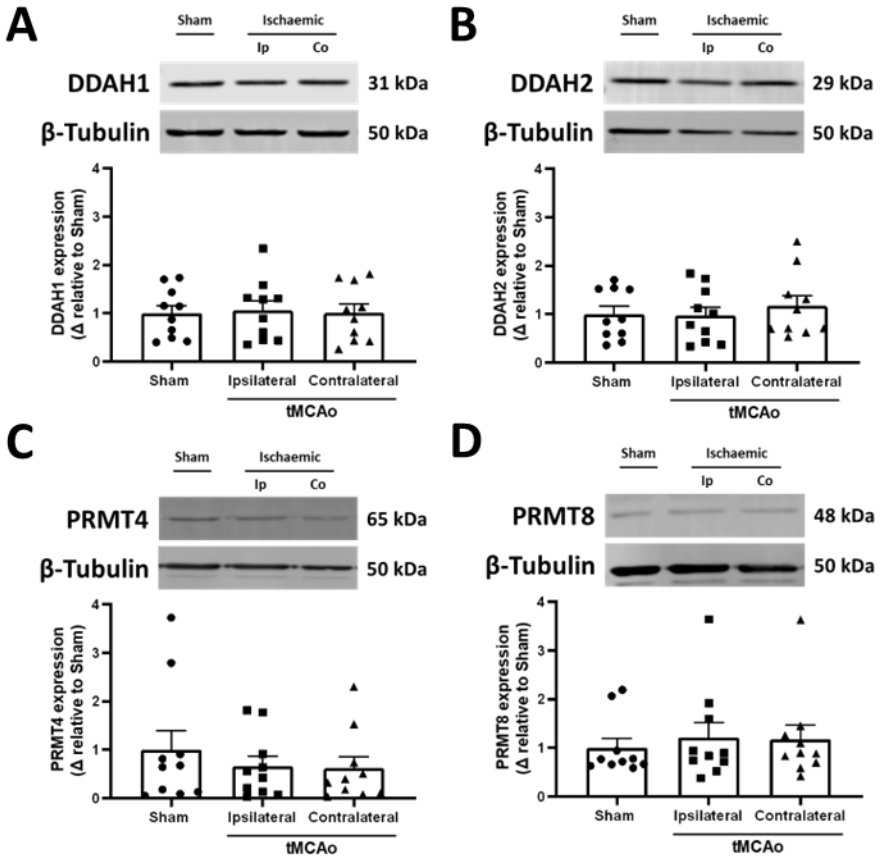

Figure 8-2. Effect of cerebral ischaemia on DDAH and PRMT protein expression in mouse brain tissue 72-hours after transient middle cerebral artery occlusion or sham surgery. Representative Western blots showing protein expression of DDAH1 (**A**), DDAH2 (**B**), PRMT4 (**C**), and PRMT8 (**D**) in the ischaemic (ipsilateral), non-ischaemic (contralateral), or sham control hemisphere tissues 72-hours post-surgery (top). Also shown is a summary of immunoreactive band intensities (bottom). Values are expressed as relative intensity normalised to ß-Tubulin (loading control) intensity. Data presented as mean ± SEM, n=10, *P*>0.05, one-way repeated measures ANOVA with Tukey's multiple comparisons post hoc test.

8.3 Cerebral ischaemia has no effect on ß-Tubulin protein expression 72-hours post-tMCAo

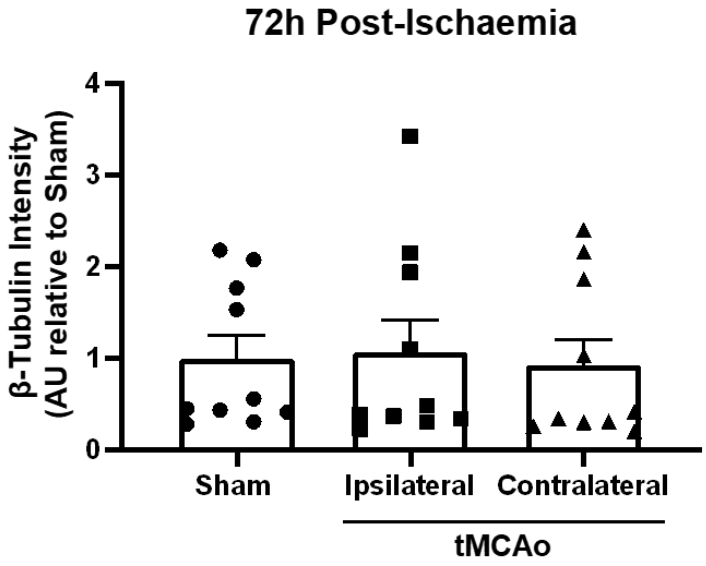

Figure 8-3. Effect of cerebral ischaemia on expression levels of the loading control ß-Tubulin in mouse brain tissue 72-hours after transient middle cerebral artery occlusion (tMCAo) or sham surgery. Relative intensities for the loading control ß-Tubulin. An average was taken for total ß-Tubulin band intensities of each sample across DDAH1, DDAH2, PRMT4, and PRMT8 blots in the 72-hour assessment. ß-Tubulin averages were normalised and expressed relative to sham mice 72-hours post-surgery. Data presented as mean ± SEM, n=10, $P>0.05$, one-way repeated measures ANOVA with Tukey's multiple comparisons post hoc test.

8.4 Western blot primary antibody selectivity

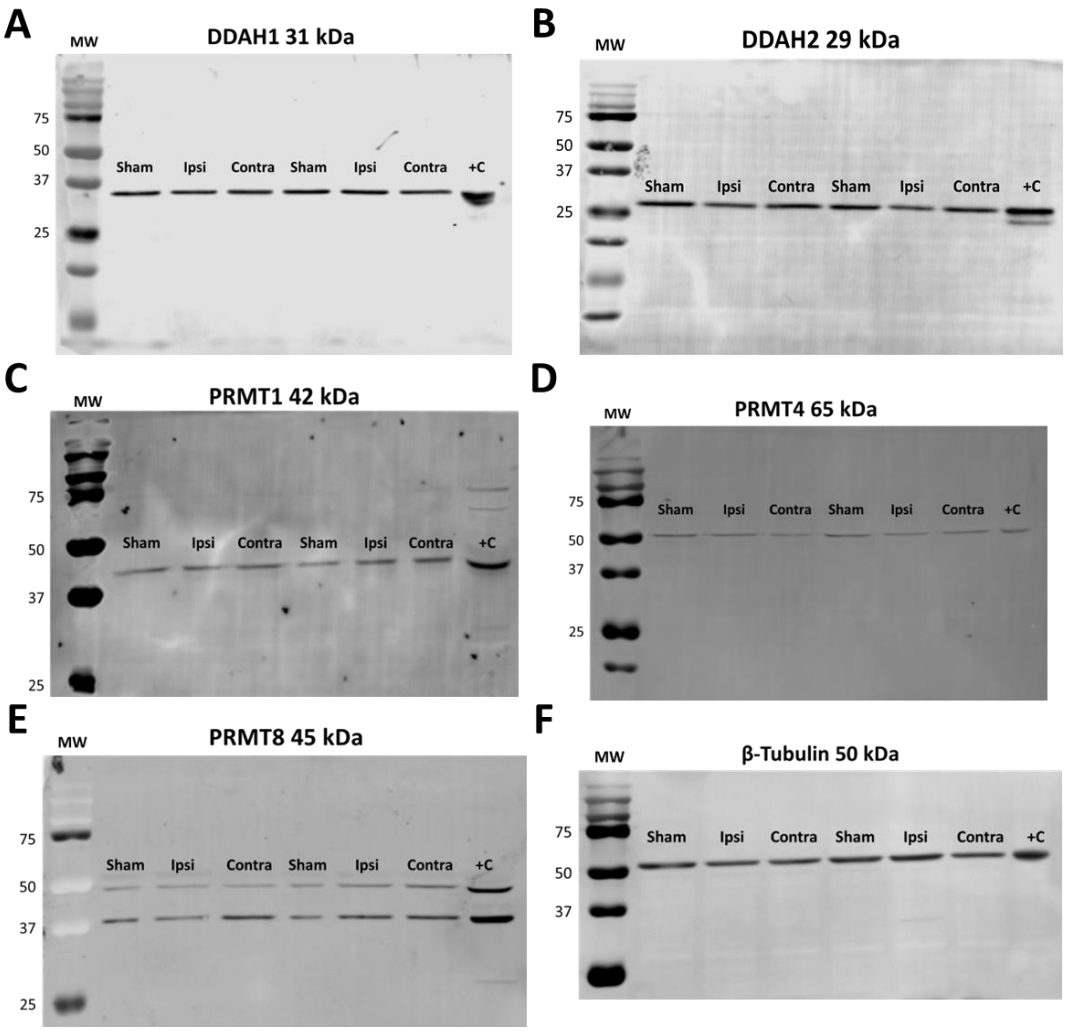

Figure 8-4. Representative images demonstrating primary antibody selectivity for Western blotting. Primary antibodies for DDAH1 (**A**), DDAH2 (**B**), PRMT1 (**C**), PRMT4 (**D**), PRMT8 (**E**), and β-Tubulin (**F**) are shown. Antibody details are described in section 2.3.5 in General Methods.

8.5 Vasorelaxation of mouse common carotid artery rings treated with suprapathophysiological concentrations of exogenous ADMA in response to rising concentrations of vasodilators

Treatment	**Acetylcholine**			**Nitroprusside**		
Group	**Vehicle**	**ADMA**	***n***	**Vehicle**	**ADMA**	***n***
KPSS (mN)	2.0±0.22	2.4±0.4	6	2.4±0.5	2.6±0.5	4
Endothelial function (%)	108.6±4	110.5±10	6	103.7±5	103.1±4	4
Pre-constriction to U46619 (% KPSS)	53.2±6	60.2±7	6	38.7±3	55.2±8	4

Table 8-1. Common carotid artery vessel integrity values that were used in acetylcholine-induced and nitroprusside-induced response curves. Maximum contractile responses to high potassium physiological salt solution (KPSS; mN); endothelial function of common carotid arteries assessed by measuring maximal relaxation response to acetylcholine (% of U46619-induced tone); and U46619 pre-constriction levels (% of KPSS) prior to commencing cumulative concentration-response curves. Values are given as mean ± SEM, where n is number of animals. There were no differences between treatment groups with all parameters, $P>0.05$, unpaired t-test.

Treatment	**Acetylcholine**			**Nitroprusside**		
Groups	**Vehicle**	**ADMA**	***n***	**Vehicle**	**ADMA**	***n***
R_{max} (% Pre-constriction to U46619)	-110.9±11.3	-56.1±12.9	6	-137.2±11	-130.6±9	4
R_{max} *P* Value	$^{**}P = 0.0095$			P = 0.651		
$logEC_{50}$	-7.06±0.1	-7.01±0.3	5-6	-7.8±0.3	-8.2±0.2	4
$logEC_{50}$ *P* Value	P = 0.889			P = 0.332		

Table 8-2. Summary of common carotid artery responses in vehicle or ADMA-treated vessels. Maximal relaxation responses (R_{max}) and half-maximal effect concentration ($logEC_{50}$) values of cumulative concentration-response curves to acetylcholine and nitroprusside in vehicle- and ADMA-treated common carotid arteries. Values are given as mean ± SEM, where n is number of animals. $^{**}P>0.01$, unpaired t-test with Welch's correction.

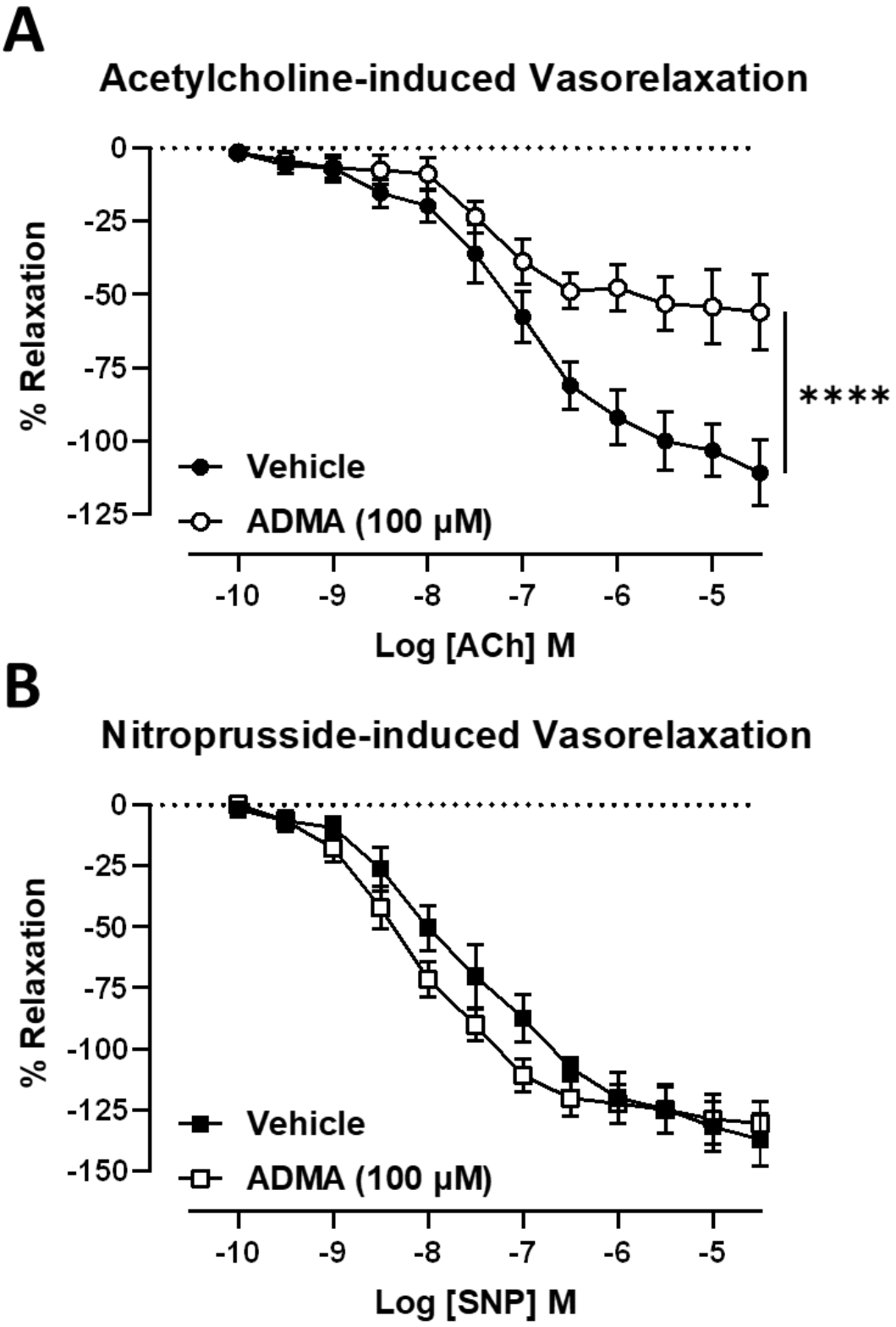

Figure 8-5. Acetylcholine- and nitroprusside-induced responses of common carotid arteries pre-treated with either vehicle or ADMA (100 µM). Cumulative concentration-response curves showing vasorelaxation responses to acetylcholine (10^{-10} to $3x10^{-5}$ M; **A**) and sodium nitroprusside (10^{-10} to $3x10^{-5}$ M; **B**) in isolated common carotid arteries treated with either vehicle (water) or ADMA (100 µM). Results are expressed as % relaxation of U46619 pre-constriction. Data presented as mean ± SEM, n=3-7, ****P<0.0001, two-way repeated measures ANOVA with Šídák's multiple comparisons test.

8.6 DDAH1 inhibition worsens ischaemic brain injury in mice following 40-minutes of tMCAo

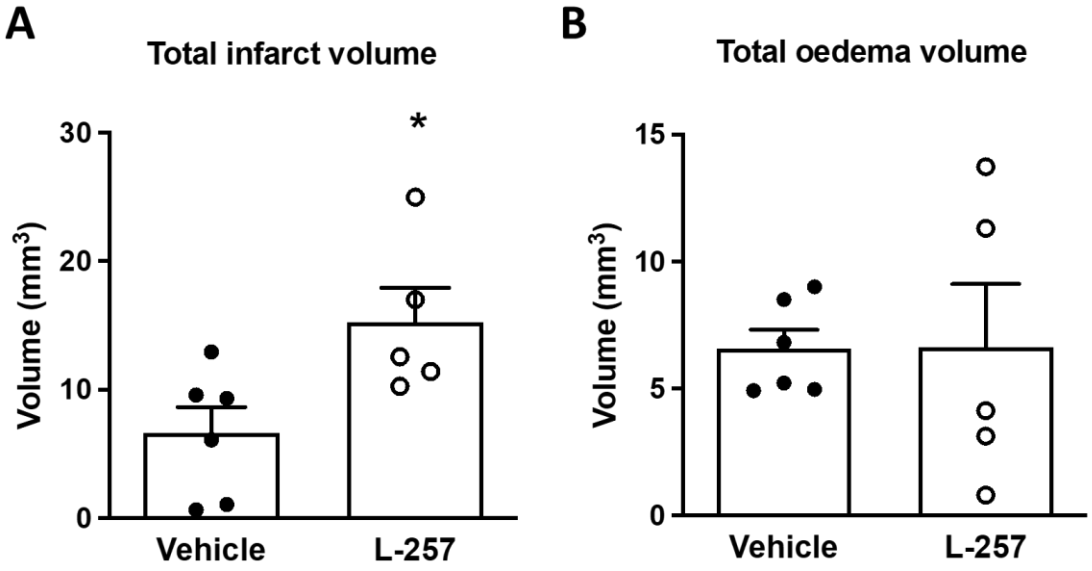

Figure 8-6. Infarct and oedema volumes of vehicle- or L-257-treated mice following 40-minutes of transient middle cerebral artery occlusion (tMCAo). Mouse brain sections in both groups were assessed for total infarct (A) and oedema volume (**B**) 3-days post-stroke. Data presented as mean ± SEM, n=5-6, **P*<0.05, unpaired t-test with Welch's correction. There were no exclusions in this study.

8.7 Additional comparisons of differentially expressed genes in DDAH1$^{En-/-}$ and DDAH1$^{fl/fl}$ cerebral microvessels

Group	Description	*n*
Group 1	Naïve DDAH1$^{fl/fl}$	4
Group 2	Naïve DDAH1$^{En-/-}$	4
Group 3	Stroke DDAH1$^{fl/fl}$, ipsilateral (ischaemic) hemisphere	3
Group 4	Stroke DDAH1$^{fl/fl}$, contralateral (non-ischaemic) hemisphere	3
Group 5	Stroke DDAH1$^{En-/-}$, ipsilateral (ischaemic) hemisphere	3
Group 6	Stroke DDAH1$^{En-/-}$, contralateral (non-ischaemic) hemisphere	3

Table 8-3. Details of the sample groups used for comparisons of differentially expressed genes by bulk RNA sequencing.

Comparison	Details
Comparison 1	Naïve DDAH1$^{fl/fl}$ *vs* naïve DDAH1$^{En-/-}$
Comparison 2	Stroke DDAH1$^{fl/fl}$ *vs* DDAH1$^{En-/-}$ ischaemic hemispheres
Comparison 3	Stroke DDAH1$^{fl/fl}$ ipsilateral *vs* contralateral hemisphere
Comparison 4	Stroke DDAH1$^{En-/-}$ ipsilateral *vs* contralateral hemisphere
Comparison 5	Naïve DDAH1$^{fl/fl}$ *vs* Stroke DDAH1$^{fl/fl}$ ipsilateral hemisphere
Comparison 6	Naïve DDAH1$^{En-/-}$ *vs* Stroke DDAH1$^{En-/-}$ ipsilateral hemisphere

Table 8-4. Details of the comparisons of differentially expressed genes by bulk RNA sequencing. Ipsilateral and contralateral hemispheres refer to the ischaemic and non-ischaemic hemispheres, respectively.

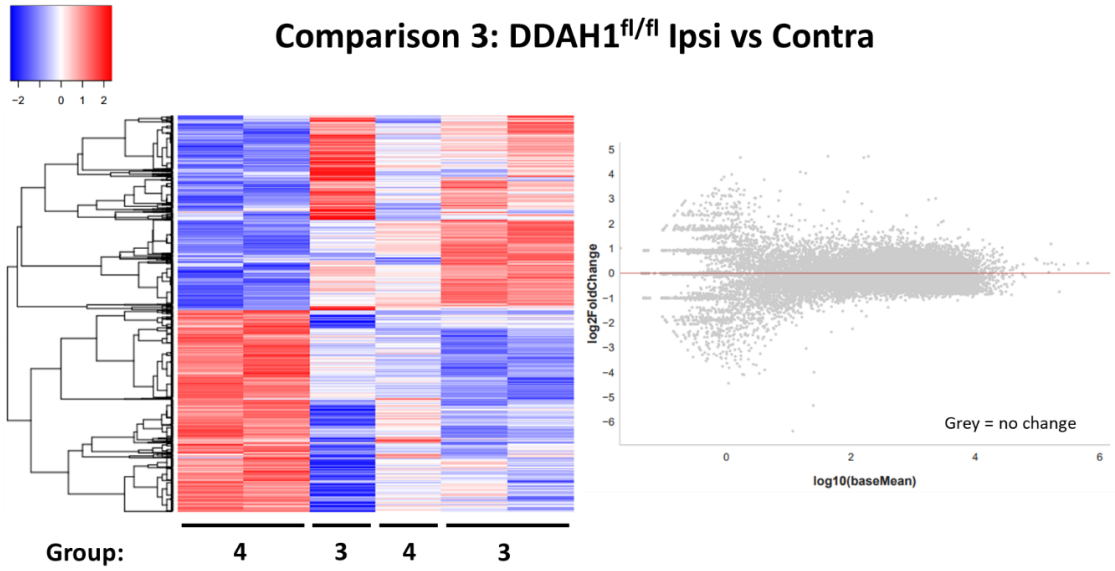

Figure 8-7. Heatmap and MA plot of transcriptome gene expressions in isolated cerebral microvessels from the ipsilateral and contralateral hemispheres of endothelial-specific DDAH1 control mice after 40-minutes transient middle cerebral artery occlusion. A colour key indicating upregulated and downregulated genes in the heatmap (left) is shown in the top left-hand corner. Grey dots in the MA plot (right) indicate no change of expression between groups.

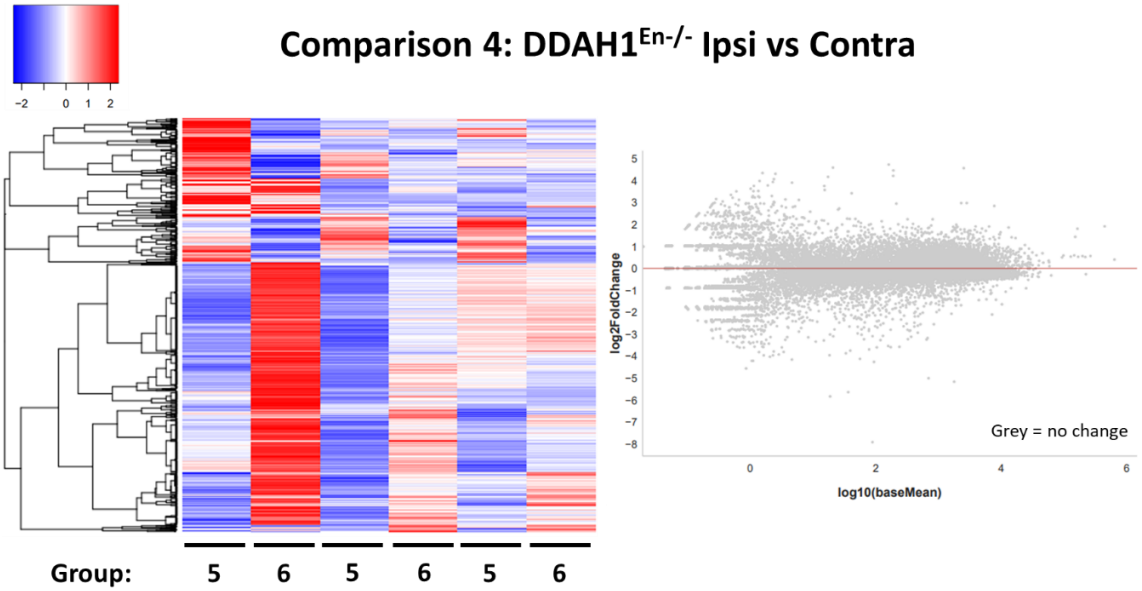

Figure 8-8. Heatmap and MA plot of transcriptome gene expressions in isolated cerebral microvessels from the ipsilateral and contralateral hemispheres of endothelial-specific DDAH1 knockout mice after 40-minutes transient middle cerebral artery occlusion. A colour key indicating upregulated and downregulated genes in the heatmap (left) is shown in the top left-hand corner. Grey dots in the MA plot (right) indicate no change of expression between groups.

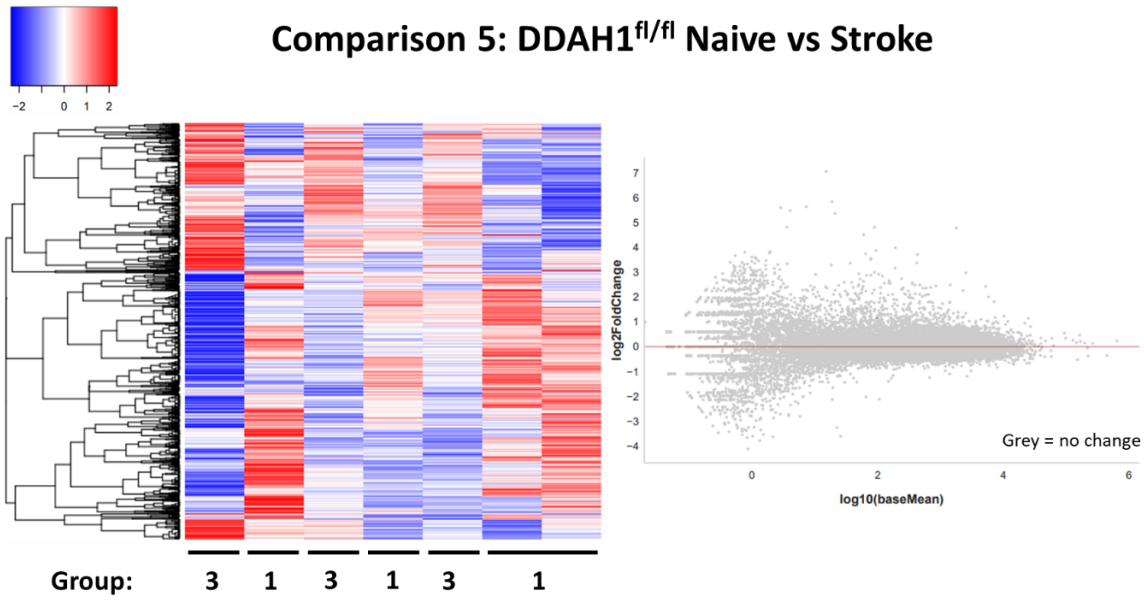

Figure 8-9. Heatmap and MA plot of transcriptome gene expressions in isolated cerebral microvessels from the naïve and ischaemic hemispheres endothelial-specific DDAH1 control mice. A colour key indicating upregulated and downregulated genes in the heatmap (left) is shown in the top left-hand corner. Grey dots in the MA plot (right) indicate no change of expression between groups.

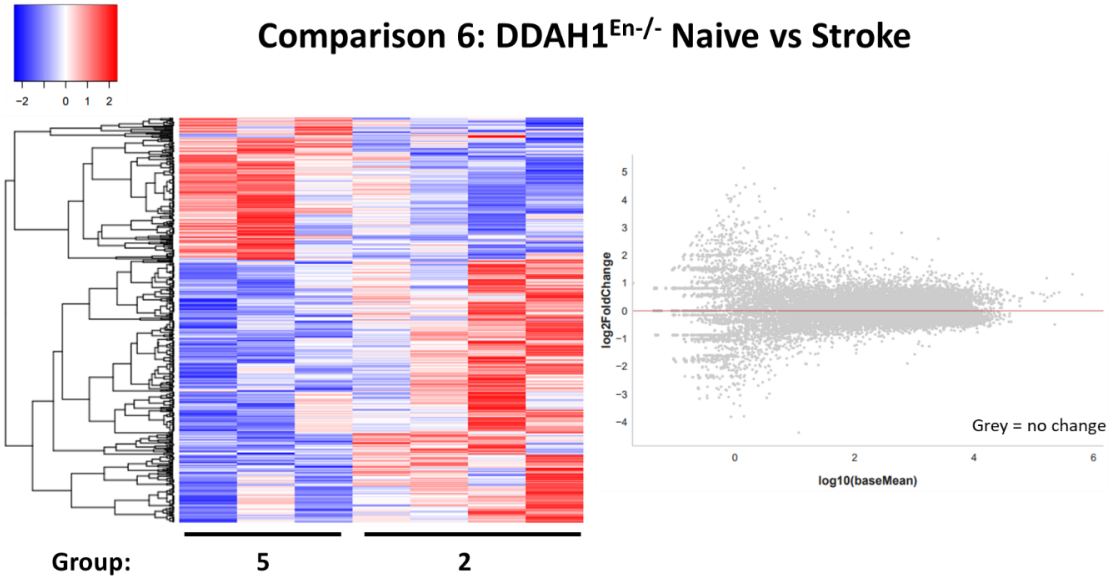

Figure 8-10. Heatmap and MA plot of transcriptome gene expressions in isolated cerebral microvessels from the naïve and ischaemic hemispheres endothelial-specific DDAH1 knockout mice. A colour key indicating upregulated and downregulated genes in the heatmap (left) is shown in the top left-hand corner. Grey dots in the MA plot (right) indicate no change of expression between groups.

References

Abbasi, F. *et al.* (2001) 'Plasma concentrations of asymmetric dimethylarginine are increased in patients with type 2 diabetes mellitus', *The American Journal of Cardiology*, 88(10), pp. 1201–1203. Available at: https://doi.org/10.1016/S0002-9149(01)02063-X.

Abbott, N.J. *et al.* (1992) 'Development and characterisation of a rat brain capillary endothelial culture: towards an *in vitro* blood-brain barrier', *Journal of Cell Science*, 103(1), pp. 23–37. Available at: https://doi.org/10.1242/jcs.103.1.23.

Abeysinghe, H.C.S. *et al.* (2014) 'Brain Remodelling following Endothelin-1 Induced Stroke in Conscious Rats', *PLoS ONE*, 9(5), p. e97007. Available at: https://doi.org/10.1371/journal.pone.0097007.

Abhary, S. *et al.* (2010) 'Sequence Variation in DDAH1 and DDAH2 Genes Is Strongly and Additively Associated with Serum ADMA Concentrations in Individuals with Type 2 Diabetes', *PLoS ONE*, 5(3), p. e9462. Available at: https://doi.org/10.1371/journal.pone.0009462.

Achan, V. *et al.* (2003) 'Asymmetric Dimethylarginine Causes Hypertension and Cardiac Dysfunction in Humans and Is Actively Metabolized by Dimethylarginine Dimethylaminohydrolase', *Arteriosclerosis, Thrombosis, and Vascular Biology*, 23(8), pp. 1455–1459. Available at: https://doi.org/10.1161/01.ATV.0000081742.92006.59.

Achan, V. *et al.* (2005) 'ADMA regulates angiogenesis: genetic and metabolic evidence', *Vascular Medicine*, 10(1), pp. 7–14. Available at: https://doi.org/10.1191/1358863x05vm580oa.

Adams, H.P. *et al.* (1993) 'Classification of subtype of acute ischemic stroke. Definitions for use in a multicenter clinical trial. TOAST. Trial of Org 10172 in Acute Stroke Treatment.', *Stroke*, 24(1), pp. 35–41. Available at: https://doi.org/10.1161/01.STR.24.1.35.

Aihara, Y. *et al.* (2008) 'Induction of housekeeping gene expression after subarachnoid hemorrhage in dogs', *Journal of Neuroscience Methods*, 172(1), pp. 1–7. Available at: https://doi.org/10.1016/j.jneumeth.2008.03.020.

Albers, G.W. *et al.* (2011) 'Stroke Treatment Academic Industry Roundtable (STAIR) Recommendations for Maximizing the Use of Intravenous Thrombolytics and Expanding Treatment Options With Intra-arterial and Neuroprotective Therapies', *Stroke*, 42(9), pp. 2645–2650. Available at: https://doi.org/10.1161/STROKEAHA.111.618850.

Albers, G.W. *et al.* (2018) 'Thrombectomy for Stroke at 6 to 16 Hours with Selection by Perfusion Imaging', *New England Journal of Medicine*, 378(8), pp. 708–718. Available at: https://doi.org/10.1056/NEJMoa1713973.

Allen, C.L. and Bayraktutan, U. (2008) 'Risk Factors for Ischaemic Stroke', *International Journal of Stroke*, 3(2), pp. 105–116. Available at: https://doi.org/10.1111/j.1747-4949.2008.00187.x.

Altmann, K.S. *et al.* (2012) 'Dimethylarginine-Dimethylaminohydrolase-2 (DDAH-2) Does Not Metabolize Methylarginines', *ChemBioChem*, 13(17), pp. 2599–2604. Available at: https://doi.org/10.1002/cbic.201200499.

Font, M., Arboix, A. and Krupinski, J. (2010) 'Angiogenesis, Neurogenesis and Neuroplasticity in Ischemic Stroke', *Current Cardiology Reviews*, 6(3), pp. 238–244. Available at: https://doi.org/10.2174/157340310791658802.

Angerova, Y. *et al.* (2020) 'Cost and cost-effectiveness of early inpatient rehabilitation after stroke varies with initial disability: the Czech Republic perspective', *International Journal of Rehabilitation Research*, 43(4), pp. 376–382. Available at: https://doi.org/10.1097/MRR.0000000000000440.

Antoniades, C. *et al.* (2009) 'Association of plasma asymmetrical dimethylarginine (ADMA) with elevated vascular superoxide production and endothelial nitric oxide synthase uncoupling: implications for endothelial function in human atherosclerosis', *European Heart Journal*, 30(9), pp. 1142–1150. Available at: https://doi.org/10.1093/eurheartj/ehp061.

Appel, D. *et al.* (2018) 'Asymmetric and Symmetric Dimethylarginines are Markers of Delayed Cerebral Ischemia and Neurological Outcome in Patients with Subarachnoid Hemorrhage', *Neurocritical Care*, 29(1), pp. 84–93. Available at: https://doi.org/10.1007/s12028-018-0520-1.

Baird, A.E. *et al.* (1994) 'Reperfusion after thrombolytic therapy in ischemic stroke measured by single-photon emission computed tomography.', *Stroke*, 25(1), pp. 79–85. Available at: https://doi.org/10.1161/01.STR.25.1.79.

Baker, M. *et al.* (2012) 'Use of the mouse aortic ring assay to study angiogenesis', *Nature Protocols*, 7(1), pp. 89–104. Available at: https://doi.org/10.1038/nprot.2011.435.

Barleon, B. *et al.* (1996) 'Migration of human monocytes in response to vascular endothelial growth factor (VEGF) is mediated via the VEGF receptor flt-1', *Blood*, 87(8), pp. 3336–3343. Available at: https://doi.org/10.1182/blood.V87.8.3336.bloodjournal8783336.

Barone, F.C. *et al.* (1993) 'Mouse Strain Differences in Susceptibility to Cerebral Ischemia are Related to Cerebral Vascular Anatomy', *Journal of Cerebral Blood Flow & Metabolism*, 13(4), pp. 683–692. Available at: https://doi.org/10.1038/jcbfm.1993.87.

Barth, T.M., Jones, T.A. and Schallert, T. (1990) 'Functional subdivisions of the rat somatic sensorimotor cortex', *Behavioural Brain Research*, 39(1), pp. 73–95. Available at: https://doi.org/10.1016/0166-4328(90)90122-U.

Baumbach, G.L., Sigmund, C.D. and Faraci, F.M. (2004) 'Structure of Cerebral Arterioles in Mice Deficient in Expression of the Gene for Endothelial Nitric Oxide Synthase', *Circulation Research*, 95(8), pp. 822–829. Available at: https://doi.org/10.1161/01.RES.0000146279.11923.14.

van Beek, A.H. *et al.* (2008) 'Cerebral Autoregulation: An Overview of Current Concepts and Methodology with Special Focus on the Elderly', *Journal of Cerebral Blood Flow & Metabolism*, 28(6), pp. 1071–1085. Available at: https://doi.org/10.1038/jcbfm.2008.13.

Berkhemer, O.A. *et al.* (2015) 'A Randomized Trial of Intraarterial Treatment for Acute Ischemic Stroke', *New England Journal of Medicine*, 372(1), pp. 11–20. Available at: https://doi.org/10.1056/NEJMoa1411587.

Bieber, M. *et al.* (2019) 'Validity and Reliability of Neurological Scores in Mice Exposed to Middle Cerebral Artery Occlusion', *Stroke*, 50(10), pp. 2875–2882. Available at: https://doi.org/10.1161/STROKEAHA.119.026652.

Bir, S. and Kelley, R. (2022) 'Carotid atherosclerotic disease: A systematic review of pathogenesis and management', *Brain Circulation*, 8(3), p. 127. Available at: https://doi.org/10.4103/bc.bc_36_22.

Bodeboger, S., Scalera, F. and Ignarro, L. (2007) 'The L-arginine paradox: Importance of the L-arginine/asymmetrical dimethylarginine ratio', *Pharmacology & Therapeutics*, 114(3), pp. 295–306. Available at: https://doi.org/10.1016/j.pharmthera.2007.03.002.

Bode-Böger, S.M. *et al.* (2003) 'Oral L-arginine improves endothelial function in healthy individuals older than 70 years', *Vascular Medicine*, 8(2), pp. 77–81. Available at: https://doi.org/10.1191/1358863x03vm474oa.

Boehme, A.K., Esenwa, C. and Elkind, M.S.V. (2017) 'Stroke Risk Factors, Genetics, and Prevention', *Circulation Research*, 120(3), pp. 472–495. Available at: https://doi.org/10.1161/CIRCRESAHA.116.308398.

Bo̧ger, R.H. *et al.* (1997) 'Dietary L-Arginine Reduces the Progression of Atherosclerosis in Cholesterol-Fed Rabbits', *Circulation*, 96(4), pp. 1282–1290. Available at: https://doi.org/10.1161/01.CIR.96.4.1282.

Bo̧ger, R.H. *et al.* (1998) 'Asymmetric Dimethylarginine (ADMA): A Novel Risk Factor for Endothelial Dysfunction', *Circulation*, 98(18), pp. 1842–1847. Available at: https://doi.org/10.1161/01.CIR.98.18.1842.

Bo̧ger, R.H. *et al.* (2000) 'LDL Cholesterol Upregulates Synthesis of Asymmetrical Dimethylarginine in Human Endothelial Cells', *Circulation Research*, 87(2), pp. 99–105. Available at: https://doi.org/10.1161/01.RES.87.2.99.

Boo, Y.C. *et al.* (2002) 'Shear stress stimulates phosphorylation of eNOS at Ser ^{635} by a protein kinase A-dependent mechanism', *American Journal of Physiology-Heart and Circulatory Physiology*, 283(5), pp. H1819–H1828. Available at: https://doi.org/10.1152/ajpheart.00214.2002.

Bots, M.L. *et al.* (1997) 'Common Carotid Intima-Media Thickness and Risk of Stroke and Myocardial Infarction', *Circulation*, 96(5), pp. 1432–1437. Available at: https://doi.org/10.1161/01.CIR.96.5.1432.

Bots, M.L. *et al.* (1999) 'Cross-sectionally assessed carotid intima–media thickness relates to long-term risk of stroke, coronary heart disease and death as estimated by available risk functions', *Journal of Internal Medicine*, 245(3), pp. 269–276. Available at: https://doi.org/10.1046/j.1365-2796.1999.0442f.x.

Bowler, J. V *et al.* (1998) 'Natural history of the spontaneous reperfusion of human cerebral infarcts as assessed by 99mTc HMPAO SPECT', *Journal of Neurology, Neurosurgery & Psychiatry*, 64(1), pp. 90–97. Available at: https://doi.org/10.1136/jnnp.64.1.90.

Brinkmann, S. *et al.* (2015) 'The Arginine/ADMA Ratio Is Related to the Prevention of Atherosclerotic Plaques in Hypercholesterolemic Rabbits When Giving a Combined Therapy with Atorvastatine and Arginine', *International Journal of Molecular Sciences*, 16(12), pp. 12230–12242. Available at: https://doi.org/10.3390/ijms160612230.

Brott, T. *et al.* (1989) 'Measurements of acute cerebral infarction: lesion size by computed tomography.', *Stroke*, 20(7), pp. 871–875. Available at: https://doi.org/10.1161/01.STR.20.7.871.

Broughton, B.R.S. *et al.* (2013) 'Stroke Increases G Protein-Coupled Estrogen Receptor Expression in the Brain of Male but Not Female Mice', *Neurosignals*, 21(3–4), pp. 229–239. Available at: https://doi.org/10.1159/000338019.

Broughton, B.R.S. *et al.* (2014) 'Sex-Dependent Effects of G Protein–Coupled Estrogen Receptor Activity on Outcome After Ischemic Stroke', *Stroke*, 45(3), pp. 835–841. Available at: https://doi.org/10.1161/STROKEAHA.113.001499.

Brouns, R. *et al.* (2009) 'Dimethylarginine Levels in Cerebrospinal Fluid of Hyperacute Ischemic Stroke Patients are Associated with Stroke Severity', *Neurochemical Research*, 34(9), pp. 1642–1649. Available at: https://doi.org/10.1007/s11064-009-9954-3.

Bryant, C.D. (2011) 'The blessings and curses of C57BL/6 substrains in mouse genetic studies', *Annals of the New York Academy of Sciences*, 1245(1), pp. 31–33. Available at: https://doi.org/10.1111/j.1749-6632.2011.06325.x.

Cai, L. *et al.* (2015) 'Weight loss: indication of brain damage and effect of combined normobaric oxygen and ethanol therapy after stroke', *Neurological Research*, 37(5), pp. 441–446. Available at: https://doi.org/10.1179/1743132815Y.0000000033.

Cao, J.-X. *et al.* (2020) 'Escitalopram improves neural functional prognosis and endothelial dysfunction in patients with acute cerebral infarction', *Restorative Neurology and Neuroscience*, 38(5), pp. 385–393. Available at: https://doi.org/10.3233/RNN-201041.

Caplin, B. *et al.* (2010) 'Circulating methylarginine levels and the decline in renal function in patients with chronic kidney disease are modulated by DDAH1 polymorphisms', *Kidney International*, 77(5), pp. 459–467. Available at: https://doi.org/10.1038/ki.2009.463.

Caplin, B. and Leiper, J. (2012) 'Endogenous Nitric Oxide Synthase Inhibitors in the Biology of Disease', *Arteriosclerosis, Thrombosis, and Vascular Biology*, 32(6), pp. 1343–1353. Available at: https://doi.org/10.1161/ATVBAHA.112.247726.

Carmeliet, P. (2000) 'Mechanisms of angiogenesis and arteriogenesis', *Nature Medicine*, 6(4), pp. 389–395. Available at: https://doi.org/10.1038/74651.

Carmeliet, P. and Jain, R.K. (2011) 'Principles and mechanisms of vessel normalization for cancer and other angiogenic diseases', *Nature Reviews Drug Discovery*, 10(6), pp. 417–427. Available at: https://doi.org/10.1038/nrd3455.

Carmichael, S.T. (2005) 'Rodent models of focal stroke: Size, mechanism, and purpose', *NeuroRX*, 2(3), pp. 396–409. Available at: https://doi.org/10.1602/neurorx.2.3.396.

De Caterina, R. *et al.* (1995) 'Nitric oxide decreases cytokine-induced endothelial activation. Nitric oxide selectively reduces endothelial expression of adhesion molecules and proinflammatory cytokines.', *Journal of Clinical Investigation*, 96(1), pp. 60–68. Available at: https://doi.org/10.1172/JCI118074.

Chalos, V. *et al.* (2020) 'National Institutes of Health Stroke Scale', *Stroke*, 51(1), pp. 282–290. Available at: https://doi.org/10.1161/STROKEAHA.119.026791.

Chan, Y.-H. *et al.* (2008) 'Reduction of C-reactive protein with isoflavone supplement reverses endothelial dysfunction in patients with ischaemic stroke', *European Heart Journal*, 29(22), pp. 2800–2807. Available at: https://doi.org/10.1093/eurheartj/ehn409.

Chen, S.T. *et al.* (1986) 'A model of focal ischemic stroke in the rat: reproducible extensive cortical infarction.', *Stroke*, 17(4), pp. 738–743. Available at: https://doi.org/10.1161/01.STR.17.4.738.

Chen, Z. *et al.* (2017) 'The role of nitric oxide in stroke', *Medical Gas Research*, 7(3), p. 194. Available at: https://doi.org/10.4103/2045-9912.215750.

Cheng, M. *et al.* (2012) 'The Outcomes of Stroke Induced by Middle Cerebral Artery Occlusion in Different Strains of Mice', *CNS Neuroscience & Therapeutics*, 18(9), pp. 794–795. Available at: https://doi.org/10.1111/j.1755-5949.2012.00361.x.

Cipolla, M.J. *et al.* (2009) 'SK,Ca and IK,Ca Channels, Myogenic Tone, and Vasodilator Responses in Middle Cerebral Arteries and Parenchymal Arterioles', *Stroke*, 40(4), pp. 1451–1457. Available at: https://doi.org/10.1161/STROKEAHA.108.535435.

Cipolla, M.J. and Bullinger, L. V. (2008) 'Reactivity of Brain Parenchymal Arterioles after Ischemia and Reperfusion', *Microcirculation*, 15(6), pp. 495–501. Available at: https://doi.org/10.1080/10739680801986742.

Closs, E.I. *et al.* (1997) 'Interference ofL-Arginine Analogues withL-Arginine Transport Mediated by the y+Carrier hCAT-2B', *Nitric Oxide*, 1(1), pp. 65–73. Available at: https://doi.org/10.1006/niox.1996.0106.

Comajoan, P. *et al.* (2018) 'Evaluation of common housekeeping proteins under ischemic conditions and/or rt-PA treatment in bEnd.3 cells', *Journal of Proteomics*, 184, pp. 10–15. Available at: https://doi.org/10.1016/j.jprot.2018.06.011.

Connolly, E.S. *et al.* (1996) 'Cerebral protection in homozygous null ICAM-1 mice after middle cerebral artery occlusion. Role of neutrophil adhesion in the pathogenesis of stroke.', *Journal of Clinical Investigation*, 97(1), pp. 209–216. Available at: https://doi.org/10.1172/JCI118392.

Cooke, J.P. (2003) 'NO and angiogenesis', *Atherosclerosis Supplements*, 4(4), pp. 53–60. Available at: https://doi.org/10.1016/S1567-5688(03)00034-5.

Couto e Silva, A. *et al.* (2020) 'Protein Arginine Methyltransferases in Cardiovascular and Neuronal Function', *Molecular Neurobiology*, 57(3), pp. 1716–1732. Available at: https://doi.org/10.1007/s12035-019-01850-z.

Cui, X. *et al.* (2013) 'Endothelial Nitric Oxide Synthase Regulates White Matter Changes via the BDNF/TrkB Pathway after Stroke in Mice', *PLoS ONE*, 8(11), p. e80358. Available at: https://doi.org/10.1371/journal.pone.0080358.

Dayoub, H. *et al.* (2008) 'Overexpression of Dimethylarginine Dimethylaminohydrolase Inhibits Asymmetric Dimethylarginine–Induced Endothelial Dysfunction in the Cerebral Circulation', *Stroke*, 39(1), pp. 180–184. Available at: https://doi.org/10.1161/STROKEAHA.107.490631.

Deacon, R.M. (2006) 'Assessing nest building in mice', *Nature Protocols*, 1(3), pp. 1117–1119. Available at: https://doi.org/10.1038/nprot.2006.170.

Delles, C. *et al.* (2004) 'Impaired Endothelial Function of the Retinal Vasculature in Hypertensive Patients', *Stroke*, 35(6), pp. 1289–1293. Available at: https://doi.org/10.1161/01.STR.0000126597.11534.3b.

DeVries, A.C. *et al.* (2001) 'Cognitive and behavioral assessment in experimental stroke research: will it prove useful?', *Neuroscience & Biobehavioral Reviews*, 25(4), pp. 325–342. Available at: https://doi.org/10.1016/S0149-7634(01)00017-3.

Didion, S.P., Hathaway, C.A. and Faraci, F.M. (2001) 'Superoxide levels and function of cerebral blood vessels after inhibition of CuZn-SOD', *American Journal of Physiology-Heart and Circulatory Physiology*, 281(4), pp. H1697–H1703. Available at: https://doi.org/10.1152/ajpheart.2001.281.4.H1697.

Dimmeler, S., Fleming, I., *et al.* (1999) 'Activation of nitric oxide synthase in endothelial cells by Akt-dependent phosphorylation', *Nature*, 399(6736), pp. 601–605. Available at: https://doi.org/10.1038/21224.

Dimmeler, S., Hermann, C., *et al.* (1999) 'Upregulation of Superoxide Dismutase and Nitric Oxide Synthase Mediates the Apoptosis-Suppressive Effects of Shear Stress on

Endothelial Cells', *Arteriosclerosis, Thrombosis, and Vascular Biology*, 19(3), pp. 656–664. Available at: https://doi.org/10.1161/01.ATV.19.3.656.

DiNapoli, V.A. *et al.* (2006) 'Selective MCA occlusion: A precise embolic stroke model', *Journal of Neuroscience Methods*, 154(1–2), pp. 233–238. Available at: https://doi.org/10.1016/j.jneumeth.2005.12.026.

Ding, H. *et al.* (2010) 'A Novel Loss-of-Function *DDAH1* Promoter Polymorphism Is Associated With Increased Susceptibility to Thrombosis Stroke and Coronary Heart Disease', *Circulation Research*, 106(6), pp. 1145–1152. Available at: https://doi.org/10.1161/CIRCRESAHA.109.215616.

Dioguardi, F.S. (2011) 'To Give or Not to Give? Lessons from the Arginine Paradox', *Lifestyle Genomics*, 4(2), pp. 90–98. Available at: https://doi.org/10.1159/000327777.

Dirnagl, U., Iadecola, C. and Moskowitz, M.A. (1999) 'Pathobiology of ischaemic stroke: an integrated view', *Trends in Neurosciences*, 22(9), pp. 391–397. Available at: https://doi.org/10.1016/S0166-2236(99)01401-0.

Doehner, W. *et al.* (2013) 'Overweight and obesity are associated with improved survival, functional outcome, and stroke recurrence after acute stroke or transient ischaemic attack: observations from the TEMPiS trial', *European Heart Journal*, 34(4), pp. 268–277. Available at: https://doi.org/10.1093/eurheartj/ehs340.

Dogan, O. *et al.* (2018) 'Oxidative and nitrosative stress in patients with ischemic stroke', *LaboratoriumsMedizin*, 42(5), pp. 195–200. Available at: https://doi.org/10.1515/labmed-2018-0036.

Dowsett, L. *et al.* (2015) 'Endothelial Dimethylarginine Dimethylaminohydrolase 1 Is an Important Regulator of Angiogenesis but Does Not Regulate Vascular Reactivity or Hemodynamic Homeostasis', *Circulation*, 131(25), pp. 2217–2225. Available at: https://doi.org/10.1161/CIRCULATIONAHA.114.015064.

Dowsett, L. *et al.* (2020) 'ADMA: A Key Player in the Relationship between Vascular Dysfunction and Inflammation in Atherosclerosis', *Journal of Clinical Medicine*, 9(9), p. 3026. Available at: https://doi.org/10.3390/jcm9093026.

Dulak, J. *et al.* (2000) 'Nitric Oxide Induces the Synthesis of Vascular Endothelial Growth Factor by Rat Vascular Smooth Muscle Cells', *Arteriosclerosis, Thrombosis, and Vascular Biology*, 20(3), pp. 659–666. Available at: https://doi.org/10.1161/01.ATV.20.3.659.

Durukan, A. and Tatlisumak, T. (2007) 'Acute ischemic stroke: Overview of major experimental rodent models, pathophysiology, and therapy of focal cerebral ischemia', *Pharmacology Biochemistry and Behavior*, 87(1), pp. 179–197. Available at: https://doi.org/10.1016/j.pbb.2007.04.015.

Ebrahim, S. *et al.* (1999) 'Carotid Plaque, Intima Media Thickness, Cardiovascular Risk Factors, and Prevalent Cardiovascular Disease in Men and Women', *Stroke*, 30(4), pp. 841–850. Available at: https://doi.org/10.1161/01.STR.30.4.841.

Eilken, H.M. and Adams, R.H. (2010) 'Dynamics of endothelial cell behavior in sprouting angiogenesis', *Current Opinion in Cell Biology*, 22(5), pp. 617–625. Available at: https://doi.org/10.1016/j.ceb.2010.08.010.

Engel, O. *et al.* (2011) 'Modeling Stroke in Mice - Middle Cerebral Artery Occlusion with the Filament Model', *Journal of Visualized Experiments* [Preprint], (47). Available at: https://doi.org/10.3791/2423.

Ettehad, D. *et al.* (2016) 'Blood pressure lowering for prevention of cardiovascular disease and death: a systematic review and meta-analysis', *The Lancet*, 387(10022), pp. 957–967. Available at: https://doi.org/10.1016/S0140-6736(15)01225-8.

Fallah, A. *et al.* (2019) 'Therapeutic targeting of angiogenesis molecular pathways in angiogenesis-dependent diseases', *Biomedicine & Pharmacotherapy*, 110, pp. 775–785. Available at: https://doi.org/10.1016/j.biopha.2018.12.022.

Faraci, F.M. *et al.* (2006) 'Selective cerebral vascular dysfunction in Mn-SOD-deficient mice', *Journal of Applied Physiology*, 100(6), pp. 2089–2093. Available at: https://doi.org/10.1152/japplphysiol.00939.2005.

Faraci, F.M. (2011) 'Protecting against vascular disease in brain', *American Journal of Physiology-Heart and Circulatory Physiology*, 300(5), pp. H1566–H1582. Available at: https://doi.org/10.1152/ajpheart.01310.2010.

Faraci, F.M., Brian, J.E. and Heistad, D.D. (1995) 'Response of cerebral blood vessels to an endogenous inhibitor of nitric oxide synthase', *American Journal of Physiology-Heart and Circulatory Physiology*, 269(5), pp. H1522–H1527. Available at: https://doi.org/10.1152/ajpheart.1995.269.5.H1522.

Faraci, F.M. and Heistad, D.D. (1990) 'Regulation of large cerebral arteries and cerebral microvascular pressure.', *Circulation Research*, 66(1), pp. 8–17. Available at: https://doi.org/10.1161/01.RES.66.1.8.

Faraci, F.M. and Heistad, D.D. (1998) 'Regulation of the Cerebral Circulation: Role of Endothelium and Potassium Channels', *Physiological Reviews*, 78(1), pp. 53–97. Available at: https://doi.org/10.1152/physrev.1998.78.1.53.

Feigin, V.L. *et al.* (2022) 'World Stroke Organization (WSO): Global Stroke Fact Sheet 2022', *International Journal of Stroke*, 17(1), pp. 18–29. Available at: https://doi.org/10.1177/17474930211065917.

Fiedler, L.R. *et al.* (2009) 'The ADMA/DDAH Pathway Regulates VEGF-Mediated Angiogenesis', *Arteriosclerosis, Thrombosis, and Vascular Biology*, 29(12), pp. 2117–2124. Available at: https://doi.org/10.1161/ATVBAHA.109.194035.

Fisher, M. *et al.* (2009) 'Update of the Stroke Therapy Academic Industry Roundtable Preclinical Recommendations', *Stroke*, 40(6), pp. 2244–2250. Available at: https://doi.org/10.1161/STROKEAHA.108.541128.

Fisslthaler, B. *et al.* (2003) 'Insulin enhances the expression of the endothelial nitric oxide synthase in native endothelial cells: a dual role for Akt and AP-1', *Nitric Oxide*, 8(4), pp. 253–261. Available at: https://doi.org/10.1016/S1089-8603(03)00042-9.

Fleck, C. *et al.* (2003) 'Serum concentrations of asymmetric (ADMA) and symmetric (SDMA) dimethylarginine in patients with chronic kidney diseases', *Clinica Chimica Acta*, 336(1–2), pp. 1–12. Available at: https://doi.org/10.1016/S0009-8981(03)00338-3.

FOOD Trial Collaboration (2003) 'Poor Nutritional Status on Admission Predicts Poor Outcomes After Stroke', *Stroke*, 34(6), pp. 1450–1456. Available at: https://doi.org/10.1161/01.STR.0000074037.49197.8C.

Forstermann, U. and Sessa, W.C. (2012) 'Nitric oxide synthases: regulation and function', *European Heart Journal*, 33(7), pp. 829–837. Available at: https://doi.org/10.1093/eurheartj/ehr304.

Fuhrmann, J., Clancy, K.W. and Thompson, P.R. (2015) 'Chemical Biology of Protein Arginine Modifications in Epigenetic Regulation', *Chemical Reviews*, 115(11), pp. 5413–5461. Available at: https://doi.org/10.1021/acs.chemrev.5b00003.

Fujii, M. *et al.* (1997) 'Strain-Related Differences in Susceptibility to Transient Forebrain Ischemia in SV-129 and C57Black/6 Mice', *Stroke*, 28(9), pp. 1805–1811. Available at: https://doi.org/10.1161/01.STR.28.9.1805.

Fulton, M.D., Brown, T. and Zheng, Y.G. (2019) 'The Biological Axis of Protein Arginine Methylation and Asymmetric Dimethylarginine', *International Journal of Molecular Sciences*, 20(13), p. 3322. Available at: https://doi.org/10.3390/ijms20133322.

Furchgott, R.F. and Zawadzki, J. V. (1980) 'The obligatory role of endothelial cells in the relaxation of arterial smooth muscle by acetylcholine', *Nature*, 288(5789), pp. 373–376. Available at: https://doi.org/10.1038/288373a0.

Gaskill, B.N. *et al.* (2013) 'Nest Building as an Indicator of Health and Welfare in Laboratory Mice', *Journal of Visualized Experiments* [Preprint], (82). Available at: https://doi.org/10.3791/51012.

Gerhardt, H. *et al.* (2003) 'VEGF guides angiogenic sprouting utilizing endothelial tip cell filopodia', *The Journal of Cell Biology*, 161(6), pp. 1163–1177. Available at: https://doi.org/10.1083/jcb.200302047.

Gharbawie, O.A., Auer, R.N. and Whishaw, I.Q. (2006) 'Subcortical middle cerebral artery ischemia abolishes the digit flexion and closing used for grasping in rat skilled reaching', *Neuroscience*, 137(4), pp. 1107–1118. Available at: https://doi.org/10.1016/j.neuroscience.2005.10.043.

Ghebremariam, Y.T., Erlanson, D.A. and Cooke, J.P. (2014) 'A Novel and Potent Inhibitor of Dimethylarginine Dimethylaminohydrolase: A Modulator of Cardiovascular Nitric Oxide', *Journal of Pharmacology and Experimental Therapeutics*, 348(1), pp. 69–76. Available at: https://doi.org/10.1124/jpet.113.206847.

Goasdoue, K. *et al.* (2016) 'Standard loading controls are not reliable for Western blot quantification across brain development or in pathological conditions', *Electrophoresis*, 37(4), pp. 630–634. Available at: https://doi.org/10.1002/elps.201500385.

Grammas, P., Martinez, J. and Miller, B. (2011) 'Cerebral microvascular endothelium and the pathogenesis of neurodegenerative diseases', *Expert Reviews in Molecular Medicine*, 13, p. e19. Available at: https://doi.org/10.1017/S1462399411001918.

Griffiths, K. and Madhani, M. (2022) 'The Use of Wire Myography to Investigate Vascular Tone and Function', in, pp. 361–376. Available at: https://doi.org/10.1007/978-1-0716-1924-7_23.

Grody, W.W. *et al.* (1989) 'Differential expression of the two human arginase genes in hyperargininemia. Enzymatic, pathologic, and molecular analysis.', *Journal of Clinical Investigation*, 83(2), pp. 602–609. Available at: https://doi.org/10.1172/JCI113923.

Grosse, G.M. *et al.* (2020) 'Arginine Derivatives in Cerebrovascular Diseases: Mechanisms and Clinical Implications', *International Journal of Molecular Sciences*, 21(5), p. 1798. Available at: https://doi.org/10.3390/ijms21051798.

Grover-Páez, F. and Zavalza-Gómez, A.B. (2009) 'Endothelial dysfunction and cardiovascular risk factors', *Diabetes Research and Clinical Practice*, 84(1), pp. 1–10. Available at: https://doi.org/10.1016/j.diabres.2008.12.013.

Haley, M.J. *et al.* (2017) 'Adipose tissue, metabolic and inflammatory responses to stroke are altered in obese mice', *Disease Models & Mechanisms* [Preprint]. Available at: https://doi.org/10.1242/dmm.030411.

Haley, M.J. *et al.* (2020) 'Stroke Induces Prolonged Changes in Lipid Metabolism, the Liver and Body Composition in Mice', *Translational Stroke Research*, 11(4), pp. 837–850. Available at: https://doi.org/10.1007/s12975-019-00763-2.

Hannemann, J. *et al.* (2020) 'Sequence Variation in the DDAH1 Gene Predisposes for Delayed Cerebral Ischemia in Subarachnoidal Hemorrhage', *Journal of Clinical Medicine*, 9(12), p. 3900. Available at: https://doi.org/10.3390/jcm9123900.

Hara, H. *et al.* (1996) 'Reduced Brain Edema and Infarction Volume in Mice Lacking the Neuronal Isoform of Nitric Oxide Synthase after Transient MCA Occlusion', *Journal of Cerebral Blood Flow & Metabolism*, 16(4), pp. 605–611. Available at: https://doi.org/10.1097/00004647-199607000-00010.

Harrison, J.E. *et al.* (2021) 'ICD-11: an international classification of diseases for the twenty-first century', *BMC Medical Informatics and Decision Making*, 21(S6), p. 206. Available at: https://doi.org/10.1186/s12911-021-01534-6.

Hayashi, T. *et al.* (1997) 'Rapid Induction of Vascular Endothelial Growth Factor Gene Expression After Transient Middle Cerebral Artery Occlusion in Rats', *Stroke*, 28(10), pp. 2039–2044. Available at: https://doi.org/10.1161/01.STR.28.10.2039.

Higashi, Y. (2022) 'Roles of Oxidative Stress and Inflammation in Vascular Endothelial Dysfunction-Related Disease', *Antioxidants*, 11(10), p. 1958. Available at: https://doi.org/10.3390/antiox11101958.

Hink, U. *et al.* (2003) 'Mechanisms Underlying Endothelial Dysfunction in Diabetes Mellitus', *Treatments in Endocrinology*, 2(5), pp. 293–304. Available at: https://doi.org/10.2165/00024677-200302050-00001.

Horie, N. *et al.* (2008) 'Mouse model of focal cerebral ischemia using endothelin-1', *Journal of Neuroscience Methods*, 173(2), pp. 286–290. Available at: https://doi.org/10.1016/j.jneumeth.2008.06.013.

Horowitz, J.D. and Heresztyn, T. (2007) 'An overview of plasma concentrations of asymmetric dimethylarginine (ADMA) in health and disease and in clinical studies: Methodological considerations', *Journal of Chromatography B*, 851(1–2), pp. 42–50. Available at: https://doi.org/10.1016/j.jchromb.2006.09.023.

Hossmann, K.-A. (2006) 'Pathophysiology and Therapy of Experimental Stroke', *Cellular and Molecular Neurobiology*, 26(7–8), pp. 1055–1081. Available at: https://doi.org/10.1007/s10571-006-9008-1.

Hu, X. *et al.* (2017) 'Cerebral Vascular Disease and Neurovascular Injury in Ischemic Stroke', *Circulation Research*, 120(3), pp. 449–471. Available at: https://doi.org/10.1161/CIRCRESAHA.116.308427.

Huang, Z. *et al.* (1994) 'Effects of Cerebral Ischemia in Mice Deficient in Neuronal Nitric Oxide Synthase', *Science*, 265(5180), pp. 1883–1885. Available at: https://doi.org/10.1126/science.7522345.

Huang, Z. *et al.* (1996) 'Enlarged Infarcts in Endothelial Nitric Oxide Synthase Knockout Mice are Attenuated by Nitro-L-Arginine', *Journal of Cerebral Blood Flow & Metabolism*, 16(5), pp. 981–987. Available at: https://doi.org/10.1097/00004647-199609000-00023.

Hurn, P.D. and Brass, L.M. (2003) 'Estrogen and Stroke', *Stroke*, 34(2), pp. 338–341. Available at: https://doi.org/10.1161/01.STR.0000054051.88378.25.

Iadecola, C. *et al.* (1997) 'Delayed Reduction of Ischemic Brain Injury and Neurological Deficits in Mice Lacking the Inducible Nitric Oxide Synthase Gene', *The Journal of Neuroscience*, 17(23), pp. 9157–9164. Available at: https://doi.org/10.1523/JNEUROSCI.17-23-09157.1997.

Iadecola, C. (2017) 'The Neurovascular Unit Coming of Age: A Journey through Neurovascular Coupling in Health and Disease', *Neuron*, 96(1), pp. 17–42. Available at: https://doi.org/10.1016/j.neuron.2017.07.030.

Iadecola, C. and Nedergaard, M. (2007) 'Glial regulation of the cerebral microvasculature', *Nature Neuroscience*, 10(11), pp. 1369–1376. Available at: https://doi.org/10.1038/nn2003.

Jackman, K. *et al.* (2009) 'Reduction of cerebral infarct volume by apocynin requires pretreatment and is absent in Nox2-deficient mice', *British Journal of Pharmacology*, 156(4), pp. 680–688. Available at: https://doi.org/10.1111/j.1476-5381.2008.00073.x.

Jackman, K. and Iadecola, C. (2015) 'Neurovascular Regulation in the Ischemic Brain', *Antioxidants & Redox Signaling*, 22(2), pp. 149–160. Available at: https://doi.org/10.1089/ars.2013.5669.

Jacobi, J. *et al.* (2010) 'Dimethylarginine Dimethylaminohydrolase Overexpression Ameliorates Atherosclerosis in Apolipoprotein E-Deficient Mice by Lowering Asymmetric Dimethylarginine', *The American Journal of Pathology*, 176(5), pp. 2559–2570. Available at: https://doi.org/10.2353/ajpath.2010.090614.

Jiang, J.-L. *et al.* (2006) 'Probucol Decreases Asymmetrical Dimethylarginine Level by Alternation of Protein Arginine Methyltransferase I and Dimethylarginine Dimethylaminohydrolase Activity', *Cardiovascular Drugs and Therapy*, 20(4), pp. 281–294. Available at: https://doi.org/10.1007/s10557-006-9065-1.

Jiang, M. *et al.* (2017) 'Neuroprotection provided by isoflurane pre-conditioning and post-conditioning', *Medical Gas Research*, 7(1), p. 48. Available at: https://doi.org/10.4103/2045-9912.202910.

Jönsson, A.-C. *et al.* (2008) 'Weight Loss After Stroke', *Stroke*, 39(3), pp. 918–923. Available at: https://doi.org/10.1161/STROKEAHA.107.497602.

Jørgensen, H.S. *et al.* (1994) 'Spontaneous Reperfusion of Cerebral Infarcts in Patients With Acute Stroke', *Archives of Neurology*, 51(9), p. 865. Available at: https://doi.org/10.1001/archneur.1994.00540210037011.

Jovin, T.G., Albers, G.W. and Liebeskind, D.S. (2016) 'Stroke Treatment Academic Industry Roundtable', *Stroke*, 47(10), pp. 2656–2665. Available at: https://doi.org/10.1161/STROKEAHA.116.013578.

Kakimoto, Y. and Akawaza, S. (1970) 'Isolation and identification of N-G,N-G- and N-G,N'-G-dimethyl-arginine, N-epsilon-mono-, di-, and trimethyllysine, and glucosylgalactosyl- and galactosyl-delta-hydroxylysine from human urine', *Journal of Biological Chemistry*, 245.

Kalucka, J. *et al.* (2020) 'Single-Cell Transcriptome Atlas of Murine Endothelial Cells', *Cell*, 180(4), pp. 764-779.e20. Available at: https://doi.org/10.1016/j.cell.2020.01.015.

Kawaguchi, M., Furuya, H. and Patel, P.M. (2005) 'Neuroprotective effects of anesthetic agents', *Journal of Anesthesia*, 19(2), pp. 150–156. Available at: https://doi.org/10.1007/s00540-005-0305-5.

Keaney, J. and Campbell, M. (2015) 'The dynamic blood–brain barrier', *The FEBS Journal*, 282(21), pp. 4067–4079. Available at: https://doi.org/10.1111/febs.13412.

Keum, S. and Marchuk, D.A. (2009) 'A Locus Mapping to Mouse Chromosome 7 Determines Infarct Volume in a Mouse Model of Ischemic Stroke', *Circulation: Cardiovascular Genetics*, 2(6), pp. 591–598. Available at: https://doi.org/10.1161/CIRCGENETICS.109.883231.

Khurana, R. *et al.* (2005) 'Role of Angiogenesis in Cardiovascular Disease', *Circulation*, 112(12), pp. 1813–1824. Available at: https://doi.org/10.1161/CIRCULATIONAHA.105.535294.

Kiechl, S. *et al.* (2009) 'Asymmetric and symmetric dimethylarginines are of similar predictive value for cardiovascular risk in the general population', *Atherosclerosis*, 205(1), pp. 261–265. Available at: https://doi.org/10.1016/j.atherosclerosis.2008.10.040.

Kielstein, J.T. *et al.* (2006) 'ADMA Increases Arterial Stiffness and Decreases Cerebral Blood Flow in Humans', *Stroke*, 37(8), pp. 2024–2029. Available at: https://doi.org/10.1161/01.STR.0000231640.32543.11.

Kilkenny, C. *et al.* (2010) 'Improving Bioscience Research Reporting: The ARRIVE Guidelines for Reporting Animal Research', *PLoS Biology*, 8(6), p. e1000412. Available at: https://doi.org/10.1371/journal.pbio.1000412.

Kitagawa, K. *et al.* (1998) 'Cerebral Ischemia after Bilateral Carotid Artery Occlusion and Intraluminal Suture Occlusion in Mice: Evaluation of the Patency of the Posterior Communicating Artery', *Journal of Cerebral Blood Flow & Metabolism*, 18(5), pp. 570–579. Available at: https://doi.org/10.1097/00004647-199805000-00012.

Kojima, T. *et al.* (2010) 'Subventricular Zone-Derived Neural Progenitor Cells Migrate Along a Blood Vessel Scaffold Toward The Post-stroke Striatum', *Stem Cells*, 28(3), pp. 545–554. Available at: https://doi.org/10.1002/stem.306.

Kovács, Z. *et al.* (1996) 'VEGF and flt', *Stroke*, 27(10), pp. 1865–1873. Available at: https://doi.org/10.1161/01.STR.27.10.1865.

Kozlova, A.A. *et al.* (2022) 'Divergent Dimethylarginine Dimethylaminohydrolase Isoenzyme Expression in the Central Nervous System', *Cellular and Molecular Neurobiology*, 42(7), pp. 2273–2288. Available at: https://doi.org/10.1007/s10571-021-01101-7.

Krempl, T.K. *et al.* (2005) 'Elevation of asymmetric dimethylarginine in patients with unstable angina and recurrent cardiovascular events', *European Heart Journal*, 26(18), pp. 1846–1851. Available at: https://doi.org/10.1093/eurheartj/ehi287.

Krock, B.L., Skuli, N. and Simon, M.C. (2011) 'Hypoxia-Induced Angiogenesis: Good and Evil', *Genes & Cancer*, 2(12), pp. 1117–1133. Available at: https://doi.org/10.1177/1947601911423654.

Krupinski, J. *et al.* (1994) 'Role of angiogenesis in patients with cerebral ischemic stroke.', *Stroke*, 25(9), pp. 1794–1798. Available at: https://doi.org/10.1161/01.STR.25.9.1794.

Krupinski, J. *et al.* (1997) 'A Putative Role for Platelet-Derived Growth Factor in Angiogenesis and Neuroprotection After Ischemic Stroke in Humans', *Stroke*, 28(3), pp. 564–573. Available at: https://doi.org/10.1161/01.STR.28.3.564.

Ku, J.M. *et al.* (2016) 'Protective actions of des-acylated ghrelin on brain injury and blood–brain barrier disruption after stroke in mice', *Clinical Science*, 130(17), pp. 1545–1558. Available at: https://doi.org/10.1042/CS20160077.

Kubes, P., Suzuki, M. and Granger, D.N. (1991) 'Nitric oxide: an endogenous modulator of leukocyte adhesion.', *Proceedings of the National Academy of Sciences*, 88(11), pp. 4651–4655. Available at: https://doi.org/10.1073/pnas.88.11.4651.

Kuriakose, D. and Xiao, Z. (2020) 'Pathophysiology and Treatment of Stroke: Present Status and Future Perspectives', *International Journal of Molecular Sciences*, 21(20), p. 7609. Available at: https://doi.org/10.3390/ijms21207609.

Kyrylkova, K. *et al.* (2012) 'Detection of Apoptosis by TUNEL Assay', in, pp. 41–47. Available at: https://doi.org/10.1007/978-1-61779-860-3_5.

Labat-gest, V. and Tomasi, S. (2013) 'Photothrombotic Ischemia: A Minimally Invasive and Reproducible Photochemical Cortical Lesion Model for Mouse Stroke Studies', *Journal of Visualized Experiments* [Preprint], (76). Available at: https://doi.org/10.3791/50370.

Lambden, S. *et al.* (2015) 'Dimethylarginine Dimethylaminohydrolase 2 Regulates Nitric Oxide Synthesis and Hemodynamics and Determines Outcome in Polymicrobial Sepsis', *Arteriosclerosis, Thrombosis, and Vascular Biology*, 35(6), pp. 1382–1392. Available at: https://doi.org/10.1161/ATVBAHA.115.305278.

Lang, C.E., MacDonald, J.R. and Gnip, C. (2007) 'Counting Repetitions: An Observational Study of Outpatient Therapy for People with Hemiparesis Post-Stroke', *Journal of Neurologic Physical Therapy*, 31(1), pp. 3–10. Available at: https://doi.org/10.1097/01.NPT.0000260568.31746.34.

Lattanzi, S., Brigo, F. and Silvestrini, M. (2019) 'Blood pressure and stroke: From incidence to outcome', *The Journal of Clinical Hypertension*, 21(5), pp. 605–607. Available at: https://doi.org/10.1111/jch.13525.

Laurent, S. *et al.* (2003) 'Aortic Stiffness Is an Independent Predictor of Fatal Stroke in Essential Hypertension', *Stroke*, 34(5), pp. 1203–1206. Available at: https://doi.org/10.1161/01.STR.0000065428.03209.64.

Lee, C.T. (1972) 'The development of nest-building behaviour in inbred mice', *Journal of General Psychology*, 87(1).

Lee, J. *et al.* (2005) 'PRMT8, a New Membrane-bound Tissue-specific Member of the Protein Arginine Methyltransferase Family', *Journal of Biological Chemistry*, 280(38), pp. 32890–32896. Available at: https://doi.org/10.1074/jbc.M506944200.

Leiper, J. *et al.* (1999) 'Identification of two human dimethylarginine dimethylaminohydrolases with distinct tissue distributions and homology with microbial arginine deiminases.', *Biochemical Journal* [Preprint].

Leiper, J. *et al.* (2002) 'S-nitrosylation of dimethylarginine dimethylaminohydrolase regulates enzyme activity: Further interactions between nitric oxide synthase and dimethylarginine dimethylaminohydrolase', *Proceedings of the National Academy of Sciences*, 99(21), pp. 13527–13532. Available at: https://doi.org/10.1073/pnas.212269799.

Leiper, J. *et al.* (2007) 'Disruption of methylarginine metabolism impairs vascular homeostasis', *Nature Medicine*, 13(2), pp. 198–203. Available at: https://doi.org/10.1038/nm1543.

Leiper, J. and Nandi, M. (2011) 'The therapeutic potential of targeting endogenous inhibitors of nitric oxide synthesis', *Nature Reviews Drug Discovery*, 10(4), pp. 277–291. Available at: https://doi.org/10.1038/nrd3358.

Leone, A. *et al.* (1992) 'Accumulation of an endogenous inhibitor of nitric oxide synthesis in chronic renal failure', *The Lancet*, 339(8793), pp. 572–575. Available at: https://doi.org/10.1016/0140-6736(92)90865-Z.

Lewington, S. *et al.* (2002) 'Age-specific relevance of usual blood pressure to vascular mortality: a meta-analysis of individual data for one million adults in 61 prospective studies', *The Lancet*, 360(9349), pp. 1903–1913. Available at: https://doi.org/10.1016/S0140-6736(02)11911-8.

Leypoldt, F. *et al.* (2009) 'Dimethylarginine Dimethylaminohydrolase-1 Transgenic Mice Are Not Protected from Ischemic Stroke', *PLoS ONE*, 4(10), p. e7337. Available at: https://doi.org/10.1371/journal.pone.0007337.

Li, R. *et al.* (2006) 'Nicotiflorin reduces cerebral ischemic damage and upregulates endothelial nitric oxide synthase in primarily cultured rat cerebral blood vessel endothelial cells', *Journal of Ethnopharmacology*, 107(1), pp. 143–150. Available at: https://doi.org/10.1016/j.jep.2006.04.024.

Li, T. *et al.* (2022) 'Depletion of iNOS-positive inflammatory cells decelerates neuronal degeneration and alleviates cerebral ischemic damage by suppressing the inflammatory response', *Free Radical Biology and Medicine*, 181, pp. 209–220. Available at: https://doi.org/10.1016/j.freeradbiomed.2022.02.008.

Li, X. *et al.* (2004) 'Chronic behavioral testing after focal ischemia in the mouse: functional recovery and the effects of gender', *Experimental Neurology*, 187(1), pp. 94–104. Available at: https://doi.org/10.1016/j.expneurol.2004.01.004.

Liang, C.-C., Park, A.Y. and Guan, J.-L. (2007) 'In vitro scratch assay: a convenient and inexpensive method for analysis of cell migration in vitro', *Nature Protocols*, 2(2), pp. 329–333. Available at: https://doi.org/10.1038/nprot.2007.30.

van Lieshout, E.C.C. *et al.* (2021) 'Translational Value of Skilled Reaching Assessment in Clinical and Preclinical Studies on Motor Recovery After Stroke', *Neurorehabilitation and Neural Repair*, 35(5), pp. 457–467. Available at: https://doi.org/10.1177/15459683211005022.

Lin, K.Y. *et al.* (2002) 'Impaired Nitric Oxide Synthase Pathway in Diabetes Mellitus', *Circulation*, 106(8), pp. 987–992. Available at: https://doi.org/10.1161/01.CIR.0000027109.14149.67.

Lin, T.-N. *et al.* (2001) 'Induction of Tie-1 and Tie-2 Receptor Protein Expression after Cerebral Ischemia—Reperfusion', *Journal of Cerebral Blood Flow & Metabolism*, 21(6), pp. 690–701. Available at: https://doi.org/10.1097/00004647-200106000-00007.

Lindley, R.I. *et al.* (2004) 'Frequency and risk factors for spontaneous hemorrhagic transformation of cerebral infarction', *Journal of Stroke and Cerebrovascular Diseases*, 13(6), pp. 235–246. Available at: https://doi.org/10.1016/j.jstrokecerebrovasdis.2004.03.003.

Lisabeth, L. and Bushnell, C. (2012) ‘Stroke risk in women: the role of menopause and hormone therapy’, *The Lancet Neurology*, 11(1), pp. 82–91. Available at: https://doi.org/10.1016/S1474-4422(11)70269-1.

Liu, N.-W. *et al.* (2017) ‘Evolutional Characterization of Photochemically Induced Stroke in Rats: a Multimodality Imaging and Molecular Biological Study’, *Translational Stroke Research*, 8(3), pp. 244–256. Available at: https://doi.org/10.1007/s12975-016-0512-4.

Liu, R.-Y. *et al.* (2014) ‘Acute hyperglycemia together with hematoma of high-glucose blood exacerbates neurological injury in a rat model of intracerebral hemorrhage’, *Neuroscience Bulletin*, 30(1), pp. 90–98. Available at: https://doi.org/10.1007/s12264-013-1371-6.

Liu, S. *et al.* (2009) ‘RODENT STROKE MODEL GUIDELINES FOR PRECLINICAL STROKE TRIALS (1ST EDITION)’, *Journal of Experimental Stroke and Translational Medicine*, 2(2), pp. 2–27. Available at: https://doi.org/10.6030/1939-067X-2.2.2.

Liu, X. *et al.* (2018) ‘Asymmetric dimethylarginine (ADMA) as an important risk factor for the increased cardiovascular diseases and heart failure in chronic kidney disease’, *Nitric Oxide*, 78, pp. 113–120. Available at: https://doi.org/10.1016/j.niox.2018.06.004.

Lorenz, M.W. *et al.* (2007) ‘Prediction of Clinical Cardiovascular Events With Carotid Intima-Media Thickness’, *Circulation*, 115(4), pp. 459–467. Available at: https://doi.org/10.1161/CIRCULATIONAHA.106.628875.

Lubarsky, B. and Krasnow, M.A. (2003) ‘Tube Morphogenesis’, *Cell*, 112(1), pp. 19–28. Available at: https://doi.org/10.1016/S0092-8674(02)01283-7.

Lucas-Noll, J. *et al.* (2023) ‘The costs associated with stroke care continuum: a systematic review’, *Health Economics Review*, 13(1), p. 32. Available at: https://doi.org/10.1186/s13561-023-00439-6.

Macrae, I. (2011) ‘Preclinical stroke research – advantages and disadvantages of the most common rodent models of focal ischaemia’, *British Journal of Pharmacology*, 164(4), pp. 1062–1078. Available at: https://doi.org/10.1111/j.1476-5381.2011.01398.x.

Maguida, G. and Shuaib, A. (2023) ‘Collateral Circulation in Ischemic Stroke: An Updated Review’, *Journal of Stroke*, 25(2), pp. 179–198. Available at: https://doi.org/10.5853/jos.2022.02936.

Malinda, K.M. (2009) ‘In Vivo Matrigel Migration and Angiogenesis Assay’, in, pp. 287–294. Available at: https://doi.org/10.1007/978-1-59745-241-0_17.

Mamatha, S.N. *et al.* (2011) ‘Asymmetric dimethylarginine as a risk marker for early-onset ischemic stroke in Indian population’, *Clinica Chimica Acta*, 412(1–2), pp. 139–142. Available at: https://doi.org/10.1016/j.cca.2010.09.026.

Manolio, T.A. *et al.* (1999) ‘Relationships of Cerebral MRI Findings to Ultrasonographic Carotid Atherosclerosis in Older Adults’, *Arteriosclerosis, Thrombosis, and Vascular Biology*, 19(2), pp. 356–365. Available at: https://doi.org/10.1161/01.ATV.19.2.356.

Marescau, B. *et al.* (1997) ‘Guanidino compounds in serum and urine of nondialyzed patients with chronic renal insufficiency’, *Metabolism*, 46(9), pp. 1024–1031. Available at: https://doi.org/10.1016/S0026-0495(97)90273-0.

Martens-Lobenhoffer, J., Bode-Böger, S.M. and Clement, B. (2016) ‘First detection and quantification of Nδ-monomethylarginine, a structural isomer of NG-

monomethylarginine, in humans using MS3', *Analytical Biochemistry*, 493, pp. 14–20. Available at: https://doi.org/10.1016/j.ab.2015.10.001.

Masuda, H. *et al.* (1999) 'Accelerated intimal hyperplasia and increased endogenous inhibitors for NO synthesis in rabbits with alloxan-induced hyperglycaemia', *British Journal of Pharmacology*, 126(1), pp. 211–218. Available at: https://doi.org/10.1038/sj.bjp.0702298.

McColl, B.W. *et al.* (2004) 'Extension of cerebral hypoperfusion and ischaemic pathology beyond MCA territory after intraluminal filament occlusion in C57Bl/6J mice', *Brain Research*, 997(1), pp. 15–23. Available at: https://doi.org/10.1016/j.brainres.2003.10.028.

McKeown, M.E. *et al.* (2022) 'Midline Shift Greater than 3 mm Independently Predicts Outcome After Ischemic Stroke', *Neurocritical Care*, 36(1), pp. 46–51. Available at: https://doi.org/10.1007/s12028-021-01341-x.

McMeekin, P. *et al.* (2017) 'Estimating the number of UK stroke patients eligible for endovascular thrombectomy', *European Stroke Journal*, 2(4), pp. 319–326. Available at: https://doi.org/10.1177/2396987317733343.

McNeill, A.M. *et al.* (2002) 'Estrogen Increases Endothelial Nitric Oxide Synthase via Estrogen Receptors in Rat Cerebral Blood Vessels', *Stroke*, 33(6), pp. 1685–1691. Available at: https://doi.org/10.1161/01.STR.0000016325.54374.93.

Medina-Leyte, D.J. *et al.* (2021) 'Endothelial Dysfunction, Inflammation and Coronary Artery Disease: Potential Biomarkers and Promising Therapeutical Approaches', *International Journal of Molecular Sciences*, 22(8), p. 3850. Available at: https://doi.org/10.3390/ijms22083850.

Miller, A.A. *et al.* (2005) 'NADPH Oxidase Activity and Function Are Profoundly Greater in Cerebral Versus Systemic Arteries', *Circulation Research*, 97(10), pp. 1055–1062. Available at: https://doi.org/10.1161/01.RES.0000189301.10217.87.

Miller, A.A. *et al.* (2009) 'NADPH oxidase activity is higher in cerebral versus systemic arteries of four animal species: role of Nox2', *American Journal of Physiology-Heart and Circulatory Physiology*, 296(1), pp. H220–H225. Available at: https://doi.org/10.1152/ajpheart.00987.2008.

Miller, A.A. *et al.* (2010) 'Augmented Superoxide Production By Nox2-Containing NADPH Oxidase Causes Cerebral Artery Dysfunction During Hypercholesterolemia', *Stroke*, 41(4), pp. 784–789. Available at: https://doi.org/10.1161/STROKEAHA.109.575365.

Miyazaki, H. *et al.* (1999) 'Endogenous Nitric Oxide Synthase Inhibitor', *Circulation*, 99(9), pp. 1141–1146. Available at: https://doi.org/10.1161/01.CIR.99.9.1141.

Montezano, A.C. *et al.* (2011) 'Novel Nox homologues in the vasculature: focusing on Nox4 and Nox5', *Clinical Science*, 120(4), pp. 131–141. Available at: https://doi.org/10.1042/CS20100384.

Moore, J.P. *et al.* (2015) 'M2 macrophage accumulation in the aortic wall during angiotensin II infusion in mice is associated with fibrosis, elastin loss, and elevated blood pressure', *American Journal of Physiology-Heart and Circulatory Physiology*, 309(5), pp. H906–H917. Available at: https://doi.org/10.1152/ajpheart.00821.2014.

Moskowitz, M.A., Lo, E.H. and Iadecola, C. (2010) 'The Science of Stroke: Mechanisms in Search of Treatments', *Neuron*, 67(2), pp. 181–198. Available at: https://doi.org/10.1016/j.neuron.2010.07.002.

Nagafuji, T. *et al.* (1995) 'The neuroprotective effect of a potent and selective inhibitor of type I NOS (L-MIN) in a rat model of focal cerebral ischaemia', *NeuroReport*, 6(11), pp. 1541–1545. Available at: https://doi.org/10.1097/00001756-199507310-00019.

Nandi, M. *et al.* (2012) 'Genetic and Pharmacological Inhibition of Dimethylarginine Dimethylaminohydrolase 1 Is Protective in Endotoxic Shock', *Arteriosclerosis, Thrombosis, and Vascular Biology*, 32(11), pp. 2589–2597. Available at: https://doi.org/10.1161/ATVBAHA.112.300232.

Ng, Y.S. *et al.* (2007) 'Comparison of Clinical Characteristics and Functional Outcomes of Ischemic Stroke in Different Vascular Territories', *Stroke*, 38(8), pp. 2309–2314. Available at: https://doi.org/10.1161/STROKEAHA.106.475483.

Nicosia, R.F. *et al.* (2005) 'A New ex vivo Model to Study Venous Angiogenesis and Arterio-Venous Anastomosis Formation', *Journal of Vascular Research*, 42(2), pp. 111–119. Available at: https://doi.org/10.1159/000083457.

Nicosia, R.F. (2009) 'The aortic ring model of angiogenesis: a quarter century of search and discovery', *Journal of Cellular and Molecular Medicine*, 13(10), pp. 4113–4136. Available at: https://doi.org/10.1111/j.1582-4934.2009.00891.x.

Nishiyama, Y. *et al.* (2010) 'Asymmetric dimethylarginine (ADMA) as a possible risk marker for ischemic stroke', *Journal of the Neurological Sciences*, 290(1–2), pp. 12–15. Available at: https://doi.org/10.1016/j.jns.2009.12.020.

Nogueira, R.G. *et al.* (2018) 'Thrombectomy 6 to 24 Hours after Stroke with a Mismatch between Deficit and Infarct', *New England Journal of Medicine*, 378(1), pp. 11–21. Available at: https://doi.org/10.1056/NEJMoa1706442.

Nowak, T.S. and Mulligan, M.K. (2019) 'Impact of C57BL/6 substrain on sex-dependent differences in mouse stroke models', *Neurochemistry International*, 127, pp. 12–21. Available at: https://doi.org/10.1016/j.neuint.2018.11.011.

Nowak-Sliwinska, P. *et al.* (2018) 'Consensus guidelines for the use and interpretation of angiogenesis assays', *Angiogenesis*, 21(3), pp. 425–532. Available at: https://doi.org/10.1007/s10456-018-9613-x.

Ogawa, T., Kimoto, M. and Sasoaka, K. (1990) 'Dimethylarginine:Pyruvate Aminotransferase in Rats', *The Journal of Biological Chemistry*, 264.

Ohashi, M. *et al.* (2006) 'MnSOD Deficiency Increases Endothelial Dysfunction in ApoE-Deficient Mice', *Arteriosclerosis, Thrombosis, and Vascular Biology*, 26(10), pp. 2331–2336. Available at: https://doi.org/10.1161/01.ATV.0000238347.77590.c9.

Oldendorf, W.H., Cornford, M.E. and Brown, W.J. (1977) 'The large apparent work capability of the blood-brain barrier: A study of the mitochondrial content of capillary endothelial cells in brain and other tissues of the rat', *Annals of Neurology*, 1(5), pp. 409–417. Available at: https://doi.org/10.1002/ana.410010502.

O'Leary, D.H. *et al.* (1992) 'Distribution and correlates of sonographically detected carotid artery disease in the Cardiovascular Health Study. The CHS Collaborative Research Group.', *Stroke*, 23(12), pp. 1752–1760. Available at: https://doi.org/10.1161/01.STR.23.12.1752.

Pannu, R. and Singh, I. (2006) 'Pharmacological strategies for the regulation of inducible nitric oxide synthase: Neurodegenerative versus neuroprotective mechanisms', *Neurochemistry International*, 49(2), pp. 170–182. Available at: https://doi.org/10.1016/j.neuint.2006.04.010.

Papapetropoulos, A. *et al.* (1997) 'Nitric oxide production contributes to the angiogenic properties of vascular endothelial growth factor in human endothelial cells.', *Journal of Clinical Investigation*, 100(12), pp. 3131–3139. Available at: https://doi.org/10.1172/JCI119868.

Pedrono, E. *et al.* (2010) 'An Optimized Mouse Model for Transient Ischemic Attack', *Journal of Neuropathology & Experimental Neurology*, 69(2), pp. 188–195. Available at: https://doi.org/10.1097/NEN.0b013e3181cd331c.

Percie du Sert, N. *et al.* (2017) 'The IMPROVE Guidelines (Ischaemia Models: Procedural Refinements Of in Vivo Experiments)', *Journal of Cerebral Blood Flow & Metabolism*, 37(11), pp. 3488–3517. Available at: https://doi.org/10.1177/0271678X17709185.

Peters, S.A.E. *et al.* (2020) 'Sex differences in the association between major risk factors and the risk of stroke in the UK Biobank cohort study', *Neurology*, 95(20), pp. e2715–e2726. Available at: https://doi.org/10.1212/WNL.0000000000010982.

Phipps, M.A. (1991) 'Assessment of Neurologic Deficits in Stroke', *Nursing Clinics of North America*, 26(4), pp. 957–970. Available at: https://doi.org/10.1016/S0029-6465(22)00308-5.

Pistoia, F. *et al.* (2016) 'Hypertension and Stroke: Epidemiological Aspects and Clinical Evaluation', *High Blood Pressure & Cardiovascular Prevention*, 23(1), pp. 9–18. Available at: https://doi.org/10.1007/s40292-015-0115-2.

Plate, K.H. (1999) 'Mechanisms of Angiogenesis in the Brain', *Journal of Neuropathology and Experimental Neurology*, 58(4), pp. 313–320. Available at: https://doi.org/10.1097/00005072-199904000-00001.

Quick, S. *et al.* (2021) 'A Vessel for Change: Endothelial Dysfunction in Cerebral Small Vessel Disease', *Trends in Neurosciences*, 44(4), pp. 289–305. Available at: https://doi.org/10.1016/j.tins.2020.11.003.

Ragavan, V.N. *et al.* (2023) 'A multicentric consortium study demonstrates that dimethylarginine dimethylaminohydrolase 2 is not a dimethylarginine dimethylaminohydrolase', *Nature Communications*, 14(1), p. 3392. Available at: https://doi.org/10.1038/s41467-023-38467-9.

Rehani, B. *et al.* (2020) 'A New Era of Extended Time Window Acute Stroke Interventions Guided by Imaging', *The Neurohospitalist*, 10(1), pp. 29–37. Available at: https://doi.org/10.1177/1941874419870701.

Rha, J.-H. and Saver, J.L. (2007) 'The Impact of Recanalization on Ischemic Stroke Outcome', *Stroke*, 38(3), pp. 967–973. Available at: https://doi.org/10.1161/01.STR.0000258112.14918.24.

Ribatti, D. and Crivellato, E. (2012) '"Sprouting angiogenesis", a reappraisal', *Developmental Biology*, 372(2), pp. 157–165. Available at: https://doi.org/10.1016/j.ydbio.2012.09.018.

Riddell, D.R. and Owen, J.S. (1997) 'Nitric Oxide and Platelet Aggregation', in, pp. 25–48. Available at: https://doi.org/10.1016/S0083-6729(08)60639-1.

Rock, M.L. *et al.* (2014) 'The time-to-integrate-to-nest test as an indicator of wellbeing in laboratory mice', *Journal of American Association for Laboratory Animal Science*, 53(1), pp. 24–28.

Rodionov, R.N. *et al.* (2010) 'Overexpression of Dimethylarginine Dimethylaminohydrolase Protects Against Cerebral Vascular Effects of

Hyperhomocysteinemia', *Circulation Research*, 106(3), pp. 551–558. Available at: https://doi.org/10.1161/CIRCRESAHA.109.200360.

Rogers, D.C. *et al*. (1997) 'Correlation Between Motor Impairment and Infarct Volume After Permanent and Transient Middle Cerebral Artery Occlusion in the Rat', *Stroke*, 28(10), pp. 2060–2066. Available at: https://doi.org/10.1161/01.STR.28.10.2060.

Rössig, L. *et al*. (1999) 'Nitric Oxide Inhibits Caspase-3 by S-Nitrosation in Vivo', *Journal of Biological Chemistry*, 274(11), pp. 6823–6826. Available at: https://doi.org/10.1074/jbc.274.11.6823.

Rothwell, P.M. (2000) 'Carotid Artery Disease and the Risk of Ischaemic Stroke and Coronary Vascular Events', *Cerebrovascular Diseases*, 10(Suppl. 5), pp. 21–33. Available at: https://doi.org/10.1159/000047601.

Ruan, J. and Yao, Y. (2020) 'Behavioral tests in rodent models of stroke', *Brain Hemorrhages*, 1(4), pp. 171–184. Available at: https://doi.org/10.1016/j.hest.2020.09.001.

Sashindranath, M. and Nandurkar, H.H. (2021) 'Endothelial Dysfunction in the Brain', *Stroke*, 52(5), pp. 1895–1904. Available at: https://doi.org/10.1161/STROKEAHA.120.032711.

Satoh, S., Shirane, R. and Yoshimoto, T. (1991) 'Clinical survey of ischemic cerebrovascular disease in children in a district of Japan.', *Stroke*, 22(5), pp. 586–589. Available at: https://doi.org/10.1161/01.STR.22.5.586.

Saver, J.L. *et al*. (2013) 'Stroke Treatment Academic Industry Roundtable', *Stroke*, 44(12), pp. 3596–3601. Available at: https://doi.org/10.1161/STROKEAHA.113.002769.

Savitz, S.I. *et al*. (2019) 'Stroke Treatment Academic Industry Roundtable X', *Stroke*, 50(4), pp. 1026–1031. Available at: https://doi.org/10.1161/STROKEAHA.118.023927.

Schaar, K.L., Brenneman, M.M. and Savitz, S.I. (2010) 'Functional assessments in the rodent stroke model', *Experimental & Translational Stroke Medicine*, 2(1), p. 13. Available at: https://doi.org/10.1186/2040-7378-2-13.

Schallert, T. (2006) 'Behavioral tests for preclinical intervention assessment', *NeuroRX*, 3(4), pp. 497–504. Available at: https://doi.org/10.1016/j.nurx.2006.08.001.

Scherbakov, N. *et al*. (2019) 'Body weight changes and incidence of cachexia after stroke', *Journal of Cachexia, Sarcopenia and Muscle*, 10(3), pp. 611–620. Available at: https://doi.org/10.1002/jcsm.12400.

Scherbakov, N., Dirnagl, U. and Doehner, W. (2011) 'Body Weight After Stroke', *Stroke*, 42(12), pp. 3646–3650. Available at: https://doi.org/10.1161/STROKEAHA.111.619163.

Schlesinger, S. *et al*. (2016) 'Asymmetric and Symmetric Dimethylarginine as Risk Markers for Total Mortality and Cardiovascular Outcomes: A Systematic Review and Meta-Analysis of Prospective Studies', *PLOS ONE*, 11(11), p. e0165811. Available at: https://doi.org/10.1371/journal.pone.0165811.

Schmittgen, T.D. and Livak, K.J. (2008) 'Analyzing real-time PCR data by the comparative CT method', *Nature Protocols*, 3(6), pp. 1101–1108. Available at: https://doi.org/10.1038/nprot.2008.73.

Schwedhelm, E. and Böger, R.H. (2011) 'The role of asymmetric and symmetric dimethylarginines in renal disease', *Nature Reviews Nephrology*, 7(5), pp. 275–285. Available at: https://doi.org/10.1038/nrneph.2011.31.

Segarra, G. *et al.* (1999) 'Effects of Some Guanidino Compounds on Human Cerebral Arteries', *Stroke*, 30(10), pp. 2206–2211. Available at: https://doi.org/10.1161/01.STR.30.10.2206.

Sena, C.M. *et al.* (2018) 'Vascular Oxidative Stress: Impact and Therapeutic Approaches', *Frontiers in Physiology*, 9. Available at: https://doi.org/10.3389/fphys.2018.01668.

Shakir, R. (2018) 'The struggle for stroke reclassification', *Nature Reviews Neurology*, 14(8), pp. 447–448. Available at: https://doi.org/10.1038/s41582-018-0036-5.

Sibal, L. *et al.* (2010) 'The Role of Asymmetric Dimethylarginine (ADMA) in Endothelial Dysfunction and Cardiovascular Disease', *Current Cardiology Reviews*, 6(2), pp. 82–90. Available at: https://doi.org/10.2174/157340310791162659.

De Silva, T.M. *et al.* (2009) 'Gender Influences Cerebral Vascular Responses to Angiotensin II Through Nox2-Derived Reactive Oxygen Species', *Stroke*, 40(4), pp. 1091–1097. Available at: https://doi.org/10.1161/STROKEAHA.108.531707.

De Silva, T.M. *et al.* (2011) 'Nox2 Oxidase Activity Accounts for the Oxidative Stress and Vasomotor Dysfunction in Mouse Cerebral Arteries following Ischemic Stroke', *PLoS ONE*, 6(12), p. e28393. Available at: https://doi.org/10.1371/journal.pone.0028393.

Simons, M. *et al.* (2015) 'State-of-the-Art Methods for Evaluation of Angiogenesis and Tissue Vascularization', *Circulation Research*, 116(11). Available at: https://doi.org/10.1161/RES.0000000000000054.

Skalak, T.C. and Price, R.J. (1996) 'The Role of Mechanical Stresses in Microvascular Remodeling', *Microcirculation*, 3(2), pp. 143–165. Available at: https://doi.org/10.3109/10739689609148284.

Smith, C.L. *et al.* (2003) 'Dimethylarginine dimethylaminohydrolase activity modulates ADMA levels, VEGF expression, and cell phenotype', *Biochemical and Biophysical Research Communications*, 308(4), pp. 984–989. Available at: https://doi.org/10.1016/S0006-291X(03)01507-9.

Sommer, C.J. (2017) 'Ischemic stroke: experimental models and reality', *Acta Neuropathologica*, 133(2), pp. 245–261. Available at: https://doi.org/10.1007/s00401-017-1667-0.

Speer, T. *et al.* (2013) 'Abnormal High-Density Lipoprotein Induces Endothelial Dysfunction via Activation of Toll-like Receptor-2', *Immunity*, 38(4), pp. 754–768. Available at: https://doi.org/10.1016/j.immuni.2013.02.009.

Speliotes, E.K. *et al.* (1996) 'Increased expression of basic fibroblast growth factor (bFGF) following focal cerebral infarction in the rat', *Molecular Brain Research*, 39(1–2), pp. 31–42. Available at: https://doi.org/10.1016/0169-328X(95)00351-R.

Springer, J. *et al.* (2014) 'Catabolic Signaling and Muscle Wasting After Acute Ischemic Stroke in Mice', *Stroke*, 45(12), pp. 3675–3683. Available at: https://doi.org/10.1161/STROKEAHA.114.006258.

Staniszewska, A. *et al.* (2015) 'Increased levels of symmetric dimethyl-arginine are associated with all-cause mortality in patients with symptomatic peripheral arterial disease', *Journal of Vascular Surgery*, 61(5), pp. 1292–1298. Available at: https://doi.org/10.1016/j.jvs.2015.01.002.

Stiffey-Wilusz, J. *et al.* (2001) 'An ex vivo angiogenesis assay utilizing commercial porcine carotid artery: Modification of the rat aortic ring assay', *Angiogenesis*, 4(1), pp. 3–9. Available at: https://doi.org/10.1023/A:1016604327305.

Stroemer, R.P., Kent, T.A. and Hulsebosch, C.E. (1995) 'Neocortical Neural Sprouting, Synaptogenesis, and Behavioral Recovery After Neocortical Infarction in Rats', *Stroke*, 26(11), pp. 2135–2144. Available at: https://doi.org/10.1161/01.STR.26.11.2135.

Stroke Therapy Academic Industry Roundtable (STAIR) (1999) 'Recommendations for Standards Regarding Preclinical Neuroprotective and Restorative Drug Development', *Stroke*, 30(12), pp. 2752–2758. Available at: https://doi.org/10.1161/01.STR.30.12.2752.

Stuehr, D., Pou, S. and Rosen, G.M. (2001) 'Oxygen Reduction by Nitric-oxide Synthases', *Journal of Biological Chemistry*, 276(18), pp. 14533–14536. Available at: https://doi.org/10.1074/jbc.R100011200.

Surdacki, A. *et al.* (1999) 'Reduced Urinary Excretion of Nitric Oxide Metabolites and Increased Plasma Levels of Asymmetric Dimethylarginine in Men with Essential Hypertension', *Journal of Cardiovascular Pharmacology*, 33(4), pp. 652–658. Available at: https://doi.org/10.1097/00005344-199904000-00020.

Sydow, K. and Münzel, T. (2003) 'ADMA and oxidative stress', *Atherosclerosis Supplements*, 4(4), pp. 41–51. Available at: https://doi.org/10.1016/S1567-5688(03)00033-3.

Tan, X.-L. *et al.* (2015) 'Partial eNOS deficiency causes spontaneous thrombotic cerebral infarction, amyloid angiopathy and cognitive impairment', *Molecular Neurodegeneration*, 10(1), p. 24. Available at: https://doi.org/10.1186/s13024-015-0020-0.

Tang, J. *et al.* (2000) 'PRMT1 Is the Predominant Type I Protein Arginine Methyltransferase in Mammalian Cells', *Journal of Biological Chemistry*, 275(11), pp. 7723–7730. Available at: https://doi.org/10.1074/jbc.275.11.7723.

Teerlink, T. (2007) 'HPLC analysis of ADMA and other methylated l-arginine analogs in biological fluids', *Journal of Chromatography B*, 851(1–2), pp. 21–29. Available at: https://doi.org/10.1016/j.jchromb.2006.07.024.

Terpolilli, N.A., Moskowitz, M.A. and Plesnila, N. (2012) 'Nitric Oxide: Considerations for the Treatment of Ischemic Stroke', *Journal of Cerebral Blood Flow & Metabolism*, 32(7), pp. 1332–1346. Available at: https://doi.org/10.1038/jcbfm.2012.12.

The NINDS and Stroke rt-PA Stroke Study Group (1995) 'Tissue Plasminogen Activator for Acute Ischemic Stroke', *New England Journal of Medicine*, 333(24), pp. 1581–1588. Available at: https://doi.org/10.1056/NEJM199512143332401.

Theofilis, P. *et al.* (2021) 'Inflammatory Mechanisms Contributing to Endothelial Dysfunction', *Biomedicines*, 9(7), p. 781. Available at: https://doi.org/10.3390/biomedicines9070781.

Torondel, B. *et al.* (2010) 'Adenoviral-mediated overexpression of DDAH improves vascular tone regulation', *Vascular Medicine*, 15(3), pp. 205–213. Available at: https://doi.org/10.1177/1358863X09360264.

Tryambake, D. *et al.* (2013) 'Intensive Blood Pressure Lowering Increases Cerebral Blood Flow in Older Subjects With Hypertension', *Hypertension*, 61(6), pp. 1309–1315. Available at: https://doi.org/10.1161/HYPERTENSIONAHA.112.200972.

Tsihlis, N.D. *et al.* (2011) 'Nitric Oxide Inhibits Vascular Smooth Muscle Cell Proliferation and Neointimal Hyperplasia by Increasing the Ubiquitination and Degradation of UbcH10', *Cell Biochemistry and Biophysics*, 60(1–2), pp. 89–97. Available at: https://doi.org/10.1007/s12013-011-9179-3.

Turski, L. *et al.* (1998) 'ZK200775: A phosphonate quinoxalinedione AMPA antagonist for neuroprotection in stroke and trauma', *Proceedings of the National Academy of Sciences*, 95(18), pp. 10960–10965. Available at: https://doi.org/10.1073/pnas.95.18.10960.

Uzdensky, A.B. (2018) 'Photothrombotic Stroke as a Model of Ischemic Stroke', *Translational Stroke Research*, 9(5), pp. 437–451. Available at: https://doi.org/10.1007/s12975-017-0593-8.

Vanlandewijck, M. *et al.* (2018) 'A molecular atlas of cell types and zonation in the brain vasculature', *Nature*, 554(7693), pp. 475–480. Available at: https://doi.org/10.1038/nature25739.

Virani, S.S. *et al.* (2020) 'Heart Disease and Stroke Statistics—2020 Update: A Report From the American Heart Association', *Circulation*, 141(9). Available at: https://doi.org/10.1161/CIR.0000000000000757.

Vital, S.A. and Gavins, F.N.E. (2016) 'Surgical Approach for Middle Cerebral Artery Occlusion and Reperfusion Induced Stroke in Mice', *Journal of Visualized Experiments* [Preprint], (116). Available at: https://doi.org/10.3791/54302.

Wanby, P. *et al.* (2006) 'Asymmetric dimethylarginine (ADMA) as a risk marker for stroke and TIA in a Swedish population', *Atherosclerosis*, 185(2), pp. 271–277. Available at: https://doi.org/10.1016/j.atherosclerosis.2005.06.033.

Wang, L. *et al.* (2004) 'Treatment of Stroke With Erythropoietin Enhances Neurogenesis and Angiogenesis and Improves Neurological Function in Rats', *Stroke*, 35(7), pp. 1732–1737. Available at: https://doi.org/10.1161/01.STR.0000132196.49028.a4.

Wang, Y. *et al.* (2018) 'Superoxide dismutases: Dual roles in controlling ROS damage and regulating ROS signaling', *Journal of Cell Biology*, 217(6), pp. 1915–1928. Available at: https://doi.org/10.1083/jcb.201708007.

Wang, Y. *et al.* (2019) 'PRMT4 overexpression aggravates cardiac remodeling following myocardial infarction by promoting cardiomyocyte apoptosis', *Biochemical and Biophysical Research Communications*, 520(3), pp. 645–650. Available at: https://doi.org/10.1016/j.bbrc.2019.10.085.

Wayman, C. *et al.* (2016) 'Performing Permanent Distal Middle Cerebral with Common Carotid Artery Occlusion in Aged Rats to Study Cortical Ischemia with Sustained Disability', *Journal of Visualized Experiments* [Preprint], (108). Available at: https://doi.org/10.3791/53106.

Weisbrot-Lefkowitz, M. *et al.* (1998) 'Overexpression of human glutathione peroxidase protects transgenic mice against focal cerebral ischemia/reperfusion damage', *Molecular Brain Research*, 53(1–2), pp. 333–338. Available at: https://doi.org/10.1016/S0169-328X(97)00313-6.

Whiteley, W.N. *et al.* (2012) 'Risk Factors for Intracranial Hemorrhage in Acute Ischemic Stroke Patients Treated With Recombinant Tissue Plasminogen Activator', *Stroke*, 43(11), pp. 2904–2909. Available at: https://doi.org/10.1161/STROKEAHA.112.665331.

Windle, V. *et al.* (2006) 'An analysis of four different methods of producing focal cerebral ischemia with endothelin-1 in the rat', *Experimental Neurology*, 201(2), pp. 324–334. Available at: https://doi.org/10.1016/j.expneurol.2006.04.012.

Wojciak-Stothard, B. *et al.* (2007) 'The ADMA/DDAH pathway is a critical regulator of endothelial cell motility', *Journal of Cell Science*, 120(6), pp. 929–942. Available at: https://doi.org/10.1242/jcs.002212.

Wojciak-Stothard, B. *et al.* (2009) 'Modulation of Rac1 Activity by ADMA/DDAH Regulates Pulmonary Endothelial Barrier Function', *Molecular Biology of the Cell*, 20(1), pp. 33–42. Available at: https://doi.org/10.1091/mbc.e08-04-0395.

Worthmann, H. *et al.* (2011) 'High Plasma Dimethylarginine Levels are Associated with Adverse Clinical Outcome After Stroke', *Journal of Atherosclerosis and Thrombosis*, 18(9), pp. 753–761. Available at: https://doi.org/10.5551/jat.8144.

Wu, L. *et al.* (2020) 'Targeting Oxidative Stress and Inflammation to Prevent Ischemia-Reperfusion Injury', *Frontiers in Molecular Neuroscience*, 13. Available at: https://doi.org/10.3389/fnmol.2020.00028.

Xu, X. *et al.* (2017) 'Cardiomyocyte dimethylarginine dimethylaminohydrolase-1 (DDAH1) plays an important role in attenuating ventricular hypertrophy and dysfunction', *Basic Research in Cardiology*, 112(5), p. 55. Available at: https://doi.org/10.1007/s00395-017-0644-z.

Yang, Y. and Rosenberg, G.A. (2011) 'Blood–Brain Barrier Breakdown in Acute and Chronic Cerebrovascular Disease', *Stroke*, 42(11), pp. 3323–3328. Available at: https://doi.org/10.1161/STROKEAHA.110.608257.

Yoo, J. and Lee, S.-C. (2001) 'Elevated levels of plasma homocyst(e)ine and asymmetric dimethylarginine in elderly patients with stroke', *Atherosclerosis*, 158(2), pp. 425–430. Available at: https://doi.org/10.1016/S0021-9150(01)00444-0.

Yuan, D. *et al.* (2018) 'Nest-building activity as a reproducible and long-term stroke deficit test in a mouse model of stroke', *Brain and Behavior*, 8(6). Available at: https://doi.org/10.1002/brb3.993.

Zahuranec, D.B. and Majersik, J.J. (2012) 'Percentage of acute stroke patients eligible for endovascular treatment', *Neurology*, 79(Issue 13, Supplement 1), pp. S22–S25. Available at: https://doi.org/10.1212/WNL.0b013e31826957cf.

Zewinger, S. *et al.* (2017) 'Symmetric dimethylarginine, high-density lipoproteins and cardiovascular disease', *European Heart Journal*, 38(20), pp. 1597–1607. Available at: https://doi.org/10.1093/eurheartj/ehx118.

Zeynalov, E., Jones, S.M. and Elliott, J.P. (2017) 'Therapeutic time window for conivaptan treatment against stroke-evoked brain edema and blood-brain barrier disruption in mice', *PLOS ONE*, 12(8), p. e0183985. Available at: https://doi.org/10.1371/journal.pone.0183985.

Zhang, F. and Iadecola, C. (1998) 'Temporal characteristics of the protective effect of aminoguanidine on cerebral ischemic damage', *Brain Research*, 802(1–2), pp. 104–110. Available at: https://doi.org/10.1016/S0006-8993(98)00557-5.

Zhang, H.-P. *et al.* (2010) 'Isoflurane Preconditioning Induces Neuroprotection by Attenuating Ubiquitin-Conjugated Protein Aggregation in a Mouse Model of Transient Global Cerebral Ischemia', *Anesthesia & Analgesia*, 111(2), pp. 506–514. Available at: https://doi.org/10.1213/ANE.0b013e3181e45519.

Zhang, L. *et al.* (2002) 'A test for detecting long-term sensorimotor dysfunction in the mouse after focal cerebral ischemia', *Journal of Neuroscience Methods*, 117(2), pp. 207–214. Available at: https://doi.org/10.1016/S0165-0270(02)00114-0.

Zhang, M. *et al.* (2011) 'Activation of NAD(P)H Oxidases by Thromboxane A $_2$ Receptor Uncouples Endothelial Nitric Oxide Synthase', *Arteriosclerosis, Thrombosis, and Vascular Biology*, 31(1), pp. 125–132. Available at: https://doi.org/10.1161/ATVBAHA.110.207712.

Zhang, Y.-Q. *et al.* (1998) 'Effects of gender and estradiol treatment on focal brain ischemia', *Brain Research*, 784(1–2), pp. 321–324. Available at: https://doi.org/10.1016/S0006-8993(97)00502-7.

Zhang, Z.G. *et al.* (1996) 'ARL 17477, a Potent and Selective Neuronal NOS Inhibitor Decreases Infarct Volume after Transient Middle Cerebral Artery Occlusion in Rats', *Journal of Cerebral Blood Flow & Metabolism*, 16(4), pp. 599–604. Available at: https://doi.org/10.1097/00004647-199607000-00009.

Zhao, Yichen *et al.* (2021) 'DDAH-1, via regulation of ADMA levels, protects against ischemia-induced blood-brain barrier leakage', *Laboratory Investigation*, 101(7), pp. 808–823. Available at: https://doi.org/10.1038/s41374-021-00541-5.

Zhao, Yichen *et al.* (2022) 'DDAH1/ADMA Regulates Adiponectin Resistance in Cerebral Ischemia via the ROS/FOXO1/APR1 Pathway', *Oxidative Medicine and Cellular Longevity*, 2022, pp. 1–15. Available at: https://doi.org/10.1155/2022/2350857.

Zhou, L. *et al.* (2010) 'Treatment of cerebral ischemia by disrupting ischemia-induced interaction of nNOS with PSD-95', *Nature Medicine*, 16(12), pp. 1439–1443. Available at: https://doi.org/10.1038/nm.2245.

Zhou, Y. *et al.* (2010) 'Isoflurane Posttreatment Reduces Neonatal Hypoxic–Ischemic Brain Injury in Rats by the Sphingosine-1-Phosphate/Phosphatidylinositol-3-Kinase/Akt Pathway', *Stroke*, 41(7), pp. 1521–1527. Available at: https://doi.org/10.1161/STROKEAHA.110.583757.

Ziche, M. *et al.* (1994) 'Nitric oxide mediates angiogenesis in vivo and endothelial cell growth and migration in vitro promoted by substance P.', *Journal of Clinical Investigation*, 94(5), pp. 2036–2044. Available at: https://doi.org/10.1172/JCI117557.

Ziche, M. *et al.* (1997) 'Nitric Oxide Promotes Proliferation and Plasminogen Activator Production by Coronary Venular Endothelium Through Endogenous bFGF', *Circulation Research*, 80(6), pp. 845–852. Available at: https://doi.org/10.1161/01.RES.80.6.845.

Zimmermann, C., Wimmer, M. and Haberl, R.L. (2004) 'L-Arginine-Mediated Vasoreactivity in Patients with a Risk of Stroke', *Cerebrovascular Diseases*, 17(2–3), pp. 128–133. Available at: https://doi.org/10.1159/000075781.

Zobel, E.H. *et al.* (2017) 'Symmetric and asymmetric dimethylarginine as risk markers of cardiovascular disease, all-cause mortality and deterioration in kidney function in persons with type 2 diabetes and microalbuminuria', *Cardiovascular Diabetology*, 16(1), p. 88. Available at: https://doi.org/10.1186/s12933-017-0569-8.

Zonta, M. *et al.* (2003) 'Neuron-to-astrocyte signaling is central to the dynamic control of brain microcirculation', *Nature Neuroscience*, 6(1), pp. 43–50. Available at: https://doi.org/10.1038/nn980.

del Zoppo, G.J. *et al.* (1991) 'Polymorphonuclear leukocytes occlude capillaries following middle cerebral artery occlusion and reperfusion in baboons.', *Stroke*, 22(10), pp. 1276–1283. Available at: https://doi.org/10.1161/01.STR.22.10.1276.

Zuckerbraun, B.S. *et al*. (2007) ‘Nitric oxide-induced inhibition of smooth muscle cell proliferation involves *S* -nitrosation and inactivation of RhoA’, *American Journal of Physiology-Cell Physiology*, 292(2), pp. C824–C831. Available at: https://doi.org/10.1152/ajpcell.00592.2005.